BINDING SERVICES
Tel +44 (0)29 2087 4949
Fax.+44 (0)29 2037 1921
E-Mail Bindery@Cardiff.ac.uk

Effect of Rigid Vegetation on the Velocity, Turbulence, and Wave Structure in Open Channel Flows

By

Saied Ahmad Mortazavi Dorcheh

Thesis submitted for the degree of
Doctor of Philosophy

Hydro-environmental Research Centre
School of Engineering, Cardiff University

May 2007

ProQuest LLC
789 East Eisenhower Parkway
P.O. Box 1346
Ann Arbor, MI 48106-1346

In the Name of God, the Compassionate, the Merciful

أَنزَلَ مِنَ السَّمَاءِ مَاءً فَسَالَتْ أَوْدِيَةٌ بِقَدَرِهَا...

He sent down water from the sky, and the channels flow, each according to its measure... (13:17)

وَأَرْسَلْنَا الرِّيَاحَ لَوَاقِحَ فَأَنزَلْنَا مِنَ السَّمَاءِ مَاءً ...

And We sent the fecundating winds that caused the rain to descend from the sky, therewith providing you with water (in abundance)... (15:22)

وَاللَّهُ خَلَقَ كُلَّ دَابَّةٍ مِن مَّاءٍ...

And God has created from water every living creature... (24:45)

...وَجَعَلْنَا مِنَ الْمَاءِ كُلَّ شَيْءٍ حَيٍّ أَفَلَا يُؤْمِنُونَ؟

... and We have made of water every thing living; will they not then believe? (21:30)

أَفَرَأَيْتُمُ الْمَاءَ الَّذِي تَشْرَبُونَ؟

Have you thought about the water you drink? (56:68)

The Holy Quran

Acknowledgements

The research for this thesis could not have been undertaken without God's help; without his mercy, nothing is possible.

I would like to express my gratitude to my sole supervisor, **Professor Roger Falconer** for his constant help and support and his guidance throughout the duration of this research, especially during the critical period. I deeply appreciate his valuable advice and continuous encouragement and fatherly advice and support during my studies period too.

During the recent months I had a very faithful support by **Dr. Mehdi Ghomeshi**, Shahid Chamran University, IRAN, without his support my thesis would not stand as it is presented now. Therefore, I wish to thank him for that.

I wish to thank **Dr David Kennedy** as a postgraduate students tutor, for his help to overcome my difficulties during my studies, especially during the critical period and even after his responsibility ended. Also I wish to thank **Mrs Helen Kennedy** for proofreading of my thesis.

I would also like to thank **Dr Saeid Sanei** for his valuable comments and proofreading of my thesis and also for other helps and supports.

I am grateful to the members of the "Hydro-environmental Research Centre" and "Student Chapter" for the valuable meetings and discussions we have had during this period.

I also acknowledge "**The Ministry of Science, Research and Technology**" **Islamic Republic of Iran**, for the award of scholarship and their financial support.

Abstract

Vegetation plays an important role in changing the flow characteristics and flooding of natural channels. In this study a series of laboratory programmes were undertaken to investigate the effects of emergent and submerged vegetation on the flow structure in compound, simple and wide channels. The vegetation consisted of rigid rods replicating tree vegetation. In a laboratory flume, wooden rods were used to replicate this with three density states and one non-vegetated state being used to compare their effects on the flow characteristics in the flume. Velocities were measured using 3-D Acoustic Doppler Velocimeters (ADV), with one downward facing and one upward facing probe.

The results showed that the velocities decreased within and near the vegetation zones, and the flow accelerated and transferred towards the upper part of the rods, or to the non-vegetated zone, along the flume. The vegetation density was shown to control the magnitude of these effects. Also, in the transition zones between the floodplain and the main channel in the compound channel, or in transition zones between the vegetated and non-vegetation zones, or near the top of the vegetation in the simple and wide channels, the velocity fluctuations and Reynolds stresses were observed to have relatively high values. The magnitude of the velocity fluctuations and the Reynolds stresses were shown to be highly depended upon the vegetation density.

Vegetation reduces the energy and increases the flow depth, with a reduction in the velocities. It also protects the channel bed against erosion due to resistance of the flow and enhances settlement of sediment.

Behind the rods the longitudinal velocity was observed to be very low, but other velocities (transverse and vertical) were high. Also velocity fluctuations and Reynolds stress components were higher behind the rods. However, as the distance from the rods increased, then the longitudinal velocity increased and the transverse and vertical velocities and Reynolds stresses all decreased.

For many conditions in vegetated open channel flows, rods may produce transverse waves due to vortex shedding. Some experiments in the wide channel, of 1200 mm width, 10 m length, and 24 mm rods diameter were undertaken using different rod arrangements and densities to investigate

the frequency and amplitude of these waves. From these experiments, and a subsequent analysis of the results, a new equation was developed for calculating the Strouhal number for water and two new equations were established for calculating the wave amplitude for different rod arrangements and densities. These equations were experimentally proved to better match the data variations than the conventional equation.

Table of Contents

List of Figures

Number **Title** **Page**

List of Tables

CHAPTER 1
INTRODUCTION

1.1 Background

The world has faced massive floods in recent years. The increasing occurrence of extreme flood events has brought the importance of river flood protection to the forefront of society. However, flood protection is only one factor of river basin management. Considering all factors of river management there is a degree of conflict, since different factors have conflicting demands. The management of floodplains is one aspect of river basin management that has become more important with the increased occurrence of flood frequency and magnitude.

The risk of flooding has in some situations increased due to straightening, dredging, and lining of channels with unnatural materials, which have changed the behaviour of waterways. Drainage of the wetlands has diminished the natural groundwater table and thus has increased further the risk of flooding. Therefore, in the last few decades, there has been increased interest and research in the floodplain management of rivers, natural waterways and wetland restoration for a wide range of civil engineering and water resource activities

Despite dealing with resistance to flow in rivers, there is a new emphasis on river restoration and enhancement. In the past, the discharge capacity of rivers has often been increased by removing vegetation, adding revetments and other modifications to increase the discharge capacity, prevent erosion and make rivers more hydraulically efficient. This has invariably led to environmental degradation because of increased sediment loads and loss of the supported ecosystem.

1.2 Flooding

Floods from rivers, estuaries, and the sea threaten many millions of people world wide. Flooding is the most widely distributed of all natural hazards usually causing distress and damage wherever it happens. For example, around 5 million people, in 2 million properties, live in flood risk areas in England and Wales (Falconer, 2006).

England and Wales saw their wettest autumn in the year 2000 for over 270 years (Environment Agency, 2001). Parts of the UK were inundated by floodwater, sometimes on several occasions. Thousands of houses were flooded, with people losing their personal possessions and being forced into temporary accommodation. Businesses were closed and roads and railways brought to a standstill. The financial and human costs were immense.

The Easter floods of 1998 and those during the autumn of 2000 have led to many conclusions; damage was reduced by flood defences and by timely warnings and evacuations where the defences could not hold back the water. This resulted in 280,000 properties being protected from the floods. However, over 10,000 properties were still flooded at an estimated cost of £1 billion (Environment Agency, 2001a).

In some developing countries, however, the consequences of floods can be devastating, both in terms of loss of property and, in particular, loss of life. In many of these countries floods can also lead to a considerable increase in water-borne disease and engineers and scientists are extending their models to include epidemiological models and health risk assessment. According to a report of the World Health Organisation and UNICEF over half of the hospital beds in the world today are occupied by people with water-borne diseases and the prevalence of some of these diseases is exacerbated by flooding (Falconer, 2006).

Flood is a natural phenomenon and may not be prevented, with experts predicting that extreme rainfall events are likely to become more frequent. However, the impacts of flooding can be minimised through flood protection and flood forecasting. We need to have a comprehensive and effective system in place to minimise the risk of flooding.

We must learn to live with rivers, without losing sight of the fundamental aims of protecting life and property from the devastating impacts of flooding. This requires a balance to be struck, such that environmental gain is obtained whenever possible and schemes that damage the environment are avoided, unless there is no other viable option. This does not mean that we should stop building and maintaining flood defences, nor should we allow urban areas to revert to marshland.

Environmental scientists and planners seek the assistance of engineers to achieve the appropriate balance. They have faced the problem of flood flow estimation throughout the ages and have in general treated it subjectively, designing intuitively for the largest known flood. Recent research has improved our understanding of the individual factors affecting flooding, but many complex interactions need to be addressed for further flood mitigation.

Historical towns are more vulnerable and may be more damaged by floods. Furthermore recent developments in the last half century have seen the construction of large areas of new housing and commercial facilities, together with the expansion of infrastructure including: roads, rail and airport networks. Agriculture and forestry have also been intensified as have the pressure on our river systems to provide more water resources and increased drainage (Fleming, et al., 2001).

To cope with the increasing levels in flood discharges, long term measures have had to be taken and raising dykes and levees is no longer the main option. Instead, measures are considered to increase the discharge capacity of the floodplains and simultaneously develop natural floodplains. These measures involve lowering of the floodplains and reconstructing secondary channels. The combination of increasing the discharge capacity and developing nature along the floodplains can be conflicting. The growth of vegetation slows down the flow velocities and enhances the sedimentation in the floodplains, and increases the velocities in the main channel.

The conflicting interest of increasing the flood discharge capacity and developing the natural floodplain provides a challenge for researchers to focus on the processes of floodplain development. This requires a broad knowledge of hydraulic, geomorphological and biological processes. The main factors causing a flood to occur are extremes in meteorology and hydrology, coupled with changes to the river hydraulics typically caused by land use changes and alterations to the river geomorphology.

1.3 Floodplain vegetation interactions

Vegetation along floodplains impacts on the hydrodynamics and morphodynamics through affecting the hydraulic roughness, sediment erodibility and sediment trapping. At present these process interactions are not well quantified. Much research has been carried out in recent years to examine the effects of vegetation on the hydraulic roughness, but the effects of vegetation on suspended sediment transport and bed-load transport are less known (Baptist, 2002).

Also understanding the impact of vegetation on the flow characteristics has become important in river restoration projects. A better understanding of the impact of riverine vegetation on the flow characteristics is therefore necessary, as

the vegetation may increase the resistance to flow and cause higher water levels. Thus, determining the flow retardation over a natural river/floodplain system is an important aspect in environmental flood management.

In environmental river engineering, channels and floodplains are regularly being restored, providing a variety of habitats for flora and fauna. Restoration must have multifunctional considerations whether these are hydrological, morphological, ecological, water quality or aesthetic (Brookes and Shields, 1996). The hydraulics of natural channels is complex and difficult to understand. Environmental features in channels need to be both technically and environmentally understood. In rivers, vegetation is an essential part of the ecosystem. However, from a hydraulic viewpoint, vegetation causes resistance to flow and can increase the risk of flooding. In alluvial river valleys the vegetation in the rivers and floodplains can reduce the risk of bank erosion. In many cases, this is a very difficult task and compromises have to be made.

The estimation of roughness in floodplains and channels, for the case of submerged and emergent vegetation, is a difficult task. Individual factors and their effects can be determined with acceptable accuracy, but the challenge is to combine these factors together as a single coefficient. One of the most significant factors which can dominate the discharge capacity of a riverine system is the flow resistance imposed by the vegetation relative to that induced by the degree of meandering and cross-sectional shape. One of the main problems in designing and modelling natural channels and floodplains is in determining the hydraulic roughness for a heterogeneous vegetated boundary. The density, height, and type of vegetation may vary within the cross-section and in the longitudinal direction. In most cases, either the velocity profile or the roughness height can be determined.

Emergent vegetation along rivers and floodplains can absorb a great deal of energy and momentum from the flow. Estimating the roughness coefficient in this region is a key factor required for establishing the river stage-discharge curves, especially during flood events, and for determining the velocity field around hydraulic structures, located along or across rivers, such as highway bridges etc. Also, the estimation of the roughness is important in the calibration and validation of river hydraulic models and even for the whole modelling process.

Vegetated floodplains can significantly reduce the velocity along the floodplains but they can also increase the main channel velocity. This is usually represented through higher Manning's n values in the streams with in-channel vegetation in flow resistance guides (Chow, 1959; Barnes, 1967). While higher values of the resistance on floodplains and banks may have little affect on low flow conditions, the effects on flood peak flows are not well known and could be significant. In areas where flow occurs through vegetation, the characteristics of the flow are largely determined by the type and density of the vegetation, as well as the depth and velocity of the flow. The Darcy-Weisbach friction factor or the Manning's n roughness can vary greatly with the area mean channel velocity due to bending of streamlines associated with the vegetation (Fathi-Moghadam, 1996).

The use of vegetation can also provide a cost-effective form of erosion control and bioengineering techniques make use of live plants to mitigate scour. Since vegetation reduces erosion, it can be a desirable control measure in comparison with other methods that control sediment, such as gabions, rip-rap, straw bale dikes, silt fences, sediment traps and basins, etc. Vegetation provides effective erosion mitigation measures by two means including changing the flow hydraulics of a river/floodplain system (i.e. reducing the flow) and by changing the run off characteristics. Vegetation also reduces erosion by absorbing the impact of rain drops (i.e. reducing dislodging), reducing the velocity of runoff (i.e. reducing the

flux), reducing runoff volumes by increasing water percolation into the soil, binding soil with roots (i.e. reducing dislodging), and protecting soil from wind and sun effects (i.e. prevents drying) (Steven et al., 1986).

In most areas grass provides an effective type of plant for erosion control, as it grows quickly and provides good ground cover. Grass linings provide an attractive alternative for the protection of earth channels exposed to intermittent flows, with this form of protection long being used for agricultural drainage channels (Temple, 1983). Rill surface cover is a major factor in predicting the detachment and erosion of sediments. Ground cover in rills greatly reduces the shear stress and hence reduces detachment rates and the sediment transport capacity of the flow (Nearing et. al., 1990). The interaction of the flow with a vegetated boundary still provides a challenge to research hydraulics. Due to the complex nature of the flow system and the variety of conditions present when the flow interacts with vegetation, it is very difficult to develop an analytical flow model, based entirely on theoretical derivations. Therefore, much of the work done in the past has been empirical in nature.

1.4 Mangroves and Coastal Protection

Since at least the third century B.C. much has been written about mangroves (Walsh 1977), with research continuing in this field in many countries world wide.

Mangroves occur in the intertidal regions of many tropical and subtropical coastlines. Their dense networks of roots attenuate the wave energy, protect the land from erosion, and provide a nursery and habitat for many land and marine animals. They cover a significant fraction of the coastline help to stabilize the banks of tidal rivers and creeks. Figure 1.1a shows an example of one species of mangrove tree, namely *Rhizophora mangle*, with their complex system of aerial roots being in Fig. 1.1b.

(a)

(b)

Fig. 1.1 Photos of mangroves illustrating: (a) an isolated *Rhizophora mangle* with prop roots, and (b) mangrove trees along a swamp channel, illustrating typical vegetation density in a forest (taken from Bangaser 2004).

In many parts of the world, man is increasingly encroaching on mangrove forests, and land managers and developers are thriving to make best use of these valuable ecosystems. (Bangasser, 2004)

As suggested, the benefits of wetlands and mangrove swamps are now being recognised for their potential as a form of coastal protection. They act as a buffer zone along the coastline and prevent large scale erosion (Westwater, 2001). Mangroves attenuate the impact of waves along coasts by obstructing the waves with their roots and trunks. Othman (1994) observed in Malaysia, that even a 50 m wide mangrove belt can be sufficient to reduce waves of 1 m in height to less than 0.3 m. As the waves pass through the mangrove trees, the roots and trunks of the mangroves obstruct the orbital water motion transmitting the wave energy. The closer the mangrove trees are to one another, the greater will be the attenuation of the waves" (Abuodha and Kairo 2001).

This type of vegetation presents obstacles to the flow, which enhances the friction by generating "complex two dimensional currents, with jets, eddies and stagnation regions, as well as vegetation scale turbulence" (Furukawa et al. 1997). As a result

of these variations in turbulence, Fukurawa et al. found that the mangroves studied trapped up to 80% of the suspended sediment brought in from coastal to estuarine waters on spring flood tides. In this way the mangroves not only build a protective coastal buffer but can also diminish turbidity in coastal waters (Furukawa et al. 1997) and protect offshore habitats, such as coral reefs. Aboudha and Kairo (2001) were found in Kenya that clear cutting of mangroves caused hydrodynamic changes to the inshore circulation, which also tended to increase the erosion of shorelines (Bangasser, 2004). Also, Wu et al (2001) noted that overcutting of mangrove trees often led to a significant impact on the ecological system in mangrove swamps and the nearby coastal waters. This removal of mangrove trees again resulted in coastline erosion. In recognising the benefits of mangrove forests, efforts have increasingly been made in many countries to re-establish mangrove forests.

Mangroves are therefore indigenous to tropical and subtropical climates and are regarded as the equivalent to tidal salt marshes more commonly found in the UK. There are approximately 80 different species of mangrove trees and shrubs. With the prop root system proving to provide added mitigation effects against erosion processes (Westwater, 2001).

1.5 Aims and Objectives

Until fairly recently, most researchers and engineers have generally used a resistance coefficient, such as Manning's n, to model flow through vegetated floodplains. However, it is also well established that the flow through vegetation can not be completely described by simple resistance coefficients. Many of the more recent studies have sought to describe the flow through vegetation by a single velocity or turbulence intensity profile. The turbulent transport processes are strongly influenced by the velocity distribution, the bed shear stress, sediment movement, and contaminant transport (Nezu et al., 1993).

The main aim of this thesis was therefore to investigate the effects of different idealised vegetation densities on the flow structure along compound channels, rectangular wide channels and simple narrow channel flows. For this purpose in a straight flume, idealised wooden rods were used to replicate tree and mangrove type vegetation with the rods having 2 different heights and extensive experimental data being collected for different vegetation densities and flow and depth conditions. The vegetation impact on the velocity profile was also considered for emergent and submerged conditions. The velocity distributions were measured at various sections along the flume, and for the varying parameters listed above, for a compound and wide and narrow modelled rectangular channels. From these measured horizontal and vertical velocity distributions various turbulence parameters were established, leading to a better understanding of the impact of idealised vegetation on the flow structure and estimates of the grass roughness characteristics.

In this thesis the layout is as follows. Chapter 2 provides an extensive review of the corresponding literature. Details of the laboratory configuration and set up are given in Chapter 3. The measurements and analysis of these data for velocity and turbulent component profiles in a compound channel with four configurations of vegetation on the floodplain are given in Chapter 4. In Chapter 5 four different combinations of submerged and emergent rod configurations in a simple channel are investigated with the data analysis and calculation of the time-averaged velocity and turbulent components. Chapter 6 includes the data analysis for three locations of vegetation (full, one-sided, and two-sided) and two rods heights (submerged and emergent) and also four configurations for investigation of velocity and turbulence profiles in two different cross-sections. In Chapter 7 the attention has been focused on the transverse wave generation in wide open channel with different densities of rods and the frequency and amplitude are

described and calculated and new equations have been proposed. Finally the conclusion and recommendations for further research are given in Chapter 8.

CHAPTER 2
LITERATURE REVIEW

2.1 Introduction

Flow transport is always associated with energy and friction losses. There are two types of flow regimes: laminar flow at low Reynolds numbers, and turbulent flows with high Reynolds numbers. Vegetation plays a major role in contributing to friction losses in rivers, roadside drainage ditches and canals (Petryk and Bosmajian 1975; Arcement and Schneider 1989). Bank vegetation is often perceived to be a significant factor in reducing the discharge capacity of natural rivers and flood-control channels (Masterman and Thorne 1992). This perception provides one reason for expensive and environmentally detrimental maintenance procedures that remove bank vegetation, despite the acknowledged beneficial effects that vegetation cover can have on increasing bank stability, reducing erosion, and improving habitat (Stormwater Quality, Best Management Practices Report 1991).

The hydraulic computations of flow in river/floodplain systems (i.e. compound channels) are based on stage-discharge curves and involve the use of roughness coefficients that separately represent the resistance to flow in the main channel and the floodplain zone. The corresponding stage-discharge curves predicted along the channel are based on the use of numerical models that include existing vegetative resistance models, which are empirical in nature and inadequate for emergent vegetation and for overbank flow.

2.2 Velocity profile

In an open channel flow the velocity is generally not uniformly distributed throughout the cross-section. The velocity distribution depends on the cross-sectional shape, the roughness type and distribution of the vegetation across the channel. In the case of a gravel bed river with turbulent flow conditions the vertical velocity profile is often assumed to be logarithmically distributed (e.g. Chow, 1959; French, 1986; Graf 1998; and Ferro, 1999). Recently, most studies have focused on velocity profiles and turbulent characteristics of vegetated channels and these have relatively good agreement between experimental results and computational modelling results (e.g. Shimizu and Tsujimoto 1994, Tsujimoto et al. 1996, Naot et al. 1996, Nepf 1999, López and García 2001, Stephan 2002, Schnauder, 2004).

Tsujimoto and his colleagues have conducted several experimental and numerical studies to examin the impact of simulated vegetation on the velocity and turbulence fields in simple and compound channels (Tsujimoto et al., 1991a, 1991b; Tsujimoto, 1993; Shimizu and Tsujimoto, 1993). Using a modified version of the high Reynolds number k-ε model and with drag-related source terms that account for the presence of vegetation, relatively good agreement between the experimental observations and numerical predictions was obtained.

2.2.1 Velocity profile above vegetation canopy

The velocity profile above the vegetation depends on the vegetation roughness height and friction velocity. Numerous investigations have been conducted on the velocity profile above flexible submerged vegetation. Most of these studies have been made for laboratory conditions, either with natural or artificial vegetation (Kummu, 2002). In channels with submerged vegetated beds the velocity profile above the vegetation is often also assumed to follow a logarithmic profile (Kouwen

et al., 1969; Stephan, 2001; El-Hakim and Salama, 1992; Tsujimoto et al., 1992 and Kutija and Hong, 1996).

Other studies of velocity profiles above vegetated canopies have been investigated by Christensen (1985) and Shimizu and Tsujimoto (1994). Christensen (1985) focused on the high roughness characteristics for tropical and subtropical watercourses. A modified logarithmic velocity profile was developed and experimentally verified for use in such watercourses (Christensen 1985). Shimizu and Tsujimoto (1994) investigated further the turbulent flow over a simulated vegetation layer (composed of rigid rod arrays) using a k-ε turbulence model.

2.2.2 Velocity profile inside vegetation canopy

The velocity profile inside a vegetated channel, where the profile is usually assumed to be uniform, has been studies by several investigators including: Kouwen et al. (1969) and Christensen (1985). Both natural and artificial vegetation have been used and, as with the above vegetation studies, most of the investigations have been carried out in laboratory conditions. Some of the studies are briefly described below.

In experiments involving branched plastic strips El-Hakim and Salama (1992) fitted a power law velocity profile to their measured data. Quraishi (1963) defined a transition zone is a thin layer above the vegetation and the velocity profile for this zone was also determined in the study by El-Hakim and Salama (1992).

Tsujimoto et al. (1992) described the velocity profile inside the vegetated zone by assuming a similar Reynolds stress profile to that in the vegetation canopy. Experiments were undertaken in a laboratory flume using artificial cylinders to model the vegetation.

2.3 Flow resistance

The influence of friction on the velocity in channels is due primarily to the channel and the bed characteristics. Standard roughness equations are used for the quantification of resistance, with the magnitude of the resistance being described by a resistance coefficient.

Flow resistance in open-channels is a complex phenomenon and there are no exact methods to calculate that. The factors that have the greatest influence on the coefficient of roughness are described in Table 2.1. It should be noted that these factors are to ascertain extent interdependent (Chow, 1959).

It is possible to represent individual factors and their effects on resistance. In a one-dimensional approach each of the factors listed below influences the choice of the roughness coefficient and is described by one single value of the coefficient.

Table 2.1. Factors affecting flow resistance (Chow, 1959).

Boundary surface roughness	It is represented by the size and shape of the grains of the material around the wetted perimeter and producing a retarding effect on the flow. The distribution of the grains and their irregularity has an influence on the retarding effect.
Vegetation	Markedly reduces the flow capacity of the channel and retards the flow. This effect depends mainly on the plant height, plant density, distribution, stiffness, type and species of vegetation. The value of the resistance factor may increase in the growing season and diminish in the dormant season.
Channel size, shape and irregularity	Refer to variations in the channel cross-section, area, cross-sectional shape, and wetted perimeter along the longitudinal axis of the channel.
Sedimentation and erosion	May change a channel either to a more irregular or more regular form. The effects depend on the soil material, form of the channel and discharge.
Obstructions	Such as fallen trees, debris, stones, bridge piers, and log jams can have a significant impact on the flow resistance.
Stage and discharge	Normally affect the flow resistance in such a way that when the relationship increases then the roughness coefficient decreases. However, for the case of a high discharge then the water reaches the riverbank or floodplain, when the effect may be opposite to the normal condition.
Sinuosity	It is the degree of the meandering. It can be quantified as the ratio of the thalweg length of the shortest distance between two points. Flow resistance increases as sinuosity increases.
Ice	It is an important factor affecting flow resistance in certain countries. An ice layer on the river may increase the resistance.

2.4 Roughness coefficient

Resistance to flow is typically characterized by a roughness coefficient. The roughness coefficient represents the degree of energy loss in an open channel system. This section introduces some of the most common roughness coefficients and their formulae.

2.4.1 Chézy formula

According to Chow (1959) Antoine Chézy developed probably the first uniform flow formula, known as the Chézy formula. It is defined as:

$$U = C\sqrt{RS_f} \tag{2.1}$$

where U is the velocity, R is the radius hydraulic, C is the Chézy's roughness coefficient and is dimensionless and S_f is the slope of the energy grade line. With the Chézy's roughness coefficient, it is possible to define the head loss.

$$h_f = \frac{1}{C^2}\frac{LU^2}{R} \tag{2.2}$$

where L is the length of the channel and h_f is the head loss [in metres].

2.4.2 Darcy-Weisbach formula

According to Chow (1959) the area mean flow velocity can also be calculated by using Darcy-Weisbach formula:

$$U = \sqrt{\frac{8gRS_f}{f}} \tag{2.3}$$

where f is the Darcy-Weisbach friction factor, which is dimensionless. A relationship between the roughness height and the Darcy-Weisbach friction factor f has been developed by Colebrook-White. The equation is semi-empirical and valid for only turbulent and hydraulically smooth, transitional, or rough flow.

According to Graf (1998) for laminar and hydraulically smooth flow the friction factor can be defined as:

$$f = \frac{24}{\mathrm{Re}} \qquad \text{and} \qquad R_e = \frac{4RU}{\upsilon} \tag{2.4}$$

while French (1986) suggests

$$f = \frac{0.316}{\mathrm{Re}^{0.25}} \tag{2.5}$$

The Darcy-Weisbach method is recommended by French because the flow resistance coefficient is dimensionless and the formula includes Reynolds Number effects. From the Darcy-Weisbach coefficient the head loss can be expressed as:

$$h_f = f \frac{L}{4R} \frac{U^2}{2g} \tag{2.6}$$

2.4.3 Manning's *n* formula

The most commonly used equation for flow resistance in open channel flow computations is the Manning's equation defined as:

$$U = \frac{1}{n} R^{2/3} S_f^{1/2} \tag{2.7}$$

where n is the roughness coefficient [$s/m^{1/3}$] known as Manning's n. The Manning's n formula is the result of a curve-fitting process and is thus completely empirical in nature (French, 1986). The head loss can be determined from Manning's n as follows:

$$h_f = n^2 \frac{LU^2}{R^{4/3}} \tag{2.8}$$

Thus, from the Equations 2.2, 2.6 and 2.8 the connection between the Darcy-Weisbach's friction factor, the Chézy's roughness coefficient and the Manning's n can be expressed as:

$$f = \frac{8gn^2}{R^{1/3}} = \frac{8g}{C^2} \tag{2.9}$$

2.5 Drag Coefficient

The drag force due to vegetation can be formulated as (Thom, 1975):

$$F_d = \frac{1}{2}\rho C_d A V^2 \tag{2.10}$$

where F_d is the drag force ; C_d is the drag coefficient; ρ is density of water; A is projected area to the flow and V is mean velocity. The drag coefficient (C_d) generally varies vertically due to variations in the velocity, and is often averaged over the flow volume. Previous studies on the drag coefficient of rods show that it typically varies between 1.13 to 2.5.

Li and Shen (1973) used a wake superposition model and the measured data by Petryk (1969) to predict a drag coefficient. They studied numerically the effects of vegetation spacing and pattern on the drag coefficient. They found that the drag coefficient decreased slightly with increases in the vegetation spacing. Klassen and Van Der Zwaard (1974) measured the hydraulic data in open-channel flows with model vegetation of fruit trees, and they computed the drag coefficient using the

Chézy formula. They obtained a higher value for the drag coefficient than the value obtained by Li and Shen (1973). They stated that the higher value of drag coefficient might be caused by the higher turbulence intensity in the fruit tree experiments.

More recently, Dunn (1996) carried out some laboratory experiments for vegetated open channel flows. He found that the drag coefficient (C_d) for rigid vegetation was not constant in the vertical direction, but reached a maximum at a distance above the bed and close to approximately one third of the vegetation height, with a mean value close to 1.13.

2.6 Simple channel flow resistance

Resistance in open channels is generally calculated using a flow resistance formula such as the Darcy, Chézy, Manning formulations. Both the Chézy and Manning coefficients are constants and functions of the roughness only. However, it is now well established that these coefficients are only constant for a range of flow rates. Most friction coefficients are estimated empirically and apply only to fully-rough turbulent flows (Chanson, 1999).

The Chézy equation is often used to compute open channel flow resistance characteristics and is evaluated from the Darcy equation since more experimental data are available to estimate the Darcy friction factor *f*. An accurate estimate of the Darcy friction factor and Chézy coefficient is possible for standard geometries and material, but the data are less applicable to natural rivers particularly where vegetation, trees, large stones, boulders and complex roughness patterns and movable boundaries exist (Chanson, 1999).

The Manning equation has been the most widely used to represent resistance in stream flows in regular man-made channels and irregular natural waterways for

more than a century. This equation is based on the momentum-wall shear balance, with its origin based on the Chézy's equation (Chadwick and Morfett 1986). The parameters involved in this equation make it very flexible for the computation of flow in a wide range of applications with channel cross-section irregularities and particularly much data have been collected for this parameter both in laboratory experiments and in the field. The main difficulty in application of this formulation to represent roughness is that it requires engineering judgment (Fathi-Moghadam 1996).

In most open-channel flows, the Reynolds number exceeds about 12,500 and the flow regime is turbulent. Therefore, for the most part laminar flow regimes are not included in this study. The random nature of turbulence has led many investigators to assume that this phenomenon can be best described in terms of statistics of parameters. On the basis of this assumption, the instantaneous velocity is conveniently defined in terms of a time-averaged velocity and a fluctuating random variable velocity. A Cartesian coordinate system, the instantaneous velocities in the x, y, and z directions are defined as u, v and w (French 1994).

2.7 Resistance for vegetated open channel flows

A number of recent studies have focussed on the interaction of vegetation and flow in open channels. Furthermore the fundamental differences for emergent and submerged vegetation have also been studied. In an early study by Kouwen et al. (1969) the velocity profiles were measured in laboratory experiments for artificial flexible and submerged vegetation. One conclusion from these studies indicated that the vertical velocity profile above the flexible artificial vegetation followed a logarithmic profile.

Meijer and Van Velzen (1998) described their flume experiments for submerged vegetation of a different kind. Their analysis led to improvements of roughness

coefficient prediction. A number of studies with vegetated flow aim at the prediction of roughness values for specific vegetation.

In an investigation by Nepf and Vivoni (2000) the flow structure in depth-limited vegetated flows was undertaken. This experimental study focused on the transition of submerged and emerged flow for aquatic vegetation. Two regions of different velocity distributions were observed for the flow. A surface flow region with a vertical turbulent exchange in the overlying water column and a lower canopy; where turbulence is generated locally by the canopy elements. The influence of the specific vegetation on the hydraulic conditions was studied for the variations turbulence patterns.

Ghisalberti and Nepf (2002) went on to provide results for the mixing layers and the coherent flow structures in vegetated aquatic flows. The flume studies showed the results on the vortex characteristics for the interaction with the model vegetation.

Unlike both of the aforementioned studies, which concentrate mainly on the determination and description of the vertical velocity profiles for vegetated flows Carollo et al. (2002) carried out flow velocity measurements to determine the influence of different vegetation densities. They divided the velocity distribution into three zones and showed the existence of a S-profile. An analytical description of the profile has been derived.

For investigations of roughness and turbulence, the layer of high shear flow is always the most important region. There is a layer of high shear flow in atmospheric flow over a vegetated canopy. Distribution of velocity in this layer is exponential (Fathi-Moghadam, 1996). Shaw and Seginer (1987), and Hagen and Skidmore (1974) showed that all turbulent intensities and Reynolds stresses were a

maximum in this layer. The same observation has been shown to apply to the flow of water through vegetation in open channels (Tsujimoto et al, 1991; Tsujimoto and Nagasaki, 1992) and between vegetated regions and non-vegetated regions of channels by Pasche and Rouve (1985), and Tsujimoto and Kitamura (1990). For compound channels, Krishnappan and Lau (1986) and Prinos (1990) developed algebraic stress models that confirmed that the interaction between flow in the main channel and floodplains was the main reason for the generation of secondary currents.

Lemon (1967) and Thom (1971) modelled flow inside the vegetation by calculating the shear stress at the top of the canopy. The coefficient of drag was estimated by determining the momentum flux (i.e., the total downward flux of momentum) and equating this parameter to the drag force extracted by the plant community. These requirements are not met by emergent and tall vegetation in channels. In fact, for emergent flow the velocity profile is influenced by changes in the density of foliage with flow depth and the orientation of the foliage.

2.8 Compound channel flow with vegetation

In contrast to the design of grassed channels, there are only a few sources of information for determining the resistance of flow in floodplains and vegetated zones of rivers, and these are limited to site specific conditions. Chow (1959) provides Manning's n values for small creeks and waterways by presenting photographs of vegetated rivers and floodplains, together with their known Manning's n value. Barnes (1967) presents a pictorial illustration of typical rivers and creeks with their respective Manning's n values. The Manning's n values were calculated from the available information of time, discharge and flood stage events for specific vegetation conditions. The values were recorded for use in the conditions similar to those depicted in the photographs (Arcement and Schneider 1984; Arcement and Schneider 1987; Arcement and Schneider 1989). Obviously,

this method requires experience and engineering judgment for successful application.

Two desired properties of a resistance relationship can be stated here. Firstly, an equation is desirable that can relate resistance to readily defined, measurable characteristics of the vegetated zone and the river flow. The principal characteristics of a vegetated zone are type (flexibility and shape) and the density of vegetation. For the flow this characteristic is the velocity. Secondly, resistance should be described as a continuous function of the independent variables involved. The historical methods of estimating the resistance to flow in vegetated zones of rivers do not possess such properties. Usually, several types of roughness and associated n values can be recognized in a compound channel cross-section. According to Einstein and Banks (1950), frictional linearity may be applicable to vegetated channels. The essential feature of this concept is that under appropriate conditions a linear relationship can exist between the total resistance to flow and the resistance contributed by two or more classes of roughness elements of dissimilar resistance characteristics. Based on this hypothesis, several methods of combining the Manning's n values and obtaining an equivalent Manning's n value for a channel cross-section can be found in the literature. Cowen (1956) developed a procedure with a base value for Manning's n (n_b, for straight-uniform channels, and a smooth natural material above the bed and wall) and other affected factors such as:

$$n = (n_b + n_1 + n_2 + n_3 + n_4)m \qquad (2.11)$$

where $n_1, \ldots, n_4$ are the correction values to account for the effects of bed and wall irregularities, variation of shape and size of the channel cross-section, obstructions, vegetation and flow conditions respectively; m takes account of the effects of meandering of the channel.

The correction values of n_1, ..., n_4 as well as n_b and m for different channel types are tabulated in the US Department of Transportation (Arcement and Schneider 1984, 1989). According to these tables, the value of n_4 has a wide range: 0.002-0.010 for light vegetation in channels with a narrow width to 0.05-0.10 for dense-large vegetation in wide natural waterways. Since the vegetation roughness (i.e. the value of n_4) is dependent on the depth and velocity of the flow, and then the percentage of the wetted perimeter covered by vegetation, as well as the density and stiffness of the vegetation, can not reasonably be expected to be represented accurately by a simple flow chart or algorithm. In an alternative method, the cross-section is divided into subsections with individual n values and the discharge for each subsection is calculated and summed to obtain the total discharge capacity of the channel.

But, because today it is widely accepted that flow through vegetation can not be completely described by resistance coefficients, therefore, most recent researchers are interest to describe the flow through vegetation by a single velocity or turbulence intensity profile (Fairbanks, 1998).

Shimizu and Tsujimoto (1993) and Tsujimoto and Tsuji (1995) separately conducted some experiments on rectangular compound channel 12 m long and 40 cm wide. Shimizu and Tsujimoto (1993) examined the impact of compound channels with vegetated zone channel on the turbulence measurements. It showed that flow over floodplain or vegetated zone is slower than the main channel, and horizontal shear flow is formed. Also Tsujimoto and Tsuji (1995) studied the characteristics of flow in a compound channel with sparse vegetation on floodplain and compared with those of flow with vegetation zone with homogeneous concentration in three patterns of vegetation in floodplain. When the vegetation covers the edge of floodplain with the main channel, the down flow from main channel to the edge of the floodplain becomes dominant.

Naot et al. (1996a) and Thornton et al. (2000) explain that the apparent shear stress at the interface of the main channel and the floodplain can be quantified as a function of the local turbulence at the interface; and it is influenced by the main channel and floodplain velocities, flow depth and vegetation density.

The denser the floodplain vegetation, the further the point of maximum velocity moves away from the floodplain (Naot et al., 1996a). Furthermore, the denser the floodplain vegetation is, the more the turbulence energy is reduced on the floodplain and still more at the boundary of the main channel and the floodplain. When there is no floodplain vegetation, the slope of the bank between the main channel and the floodplain and, the width of floodplain have a significant effect on the shear stress at the interface; but when floodplain is vegetated, the slope has no significant influence on the shear stress (Pasche and Rouve´, 1985).

Naot et al. (1996a) found that the behaviour of the flow in a compound channel with rigid floodplain vegetation depends mainly on two vegetation parameters: the shading factor and the wake length. The shading factor increases with increases in vegetation diameter and density, and the wake length increases with increasing vegetation diameter and decreasing vegetation density.

Schnauder (2004) examined the interaction processes in an asymmetric compound channel with trapezoidal main channel cross-section with a width to depth ratio of considerably larger than those of previously mentioned studies. The floodplain was roughened using both rigid and flexible cylinders at two different densities. Results showed that plant properties and densities had an important impact on velocities and main channel/floodplain momentum exchange processes.

2.9 Experiments using flexible vegetation

For laboratory flume experiments many different set-ups have been studied to model vegetation. Simple set-ups use rigid rods as plant stems, which are mounted in a regular pattern. These set-ups represent rigid vegetation. For taking account of flexible properties of vegetation different kinds of set-ups are required. Kouwen (1992) advocated that grass behaves differently depending on whether it is erect or prone in the flow and it also varies differently depending upon the state of proneness of the grass. Plate and Qurashi (1965), Lemon (1967), Meroney (1968), Lemon and Wright (1969), Thom (1968, 1971, 1972), Landsberg and Thom (1971), Kondo and Akashi (1976), Wilson and Show (1977), Raupach et al. (1980), and Raupach and Shaw (1982), have all tried to model flow over flexible vegetated canopies (Fathi-Moghadam, 1996).

In a study by Stone and Shen (2002) the hydraulic resistance of flow with cylindrical roughness was investigated. The vegetation was modelled with cylindrical stems under emergent and submerged conditions. Meijer and Van Velzen (1998) used steel rods as well as natural reeds for their experiments. Ghisalberti and Nepf (2002) used a simple model of eelgrass meadow. This was scaled at the canopy and consisted of randomly placed model plants, each consisting of six thin flexible blades made from eelgrass meadow. They found that the vertical velocity profile above the flexible artificial roughness shows an adequate logarithmic characteristic. Also, they showed the influence of the different vegetation concentrations on hydraulic conditions, i.e. the turbulence patterns and vortex characteristics.

2.10 Field studies of flows with vegetation

Restoring rivers and channels to their natural form has raised the need to investigate how riparian vegetation (i.e. bushes, trees, grasses, reeds etc) affect the

hydraulic capacity of a river/floodplain system. Retardation due to vegetation is an important part of designing floodplains and hence estimating the flow resistance of vegetation is of great importance in river basin management, since it may have a significant effect on the conveyance of the channel.

A literature review by Petryk and Bosmajian (1975) has revealed that little is known about the variation of the value of n or any other roughness coefficient in dense vegetated channels and floodplains, except in channels with vegetation heights up to approximately 1 m in height (Kouwen et al. 1981; Kouwen 1992; USDA 1954; Ree and Crow 1977).

Christensen (1985) conducted some field experiments in several heavily vegetated rivers. Within the vegetation canopy the velocity was found to be uniform and in most cases close to zero.

In 1936 one of the first investigations into the hydraulic resistance of a vegetated channel was conducted Spartanburg, S.C., by the Soil Conservation Service (Cook 1938; Cook and Campbell 1939). They found a graphical relationship between Manning's n values and the product of average velocity of flow and hydraulic radius of the channel. Since most of the tests were carried out with the vegetation submerged, the correlation showed that the n value decreased as VR (velocity and hydraulic radius) increased. The decrease in n was associated with:

- the increase in plant streamlining as the velocity and the flow depth increased,
- the increase in plant submergence (i.e., decrease in relative roughness) as UR is increased.

The correlations were not found to be valid where the vegetation was not submerged completely by the flow, with this result being consistent with that shown in the field experimental results of Ree (1958). More results of the

hydraulic resistance measurements for additional types of grass land have been published in Ree and Crow (1977), again in terms of n values.

From a hydraulic viewpoint, vegetation generally increases the resistance to flow and therefore increases the risk of upstream flooding. The additional roughness of the channel due to vegetation growth, the reduction in channel cross-sectional flow area due to the bulk nature of the plants, the possibility of increased turbulence around trees in floods and the blockage caused by cut vegetation and trees all have an impact on the risk of flooding. In river systems vegetation causes energy loss through the creation of turbulence around the vegetation stems and leaves and creates an increased drag force on the flow.

Channel roughness caused by vegetation growth is also linked to the density, type, stiffness, height, area (projected against the flow direction) and distribution of vegetation. For small channels, vegetation growth can have a marked impact on the water levels. From a biological viewpoint, riparian vegetation provides an important habitat. Plants are vital sources of shelter and food for fish, invertebrates and some birds. In many natural, undisturbed rivers water often spills onto floodplains and can provide a good habitat for wetland plants. Vegetation on the floodplains and in river corridors is an important part of the whole river basin ecosystem (Marsh, 1991).

A diversity of plant species and types can enhance the general landscape and aesthetic appeal of a river corridor (Fisher, 1996 and; Hanski, 2000). To combine the hydraulic, aesthetic and biological characteristic requirements of a river corridor some compromises need to be made.

Chow (1959) describes that the roughness height for a natural river bed can be in the range 0.03 to 0.9 m. This shows how much variation can exist in the different

kinds of natural channel vegetation, with factors affecting flow resistance described in Table 2.1.

In 1955, Saari, conducted some field experiments in both a number of small natural channels and engineered channels to determine the corresponding resistance coefficients. The academic research tradition in this field has been weak; the only previous related doctoral thesis was published some twenty years ago by Hosia in 1983 (Järvelä, 2004).

In Finland, a number of studies have been undertaken on open channel flow with vegetation and oriented towards practical design problems. Kaitera (1934) was the first researcher to systematically investigate the magnitude and variation of resistance coefficients. Recently, a new approach to field studies was employed in three rivers and streams to support restoration and flood management efforts. A major advantage of this procedure compared with previous methods was its ability to estimate the flow resistance of woody vegetation in both leafless and leafy conditions. In determining the velocity profile and flow resistance caused by submerged flexible vegetation, the approach developed by Stephan (2002) was found to be suitable. However, a new formulation was proposed for the shear velocity based on deflected plant height. This modification offered better practical applicability than the original formulation, which requires complicated turbulence measurements (Järvelä, 2004).

2.11 Computational model studies

In numerically modelling the flow characteristics on floodplains, with the effects of vegetation, the governing equations needed to be extended to include the effects of blockage due to vegetative bodies, and form drag effects due to the fluid passing through a dense vegetative canopy.

Recent advances in computer technology have enabled hydraulic engineers to model the detailed structures of vegetated open-channel flows using CFD. At the same time, the detailed mean flow and turbulence characteristics has also been determined using advanced laboratory measuring techniques and typical CFD model studies have been shown to predict successfully the flow structures (Choi, 2005).

For vegetated open-channel flows, modelling of the vertical structure of the velocity profile has been carried out by a number of researchers (e.g. Shimizu and Tsujimoto, 1994; Lopez and Garcia, 2001; Choi and Kang, 2004). Previous studies on the 3D numerical modelling of vegetated open-channel flows are quite rare, with some of these studies including these undertaken by Shimizu and Tsujimoto (1993), Naot *et al.* (1996a), Fischer-Antze *et al.* (2001), and Xiaohui and Li (2002). Shimizu and Tsujimoto (1993) simulated a partly-vegetated rectangular channel flow using an algebraic stress model and investigated differences in the flow structure from non-vegetated compound open channel flow.

Naot *et al.* (1996a) simulated partly-vegetated open-channel flows numerically using an algebraic stress model and found that the vegetation within the watercourse tends to increase hydraulic resistance by providing additional drag force and the production of turbulence energy. Therefore, the flow decelerates in the vegetated zone, whereas it accelerates in the non-vegetated zone. This generates a shear layer along the interface between vegetated and non-vegetated zones. The shear layer is created between the vegetated and non-vegetated zones and its location varies depending upon the level of the turbulent kinetic energy.

Choi and Kang (2006) presented a 3D model for the numerical simulation of uniform, partly-vegetated open-channel flows. The Reynolds stress model (RSM) was used for the turbulence closure, with the model being applied to partly-

vegetated rectangular open-channel flows. The simulated results were compared with the measurements from laboratory data and were found to give good agreement between the measured and predicted velocities.

Lin and Falconer (1997) refined and applied their three-dimensional layer integrated numerical model TRIVAST (Three-dimensional layer Integrated Velocity and Solute Transport) to tide-induced circulation. In their model, the authors used the mode splitting method where a set of depth-integrated two-dimensional equations were first solved to give the pressure gradient and then the layer-integrated three-dimensional equations were solved to obtain the vertical distributions of the flow velocities. They applied their model to a large estuary with tidal circulation and obtained favourable results for both simple and complex flow fields.

The numerical model used in the current study, to predict the velocity distributions through vegetated floodplains such as those simulated in the laboratory, was based on a refined version of three-dimensional model, TRIVAST. This model was originally developed by Falconer (1976) and has been refined considerably by Falconer, Lin, Wu and Harris (2001).

2.12 Turbulent measurements in open channel flows

The distributions of the mean velocity and boundary shear stress in compound open-channel flows, using a Pitot static tube and/or a Preston tube, have been measured by many researchers (Myers and Elsawy, 1975; Rajaratnam and Ahmadi, 1981; Knight and Demetriou, 1983; Wormleaton *et al.*, 1982; Nalluri and Judy, 1985). However, a few measurements of the turbulence structure have been conducted in compound open-channel flows by a one component LDA (Mackee *et al.*, 1985) and later a two-component LDA (Tominaga *et al.*, 1989b; Shiono and Knight, 1989). Tominaga and Nezu (1991) conducted more accurate measurements

using a fibre-optic Laser Doppler Anemometer. In compound open channel flows, the strong inclined secondary currents generated from the junction edge were experimentally shown by Tominaga and Nezu in 1991 (Kang, 2004).

Nezu and Rodi (1985) measured the secondary currents in rectangular open-channel flows using a Laser Doppler Anemometer (LDA). They provided contour lines of the mean streamwise velocity, distributions of the wall shear stress, patterns of secondary currents and the turbulence structure in open-channel flows and for various aspect ratios. The measurements all showed the strong downward flow that occurs at the centre of a channel, resulting in the velocity-dip phenomena. Tominaga *et al.* (1989a) measured the mean velocity and turbulence structure in both rectangular and trapezoidal open-channel flow with various conditions for the wall roughness. They found that for a trapezoidal open-channel flow a vortex was generated with a reserve rotation to that of the free surface vortex and with the vortex occurring in the region between the free surface and the sidewall. This means that the velocity dip phenomenon does not appear in a trapezoidal open-channel. Although the boundary roughness condition is varied, the basic structures of the secondary currents do not change significantly.

2.13 Turbulent measurements in vegetated open channel flows

In recent years, an increase in the awareness of the importance of the ecological and environmental effects of vegetation has spurred on additional studies into the turbulence characteristics of turbulence in vegetated open channel flows. Most experimental studies focused on the mean velocity and turbulence structures in the vegetated open-channel flows.

Extensive studies have been undertaken at Kanazawa University on the measurements of turbulence characteristics for vegetated open-channel flows over rigid and flexible vegetation (Tsujimoto *et al.*, 1991; Tsujimoto and Kitamura,

1992; Shimizu and Tsujimoto, 1993). Tsujimoto *et al.* (1991) investigated the mean flow and turbulence characteristics for rigid and flexible vegetation. Their experimental results for rigid vegetation showed that an almost uniform mean velocity distribution prevailed in the region where the flow depth was smaller than the vegetation height. In this region, the turbulent momentum exchange was negligible and the turbulence intensity was relatively small. The corresponding results for flexible vegetation revealed that the mean velocity was no longer as uniform as with rigid elements for emergent vegetation. The results for submerged vegetation indicated the existence of a deflection point near the vegetation height, with a corresponding peak in the vertical distribution of the turbulence intensity.

Tsujimoto and Kitamura (1992) carried out some experiments for open channel flows with a partially vegetated zone of half the channel width. They found that there was a transitional zone between the vegetated and non-vegetated zones, where the velocity gradient and turbulence intensity showed large values. The measured water surface fluctuations had a peak at the interface between the vegetated and non-vegetated zones, and it reduced with spanwise distance from the interface.

Ikeda and Kanazawa (1996) carried out turbulence measurements for open channel flow above flexible vegetation, using 2D Laser Doppler Velocimetery (LDV) and Particle Image Velocimetery (PIV). Their experiments revealed that the turbulence intensity and the Reynolds stresses peaked around the vegetation height. Also, their experiments showed an organized vortex of elliptic shape above the top of the vegetation height. The organized vortex structure consisted of a pair of counter-rotating vortices when viewed both in horizontal and cross section.

Nepf and Vivoni (1999) measured the mean flow and turbulence structure in open channel flows over emergent and submerged vegetation. They used vinyl plastic

rods for flexible vegetation and 3D Acoustic Doppler Velocimeters (ADV) and 2D LDVs for measurement of the instantaneous velocity. They found that with the increase in submergence depth from the emergent condition, the in-vegetation momentum became increasingly dependent upon the vertical turbulence transport. For submerged conditions, turbulence shear production was predominately generated at the top of the vegetation. For emergent conditions, the shear production was negligible, and turbulence generation was dominated by wake production.

Nepf and Vivoni (2000) classified the vegetated open-channel flows to three types depending upon the relative height of vegetation to the total water depth.

1) If the vegetation height is nearly negligible compared to the water depth ($hp/H \rightarrow 0$), then the flow belongs to the first type of the terrestrial canopy flows. The flows are characterized by a strong shear layer formed around the vegetation height. The Reynolds stress at the vegetation height further exceeds the pressure gradient in the streamwise direction. For terrestrial canopy flows, the characteristic length of turbulence is about the same as the vegetation height and the turbulence production by wake is about 10% of the total turbulence production (Raupach and Shaw, 1982).
2) The second type is open channel flow with submerged vegetation affected by the water depth ($0 < hp/H < 1$). For this kind of flow, the magnitude of the Reynolds stress and the pressure gradient in the streamwise direction are about the same at the vegetation height, and the flow structure varies depending upon the relative value of h_p/H.
3) The third type is open-channel flow with emergent vegetation. Under this condition, the pressure gradient in the streamwise direction exceeds the Reynolds stress at the water surface. Since the turbulence production is made largely by the wake, the characteristic length scale of the turbulence is about the same as the stem diameter.

Nepf and Vivoni (2000) carried out further laboratory experiments for open channel flows with various submergence depths. The experiments revealed that the flow within an aquatic canopy may be divided into two regions, i.e., above and below the penetration depth. The penetration depth is defined as the distance from the top of the vegetation at which the turbulent stress has decayed to 10 % of its maximum value. The two regions are named the "vertical exchange zone" and the "longitudinal exchange zone", above and below the penetration depth, respectively. In the vertical exchange zone, the mean flow and turbulence structures are significantly influenced by the shear layer around the top of the canopy. In the longitudinal exchange zone, the turbulence is generated locally by the canopy elements, and the momentum budget is balanced by vegetative drag and pressure gradient.

Nezu and Onitsuka (2001) measured the mean flow and turbulence structure in open-channel flows with a partially vegetated zone of half the channel width, with the measurements being undertaken using LDAs and PIVs. They found that the horizontal vortices near the free surface were generated by the shear instability, and the magnitude of the vortices increased with an increase in the vegetation density. The intensities of the secondary currents and the turbulence energy increased as the Froude number increased. Also, the pattern of the secondary currents was quite different from that for plane rectangular and compound open-channel flows.

As outlined in this chapter many studies have been undertaken in the past in analysing the flow (including velocity and depth) and turbulence characteristics for simple rectangular and compound channels with emergent and submerged vegetation. The studies have primarily focused on laboratory and/or numerical model studies, but some field studies have also been undertaken. Studies relating to vegetation density and diameter for idealised vegetation have been limited and the

current study extends these investigations for a relatively wide range of parameters and flow conditions.

CHAPTER 3
EXPERIMENTAL MODEL DETAILS

3.1 Introduction

In this chapter details are given of the various setup configurations for studying the velocity and turbulence characteristics of flows through rigid vegetation in a compound channel, a narrow simple channel, and a wide rectangular channel. Experiments were conducted for fully emergent vegetation conditions on the floodplain for the compound channel configuration, and fully or partially emergent and submerged vegetation conditions were studied for the narrow simple channel and the wide rectangular channel configurations. For the compound and wide rectangular channel experiments, the velocity was measured across the entire channel cross-section, whereas for the narrow simple channel the measurements were taken at several locations within the vegetation array.

All of the laboratory experiments described in this project were conducted in the Hyder Hydraulics Laboratory, in the School of Engineering, at Cardiff University. The tests were performed during the period January 2003 to April 2006.

3.2 Flume design and details

Experiments were conducted in a recirculating flume of width 1.2 m, a length of 10 m and a maximum depth of 0.3 m with the longitudinal bed slope set at 1:1000. To ensure structural rigidity for the water pressure when the flume is in operation, the flume was strengthened with toughened glass of thickness 10 mm. The wall sides of the flume in the compound and wide channels were all glass but in narrow simple channel the wall sides and bed were made of wood. For the compound channel the wall sections were located within the main channel and were

constructed of eight 2.5 m by 0.32 m sections with all joints being waterproofed using a silicone sealant. The flume was located on a fixed steel frame structure with hollow sections and designed to reduce the stresses on the glass when the flume was operational. The flume structure is illustrated in Figs. 3.1 and 3.2.

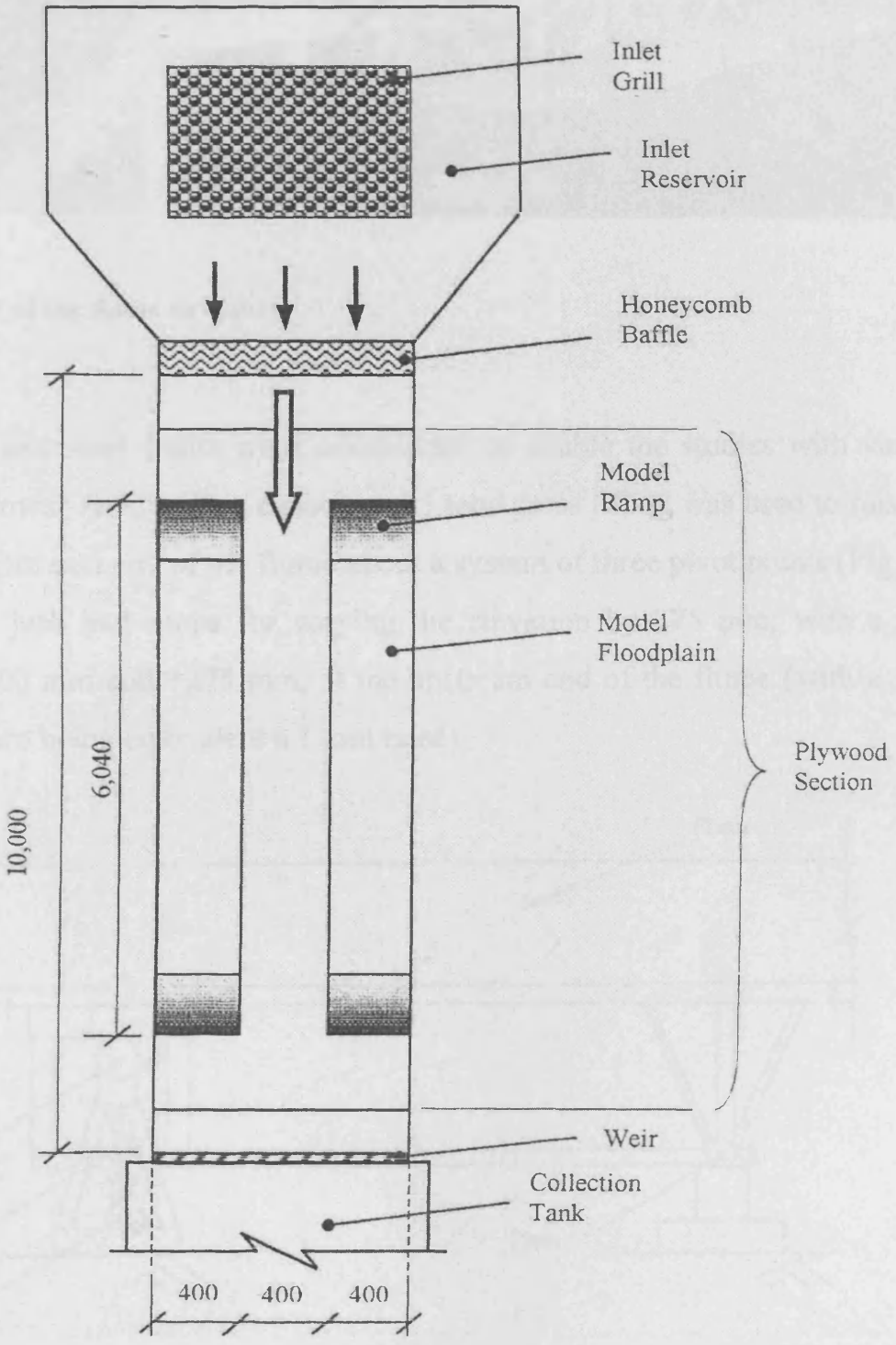

Fig. 3.1 Plan and layout of flume for the compound channel (all values are in meters).

Fig. 3.2 View of the flume structure.

The flume and steel frame were constructed to enable the studies with variable slope. A "Power Jack" with a capacity of 5 tons gross lifting was used to raise and lower the upstream end of the flume about a system of three pivot points (Fig. 3.3). The power jack had scope for varying the elevation by 375 mm, with a range between -100 mm and +275 mm, at the upstream end of the flume (with a 1 mm complete turn being equivalent a 1 mm raise).

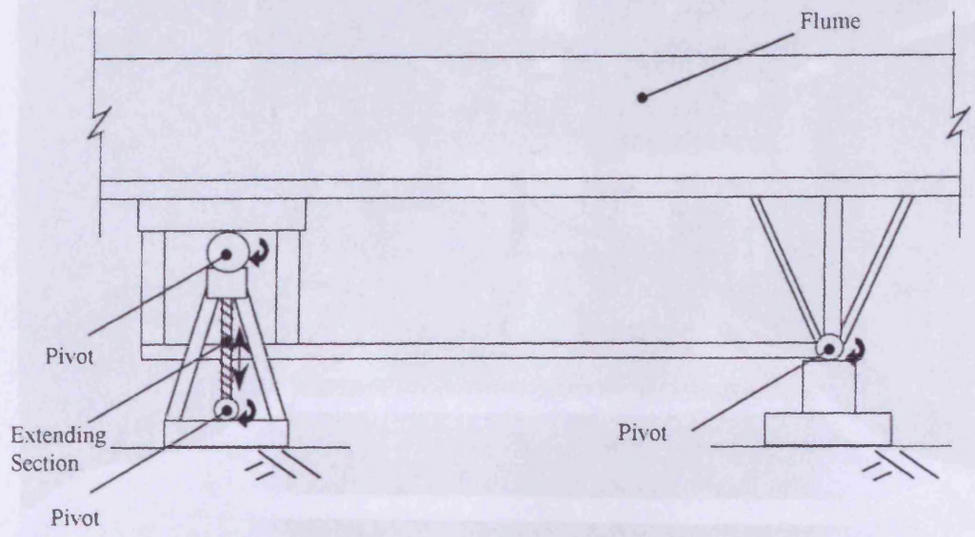

Fig. 3.3 Sketch of three point pivot slope mechanism (not to scale).

The mechanism of the three-point pivotal system is not strictly linear, due to the horizontal and vertical movement of the flume when raised. Since the effects of the bed slope were important in all experiments the bed slope was fixed at 1/1000.

A centrifuge pump (SPP AM20A) was used for recirculation in the flume, with a maximum capacity of 0.8 l/s. To ensure that the pump remained full of water a minimum water level of 1 m was maintained in the tank. Any air entertainment would result in an insufficient water delivery or, even worse, the onset of cavitations.

The water was first pumped by a delivery pipe under the glass flume, through a grill, and into the inlet reservoir at the upstream end of the flume. The water was then passed through a honeycomb baffle, to reduce the turbulence and non-uniformity in the flow structure, before entering the flume (Fig. 3.4). An adjustable steel thin plate weir was located at the downstream end to control the flow regime and depths throughout the experimental programme. This was manually operated, through a range of 0 to 330 mm above the bed (Fig. 3.5).

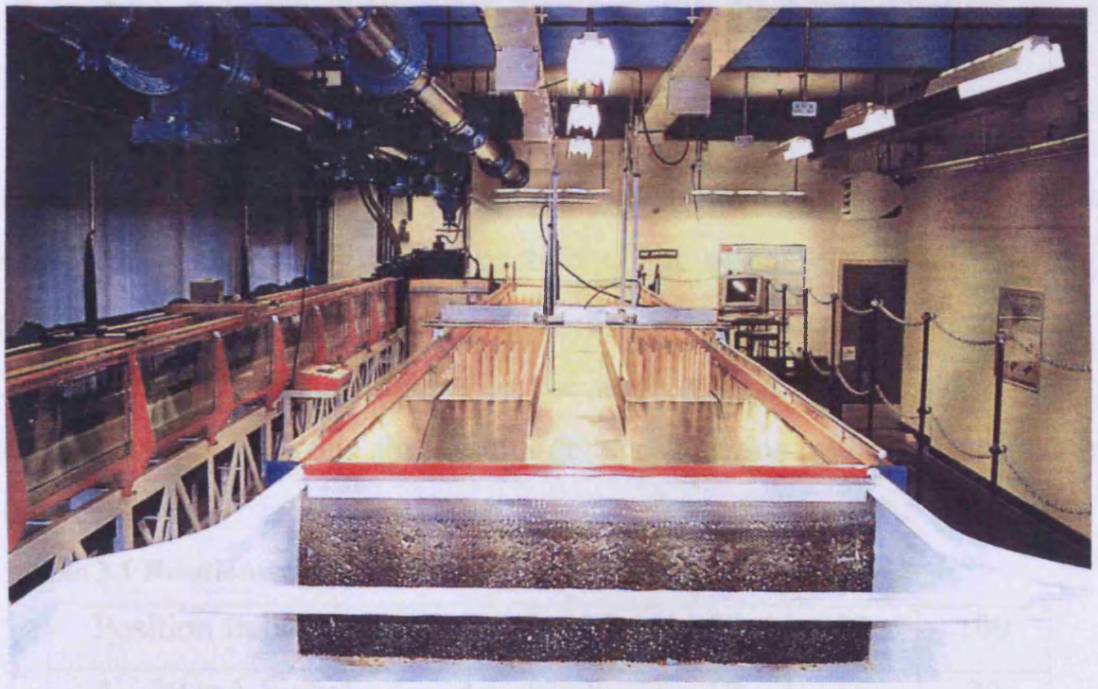

Fig. 3.4 View (looking downstream) of honeycomb baffle at the upstream end of flume.

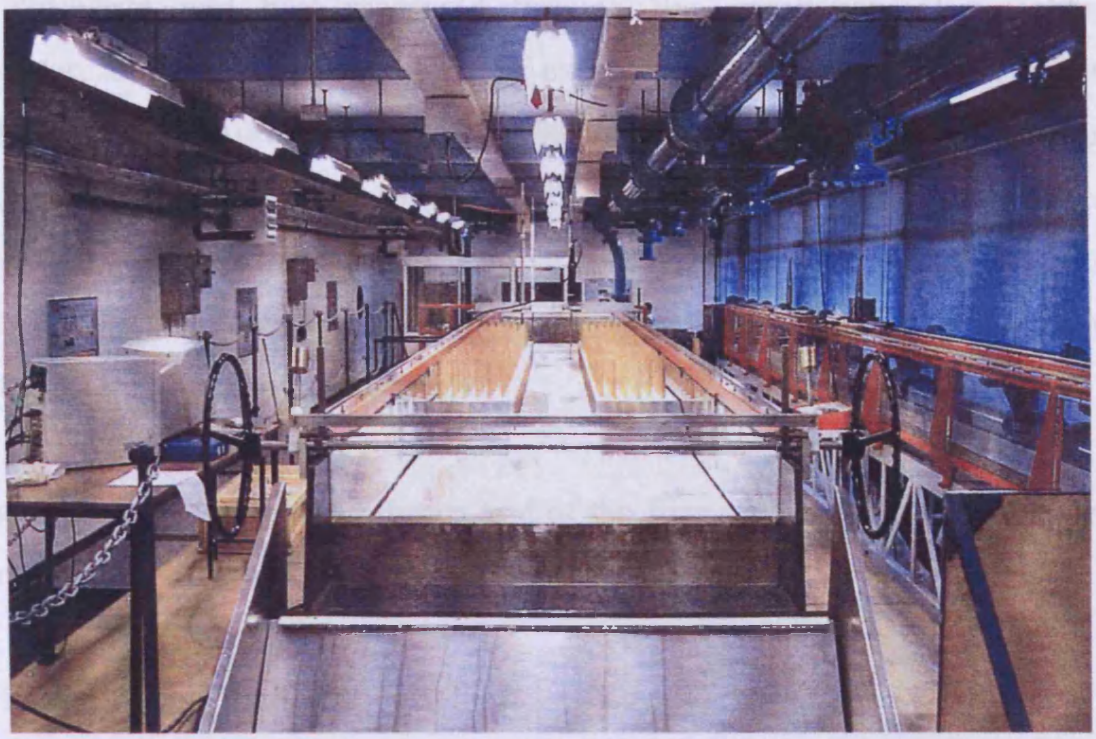

Fig. 3.5 View of weir at downstream end of flume.

The flow was adjusted manually through the use of an uncalibrated valve indicator, which showed the discharge to be between 0 and 100%. The flat plate valve regulated the flow through the inlet to the pump; therefore, it could not be assumed that there was a linear relationship between the discharge through the valve opening and the position indicator.

The valve was operated via an electronic signal in the range of 4 to 20 mA for the fully closed and open positions respectively. The actual signal and the indicator were calibrated according to Table 3.1, as described in the operating manual. This indicated a linear relationship between the valve position and the indicator, but a linear relationship between the discharge and position indicator could not be assumed.

Table 3.1 Relationship between position indicator and valve signal.

Position Indicator	0	25	50	75	100
4 – 20 mA Signal	4	8	12	16	20

The discharge was best measured through the installation of a calibrated flowmeter, attached to a computer. For experimental discharge measurements in the flume a "Flow Automation Series 4000" insertion turbine flowmeter was used. Using the Flow Automation Model 405D, the flow-computer was calibrated to produce an output registering the flow in m^3/min. The valve indicator was then calibrated against the flowmeter output, with a range of investigations being undertaken for appropriate discharges.

The tailgate weir at the downstream end of the flume was adjusted to monitor the water surface profile to establish uniform flow conditions.

3.3 Measuring equipment

A three-dimensional (3D) Acoustic Doppler Velocimeter (ADV) was used to measure the point velocity across the entire channel cross-section. This type of current meter uses an acoustic pulse emitted from a central emitter and then, through a configuration of three acoustic sensors, the reflected acoustic pulse is detected and therefore the Doppler shift is measured for a particle within the flow. From these velocimeters the data were transmitted via a conditioning module to the PC where the data were interpreted to give the instantaneous Cartesian co-ordinate velocity components at a specific point in the flow. The ADV measures the velocity components in three directions: i.e. the streamwise (u_x), transverse (v_y) and vertical (w_z) directions. A measurement duration of 3 minutes was used and the measurement frequency was set to 25 Hz. To obtain measurements near to the bed and sidewall boundaries and the water surface, the maximum number of points velocity measurements were taken, both using upward and downward-looking probe heads.

Depth measurements were made using a pointer gauge, which had a graduated millimetre scale attached. The pointer was first set to the bed level at each point,

and the scale zeroed. Then the depth was measured by moving the pointer to the free surface.

3.4 Experimental set-up

This Section gives a description of the flume configuration used in each experiment. Herein we start with compound channel, then the simple narrow channel is discussed, and finally the wide channel is explained. The above order is in line with the order of the experiments; for each a certain prior set-up and solving technical problems were required. The following sections provide more detailed information about the individual experiments.

3.4.1 Compound channel

For the compound channel experiments the flume had a symmetrical compound section, with a main channel width of 400 mm and floodplains widths of 400 mm (Fig. 3.6).

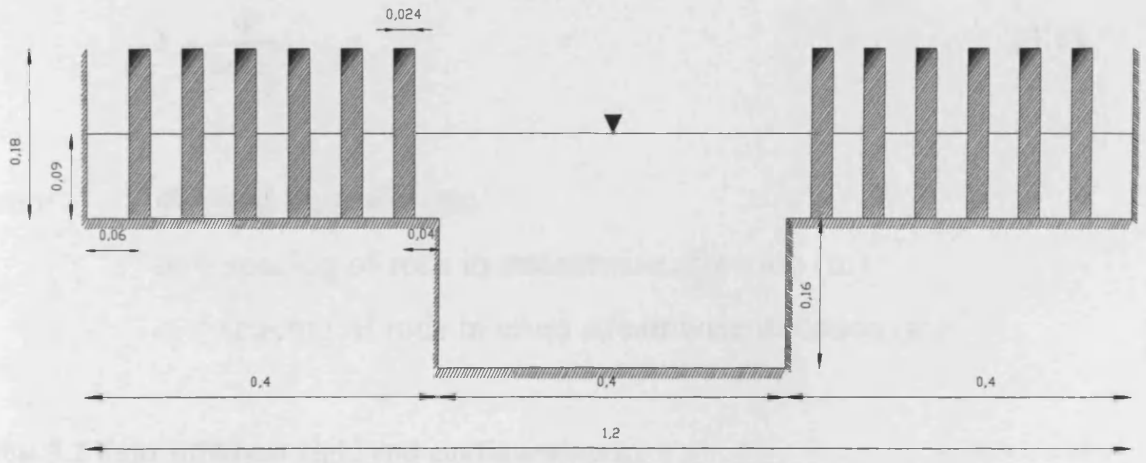

Fig. 3.6 Cross-sections of main channel and floodplain (all values are in meters).

The wooden dowels used to simulate rigid rods had a diameter of 24mm and a length of 180 mm, with the dowel of spacing along the width and channel width being typical of those found in mangroves forests with noriyoral scaling ratios in

the range 1:20 to 1:100. In the compound channel tests the dowels were always emergent on the floodplain.

The next set of tests was undertaken for a rectangular section, with a narrow constant width. The experiments were conducted for both, emergent and submerged conditions for this experimental programme. The same diameter rods were used (i.e. 24 mm), but the length of rods varied from 180 mm for the submerged case and 300 mm for the emergent case. The number and spacing between the rods were based upon the vegetation density. Four different rod configurations were investigated (Fig. 3.8) and these are summarised in Table 3.2 with the density (λ) being defined as:

$$\text{Density } \lambda = \frac{\text{Projected area of plant in control volume}}{\text{Total flow volume of control volume}}$$

$$\lambda = \frac{\Phi}{a_x . a_y} \qquad (3.1)$$

where Φ = rod diameter (m)

a_x = spacing of rods in streamwise direction (m)

a_y = spacing of rods in cross streamwise direction (m)

Table 3.2 Four different rigid rod configurations.

Density	λ (m^{-1})	a_x (mm)	a_y (mm)	Details	Cross-section N0.
High	0.004	100	60	In-line	2 (4.4, 4.5)
Medium	0.002	100	120	Staggered	2 (4.4, 4.5)
Low	0.001	200	120	In-line	2 (4.4, 4.5)
No vegetation	--	--	--	--	1 (4.4)

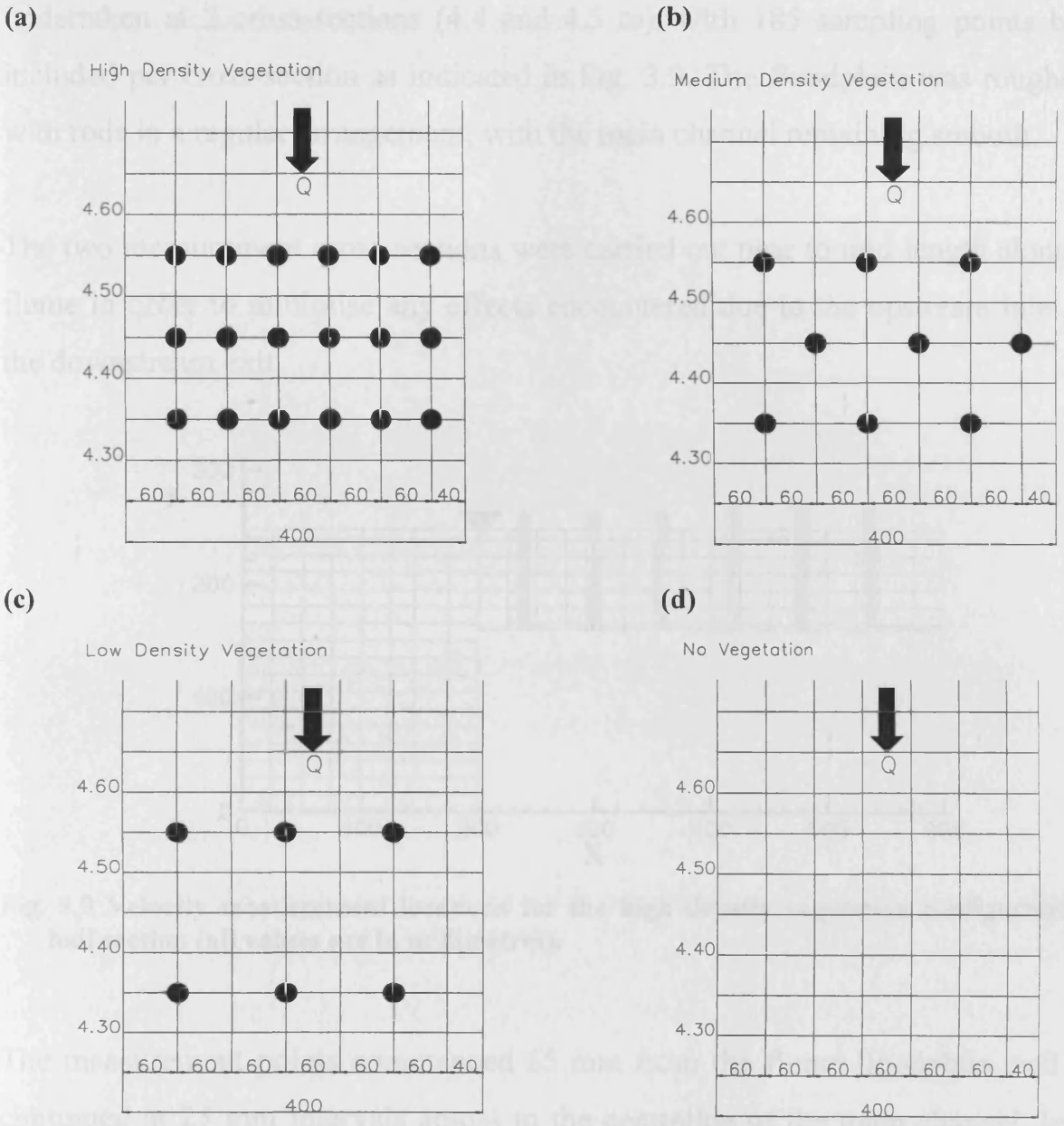

Fig. 3.8 Layout of four rod configurations on the floodplain: (a) high, (b) medium, (c) low, and (d) no vegetation.

For all experiments with differing densities in the compound channel experiments, the flow rate was kept constant at a value of 15 l/s. For the range of rod densities examined in this study, the variation in the density had little effect on the water elevation (less than 5 mm). For the achieved uniform flow condition, the flow depths in the main channel and on the floodplains were 250 mm and 90 mm respectively. For each density configuration velocity measurements were

undertaken at 2 cross-sections (4.4 and 4.5 m), with 185 sampling points being included per cross-section as indicated in Fig. 3.9. The floodplain was roughened with rods in a regular arrangement, with the main channel remaining smooth.

The two measurement cross-sections were carried out near to mid-length along the flume in order to minimise any effects encountered due to the upstream inlet and the downstream exit.

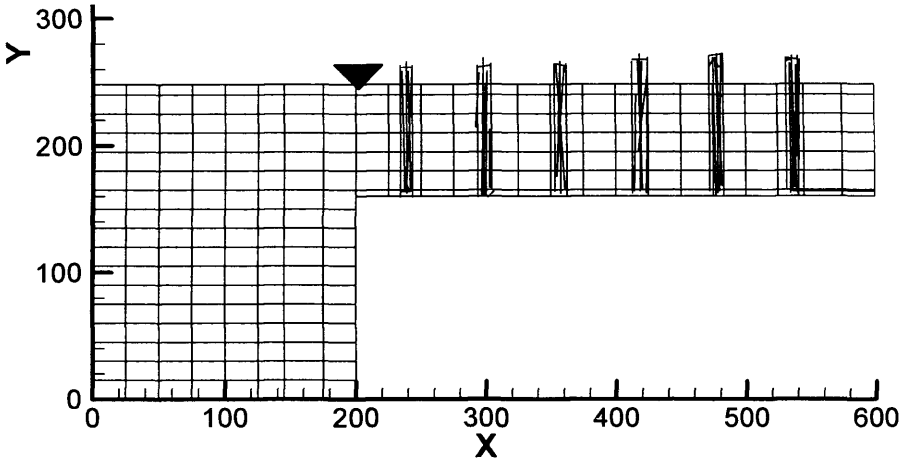

Fig. 3.9 Velocity measurement locations for the high density vegetation configuration in half section (all values are in millimetres).

The measurement points commenced 55 mm from the flume floodplain wall and continued at 25 mm intervals across to the centreline of the main channel. In the vertical plane measurement points commenced 15 mm from the bed of the main channel and 5 mm from the floodplain bed, continuing up to the water surface.

As mentioned previously, the velocity data were recorded using an ADV, with the probes being of the downward orientation type or of the upward orientation type. As the downward orientation probe was positioned along the x-axis and in the direction of flow, then the velocity in the x direction was defined as being positive, but in contrast, the upward pointing probe was in the opposite flow direction and the x-axis velocity was therefore defined as being negative. Also for both probes

the y-axis was taken as being positive in the direction towards the centreline and the z axis was taken as positive in the direction upwards from the bed.

3.4.2 Narrow simple channel

Experiments were conducted in a simple rectangular flume of 400 mm width, with the longitudinal bed slope being set at 1:1000. The bottom and side walls of the flume were made of wood and, for all conditions, the measuring equipment and vegetation densities were similar to those for the compound channel flume as described in the previous sections. For all of the experiments with differing densities the flow rate was kept constant at a value of 6.5 l/s.

For all densities, it was found that the water elevation had minor effect (less than 5 mm). For each density, the velocity was measured at different points along the middle of channel with the measuring sites being 5 mm from the bed and at 25 mm increments towards water surface (i.e. at 5, 25, 50, 75, 100, 125, 150, 175, 200, 225, 250 and 260 mm). As before, a sampling period of 3 minutes was used and the measurement frequency was set to 25 Hz. Four different combinations of submerged and emergent rods configurations were investigated. The height of the rods for the submerged state was 180 mm (Fig. 3.10) and for the emergent state was 300 mm (Fig. 3.11).

(a)

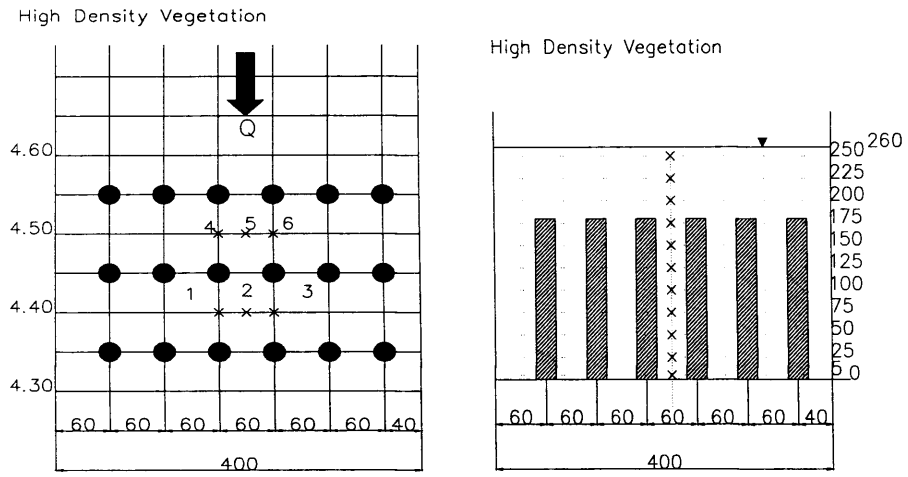
High Density Vegetation
Q
4.60
4.50
4.40
4.30
1
2
3
4
5
6
60 60 60 60 60 60 40
400
High Density Vegetation
250 260
225
200
175
150
125
100
75
50
25
5 0
60 60 60 60 60 60 40
400

(b)

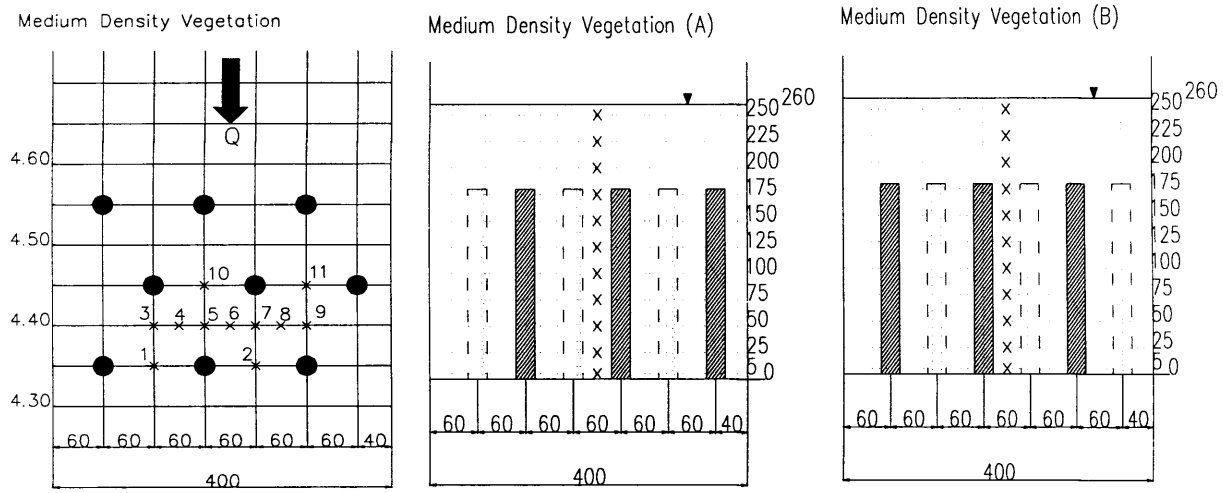
Medium Density Vegetation
Q
4.60
4.50
4.40
4.30
1
2
3
4
5
6
7
8
9
10
11
60 60 60 60 60 60 40
400
Medium Density Vegetation (A)
250 260
225
200
175
150
125
100
75
50
25
5 0
60 60 60 60 60 60 40
400
Medium Density Vegetation (B)
250 260
225
200
175
150
125
100
75
50
25
5 0
60 60 60 60 60 60 40
400

(c)

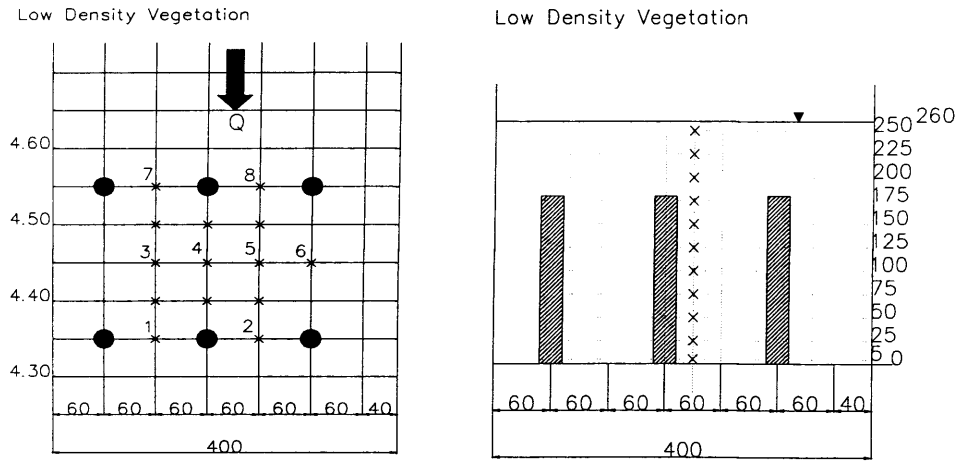
Low Density Vegetation
Q
4.60
4.50
4.40
4.30
1
2
3
4
5
6
7
8
60 60 60 60 60 60 40
400
Low Density Vegetation
250 260
225
200
175
150
125
100
75
50
25
5 0
60 60 60 60 60 60 40
400

(d)

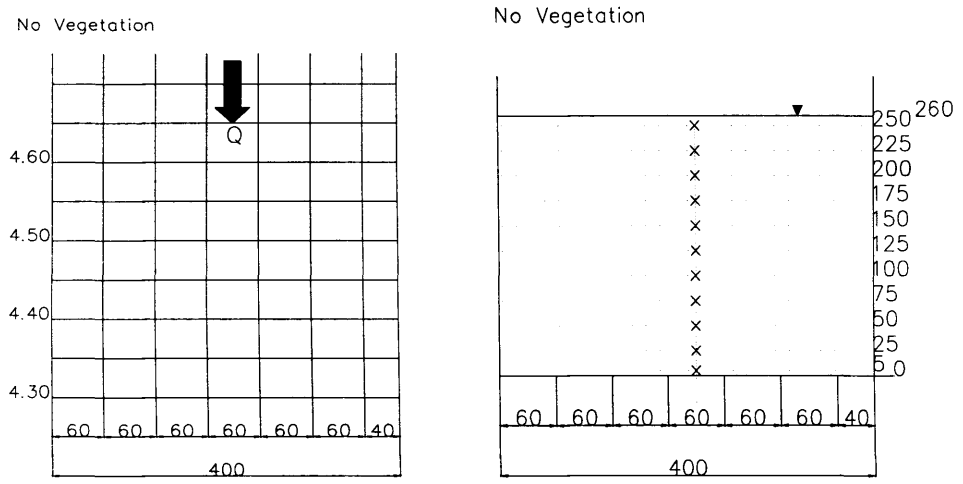

Fig. 3.10 Layout of the submerged vegetation in the simple channel showing the measuring point locations for the vertical velocity profiles in four configurations: (a) high, (b) medium, (c) low, and (d) no vegetation.

(a)

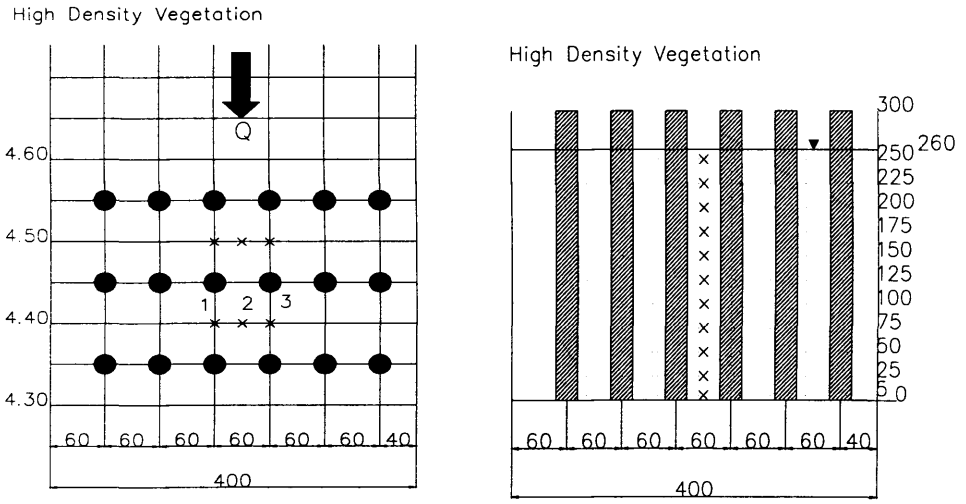

(b)

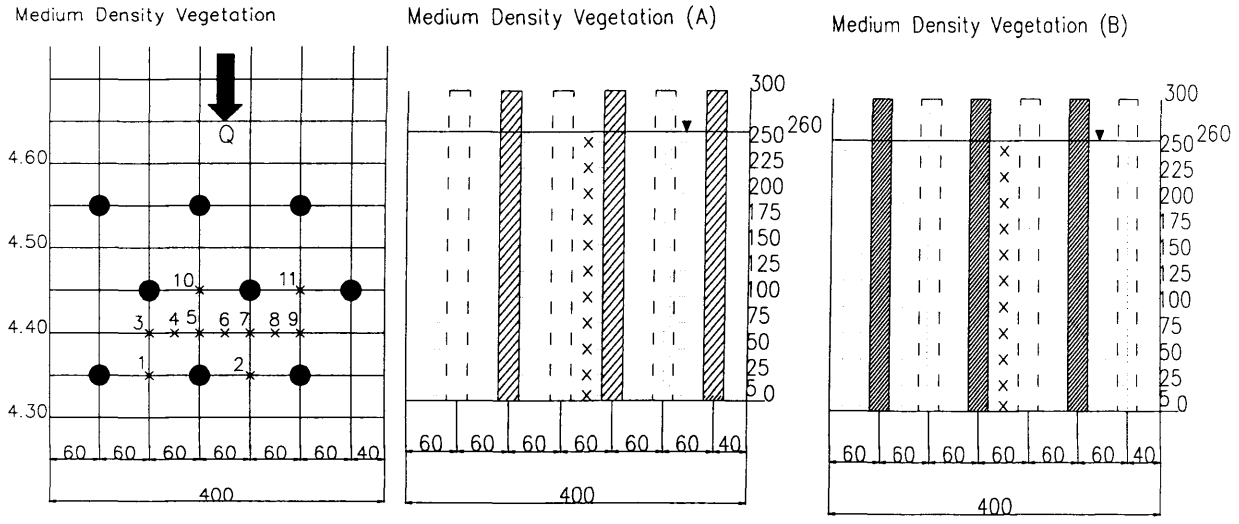

(c)

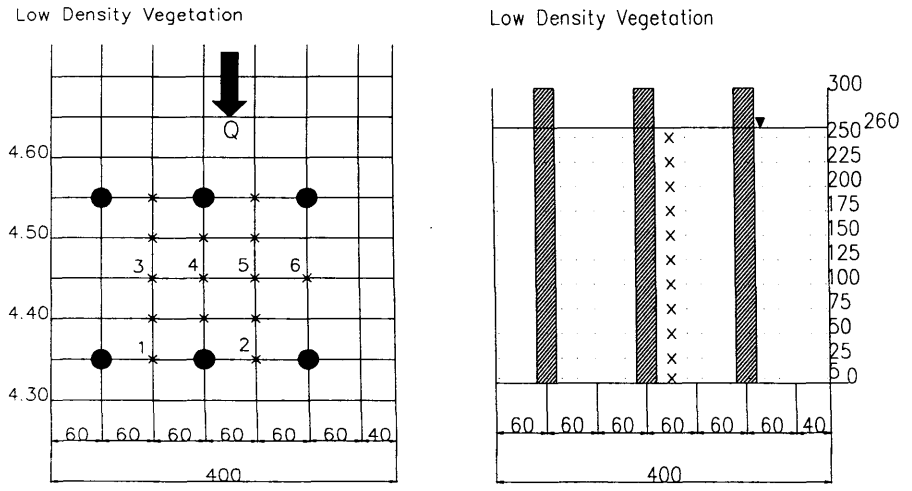

Fig. 3.11 Layout of the emergent vegetation in the simple channel showing the measuring point locations for the vertical velocity profiles in three configurations: (a) high, (b) medium, and (c) low density.

Table 3.3 Laboratory experiments of compound channel and simple narrow channel with rigid rods (diameter φ=24 mm).

No.	Rods Height	Channel Type	Density	λ	Tailgate (mm)	Q (l/s)	Flow	Depth	Channel	Rod	Rod	Data Type	
							Main ch	Floodp	Re_{mc}	$Re_{fp(y)}$	$Re_{fp(\varphi)}$	Name	No
1)	180mm	Compound Channel (Emergent)	High	0.004	290	15	250	90	1925	288	76.8	Cross Sectional	3
			Medium	0.002	"	"	250	"	1750	378	100.8	"	2
			Low	0.001	"	"	250	"	1700	396	105.6	"	1
			No Veg	--	"	"	250	"	1350	576	153.6	"	1
2)	180mm	Simple Narrow Channel (Submerged)	High	0.004	290	6.5	260	--	1625	--	150	Vertical points	6
			Medium	0.002	"	"	"	--	"	--	"	"	11
			Low	0.001	"	"	"	--	"	--	"	"	8
			No Veg	--	"	"	250	--	"	--	"	"	6
3)	300mm	Simple Narrow Channel (Emergent)	High		290	6.5	260	--	1625	--		Vertical points	3
			Medium		"	"	255	--	"	--		"	11
			Low		"	"	253	--	"	--		"	6
			No Veg		"	"	250	--	"	--		"	6

3.4.3 Wide rectangular channel

In the wide channel experiments the flume had a width of 1200 mm and a maximum depth of 300 mm height. The experiments were conducted for both emergent and submerged conditions in this flume. The rods were chosen with same diameter (i.e. 24 mm), but they were of length 180 mm for the submerged conditions and 300 mm for the emergent conditions, i.e. the same as for the narrow simple channel. The numbers and spacing between the rods were based upon the vegetation density.

For all of the experiments with different densities in the wide channel, the flow rate was kept a constant at of 15 l/s. For all of these it was observed that the variation in rod density had little effect on the water surface elevation. For uniform flow conditions the flow depth in the channel did vary somewhat, from about 275 mm to 280 mm and 290 mm for the medium and high density flow. For each density velocity measurements were undertaken at 2 cross-sections. The cross-sections were located at the midlength along the flume (i.e. 4.40 m) and near the end of the channel (i.e. 1.40 m), with the aim avoiding an analysis encountered from upstream inlet and downstream exit conditions. Lateral measurement sections commenced 60 or 90 mm from one sidewall and continued at 30 or 60 mm intervals to the other sidewall of channel. Hence measurement points were located behind or in between the rods across the channel. This meant that for the high density rods the intervals was 30 mm but for all other densities of rods the interval was 60 mm. In the vertical plane measuring distances were 50 mm from the channel bed and with 50 mm intervals towards the water surface (i.e. 50, 100, 150, 200, 250 and 275 mm). In other words the last point of measurement was 2 mm under the water surface. Other characteristics remained the same as for both the compound and narrow simple channels.

For both the emergent and submerged conditions, the experiments were performed with full vegetation, partial vegetation along half of the flume (one side) and then partial vegetation along the sides (half of the flume) for the different densities (i.e. high, medium and low). Figs. 3.12, 3.13 and 3.14 show the setup configurations for the experiments in a wide channel, together with the location of the measuring points.

(a)

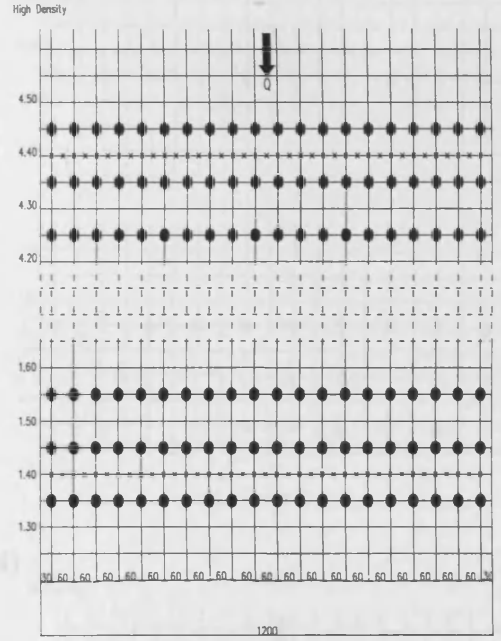

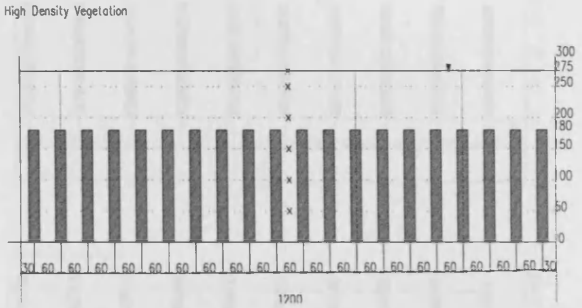

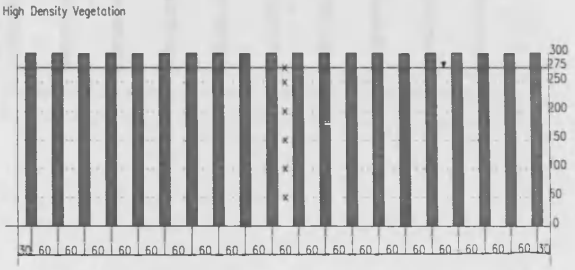

(b)

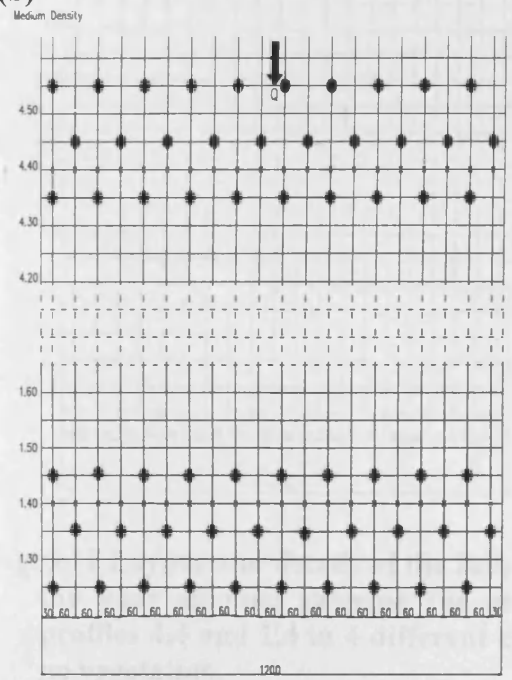

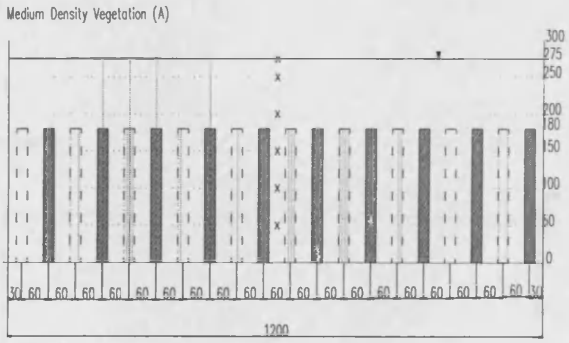

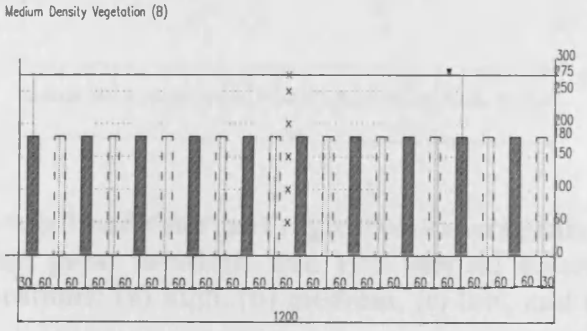

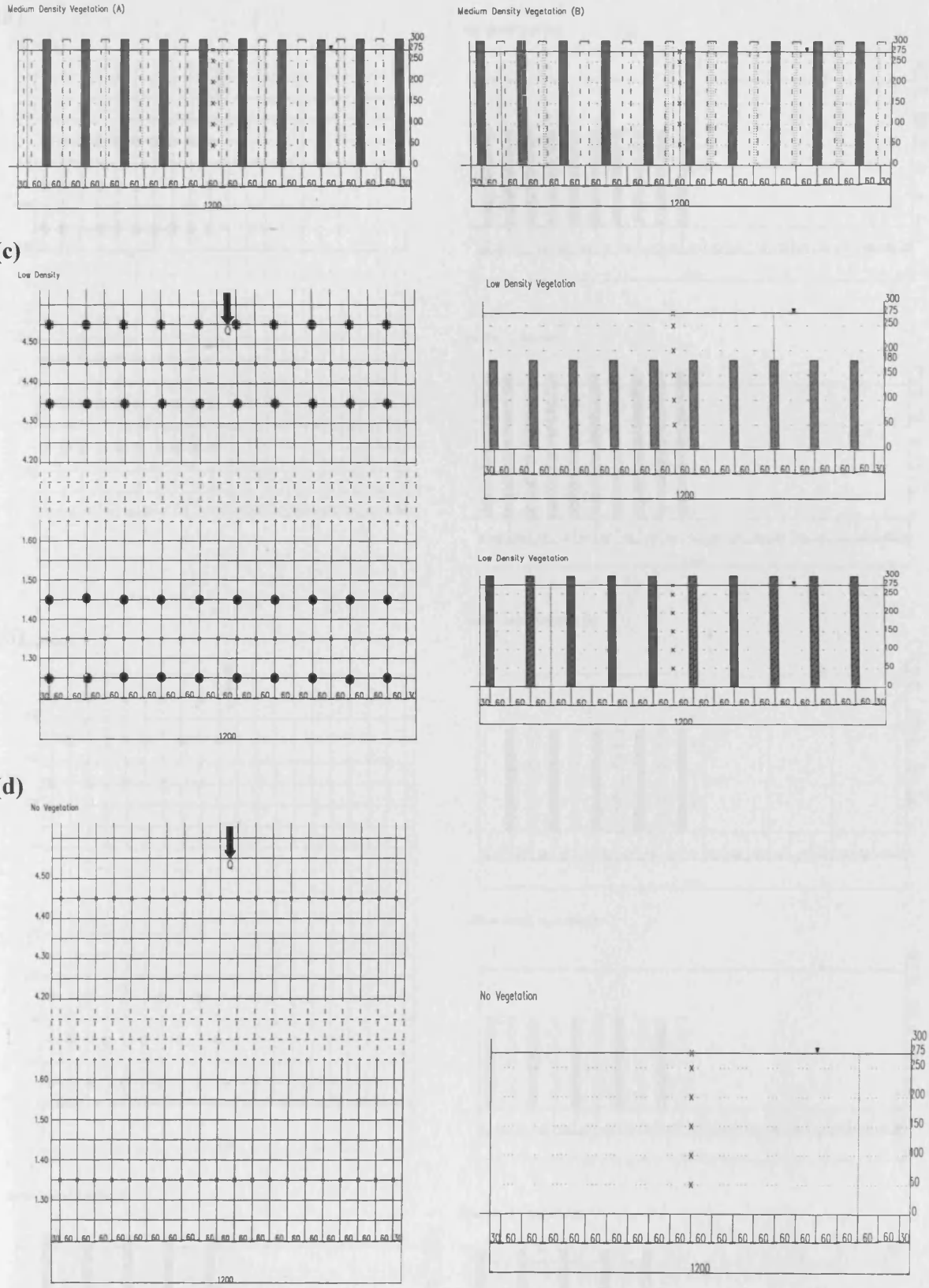

Fig. 3.12 Layout and details of the fully submerged and emergent vegetation experiments in the wide channel showing the measuring point locations and two vertical velocity profiles 4.4 and 1.4 in 4 different configurations: (a) high, (b) medium, (c) low, and (d) no vegetation.

(a)

High Density

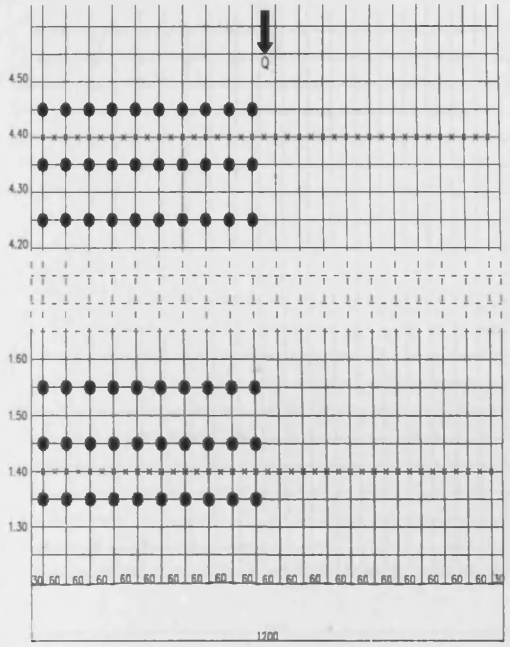

High Density Vegetation

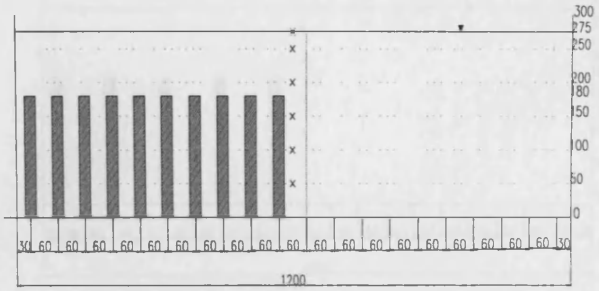

High Density Vegetation

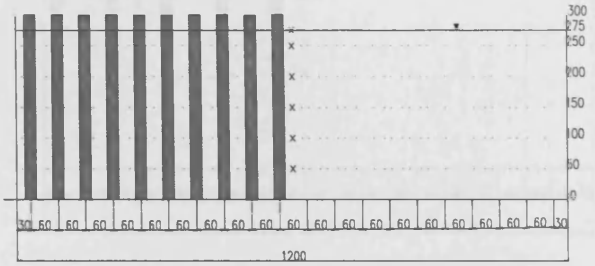

(b) Medium Density

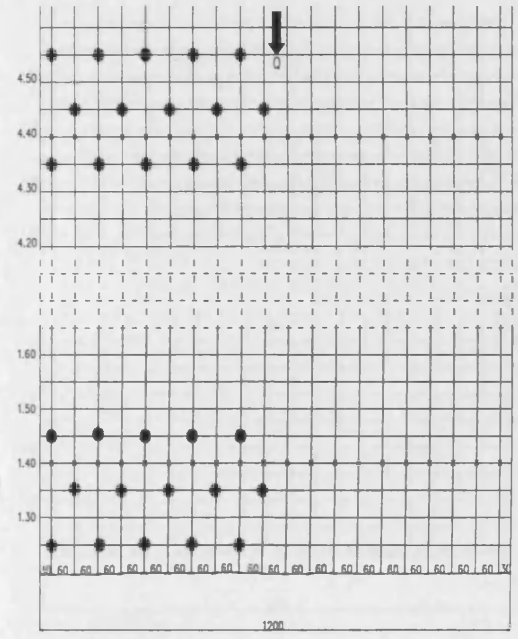

Medium Density Vegetation (A)

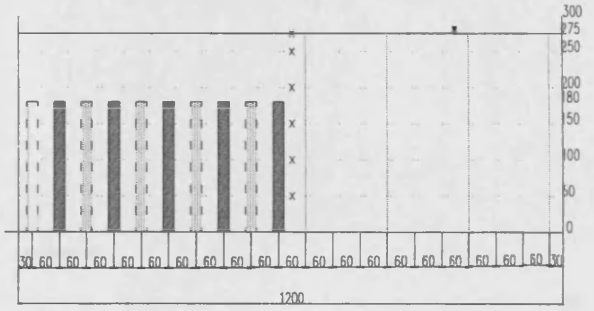

Medium Density Vegetation (B)

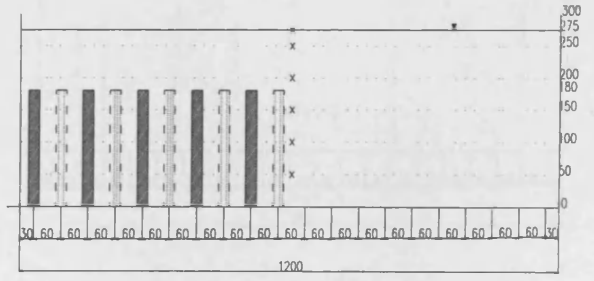

Medium Density Vegetation (A)

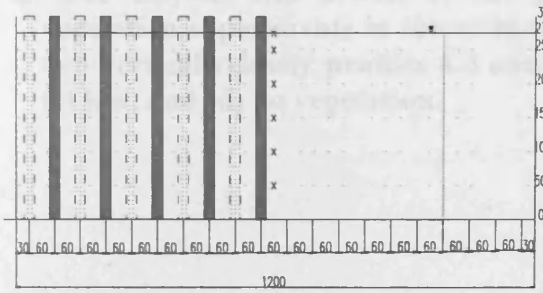

Medium Density Vegetation (B)

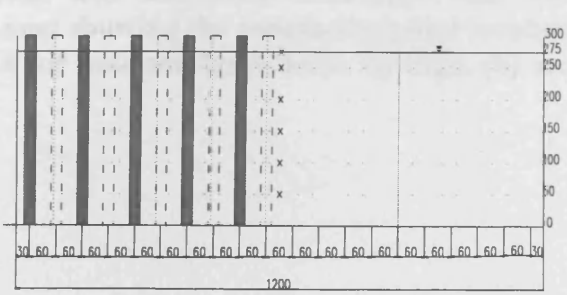

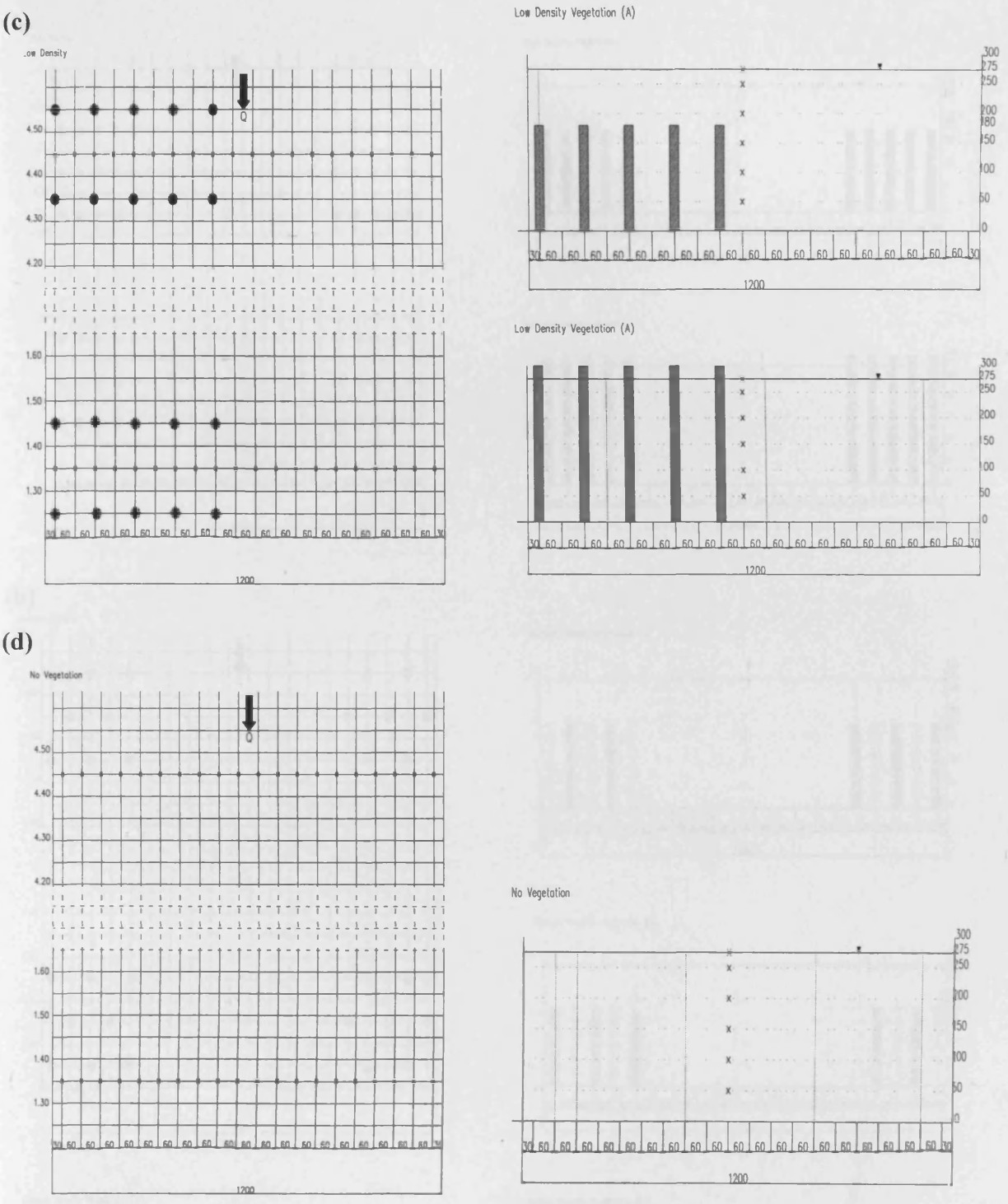

Fig. 3.13 Layout and details of the partial half one-sided submerged and emergent vegetation experiments in the wide channel showing the measuring point locations and two vertical velocity profiles 4.4 and 1.4 for four configurations: (a) high, (b) medium, (c) low, and (d) no vegetation.

(a)

High Density

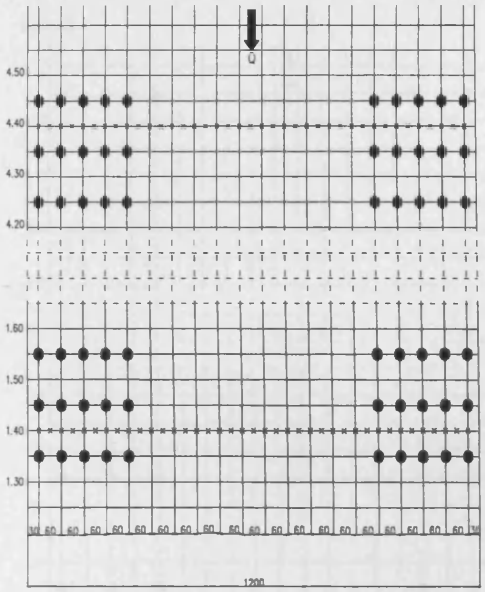

High Density Vegetation

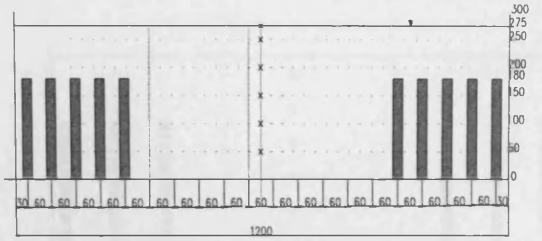

High Density Vegetation

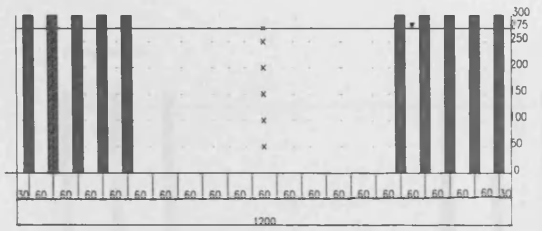

(b)

Medium Density

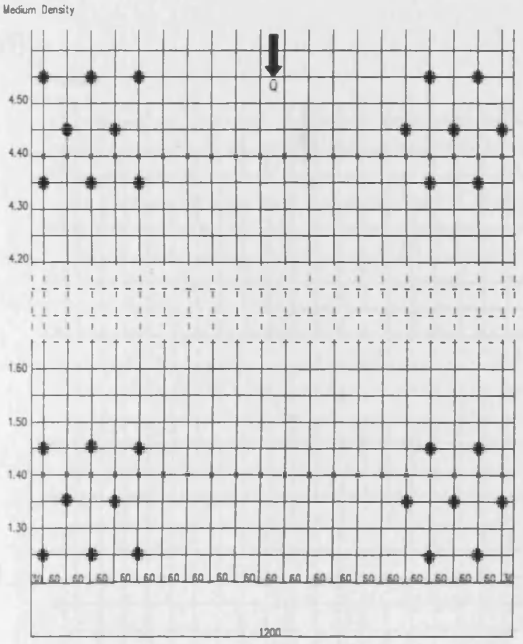

Medium Density Vegetation (A)

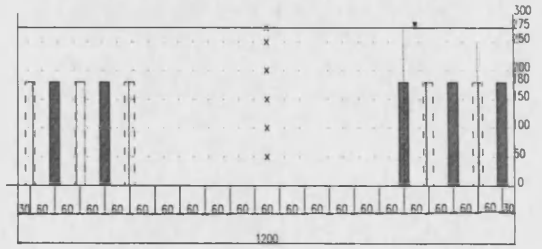

Medium Density Vegetation (B)

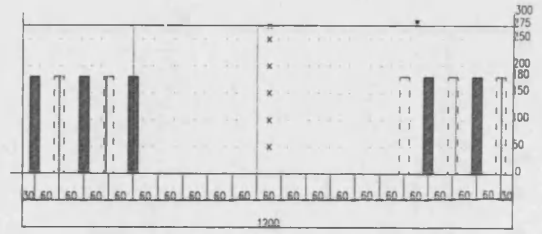

Medium Density Vegetation (A)

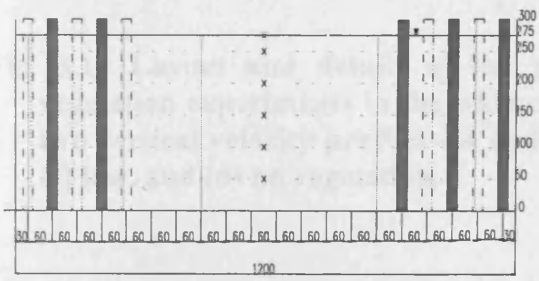

Medium Density Vegetation (B)

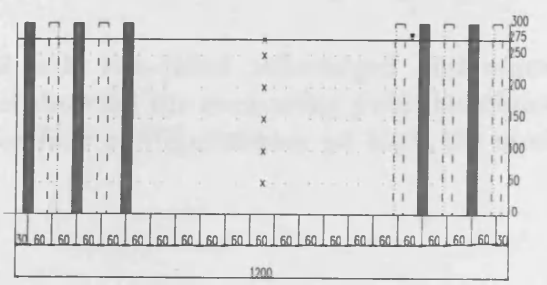

(c)

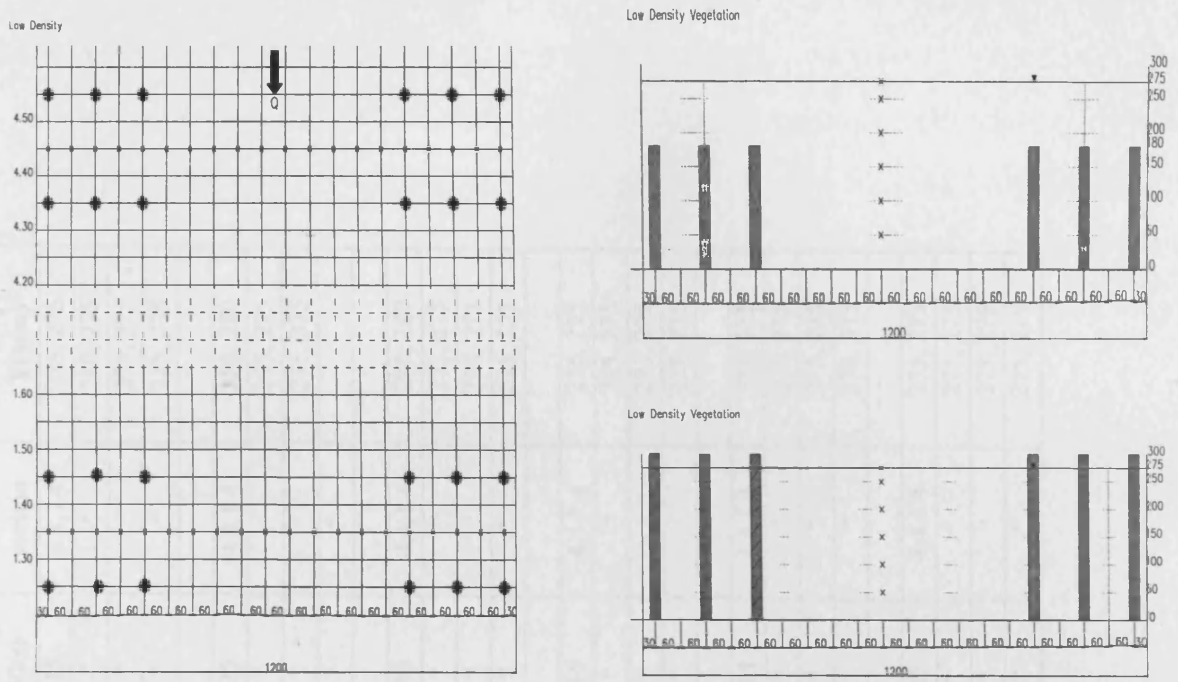

(d)

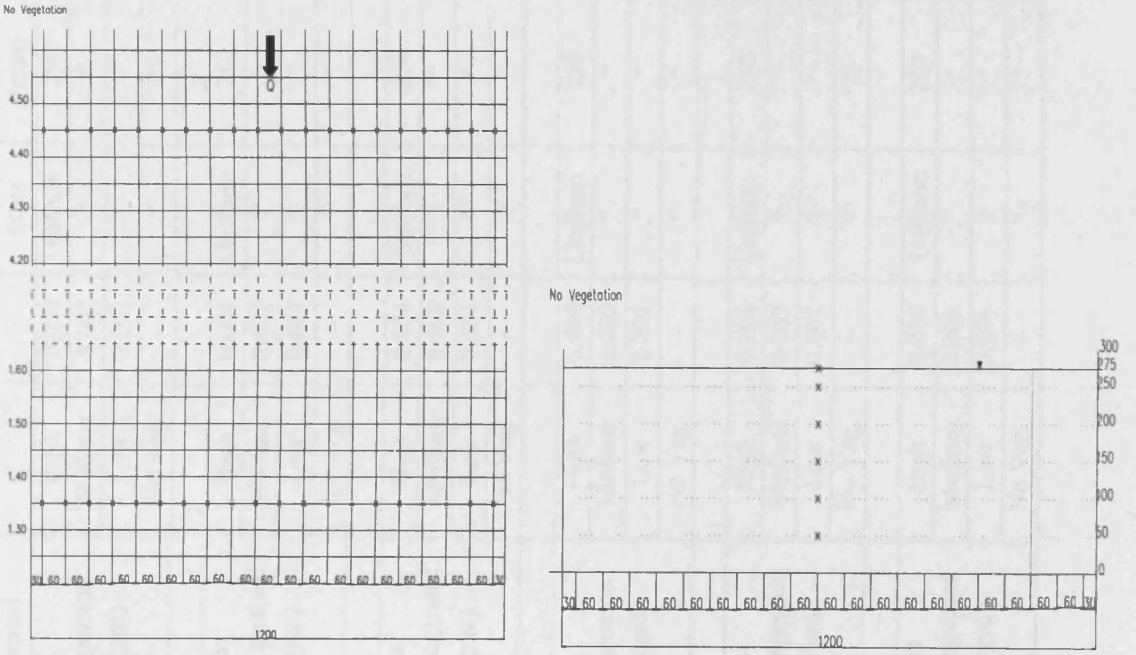

Fig. 3.14 Layout and details of the partial half two-sided submerged and emergent vegetation experiments in the wide channel showing the measuring point locations and two vertical velocity profiles 4.4 and 1.4 for four configurations: (a) high, (b) medium, (c) low, and (d) no vegetation.

Table 3.4 Wide channel experiments with rigid rods (diameter φ=24 mm).

No.	Rods Height	Situation of Rods in the Channel	Density	λ	Flow State	Tailgate (mm)	Discharge Q(l/s)	Cross-section	Flow Depth Y(mm)
1)	300mm	Fully Vegetation (Emergent)	High	0.004	Uniform	250	15	4.4,1.4	285, 275
			Medium	0.002	"	"	"	"	280, 275
			Low	0.001	"	"	"	"	275, 275
			No Veg.	--	"	"	"	"	275, 275
2)		1side Partially Vegetated (Emergent)	High	0.004	Uniform	250	15	4.4,1.4	280, 280
			Medium	0.002	"	"	"	"	275, 275
			Low	0.001	"	"	"	"	275, 275
			No Veg.	--	"	"	"	"	
3)		2sides Partially Vegetated (Emergent)	High	0.004	Uniform	250	15	4.4,1.4	280, 280
			Medium	0.002	"	"	"	"	275, 275
			Low	0.001	"	"	"	"	275, 275
			No Veg.	--	"	"	"	"	275, 275
4)	180mm	Fully Vegetation (Submerged)	High	0.004	Uniform	250	15	4.4,1.4	275, 275
			Medium	0.002	"	"	"	"	275, 275
			Low	0.001	"	"	"	"	275, 275
			No Veg.	--	"	"	"	"	275, 275
5)		1side Partially Vegetated (Submerged)	High	0.004	Uniform	250	15	4.4,1.4	275, 275
			Medium	0.002	"	"	"	"	275, 275
			Low	0.001	"	"	"	"	275, 275
			No Veg.	--	"	"	"	"	275, 275
6)		2sides Partially Vegetated (Submerged)	High	0.004	Uniform	250	15	4.4,1.4	275, 275
			Medium	0.002	"	"	"	"	275, 275
			Low	0.001	"	"	"	"	275, 275
			No Veg.	--	"	"	"	"	275, 275

3.5 Terminology definition

For each measurement point the ADV measured the instantaneous velocities u_i, v_i, w_i in the longitudinal, transverse and vertical directions respectively, for a sampling period of 3 minutes and a sampling frequency of 25 Hz. This meant that a total number of 4500 measurements were made. Three measurements were carried out for the compound, simple narrow and wide rectangular channel. This section is divided into several parts:

- Definition of the time-averaged velocity, velocity fluctuation, and Reynolds stress.
- Results of the time-averaged velocities ($\overline{U}$, $\overline{V}$, $\overline{W}$).
- Results of the time-averaged *rms* velocity fluctuations ($u'rms$, $v'rms$ $w'rms$) and the absolute value of the velocity fluctuations $ABS(u')$, $ABS(v')$, $ABS(w')$.
- Results of the turbulence Reynolds stresses ($\overline{u'v'}$, $\overline{u'w'}$, $\overline{v'w'}$), obtained from the time-averaged instantaneous velocity fluctuations
- Results of depth-averaged component of velocities, velocity fluctuations and Reynolds stresses for all cross-sections in the compound channel.

From laboratory data measurements with changes in the density of vegetation on floodplain were observed to give variations in the velocity profiles. This proved that the vegetation significantly affected the velocity profile and the turbulence in the main channel and on the floodplain. In the next chapter the research results are analysed and discussed.

3.5.1 Definition of time-averaged velocities

The resulting data was processed to give a time-averaged value of each velocity component. These values are defined as:

$$U_{bar} = \sum \frac{u_i}{n} \quad ; \qquad V_{bar} = \sum \frac{v_i}{n} \quad ; \qquad W_{bar} = \sum \frac{w_i}{n} \quad (3.2)$$

where n is the number of measures of the instantaneous velocity (more than 4500).

3.5.2 Velocity fluctuations

The instantaneous velocity fluctuations (i.e. u'_i, v'_i, w'_i) from the time-averaged velocity components are defined as:

$$u'_i = U_{bar} - u_i \qquad (3.3)$$

$$v'_i = V_{bar} - v_i \qquad (3.4)$$

$$w'_i = W_{bar} - w_i \qquad (3.5)$$

The root mean square (*rms*) value over the sampling period was also evaluated to give the time-averaged *rms* value for each component defined as:

$$u'_{rms} = \sqrt{\frac{\sum (U_{bar} - u_i)^2}{n}} \qquad (3.6)$$

$$v'_{rms} = \sqrt{\frac{\sum (V_{bar} - v_i)^2}{n}} \qquad (3.7)$$

$$w'_{rms} = \sqrt{\frac{\sum (W_{bar} - w_i)^2}{n}} \qquad (3.8)$$

Also the absolute values of the instantaneous velocity fluctuations were calculated for each component as defined by:

$$ABS(u') = \frac{\sum |Ubar - u_i|}{n} \tag{3.9}$$

$$ABS(v') = \frac{\sum |Vbar - v_i|}{n} \tag{3.10}$$

$$ABS(w') = \frac{\sum |Wbar - w_i|}{n} \tag{3.11}$$

Herein for the compound channel the values considered were $u'rms$, $v'rms$ $w'rms$ and for the simple channel the values $ABS(u')$, $ABS(v')$, $ABS(w')$ were considered.

3.5.3 Reynolds stress

In laminar flows the stress is referred to as the shear stress. In turbulent flows there is an additional turbulent stress on all planes. The Reynolds stress, in m^2s^2, is defined as the time-averaged instantaneous velocity fluctuation in one direction multiplied by the coincident instantaneous velocity fluctuation in another direction:

$$\overline{u'v'} = \frac{\sum u'_i \times v'_i}{n} \tag{3.12}$$

$$\overline{u'w'} = \frac{\sum u'_i \times w'_i}{n} \tag{3.13}$$

$$\overline{v'w'} = \frac{\sum v'_i \times w'_i}{n} \tag{3.14}$$

Also, the turbulent intensity is defined as the absolute time-averaged instantaneous velocity fluctuation in one direction, multiplied by the absolute coincident instantaneous velocity fluctuation in another direction giving:

$$\overline{u'v'} = \frac{\sum[ABS(u_i')]\times[ABS(v_i')]}{n} \tag{3.15}$$

$$\overline{u'w'} = \frac{\sum[ABS(u_i')]\times[ABS(w_i']}{n} \tag{3.16}$$

$$\overline{v'w'} = \frac{\sum[ABS(v_i')]\times[ABS(w_i']}{n} \tag{3.17}$$

For the compound channel, simple channel, and wide channel the instantaneous velocity fluctuation components (i.e, u'_i, v'_i, w'_i) were evaluated to determine the Reynolds stress components (i.e, $\overline{u'v'}$, $\overline{u'w'}$, $\overline{v'w'}$).

An indication of the turbulence characteristics can be given by the standard deviation of the instantaneous Reynolds stress value, over the sampling period, for each Reynolds stress plane. It is significant that the Reynolds stresses for all three planes are shown to be considerably higher for the test with vegetation. The turbulence characteristics play an important role in the experiments reported herein and the interaction of the vegetation and the turbulence has been analysed in some detail.

In this chapter, experimental setups for various configurations have been established to investigate the velocity and turbulence characteristics of the flow through rigid vegetation in a compound channel, a narrow simple channel, and a wide rectangular channel. Experiments were conducted for: fully emergent vegetation conditions on the floodplain in the compound channel, and fully and partially emergent and submerged vegetation conditions in both the narrow simple and the wide rectangular channel configurations. For the compound and wide rectangular channel experiments, the velocity was measured across the entire

channel cross-section, whereas for the narrow simple channel the measurements were carried out at several locations only within the vegetation array. Finally, empirical formulations have been used to calculate the velocity, velocity fluctuations, and Reynolds stress parameters for various vegetation densities.

CHAPTER 4
COMPOUND CHANNEL

4.1 Introduction

In compound open-channel flows the interaction between the main channel and floodplain is relatively complex. Hence, when there is vegetation along the floodplain then the reduced mean velocity in the floodplain enhances the difference in the mean velocities at the interface between the main channel and floodplain, thereby tending to increase the main channel velocity. In general, as the vegetation density on the floodplain increases the magnitude of secondary currents in the main channel increases, and the point of maximum streamwise velocity moves laterally. Also, the resistance at the interface is known to be further increased, in comparison with the case for non-vegetated floodplains (Shimizu and Tsujimoto, 1993). An analysis of both the velocity and the turbulence at the interface between the main channel and the floodplain provides valuable information about the effects of various vegetation configurations in compound channel flows.

In this chapter, the results of compound open-channel flows with vegetated floodplains are investigated and results of the velocity and turbulent structures are discussed. The laboratory experiments with vegetation along the floodplain primarily involved taking detailed measurements of the velocity distributions across the flow section at two cross-sections located at 4.40 m and 4.50 m from the downstream weir for various vegetation densities. The impacts of vegetation density on the mean flow and the turbulent structures have also been investigated.

For these measurements the vegetation rods were located at intervals of 60 mm along the floodplains. The positions of the measurement electrodes in between the rows of rods were located at 25 mm intervals (instead of 30 mm) which unfortunately did not enable the minimum and maximum velocities to be measured directly behind and in between the rods respectively. However, since the measurements obtained were with respect to the flow in the main channel, and disregarding the exact minimum and maximum points, the results still enabled general comparisons and evaluations to be made successfully.

The results for the compound channel are reported and discussed below. Figs. 4.1 to 4.6 show the time averaged velocities $\overline{U}$, $\overline{V}$ *and* $\overline{W}$, and Figs. 4.7 to 4.12 show the Reynolds stresses $\overline{u'v'}$, $\overline{v'w'}$ *and* $\overline{u'w'}$ for all of the densities respectively.

4.2 Time-averaged velocities ($\overline{U}$, $\overline{V}$ and $\overline{W}$)

The laboratory results show the effects of the vegetation density along the floodplain on the velocity distributions in all three directions. More importantly, the complexity of the velocity distribution along the interface is evaluated herein. Although in changing the high vegetation density to the medium vegetation density state on the floodplain, i.e. the vegetation density is halved, the corresponding change in the water velocity profile is small and almost negligible. This indicates that the vegetation has introduced a staggered state, which considerably dominates variations in the velocity profile. Therefore, for such a case a decrease in the vegetation density does not necessarily imply any considerable change in the velocity profile. A similar effect may be observed for the case where the change is from low density to no vegetation state.

4.2.1 Time-averaged longitudinal component of velocity ($\overline{U}$)

As the vegetation density increases the difference in the time-averaged longitudinal velocity ($\overline{U}$) along the floodplain and the main channel increase (see Figs. 4.1a-d and 4.2a-d). This means that the longitudinal velocity in the main channel region is considerably larger than that along the floodplain region, with the degree of the non-uniformity in the velocity between the main channel and the floodplain clearly illustrated in these figures. The greatest cross-sectional variation in the longitudinal velocity is observed for the highest vegetation density as shown in Figs. 4.1a and 4.2a. The maximum longitudinal velocity core is located near the bottom of the main channel for all configurations, while the lowest velocities are located close to the bank at the edge of floodplain and immediately downstream of the rods. The velocity distribution for the non-vegetated floodplain conditions is shown in Figs. 4.1d and 4.2d.

For normal open channel flows, in general the maximum longitudinal velocity is located in the region near the water surface. From Figs. 4.1 and 4.2 it is clearly observed that, in contrast to normal circumstances, the maximum longitudinal velocity is measured and found to occur near the bottom of the main channel. This is mainly due to the existence of the rods on the floodplain and the creation of vortex shedding and turbulence by the vegetation. The corresponding transfer of momentum towards the main channel avoids the maximum longitudinal velocity core to occur at the top of main channel (i.e. near water surface). Hence, the maximum longitudinal velocity forms near the bottom of the main channel. For the no vegetation configuration, the maximum velocity region is located near the water surface for the main channel and the floodplain. For the effects at the edge of the contact point between main channel and floodplain the maximum velocity region is separated between both reaches. This interesting effect of vortex shedding and

oscillations, introduced by vegetation in the channels, will be discussed in more detail Chapter 7.

For all cross sections, there are zones of equal velocity. In the main channel the longitudinal velocity component follows a horizontal structure where there is a degree of uniformity in the horizontal direction. However, in the floodplain the existence of the rods ensures that the velocity follows a vertical structure where uniformity is primarily in the vertical direction. For the non-vegetated condition there is a degree of uniformity horizontally both along the floodplain and the main channel as can be seen in Figs. 4.1a-d and 4.2a-d.

For the range of vegetation densities examined it can be seen that, as the vegetation density increases, then the degree of flow uniformity across the floodplain increases, leading to a corresponding decrease in the main channel. For the non-vegetated case the values of the longitudinal velocity in the main channel and over the floodplain region are comparable (see Figs. 4.1d and 4.2d). However, an interesting pattern of the flow is observed in the interface between the floodplain and main channel. As can be seen in Figs. 4.1a and 4.2a for the case of high density vegetation, a severe non-uniformity in the velocity distribution is pronounced.

(a)

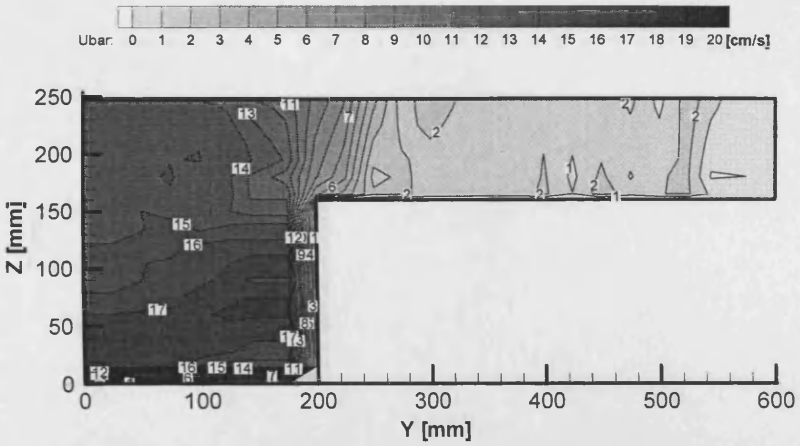

(b)

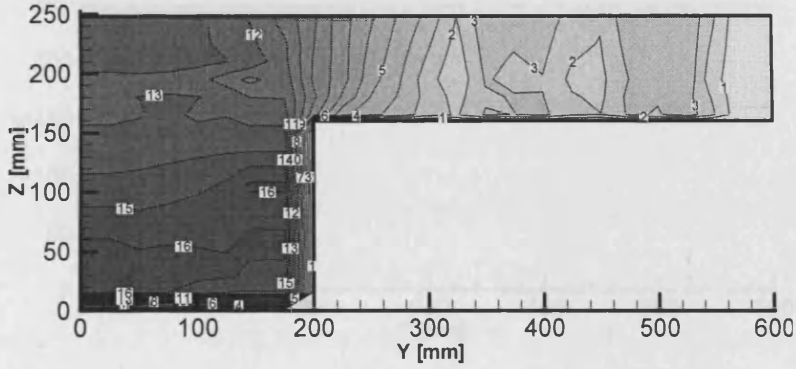

(c)

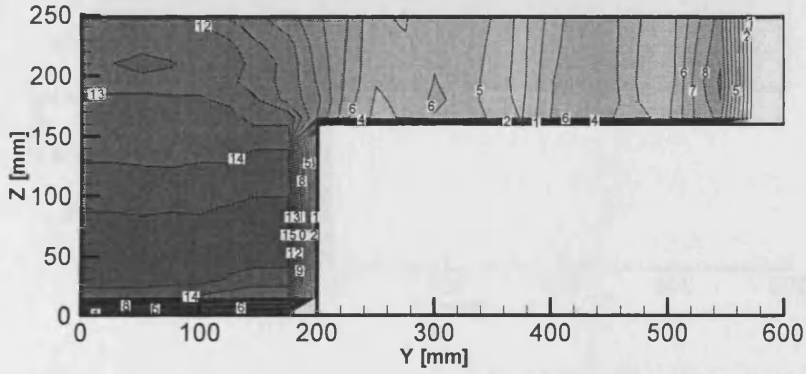

(d)

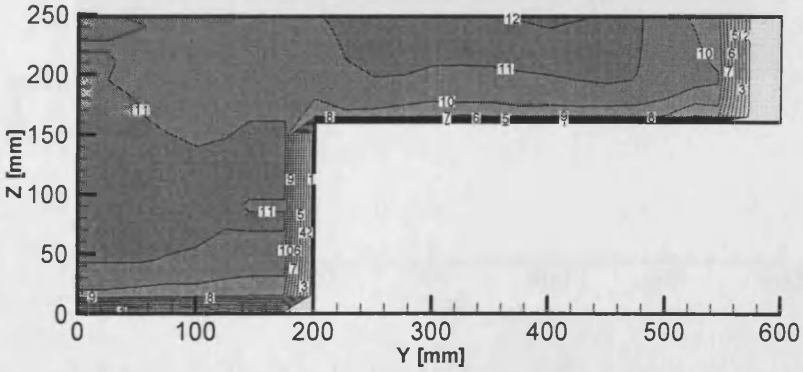

Fig. 4.1 Time-averaged longitudinal velocity ($\overline{U}$) [cms^{-1}] at cross-section 4.4 and for four configurations: (a) high, (b) medium, (c) low, and (d) no vegetation.

(a)

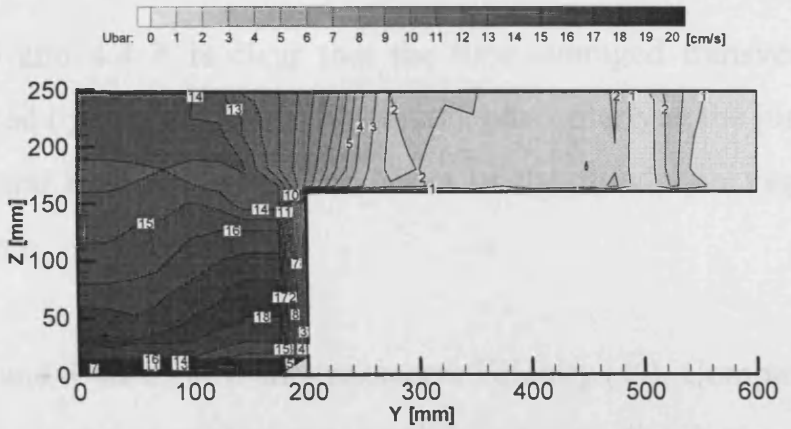

(b)

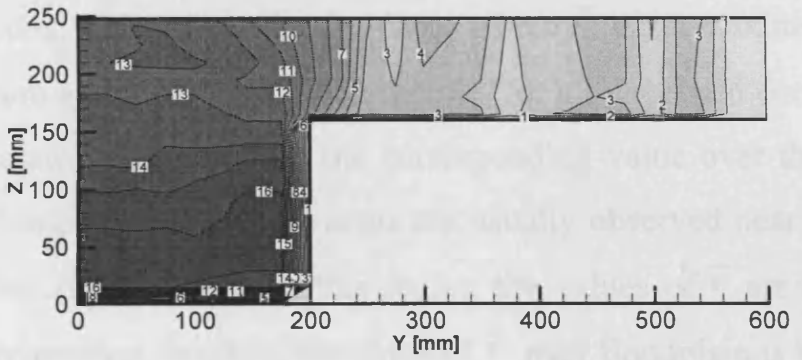

(c)

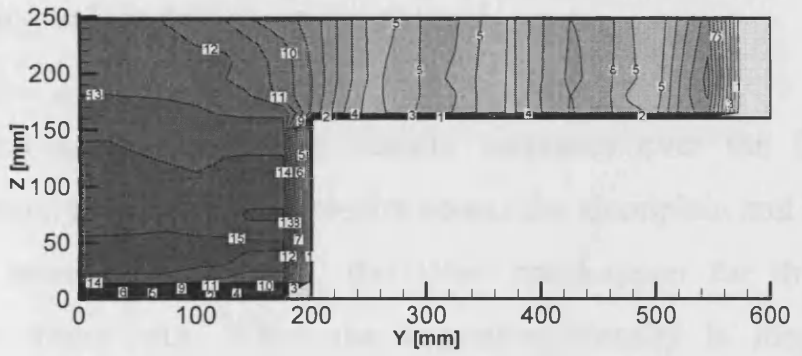

(d)

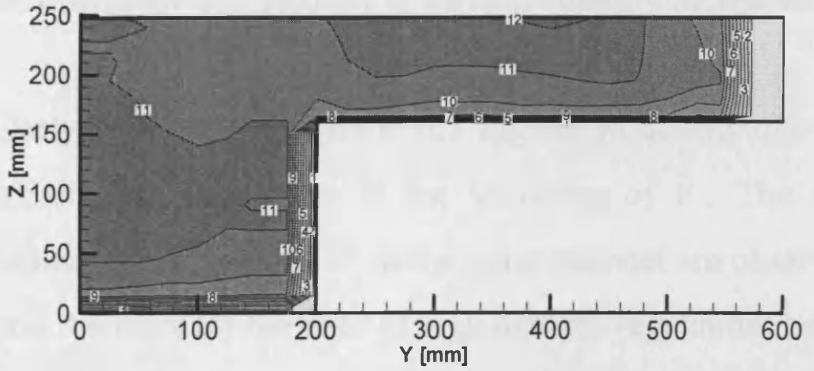

Fig. 4.2 Time-averaged longitudinal velocity ($\overline{U}$) [cms^{-1}] at cross-section 4.5 and for four configurations: (a) high, (b) medium, (c) low, and (d) no vegetation.

4.2.2 Time-averaged transverse component of velocity ($\overline{V}$)

From Figs. 4.3 and 4.4 it is clear that the time-averaged transverse velocity is greatly influenced by the floodplain vegetation, particularly at the junction between the floodplain and main channel. The effect of the floodplain vegetation is less marked elsewhere.

Figures 4.3a-d and 4.4a-d show the transverse velocity ($\overline{V}$). Comparing the results of $\overline{V}$ and $\overline{U}$, it can be seen that they exhibit velocity distributions which are in opposite directions. This means that in places where $\overline{U}$ has a maximum value then $\overline{V}$ has a minimum and vice versa. For example, for all vegetated configurations $\overline{U}$ in the main channel is higher than the corresponding value over the floodplains, since the high longitudinal velocity areas are usually observed near the bottom of the main channel. In contrast, for this region the values of $\overline{V}$ are minimum. As before, for all vegetation densities the value of $\overline{V}$ over floodplain is higher than for the corresponding values over the main channel.

This means that as the vegetation density increases over the floodplain, the difference between the transverse velocity across the floodplain and that across the main channel increases. However, this does not happen for the longitudinal velocity at the same rate. When the vegetation density is increased on the floodplain, then the transverse velocity is correspondingly increased.

Also, and similarly for $\overline{U}$, an increase in the vegetation density over the floodplain leads to an increase in the range in the variation of $\overline{V}$. The maximum and minimum variations in the velocity $\overline{V}$ in the main channel are observed as follows: between -1.4 and 0.6 cm/s for the case of high density vegetation, between -1.3 and 0.3 cm/s for medium density, between -1.1 and 0.2 cm/s for low density, and between -0.8 and 0 cm/s for no vegetation.

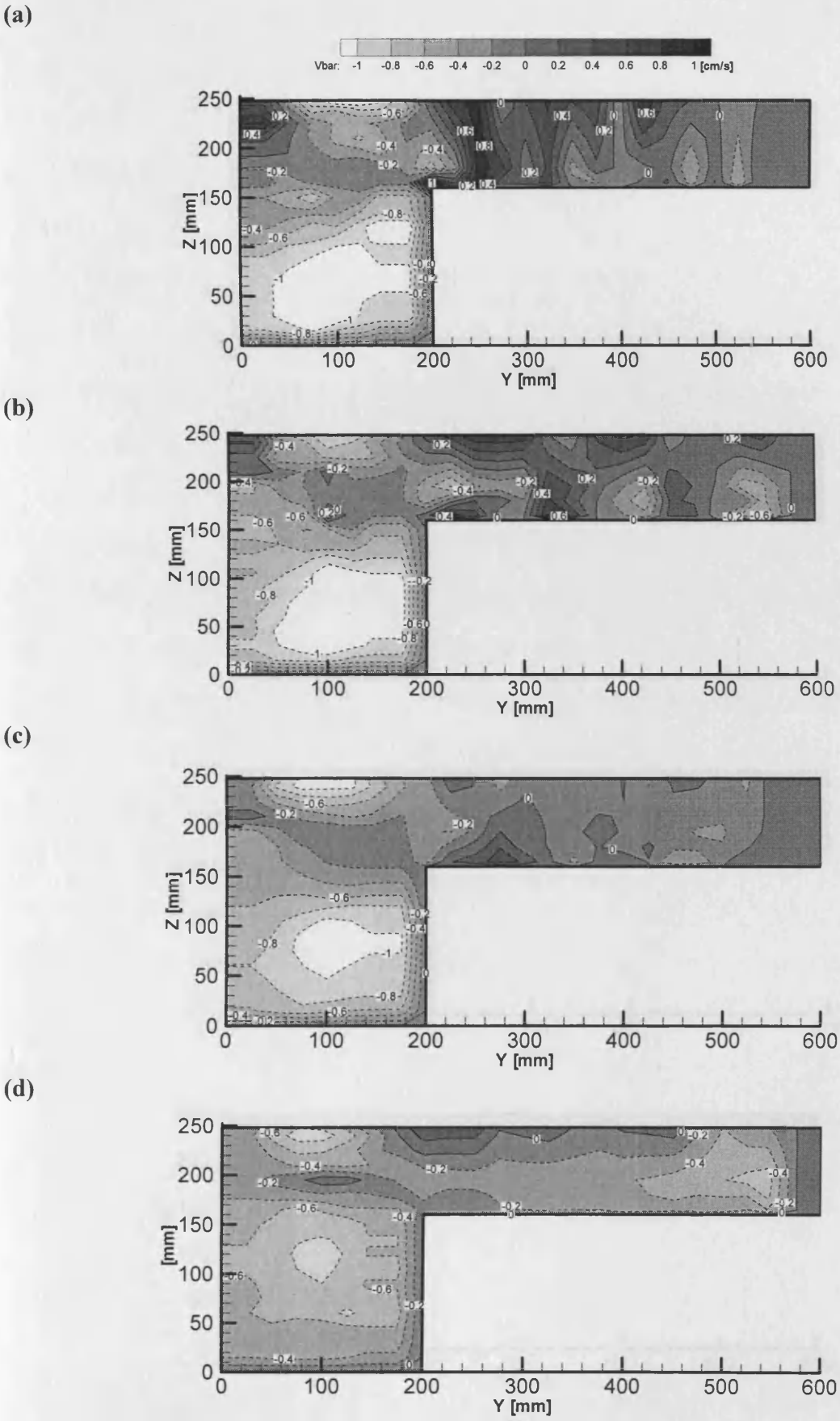

Fig. 4.3 Time-averaged transverse velocity ($\overline{V}$) [cms^{-1}] at cross-section 4.4 and for four configurations: (a) high, (b) medium, (c) low, and (d) no vegetation.

(a)

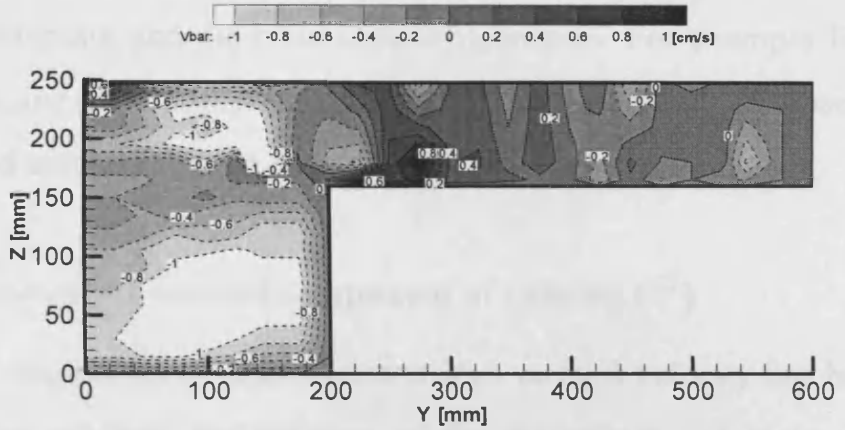

(b)

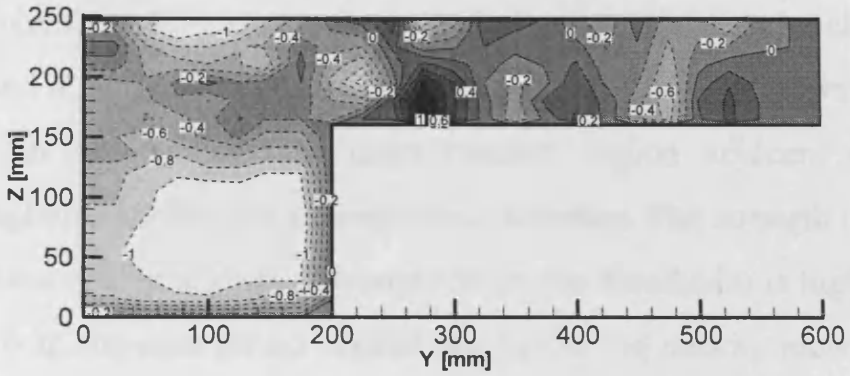

(c)

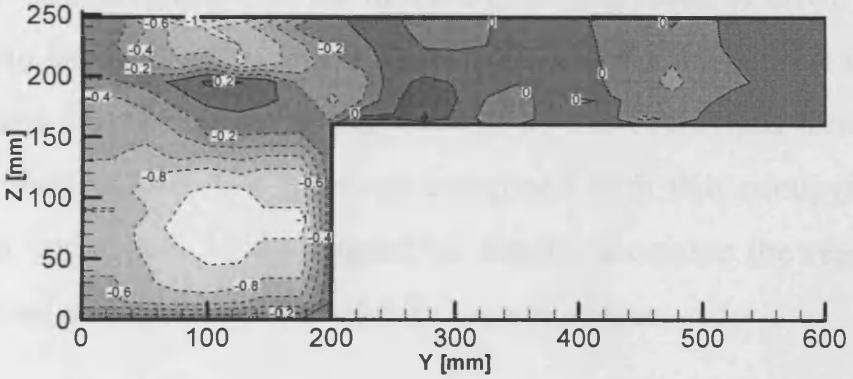

(d)

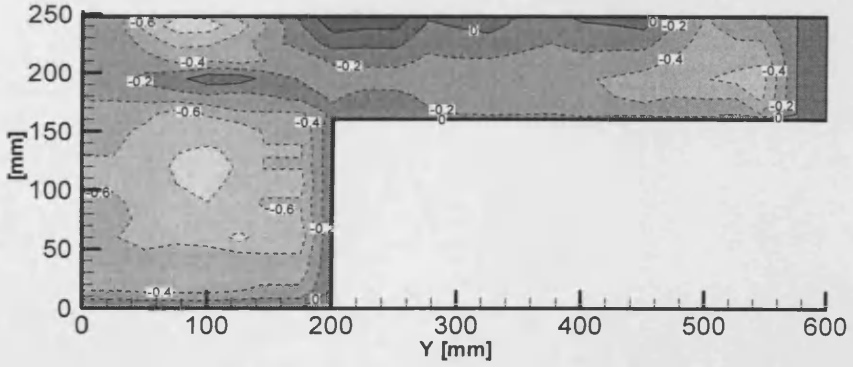

Fig. 4.4 Time-averaged transverse velocity ($\overline{V}$) [cms^{-1}] at cross-section 4.5 and for four configurations: (a) high, (b) medium, (c) low, and (d) no vegetation.

However, as the vegetation density decreases the uniformity between the velocity across the floodplain and the main channel increases. For example for the case of no vegetation, the maximum homogeneity and uniformity can be observed over the floodplain and across the main channel.

4.2.3 Time-averaged vertical component of velocity ($\overline{W}$)

The effect of vegetation on the time-averaged vertical velocity has been shown to be very prominent near the junction of the floodplain and main channel. This introduces a circular cell structure in the turbulence, which can be clearly viewed in Figs. 4.5 and 4.6. As observed in Figs. 4.5a-d and 4.6a-d, an upward transfer of momentum can be seen in the main channel region adjacent to the main channel/floodplain interface for all vegetation densities. The strength of the upward momentum transfer is marginally stronger when the floodplain is highly vegetated as compared with the case for no vegetation. As the rod density increases over the floodplain then the magnitude in the upward trend increases. A downward trend in momentum can be observed along the main channel centre line for all vegetation densities. When the floodplain is vegetated then the downward trend occupies a greater proportion of the flow depth as compared with that occupying when the channel is not vegetated. As the vegetation density increases the region occupied by the maximum downward-trend velocity core increases.

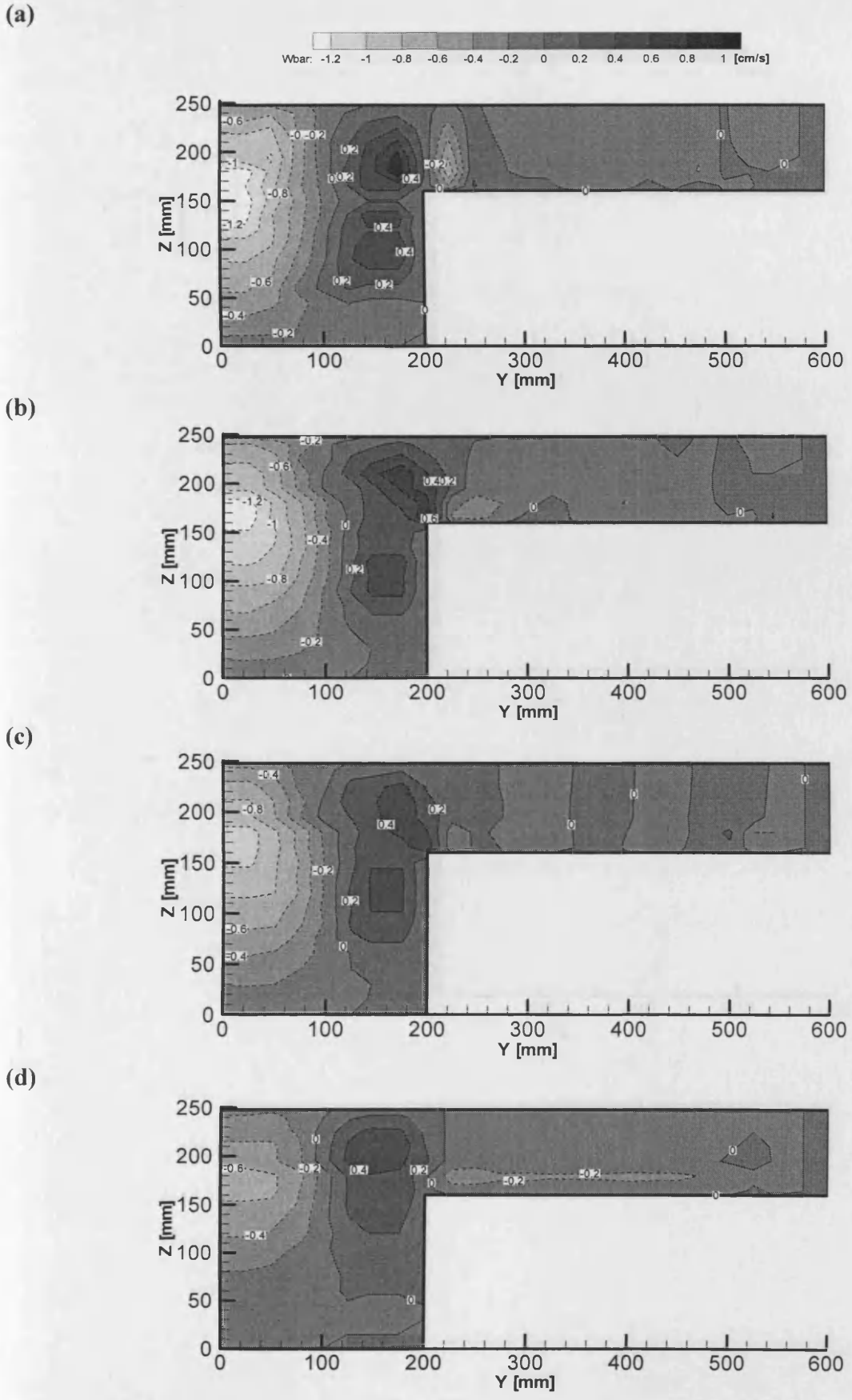

Fig. 4.5 Time-averaged vertical velocity ($\overline{W}$) [cms^{-1}] at cross-section 4.4 and for four configurations: (a) high, (b) medium, (c) low, and (d) no vegetation.

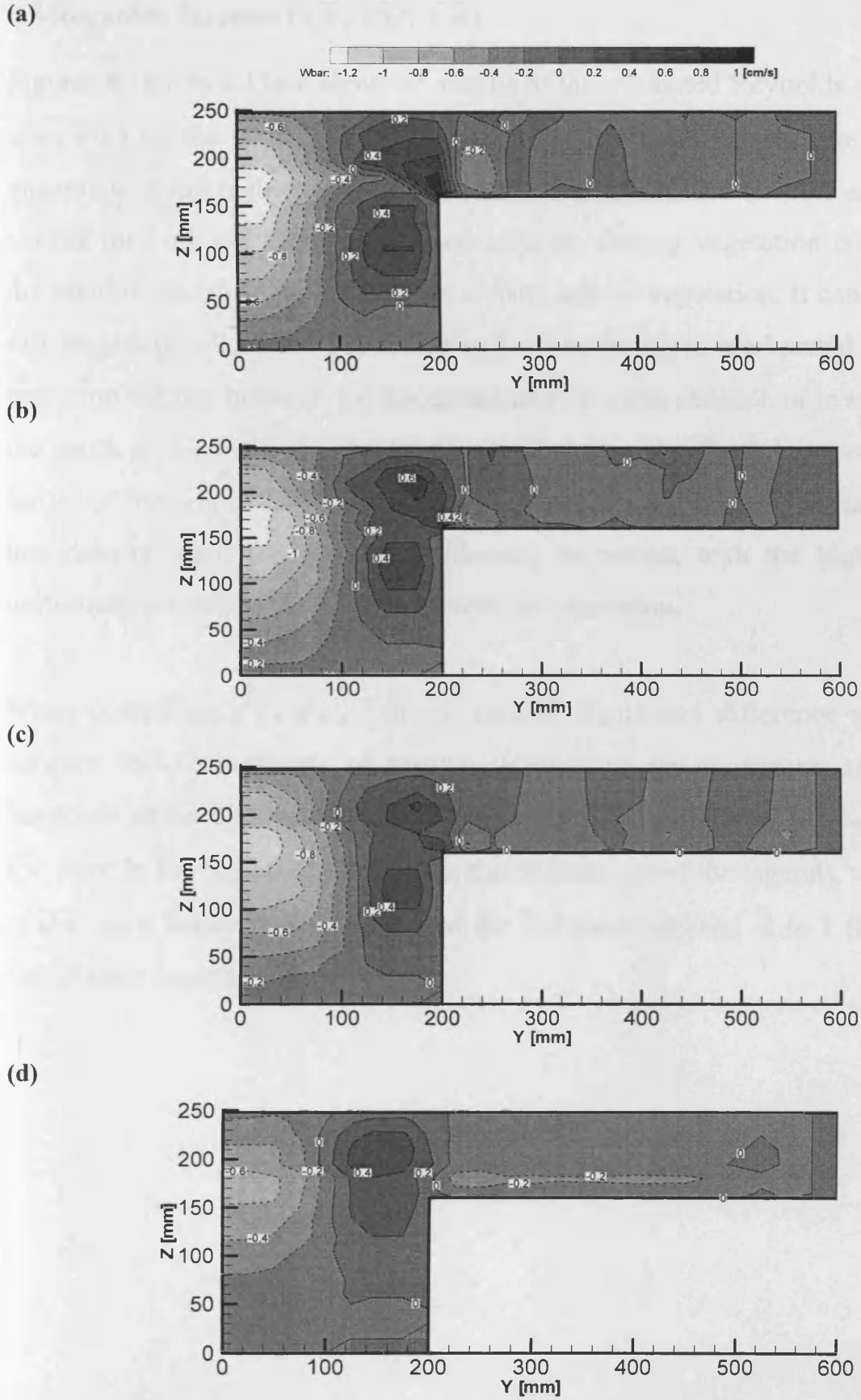

Fig. 4.6 Time-averaged vertical velocity ($\overline{W}$) [cms^{-1}] at cross-section 4.5 and for four configurations: (a) high, (b) medium, (c) low, and (d) no vegetation.

4.3 Reynolds Stresses ($\overline{u'v'}$, $\overline{u'w'}$, $\overline{v'w'}$)

Figures 4.7a-c to 4.12a-c show the results of the evaluated Reynolds stresses ($\overline{u'v'}$, $\overline{u'w'}$, $\overline{v'w'}$) for the various flow configurations. It can be seen that the approximate quantities of the highest and lowest areas of the Reynolds stresses are somewhat similar for both the high density and medium density vegetation configurations; the same is also the cases of the low density and no vegetation. It can also be seen that in general all of the maximum and minimum areas are located either in the transition regions between the floodplain and the main channel, or in regions where the depth of the main channel is close to that over the floodplain bed. Generally, for all of the results and graphs, in moving from high density vegetation towards low density, then the level of uniformity increased, with the highest level of uniformity occurring for the case of with no vegetation.

When comparing $\overline{u'v'}$, $\overline{u'w'}$, and $\overline{v'w'}$ another significant difference was observed between the various sets of results. Apart from the maximum and minimum Reynolds stress distributions, most of Reynolds stress values for each profile of $\overline{u'v'}$ were in the region of -1 to 1 (i.e. the middle part of the legend), whereas these of $\overline{u'w'}$ were between -0.4 to 0.4 and for $\overline{v'w'}$ were between -2 to 1 (i.e. the lower part of their legend).

(a)

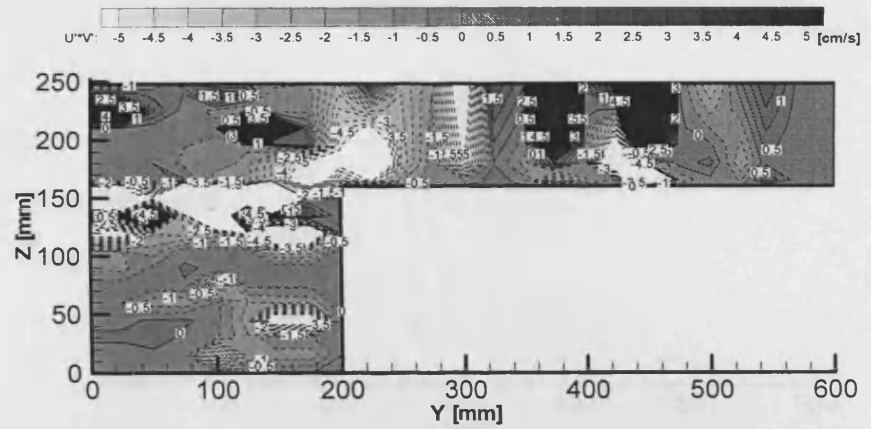

(b)

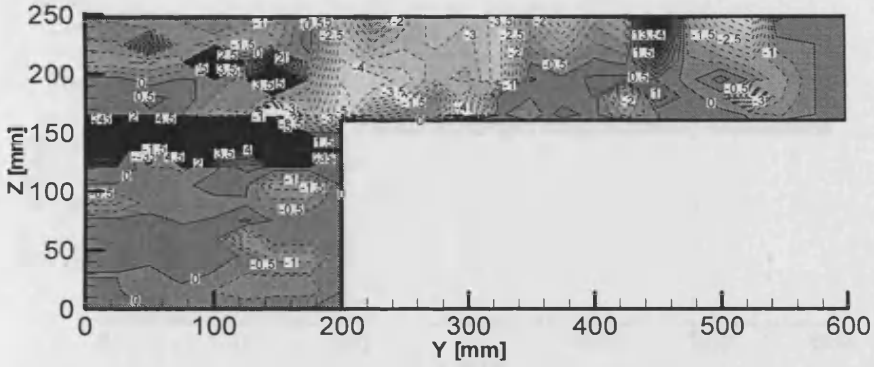

(c)

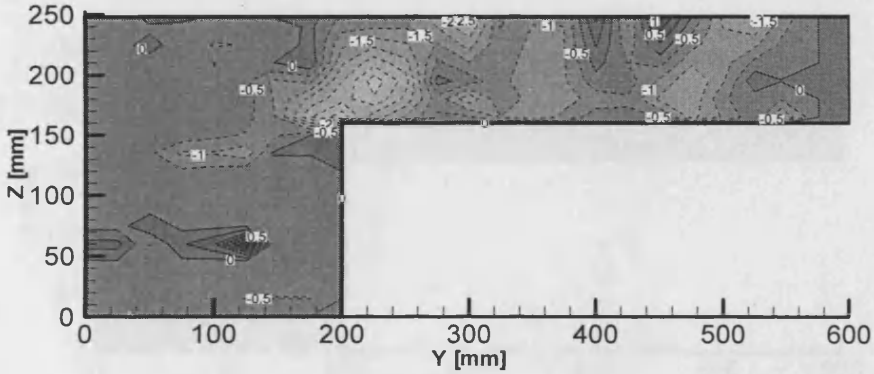

(d)

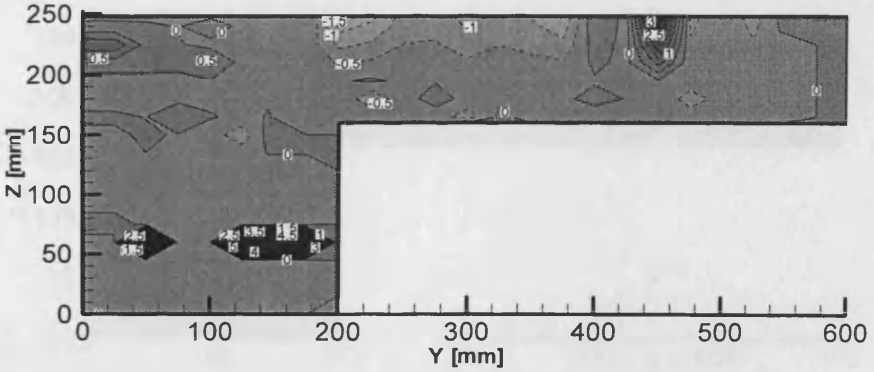

Fig. 4.7 Reynolds stress ($\overline{u'v'}$) [cm^2s^{-2}] at cross-section 4.4 and for four configurations: (a) high, (b) medium, (c) low, and (d) no vegetation.

(a)

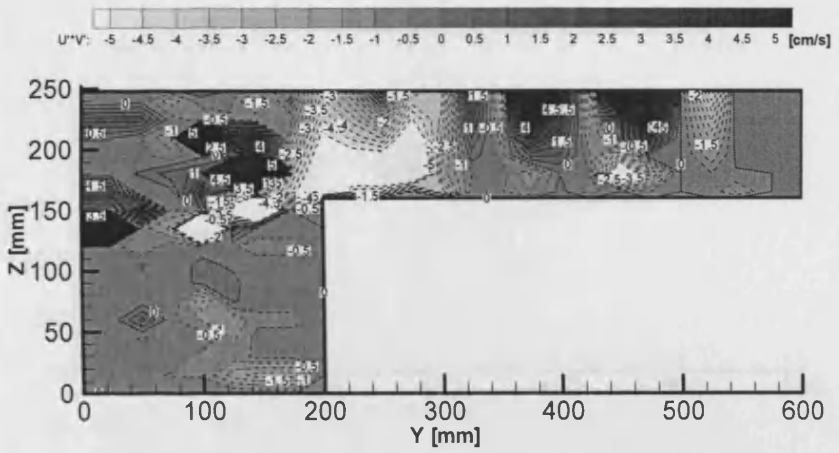

(b)

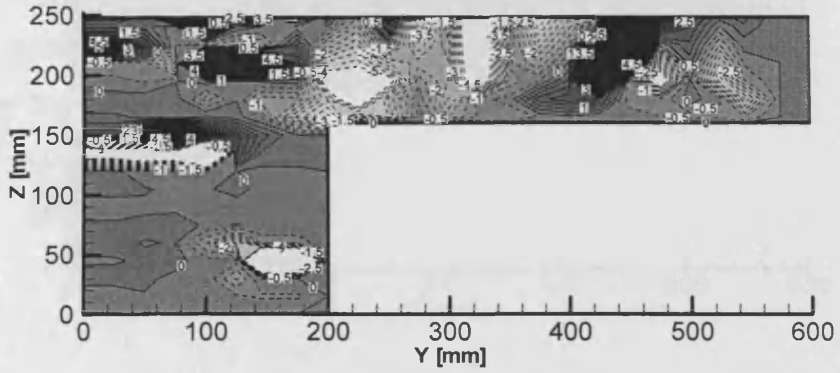

(c)

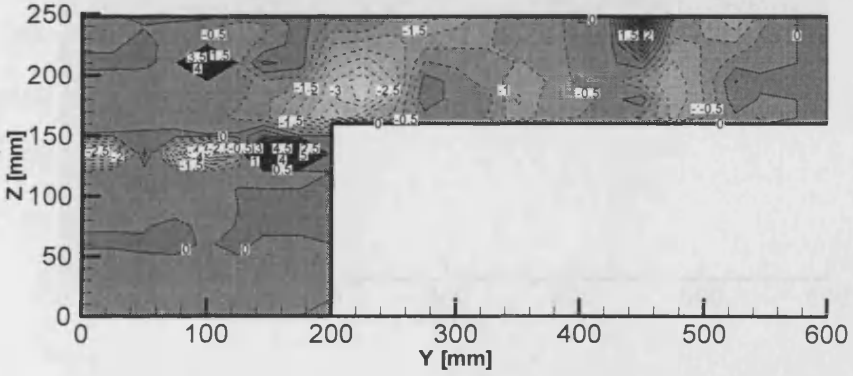

(d)

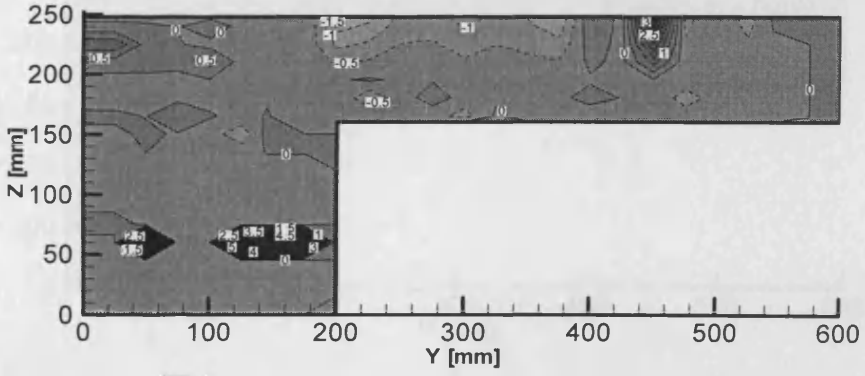

Fig. 4.8 Reynolds stress ($\overline{u'v'}$) [cm^2s^{-2}] at cross-section 4.5 and for four configurations: (a) high, (b) medium, (c) low, and (d) no vegetation.

(a)

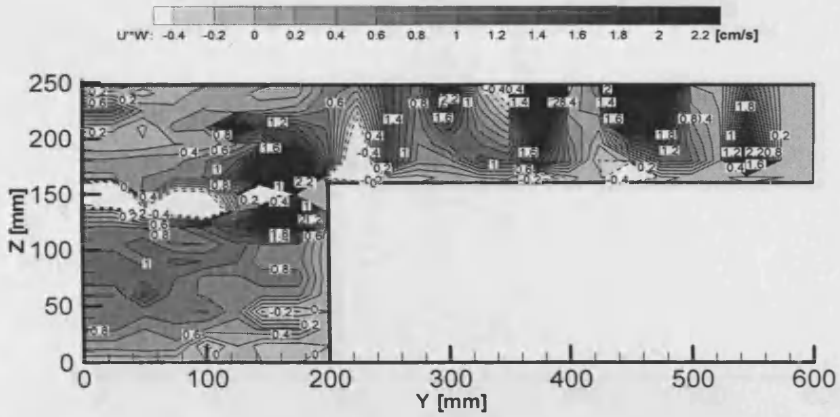

(b)

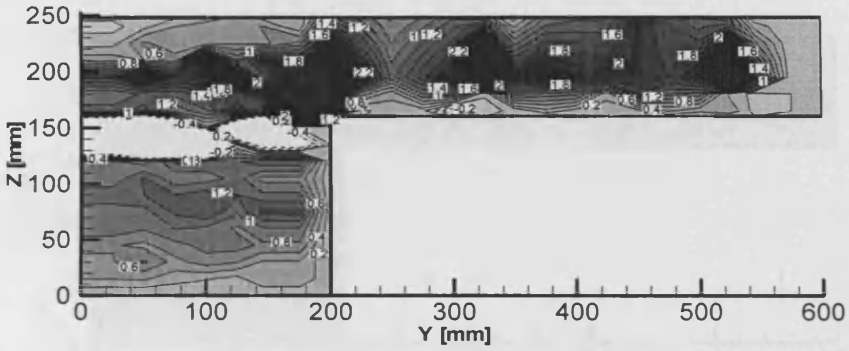

(c)

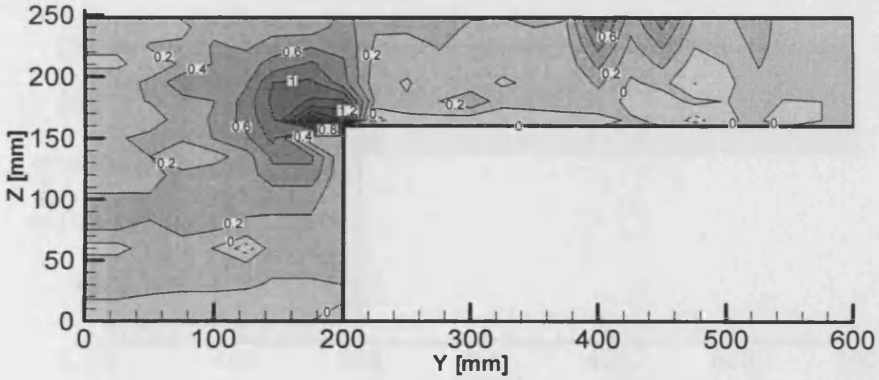

(d)

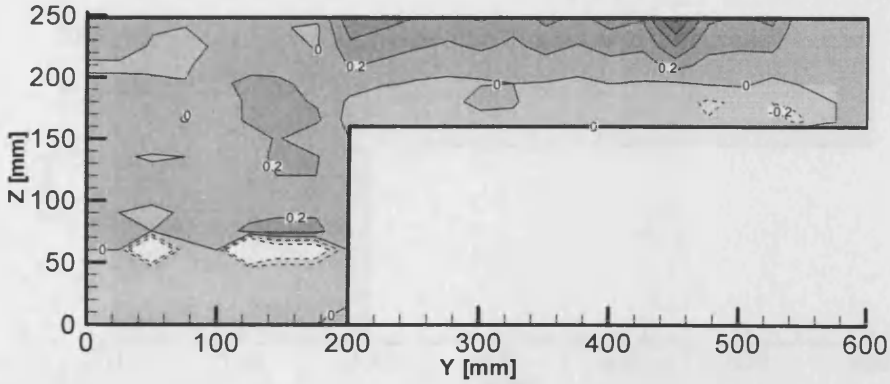

Fig. 4.9 Reynolds stress ($\overline{u'w'}$) [cm^2s^{-2}] at cross-section 4.4 and for four configurations: (a) high, (b) medium, (c) low, and (d) no vegetation.

(a)

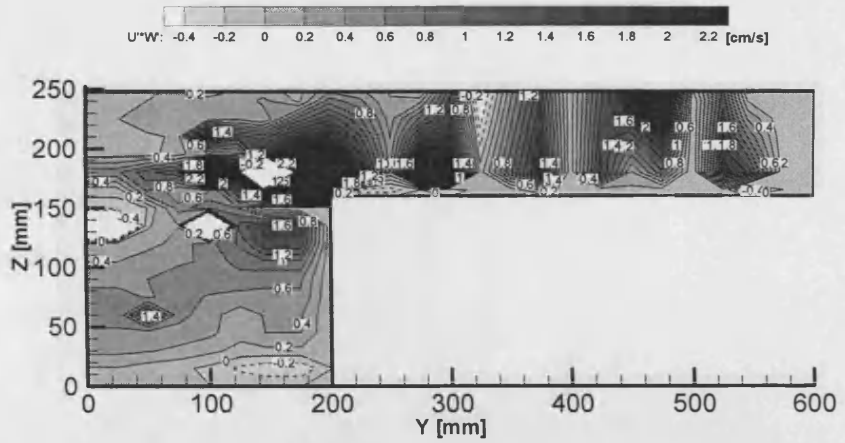

(b)

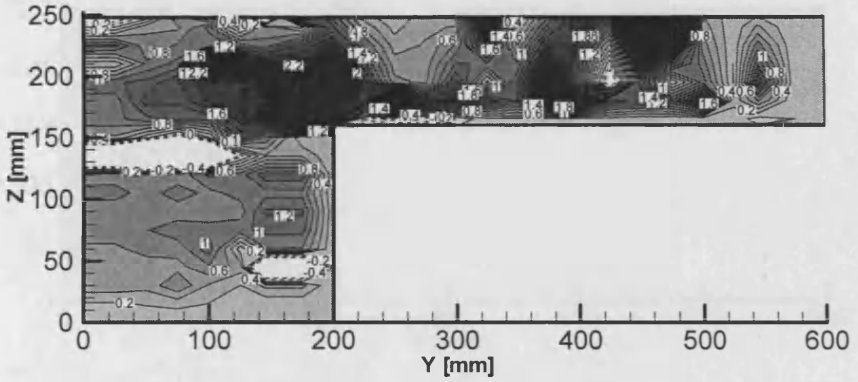

(c)

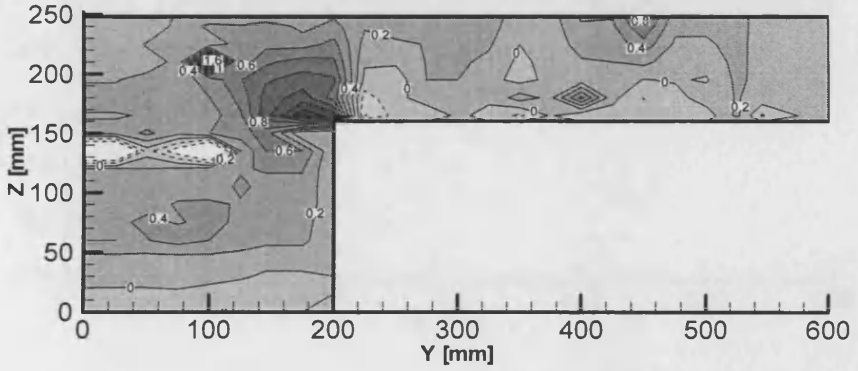

(d)

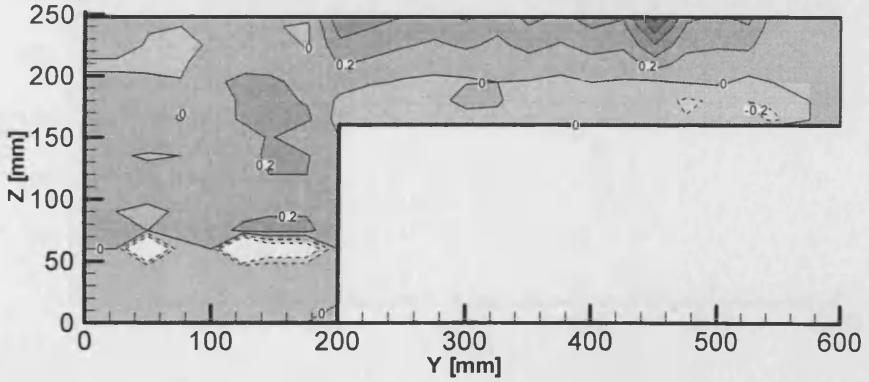

Fig. 4.10 Reynolds stress ($\overline{u'w'}$) [cm^2s^{-2}] at cross-section 4.5 and for four configurations: (a) high, (b) medium, (c) low, and (d) no vegetation.

(a)

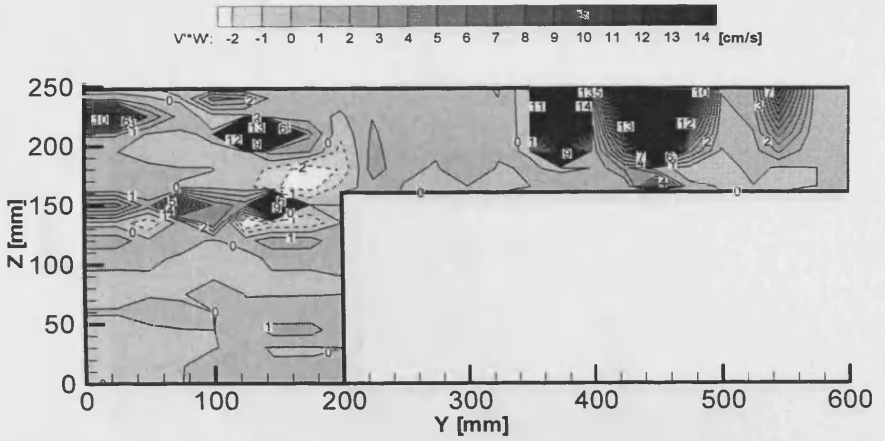

(b)

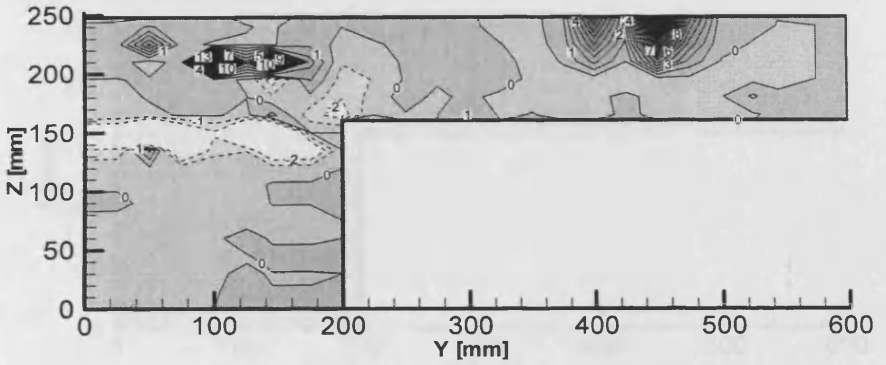

(c)

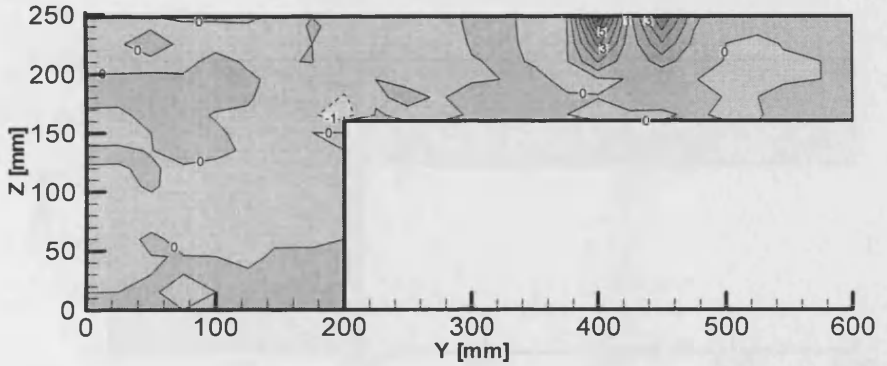

(d)

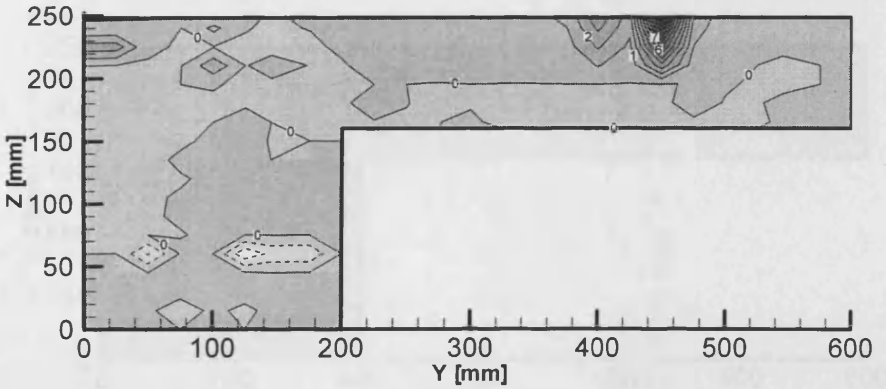

Fig. 4.11 Reynolds stress ($\overline{v'w'}$) [cm^2s^{-2}] at cross-section 4.4 and for four configurations: (a) high, (b) medium, (c) low, and (d) no vegetation.

(a)

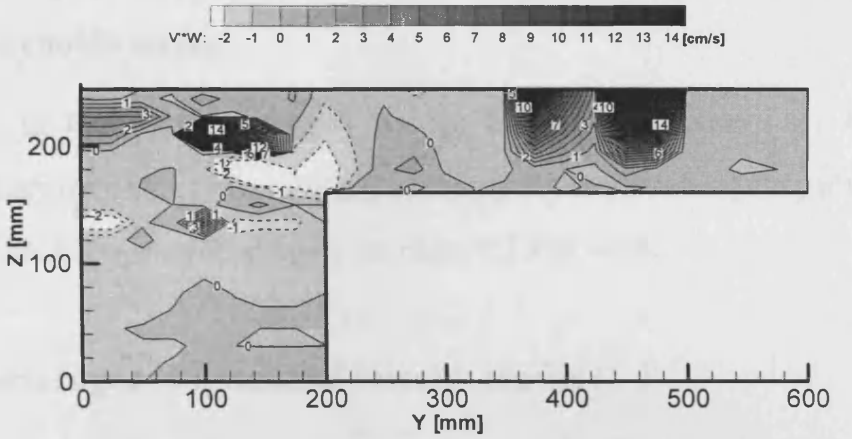

(b)

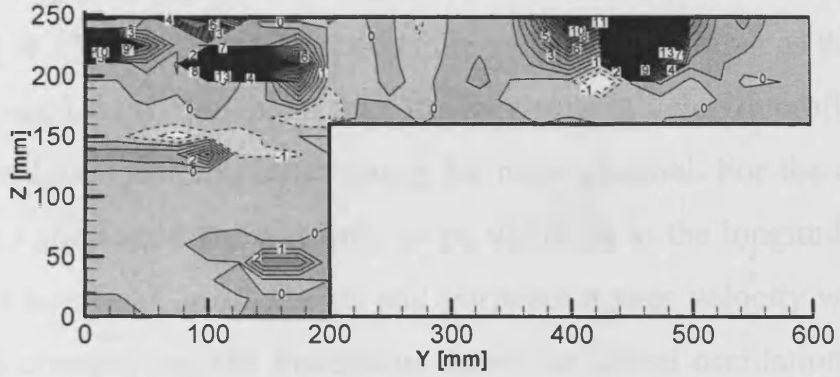

(c)

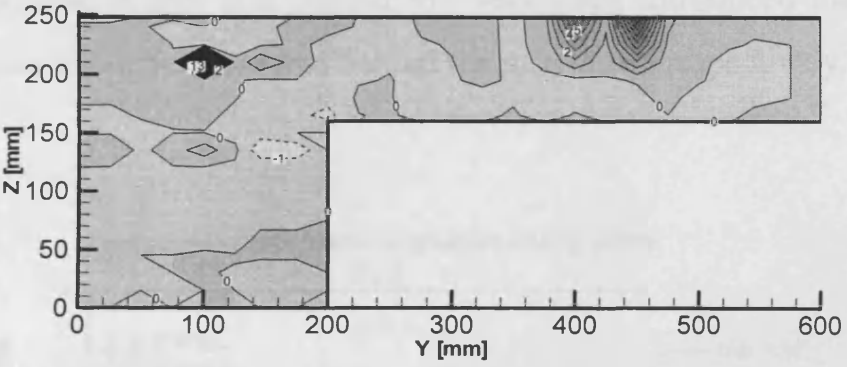

(d)

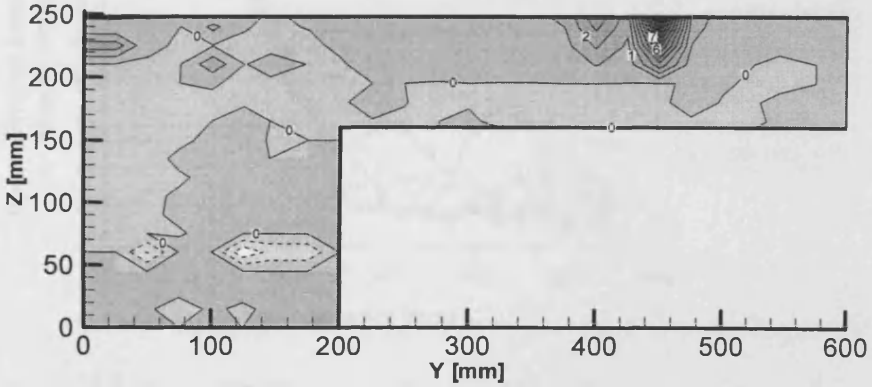

Fig. 4.12 Reynolds stress ($\overline{v'w'}$) [cm^2s^{-2}] at cross-section 4.5 and for four configurations: (a) high, (b) medium, (c) low, and (d) no vegetation.

4.4 Depth-averaged component of the velocity profile, the velocity fluctuation, and the Reynolds stress

The variation in the depth-averaged values for the velocities ($\overline{U}$, $\overline{V}$, $\overline{W}$), the velocity fluctuations (u'_{rms}, v'_{rms}, w'_{rms}) and Reynolds stresses ($\overline{u'v'}$, $\overline{u'w'}$, $\overline{v'w'}$) are illustrated for each vegetation density in Figs. 4.13 to 4.18.

4.4.1 Depth-averaged longitudinal velocity profile ($\overline{U}$)

The depth-averaged longitudinal velocity profile is illustrated across the cross-section in Fig. 4.13. For all cross-sections the results showed that as the vegetation density increased on the floodplain then the longitudinal velocity profile decreased across the floodplain and increased along the main channel. For the case with no vegetation, as expected, there was little or no variation in the longitudinal velocity over the cross-section. For all intents and purposes a near velocity was measured over the main channel and the floodplain. Also, the lateral oscillations in velocity over the floodplain meant that behind the vegetation introduced maximum and minimum velocities in between and behind the vegetation respectively.

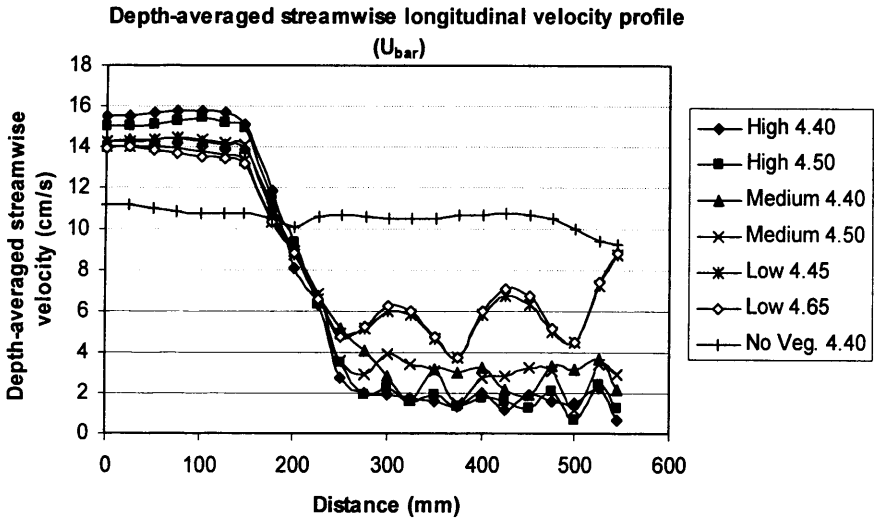

Fig. 4.13 Depth-averaged longitudinal velocity profile ($\overline{U}$).

4.4.2 Depth-averaged transverse velocity profile ($\overline{V}$)

The depth-averaged transverse velocity profile is shown in Fig. 4.14. For this case, the velocity distributions for all trials show that for all of the densities the velocity variations are similar. Clearly, variations in the main channel velocity are relatively uniform, but on the floodplain are oscillatory and in line with the vegetation distributions.

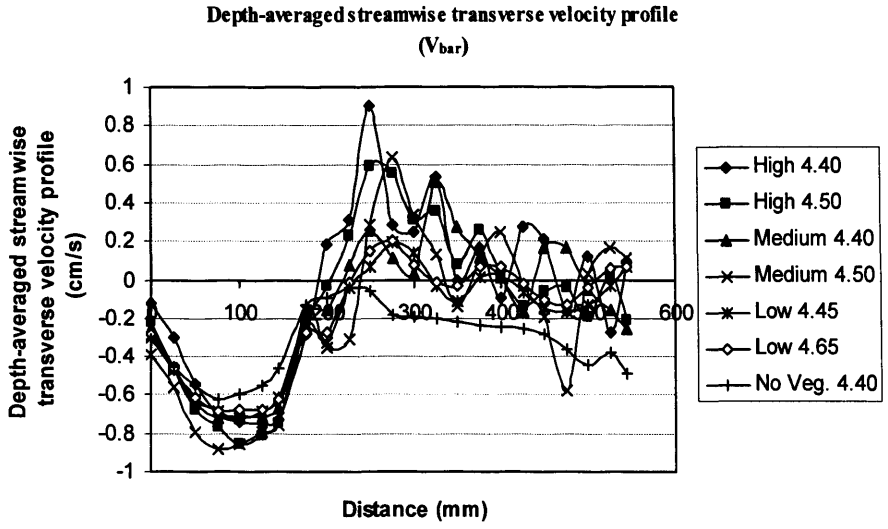

Fig. 4.14 Depth-averaged transverse velocity profile ($\overline{V}$).

Also, all of the transverse velocity profiles (i.e. $\overline{V}$) have a minimum velocity at approximately 100 mm from the centre of the main channel and 2 locations equidistant from the 100 mm point (i.e. on the central line and between the main channel and the floodplain) where the velocities are again similar in magnitude. In traversing across the section the velocities peaked just after crossing on the floodplain, and then decreased gradually towards the edge of the floodplain.

The maximum velocities across the section were higher for the high density vegetation, vis-a-vis the medium density, low density and no vegetation and the oscillatory characteristics of the lateral profile were related to the vegetation rods as discussed previously. Furthermore for the case of no vegetation, then the

variations in the transverse velocity were found to be smaller than for the other configurations with no oscillatory variations across the floodplain, in comparison with the results of the other densities.

4.4.3 Depth-averaged vertical velocity profile ($\overline{W}$)

The depth-averaged vertical velocity profile is shown in Fig. 4.15. In this case all graphs for all densities have approximately similar variations. The variations in the main channel and in the floodplain were found to be less oscillatory in comparison with those measurements recorded for $\overline{V}$.

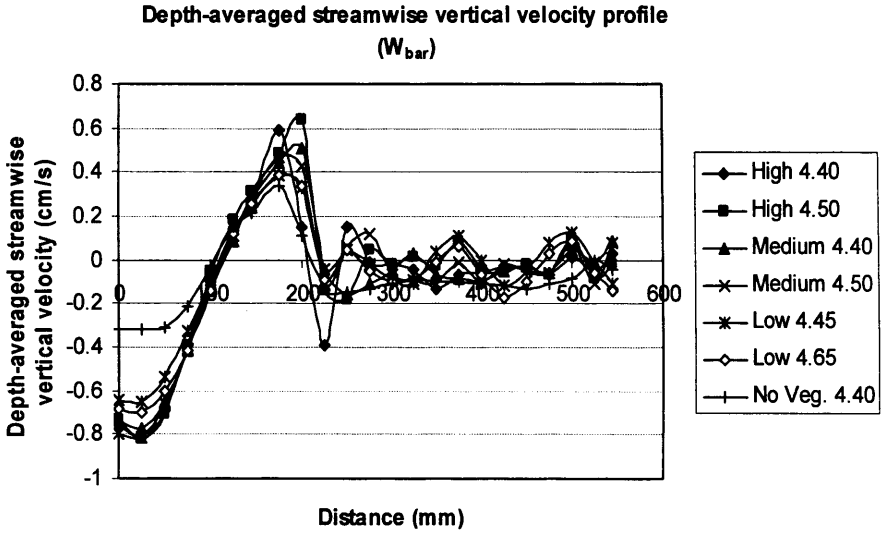

Fig. 4.15 Depth-averaged vertical velocity profile ($\overline{W}$).

For all of the different density profiles it was found that a minimum velocity point occurred along the central line of the main channel, which increased towards the end of the main channel and then decreased and continued with constant values which varied in an oscillatory manner towards the sidewalls. Whenever the vegetation densities were high, the differences between the maximum and minimum velocities were found to be high and vice versa, as for the case with no vegetation across the cross section. Again, oscillatory changes over the flood plain were related to the density of vegetation, since for the case of no vegetation clearly

there were no resistance variations over the floodplain vis-a-vis that occurring for the varying vegetation densities.

4.4.4 Depth-averaged components root mean square velocity fluctuation profile (u'_{rms}, v'_{rms}, w'_{rms})

Figure 4.16 shows the results of Depth-averaged components of the root mean square (*rms*) velocity fluctuation profiles for u'_{rms}, v'_{rms}, w'_{rms} for all vegetation densities. As can be seen from the results, all of the profiles show a similar distribution with the quantities in the main channel being relatively constant, with little variation, but variation across the floodplain and over the transition region between the main channel and the floodplain. The results for the high density vegetation always give the highest values for the Reynolds stresses, indicating a higher degree of turbulence, vis-a-vis lower quantities of the turbulence parameters for the case with no vegetation.

Furthermore, as the vegetation density decreases the variation of the Reynolds stress decreases over the floodplain, since the lowest variation was observed for the lower density and no vegetation cases. These results show that the governing velocity variations and fluctuations are caused by the vegetation on the floodplain.

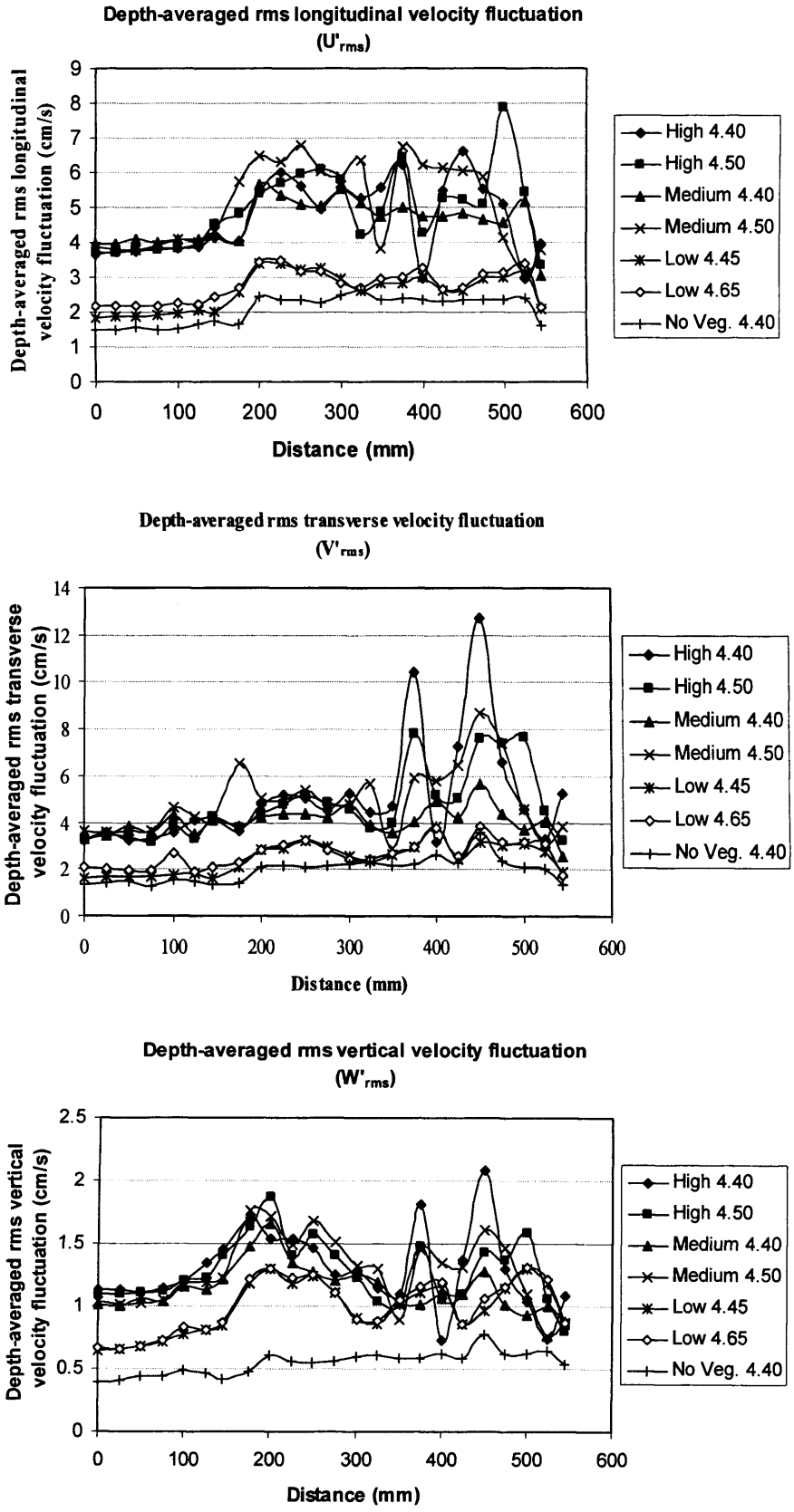

Fig. 4.16 Depth-averaged components of the root mean square velocity fluctuation (u'_{rms} ,v'_{rms}, w'_{rms}).

4.4.5 Depth-averaged component of Reynolds stresses ($\overline{u'v'}$, $\overline{u'w'}$, $\overline{v'w'}$)

Figure 4.17 shows the results of the depth-averaged components of the Reynolds stresses ($\overline{u'v'}$, $\overline{u'w'}$, $\overline{v'w'}$) for all of the vegetation densities. As can be seen for the case with no vegetation, the quantity of the Reynolds stress components are approximately constant and remain close to zero across the main channel and floodplain.

For all of the vegetation densities the Reynolds stress components in the main channel are constant and close to zero, whereas they change towards the floodplain. However, these variations are different, as for $\overline{u'v'}$, the variations in the transition region are negative and positive across the floodplain. Whereas, in $\overline{u'w'}$, for the variations these change in the transition region and continue to grow across the floodplain, with positive values. For $\overline{v'w'}$ the values are approximately constant or have negligible variations in the main channel and the transition areas for all of the vegetation densities with only minor variations occurring near the edge of the floodplains. Thus these results show that, in general, an increase in the vegetation density leads to an increase in the Reynolds stress components. The maximum values occur for the high density vegetation, with the minimum values occurring for the low density and no vegetation configurations.

Table 4.1 shows the maximum and minimum values of the velocity, the velocity fluctuations, and the Reynolds stress components for all of the densities and for the compound channel configuration. From this table the effects of the vegetation density on the velocity profile, the root mean square velocity and the Reynolds stress profiles have been studied. For the different variables, the marked consistency in the effects of the vegetation changes confirms the accuracy of the experiments undertaken.

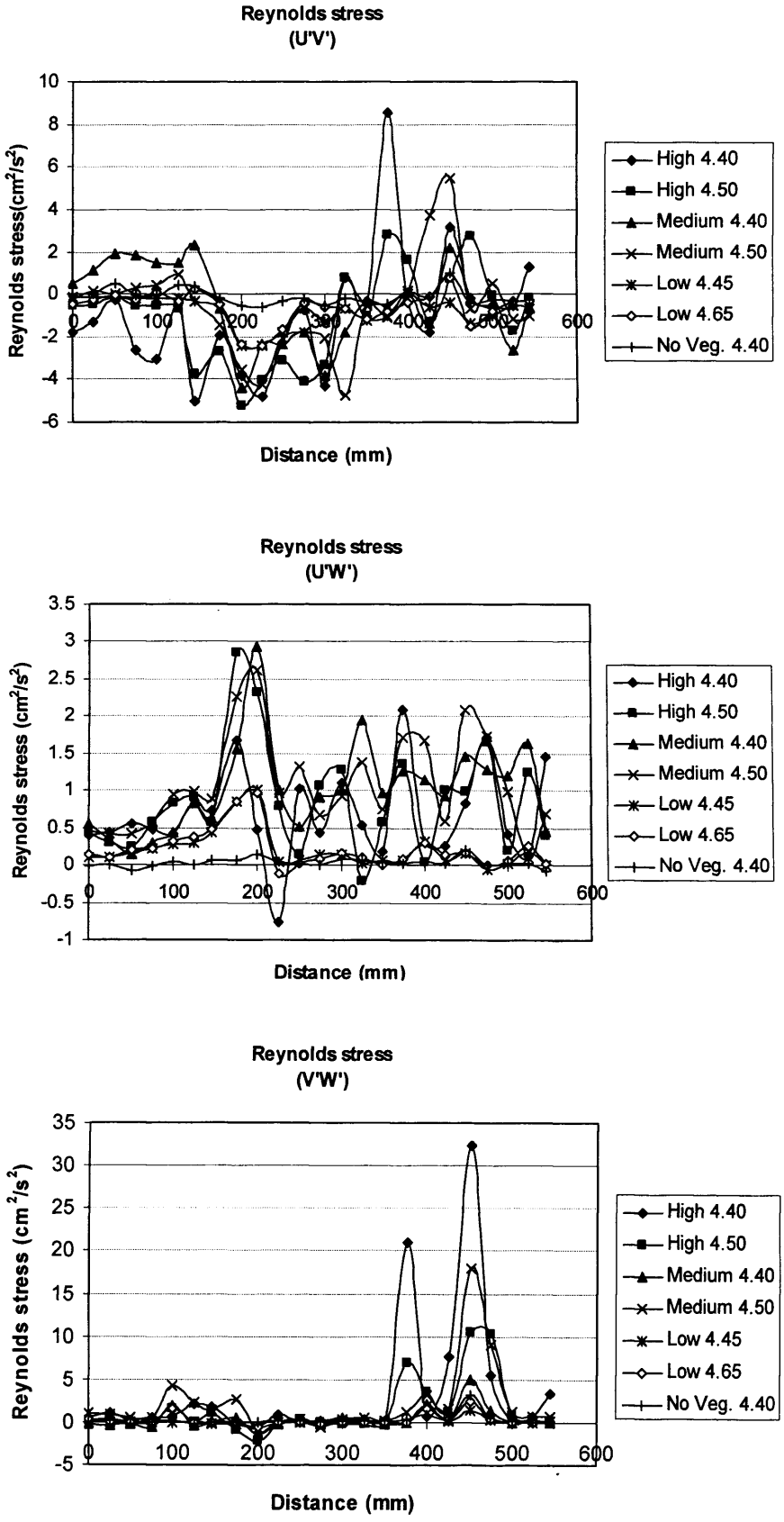

Fig. 4.17 Depth-averaged components of the Reynolds stresses ($\overline{u'v'}$, $\overline{u'w'}$, $\overline{v'w'}$).

Table 4.1 Maximum and minimum values of time-averaged velocity components, velocity fluctuation, and Reynolds stress components for all tests conducted in the compound channel.

No	Vegetation Density	$\overline{U}$ (cm/s) Min – Max	$\overline{V}$ (cm/s) Min – Max	$\overline{W}$ (cm/s) Min – Max	u'_{rms} (cm/s) Min – Max	v'_{rms} (cm/s) Min – Max	w'_{rms} (cm/s) Min – Max	$u'v'$ (cm^2/s^2) Min – Max	$u'w'$ (cm^2/s^2) Min – Max	$v'w'$ (cm^2/s^2) Min – Max
1	High Den 4.40	0 – 18	-1.4 – 0.6	-1.3 – 0.9	0 - 8	2 - 14	0 - 3	-15 -15	-1 - 3	-3 - 28
2	High Den 4.50	0 - 18	-1.5 – 0.6	-1.4 – 0.9	0 - 8	2 - 14	0 - 3	-15 -15	-1 - 3	-3 - 27
3	Medium Den 4.40	0 – 17	-1.3 – 0.4	-1.3 –0.6	0 - 8	2 - 12	0 - 2	-6 - 15	-1 - 3	-3 - 25
4	Medium Den 4.50	0 - 17	-1.4 – 0.3	-1.3 -0.6	0 - 8	2 - 12	0 - 2	-7 - 15	-1 - 3	-3 – 27
5	Low Den 4.45	0 - 16	-1.1 - 0.1	-1.1 -0.5	0 - 3	2 - 8	0 - 1.5	-3 - 1	-1 - 1.5	-3 - 6
6	Low Den 4.65	0 – 16	-1.1 - 0.1	-1.1 -0.5	0 - 3	2 - 8	0 - 1.5	-3 - 1	-1 - 1.5	-3 - 6
7	No. Veg 4.40	0 - 12	-0.9 - 0	-0.7 -0.4	0 – 3	2 – 8	0 - 1.5	-3 - 1	-1 - 1.5	-3 - 6

In this chapter details are given of a number of experiments undertaken in the compound channel to investigate the effects of emergent vegetation on the floodplain velocities, with data being collected across two cross-sections. The results showed that with an increase in vegetation density on the floodplain, the velocity in the vegetation zone (i.e. the floodplain) decreased and the main flow accelerated and transferred towards the main channel. Also, in the transition zone between the floodplain and the main channel, the velocity fluctuations and the Reynolds stresses were observed to be relatively high. The magnitude of the velocity, velocity fluctuation, and Reynolds stress components for the different zones were highly dependent upon on the vegetation density.

CHAPTER 5
SIMPLE RECTANGULAR NARROW CHANNEL

5.1 Introduction

In natural environments, flows are generally over vegetated beds. Hence, the vegetation in channels causes the water elevation to rise even further during high discharges, i.e. floods. Therefore it is important to estimate accurately the impact of vegetation on the conveying discharge of a vegetated channel. In natural rivers, vegetation is an essential part of the ecosystem. However, from a hydraulic viewpoint, vegetation causes resistance to flow and can increase the risk of flooding. In many cases, this is a very difficult task and some compromises have to be made.

Estimating the roughness in channels for the case of submerged and emergent vegetation is a difficult task. One of the most significant factors which can dominate the discharge capacity is the flow resistance imposed by vegetation. The density, height, and type of vegetation may vary across the river-section and in the longitudinal direction. In most cases, either the velocity profile or the roughness height can be determined. In areas where flow occurs through vegetation, the characteristics of the flow are largely determined by the type and density of vegetation, as well as the depth and velocity of the flow.

The main aim of this part of the study has been to investigate the effect of different vegetation densities on a simple channel flow. For this purpose, laboratory experiments were conducted in a simple narrow rectangular channel, of width 400mm, to investigate the velocity profile and turbulence structure of the flow

through and above rigid vegetation. The vegetation used in the channel varied in configurations (i.e. density) and height (including submerged and emergent).

In this chapter all densities used for the compound channel were also used for the simple channel, with the instantaneous velocity components (u_i , v_i , w_i) being measured for both the submerged and emergent cases. A 3 minute sampling period was again used and the measurement frequency was set to 25 Hz. Four different combinations of submerged and emergent rods configurations were investigated. The data were analysed and the time-averaged velocities, velocity fluctuations and Reynolds stresses were calculated for the three co-ordinate directions. The heights of the rods for the submerged and emergent cases were 180 mm and 300 mm respectively. In the following sections the emergent configurations is considered.

5.2 Fully submerged vegetation flow (Rods height = 180 mm)

Tests were first conducted for submerged vegetation, for all densities, where it was found that the water elevation had little effect. For each density, the velocity was measured at different points along the middle of channel with the measuring sites being 5 mm from the bed and at 25 mm increments towards the water surface (i.e. at 5, 25, 50, 75, 100, 125, 150, 175, 200, 225, 250 and 260 mm) (Fig. 5.1). The height of the rods for the submerged case was 180 mm.

(a)

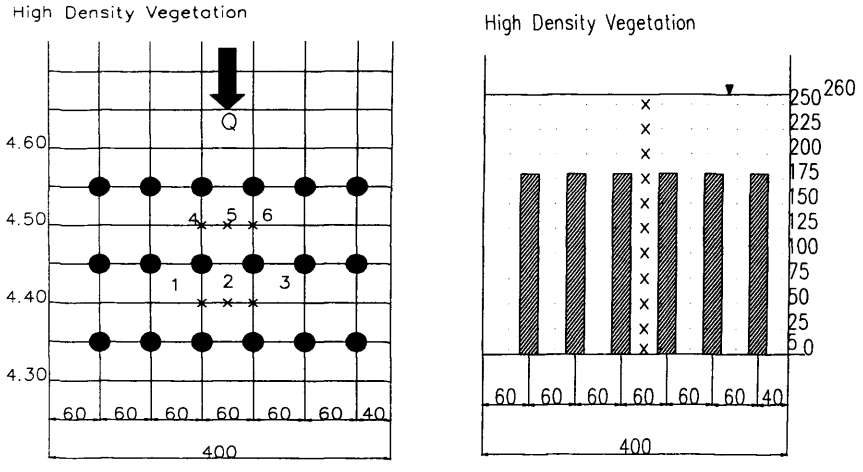

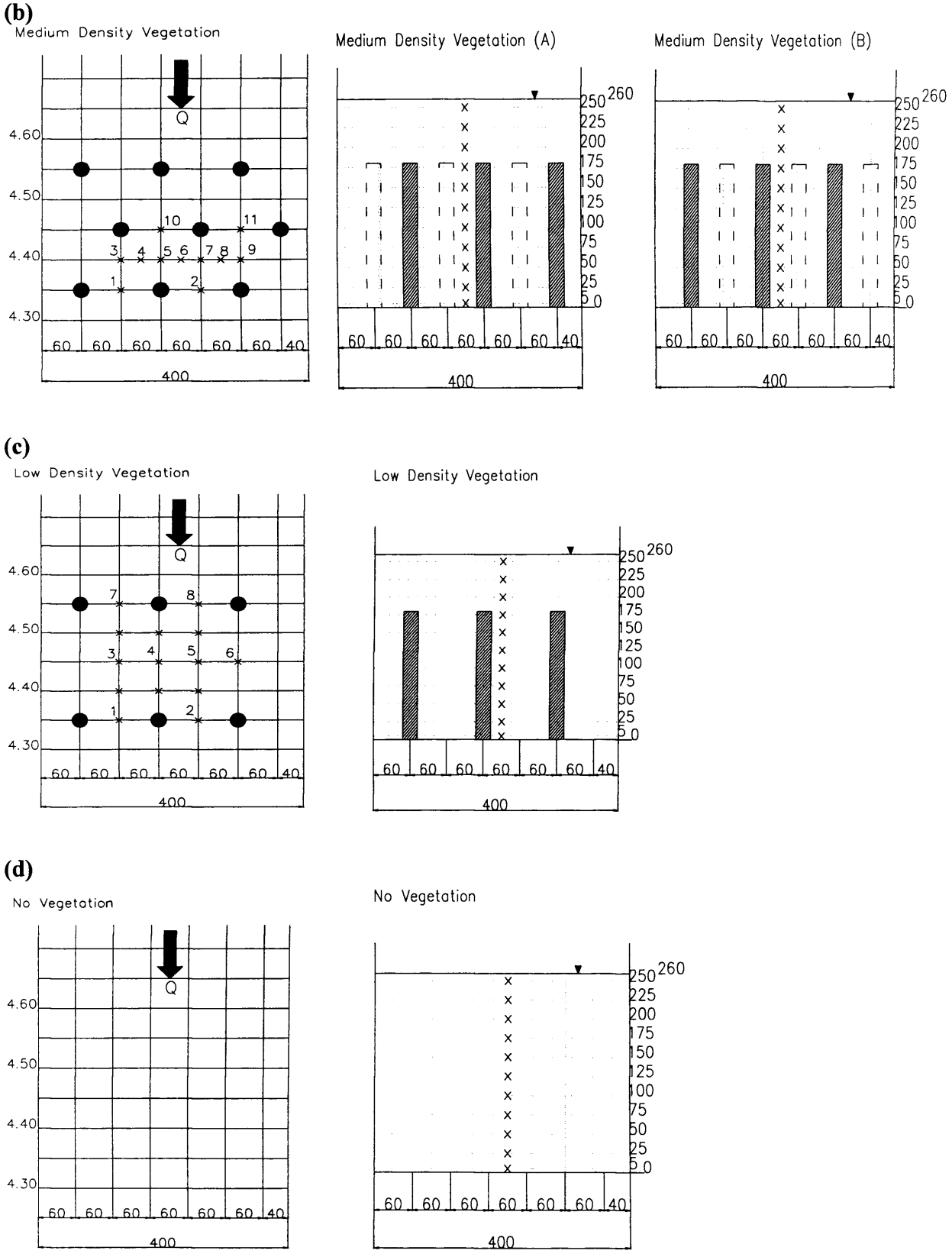

Fig. 5.1 Layout for the simple channel with the submerged rods, showing the location of the measuring points for the vertical velocity profiles at four configurations: (a) high, (b) medium, (c) low, and (d) no vegetation.

5.2.1 Time-averaged velocity components ($\overline{U}$, $\overline{V}$, $\overline{W}$)

These results show the effect of vegetation density on the velocity components in the simple channel (Figs. 5.2a-d to 5.4a-d).

a) Time-averaged longitudinal component of velocity ($\overline{U}$)

As, can be seen in Fig. 5.2a-d, when the density increases the longitudinal velocity in the rod zone decreases. Also, the velocity is constant or has little variation from the bed to near the top of the rods (150 mm) but it increases steeply from that level to the water surface. This means that the maximum velocity occurs near the water surface.

Of course, there are different changes for different densities. In a high density, the velocity is about 3 cm/s at 5 mm above the bed for all points between and behind the rods. However, with increasing depth, the velocity at locations behind the rods decreases to 1 cm/s and velocity of the points between the rods increases to 4 cm/s. In addition, the velocity at all points is approximately constant with an increase in depth up to about 150 mm above the bed. It then increases steeply and approaches 15 cm/s on the water surface. It shows that the friction caused by the bed roughness dominates and the rods have limited effect on the flow. Therefore the velocity for all the points is almost the same and constant. But with a further increase in depth it is observed that the effects of the bed roughness friction are reduced and the effects of vortex shedding and form drag develop and dominate. So, the velocity profiles behind and between the rods are completely different. As can be seen in Fig. 5.1a points 2 and 5 are in between the rods and points 1, 3, 4 and 6 are behind the rods. For these location sets the velocity profiles are completely different in shape and magnitude. However for a depth in excess of 150 mm the velocity increases sharply at the vegetation top and in the upper depths, increasing fairly uniformly to a maximum near the water surface.

For medium and low densities, the effect of the friction roughness is less than for the high density. As observed in Fig 5.2b, for medium density the velocity starts at 2 cm/s at the locations behind the rods (i.e. points 3 and 7) and about 5 cm/s in between the rods (i.e. the other points) near the bed and with a little decrease or increase up to a depth of 150 mm. In this state due to the effects of staggering near the top of the rods it was observed that a steep increase occurred in the velocity, with an increase to approximately 15 cm/s at the water surface. For the low density case, the velocity started at 4 cm/s for the points behind the rods (i.e. points 4 and 6) and 6 cm/s for the points between the rods (i.e. the other points) near the bed and remain constant or increase gradually up to 150 mm. Above this location the velocity increases up to 13 cm/s or less at the water surface (Fig. 5.2c). For the no vegetation state, the velocity starts at about 5.5 cm/s near the bed and increases steadily towards the water surface, reaching to 8.5 cm/s at the water surface (Fig. 5.2d).

In considering Fig. 5.2a-d and the different points (i.e. behind and in between the rods) for the flume, and the profiles at different depths from the bed to the water surface, the effects of vortex shedding behind the rods can be observed. For details and more information about vortex shedding, and its variation with distance from the rods, further details are included in Chapter 7.

Thus it can be observed from the data that as the density increases in the submerged state, the velocity decreases in between the rods and becomes completely constant from the bed up to near the top of the rods but the velocity increases steeply from the top of the rods towards the water surface. For the case of no rods, the velocity increases steadily from the bed up to the water surface. In other words, for the submerged state when the density of the rods increase near the channel bed, then the velocity within the rods decreases and the majority of the flow transfers to the top of the rods and towards the water surface.

(a)

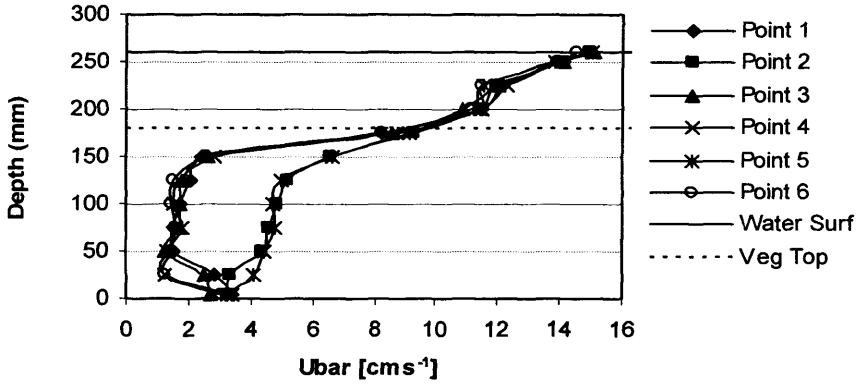

(b)

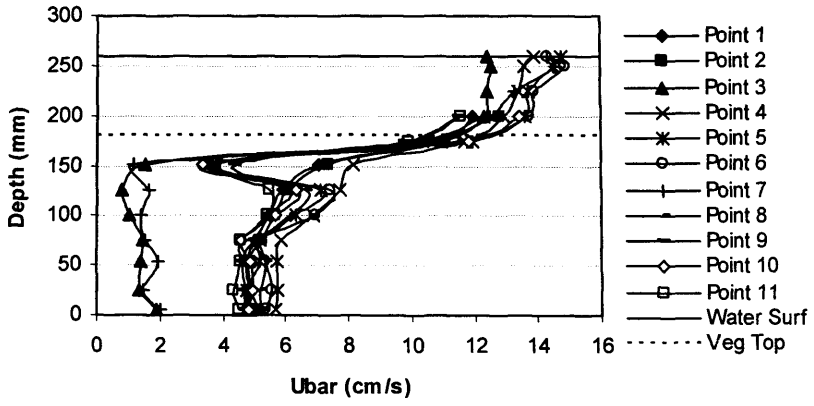

(c)

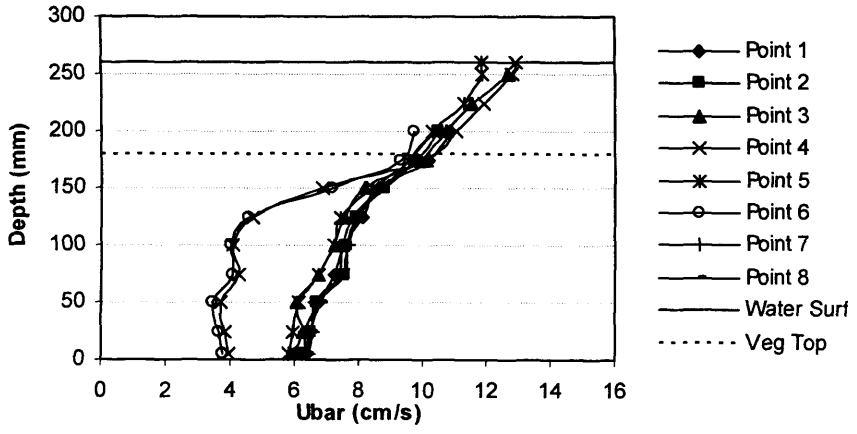

(d)

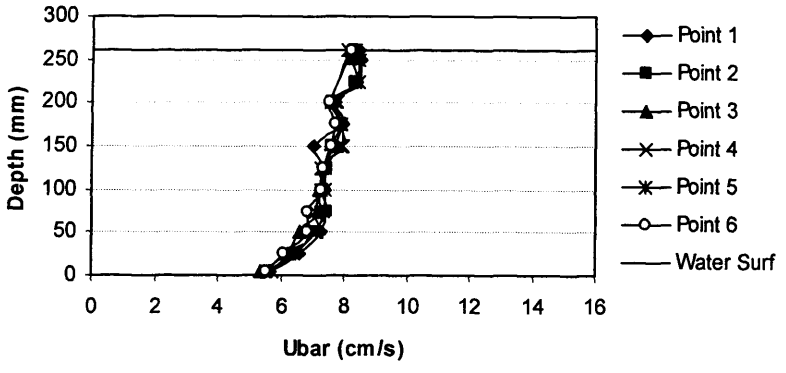

Fig. 5.2 Time-averaged longitudinal velocity ($\overline{U}$) [cms^{-1}] for four configurations: (a) high, (b) medium, (c) low, and (d) no vegetation.

b) Time-averaged transverse component of velocity ($\overline{V}$)

From Fig. 5.3a-d it can be seen that as the density increases, the dispersion of the transverse velocity in the vegetated areas increases and, above the vegetated areas towards the water surface, it reduces. In other words no vegetation and low density within the vegetation areas are observed to disperse the transverse velocity as compared with high density and medium density, where it is different in areas above the vegetation, and there is the least dispersion above the vegetation and more dispersion towards the vegetated areas. Also the staggered effect is very important, as for the medium density configuration it can be seen that the dispersion effects are more than for the high density (Fig. 5.3a-b). Therefore it shows that the effect of staggering is more important than the effect of density.

In comparing points in the channel it is observed that points between the rod columns have a maximum $\overline{U}$ and those behind the rods have a minimum $\overline{U}$. Conversely for $\overline{V}$ the result is different, i.e. the points with a high $\overline{U}$ have a low $\overline{V}$ and vice versa (Figs. 5.2a-b and 5.3a-b).

Also there is a maximum dispersion in results in medium density for staggering effect of vegetation even more than high density state. For more details about the quantity and quality of the differences between the in-line and staggered rods locations refer to Chapter 7 on wave generation.

(a)

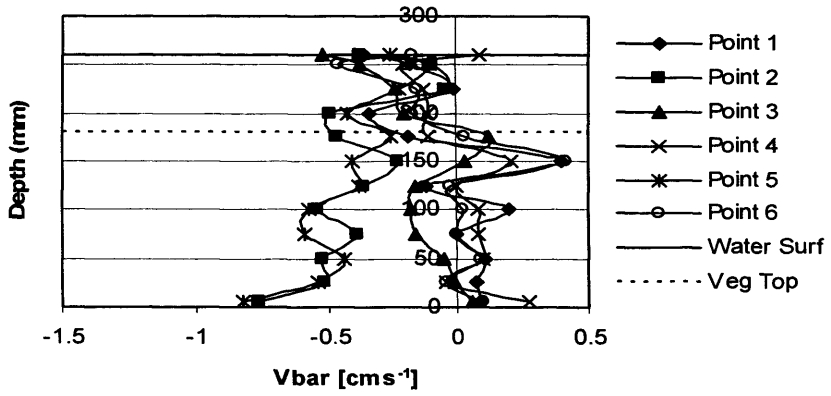

(b)

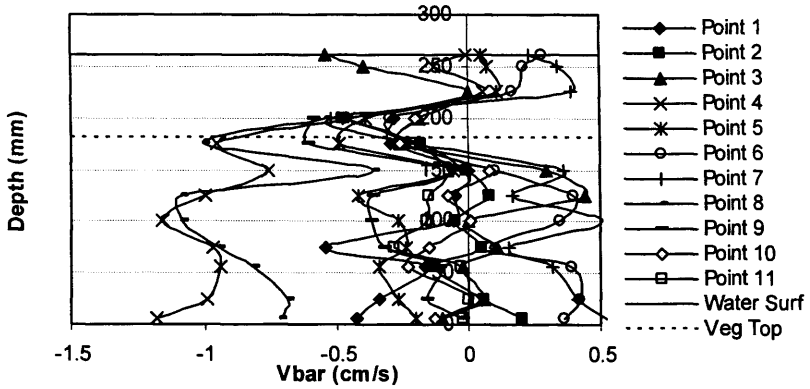

(c)

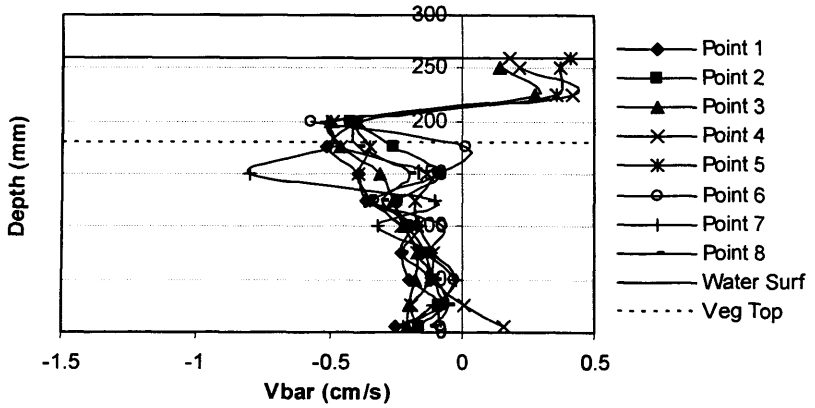

(d)

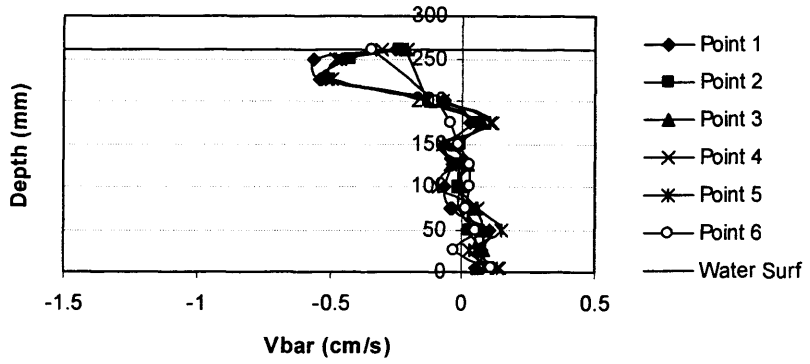

Fig. 5.3 Time-averaged transverse velocity ($\overline{V}$) [cms^{-1}] for four configurations: (a) high, (b) medium, (c) low, and (d) no vegetation.

c) Time-averaged vertical component of velocity ($\overline{W}$)

From Fig. 5.4a-d it may be estimated that from the channel bed up to 100 mm depth, the vertical velocity is approximately constant or with low variations around the 0 cm/s for all densities except that for no vegetation. However above about 100 mm depth and up to the rod tops (180 mm depth) then for the high and medium density rods a steep decrease occurs in the velocity. Beyond the top of the rods, the time averaged vertical velocity ($\overline{W}$) is constant around 0 cm/s and continues with this value to water surface. For the no vegetation case, from the bed up to 100 mm depth the velocity decreases slightly and above this elevation to the water surface there is a small increase in the velocity.

The vertical velocity component $\overline{W}$ was found to be inversely related to $\overline{U}$, so with maximum $\overline{U}$ values occurring with minimum $\overline{W}$ values and vice versa. Also as $\overline{U}$ in top vegetation area has a steep increase, then $\overline{W}$ also has a different structure in this zone (see points 2 and 5 for high density vegetation, 3 and 7 for medium density, and 4 and 6 for low density Figs. 5-2a-c and 5.4a-c).

(a)

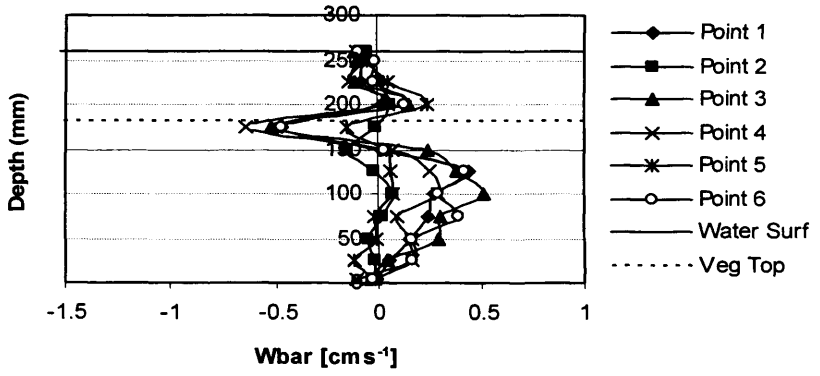

(b)

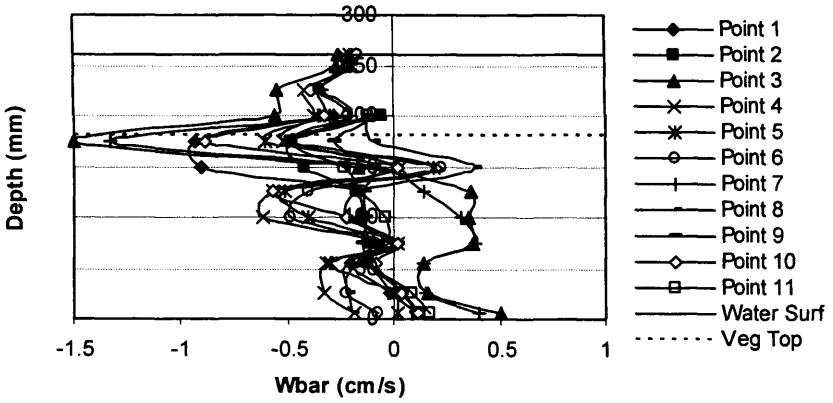

(c)

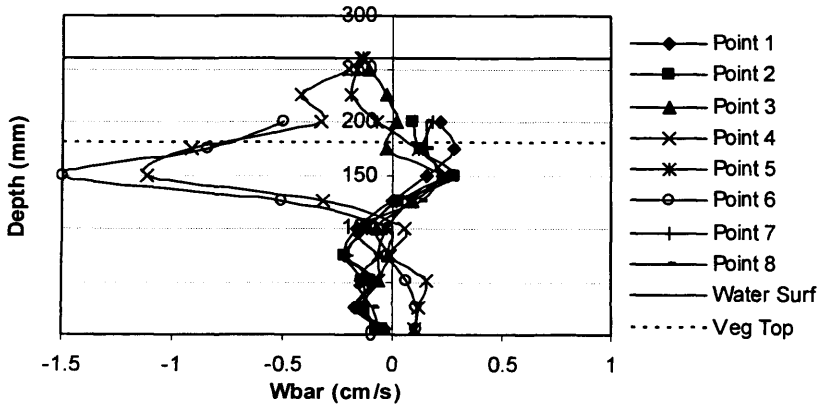

(d)

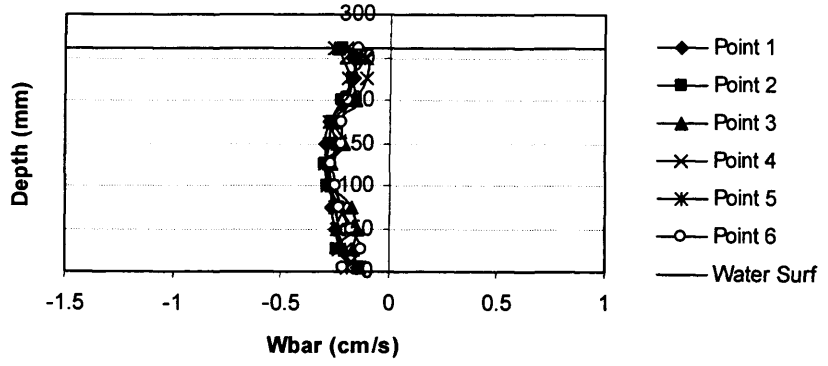

Fig. 5.4 Time-averaged vertical velocity ($\overline{W}$) [cms^{-1}] for four configurations: (a) high, (b) medium, (c) low, and (d) no vegetation.

5.2.2 Time-averaged *rms* velocity fluctuations component (*u'rms*, *v'rms* *w'rms*)

From Figs. 5.5a-d to 5.7a-d it can be seen that whenever the density increases then the velocity fluctuations for the longitudinal, transverse and vertical velocity components increase. For all densities the component fluctuation starts with a minimum rate near the bed and increases slowly up to a depth of 100 mm and then increases steeply after this elevation and reaches a peak at about 150 mm depth (i.e. just under the rod tips). The velocity components then reduce towards the water surface and reach approximately the same value as the near bed value.

For the high and low densities, more uniformity occurs in the flow structure between the points and for all depths, as can be seen in Figs. 5.5a,c to 5.7a,c. However, for the medium density more diffusion occurs between the rods. It can be concluded that the reason for this diffusion of the velocity is due to the staggering (or zigzag) effects of the rods along the channel (see Figs 5.5b to 5.7b). Therefore, for no vegetation, the fluctuating components for all points are almost constant from the bed towards the water surface. Clearly, some variation is observed near the water surface.

(a)

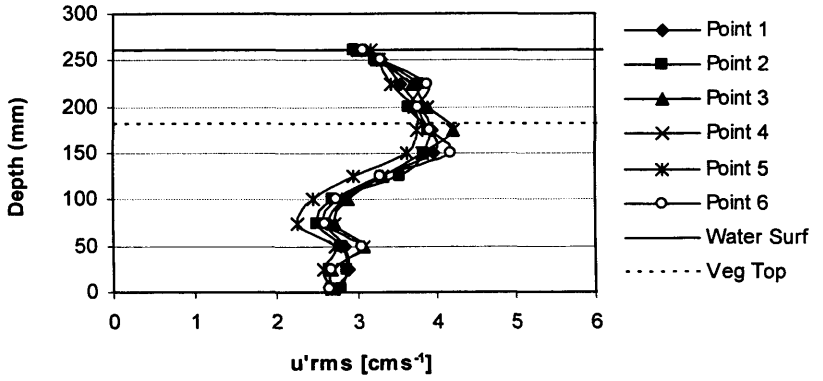

(b)

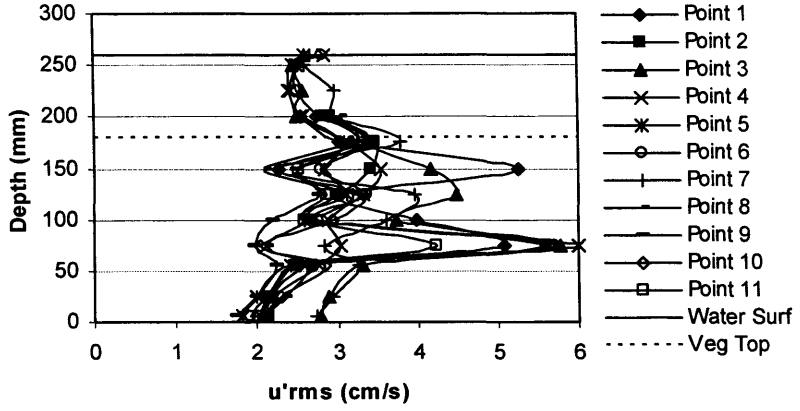

(c)

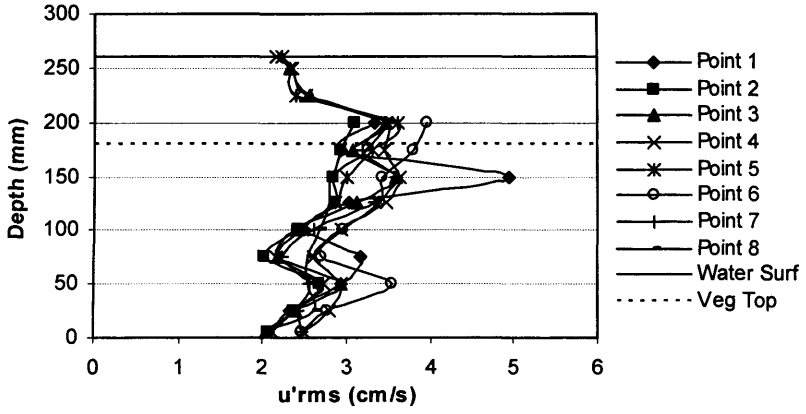

(d)

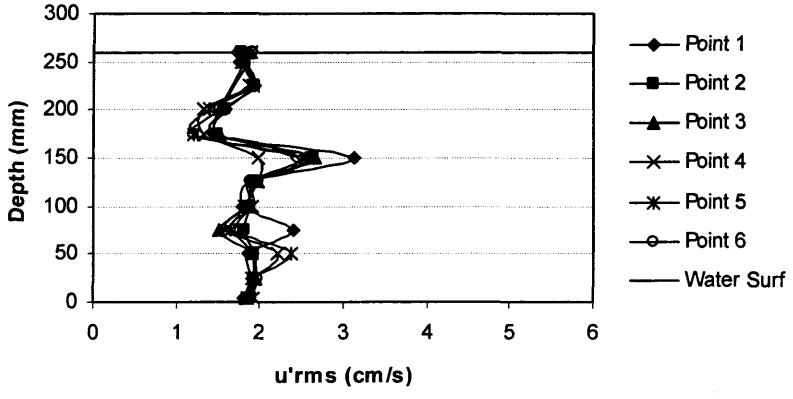

Fig. 5.5 Time-averaged *rms* velocity fluctuations ($u'rms$) [cms^{-1}] for four configurations: (a) high, (b) medium, (c) low, and (d) no vegetation.

(a)

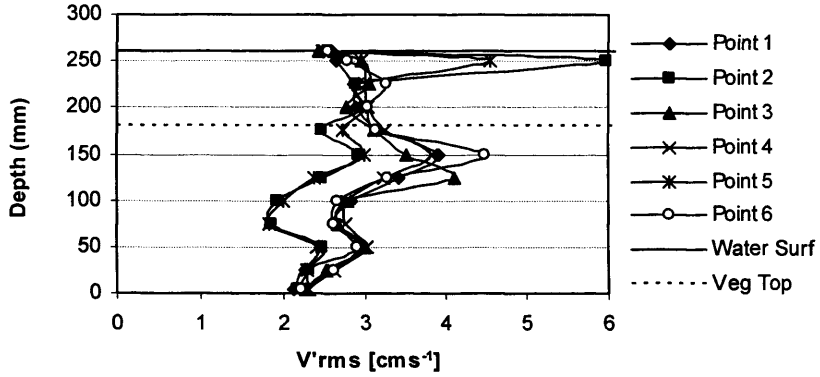

(b)

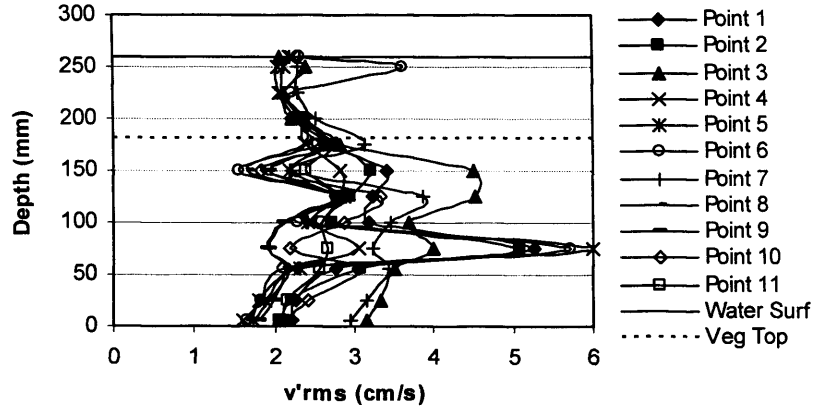

(c)

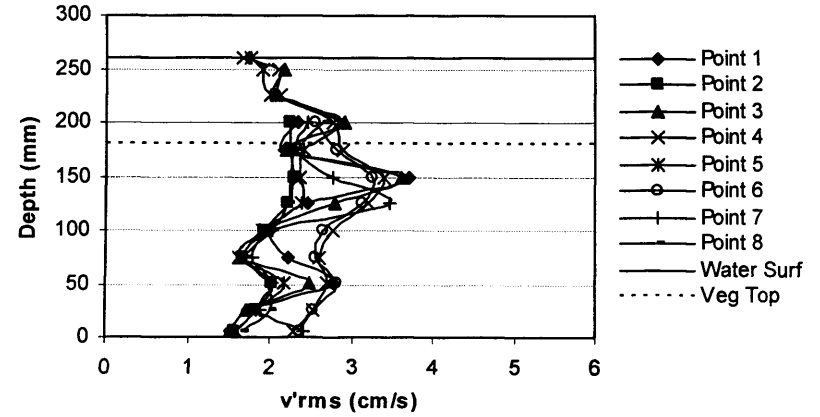

(d)

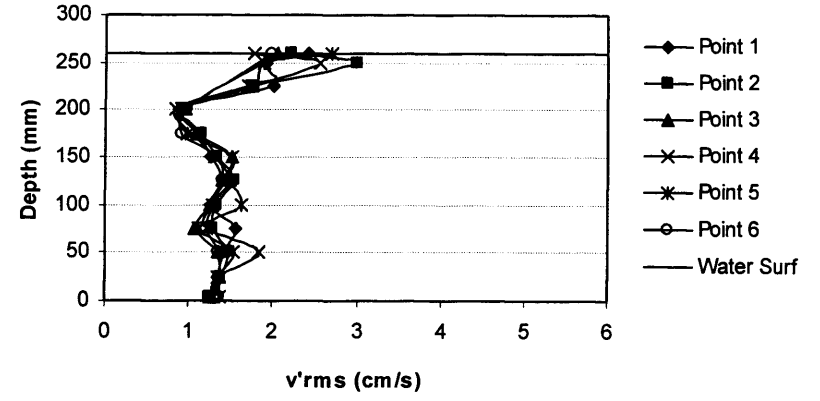

Fig. 5.6 Time-averaged *rms* velocity fluctuations ($v'rms$) [cms^{-1}] for four configurations: (a) high, (b) medium, (c) low, and (d) no vegetation.

(a)

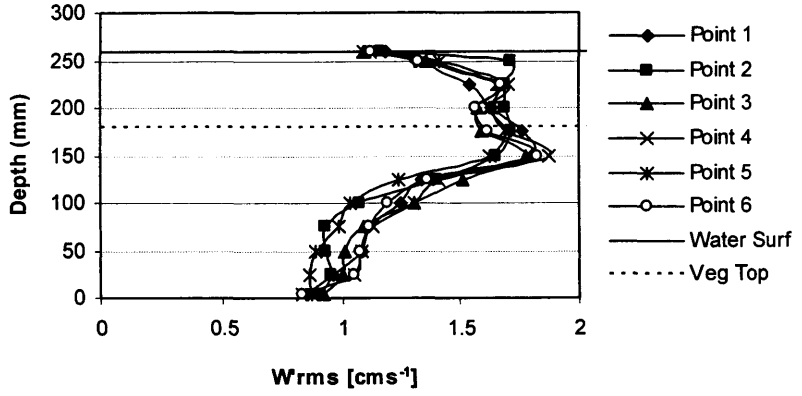

(b)

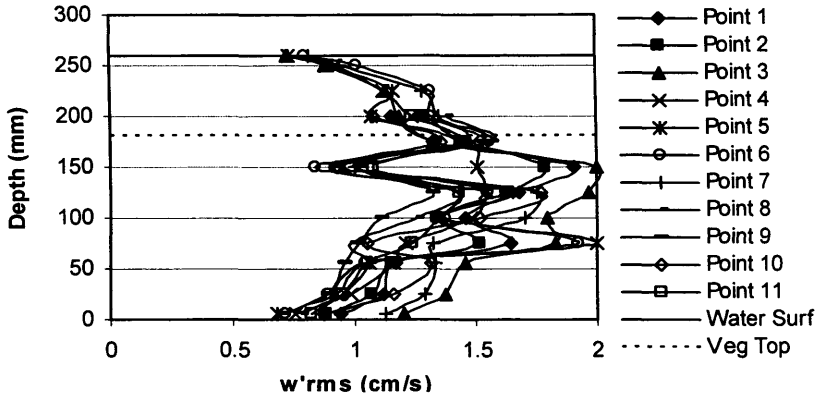

(c)

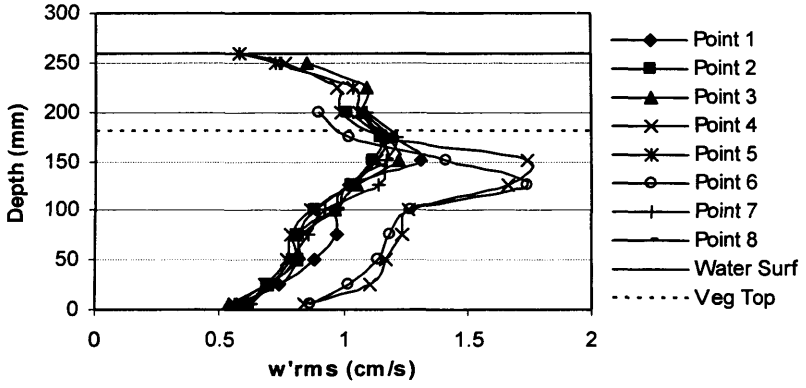

(d)

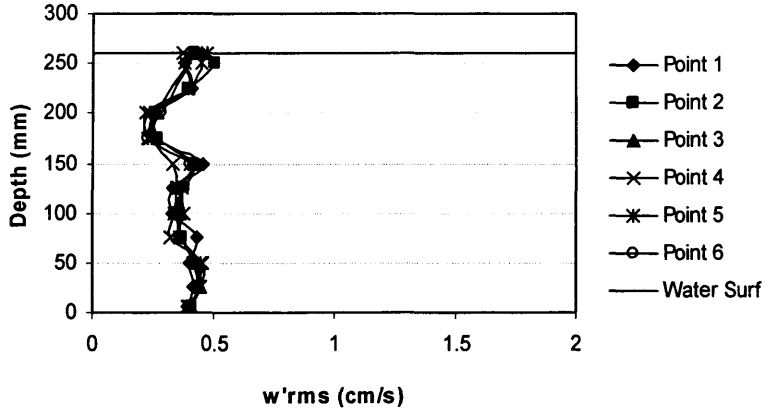

Fig. 5.7 Time-averaged *rms* velocity fluctuations ($w'rms$) [cms^{-1}] for four configurations: (a) high, (b) medium, (c) low, and (d) no vegetation.

5.2.3 Reynolds stresses ($\overline{u'v'}$, $\overline{u'w'}$, $\overline{v'w'}$)

The Reynolds stress components ($\overline{u'v'}$, $\overline{u'w'}$, $\overline{v'w'}$) in fully submerged vegetation flow for all densities and for all measuring locations, at different channel depths have been shown in Figs. 5.8a-d to 5.10a-d. It is clear that with an increase in the vegetation density, variation of the Reynolds stress components increase. Hence, from near the bed to a depth of about 100 mm these parameters remain constant or have a low rate of increase or variation, but for greater elevations the stresses rise steeply and reach a negative peak value at about 150 mm depth (i.e. near the top of the rods). The stresses then reduce again towards the water surface. Thus, more diffusion of the stresses occurs as a result of the staggering effect of the rods, as can be seen particularly in the medium density state. So in medium density some points are high scattering and out of range compared with others. Also, with no vegetation, a minimum rate of the Reynolds stress parameters can be seen and this rate is constant for all measuring points throughout the flow depth.

(a)

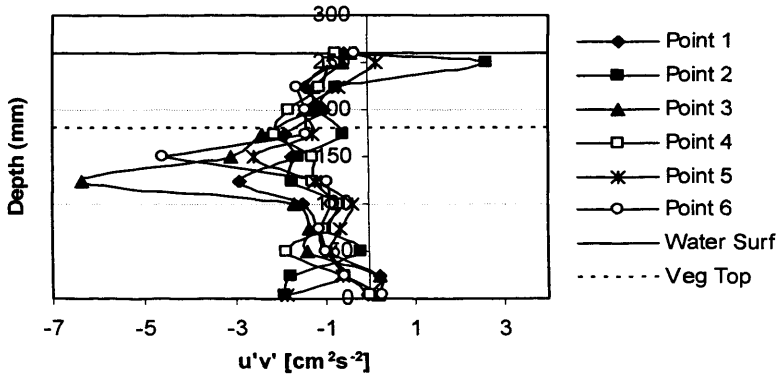

(b)

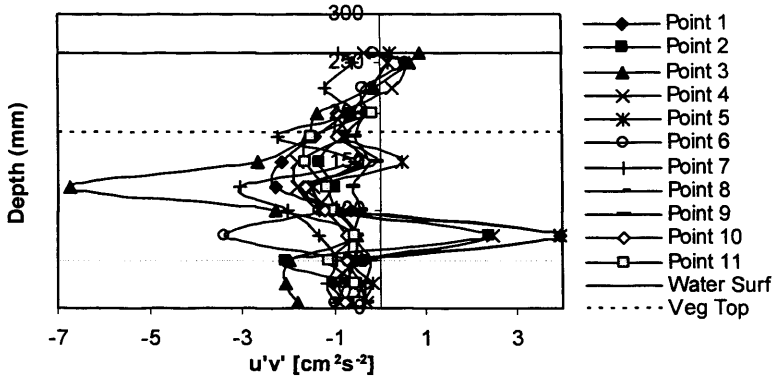

(c)

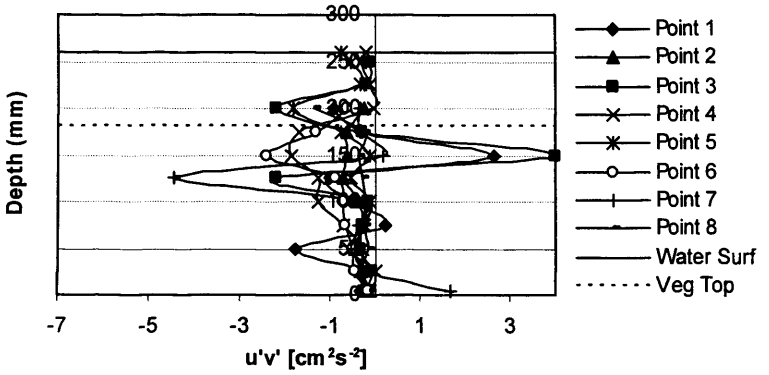

(d)

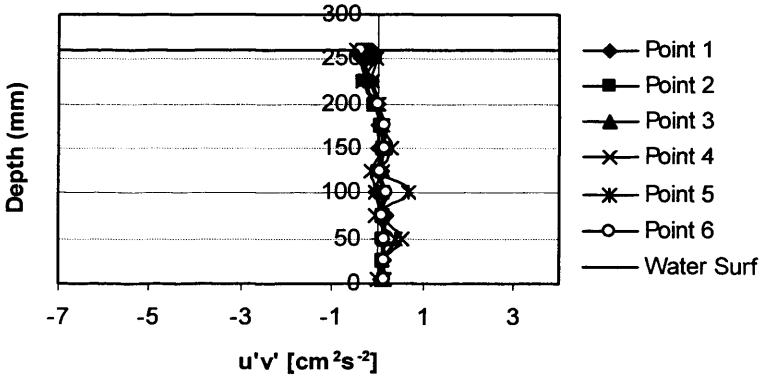

Fig. 5.8 Reynolds stress ($\overline{u'v'}$) [cm^2s^{-2}] for four configurations: (a) high, (b) medium, (c) low, and (d) no vegetation.

(a)

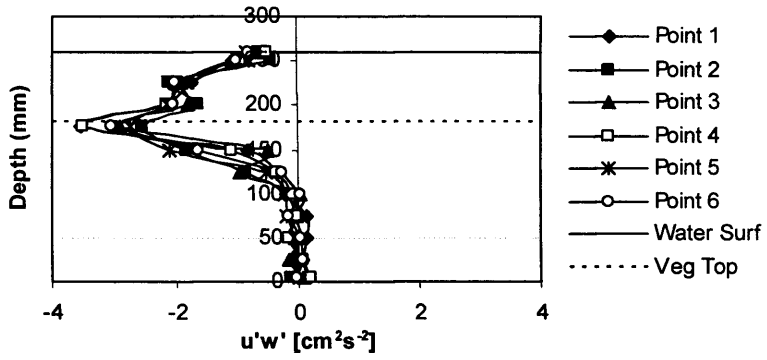

(b)

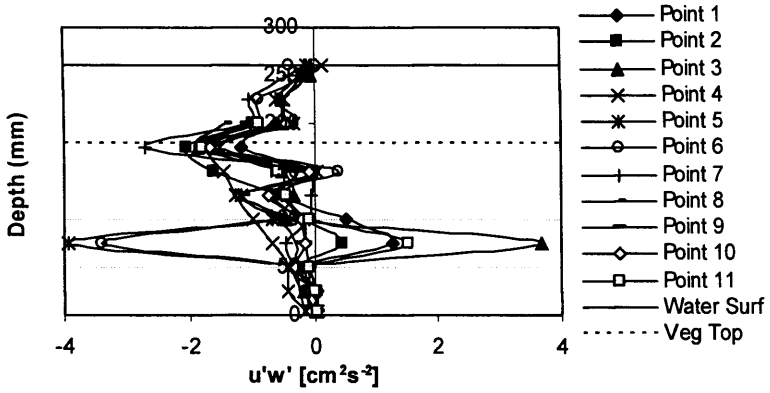

(c)

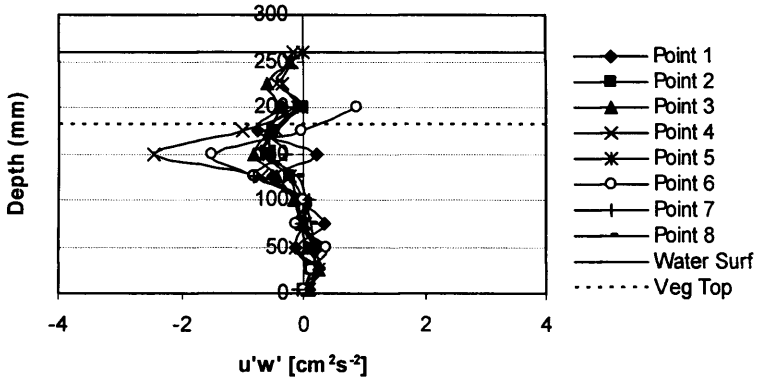

(d)

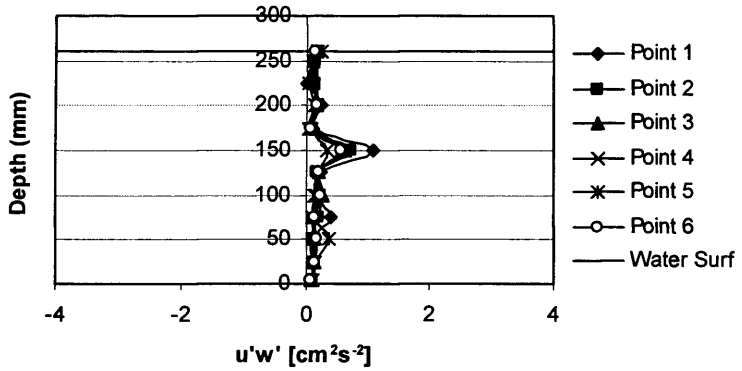

Fig. 5.9 Reynolds stress ($\overline{u'w'}$) [cm^2s^{-2}] for 4 configurations: (a) high, (b) medium, (c) low, and (d) no vegetation.

(a)

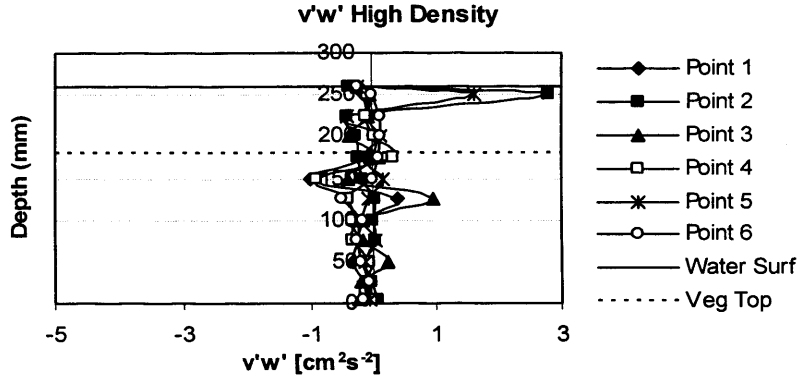

(b)

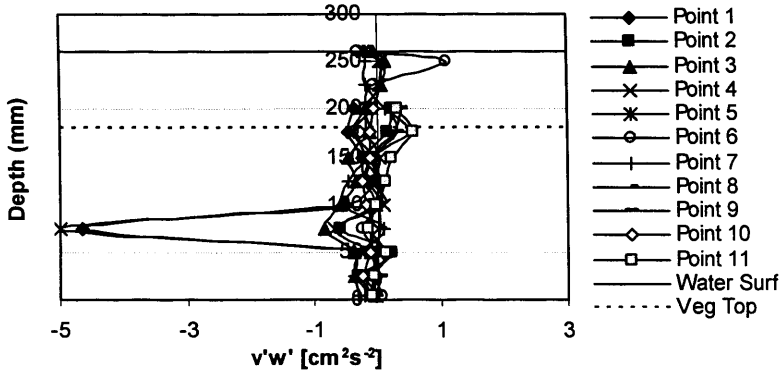

(c)

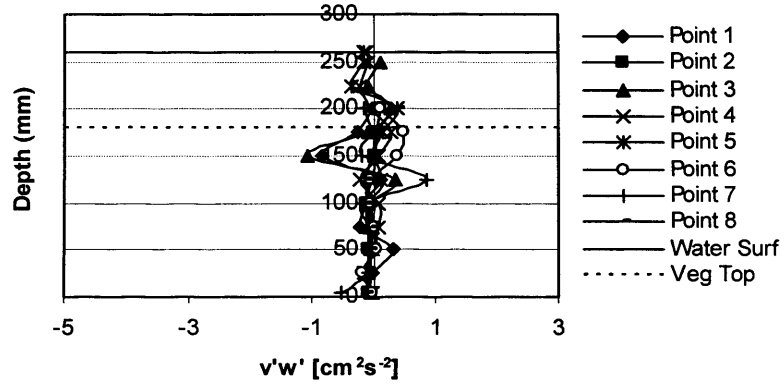

(d)

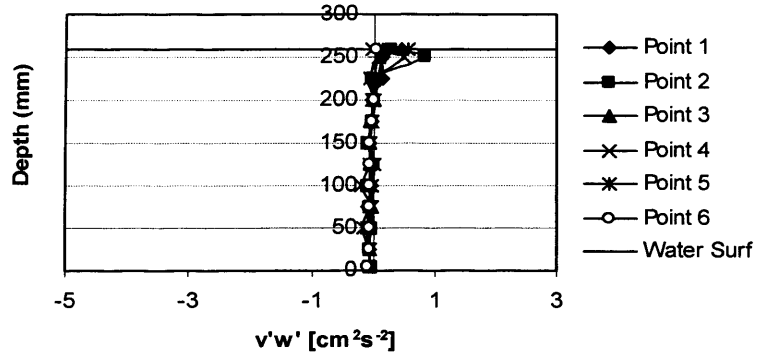

Fig. 5.10 Reynolds stress ($\overline{v'w'}$) [cm^2s^{-2}] for four configurations: (a) high, (b) medium, (c) low, and (d) no vegetation.

5.2.4 Effect of distance behind rods upon flow

As can be seen in Fig. 5.11 for the middle row and the low density state, the measuring points 4A, 4 and 4B have been located at 150, 100 and 50 mm downstream of the rods. Hence, the flow behind the rods is disturbed due to effects of vortex shedding of the rods, creating pronounced wakes and with the wake characteristics decreasing away from the rods.

In the immediate wakes of the rods (i.e. point 4B) the longitudinal velocity is very low, but the other velocity components (i.e. transverse and vertical components) are relatively high in the vegetated zone. Also, the Reynolds stress components are high behind of the rods (i.e. at point 4B). However, as the distance from the rods increases (i.e. towards points 4 and 4A) the longitudinal velocity increases and other components decrease. As can be seen from Figs. 5.12a-c to 5.14a-c, the measurements at all of the points follow approximately the same variation in structure. This means that the parameters are constant or have only a small variation from near the bed up to an elevation of 100 mm and then increase or decrease steeply up to an elevation near the top of the rods and then decrease or increase steeply up to the water surface. Since in the vegetation zone all the measured parameters follow a similar pattern, this confirms that the variations in various parameters (i.e. velocity, Reynolds stresses etc.) are caused directly as a result of the impact of the change in the above parameters on the flow.

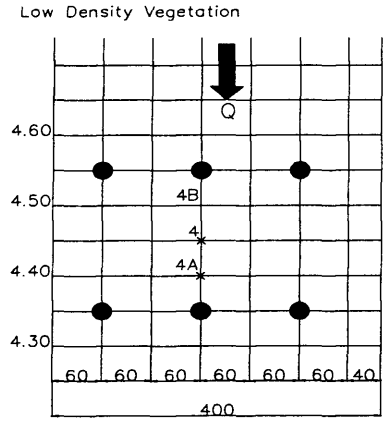

Fig. 5.11 Layout of low density vegetation in simple channel (showing measuring points 4A, 4, 4B).

(a)

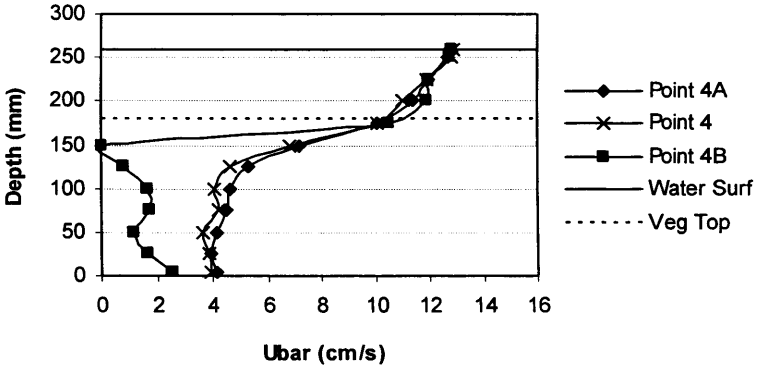

(b)

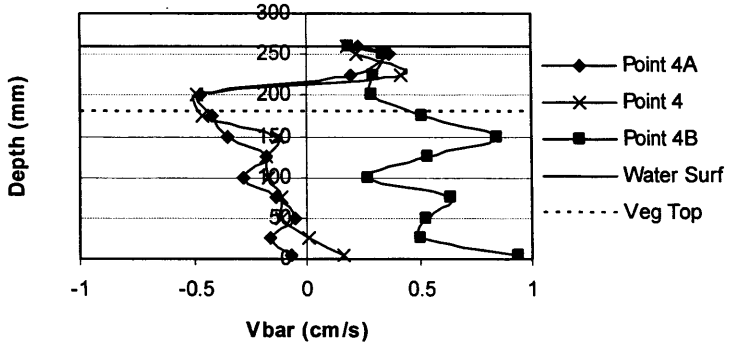

(c)

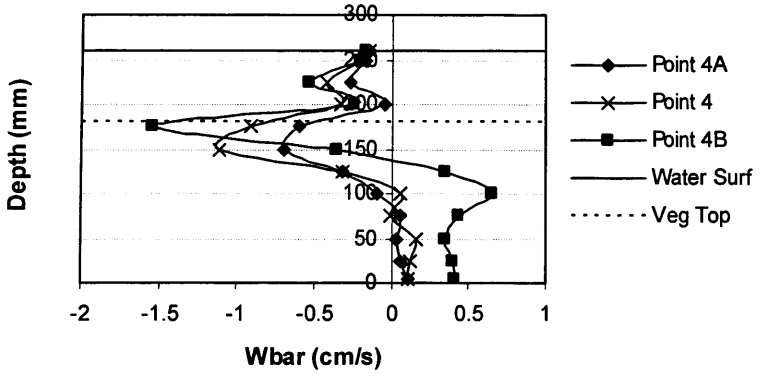

Fig. 5.12 Time-averaged velocity components [cms^{-1}] for low density configuration: (a) longitudinal $\overline{U}$, (b) transverse $\overline{V}$, and (c) vertical $\overline{W}$.

(a)

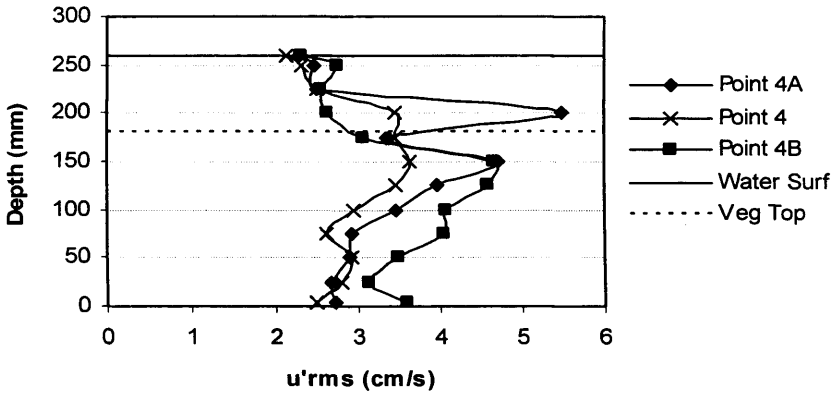

(b)

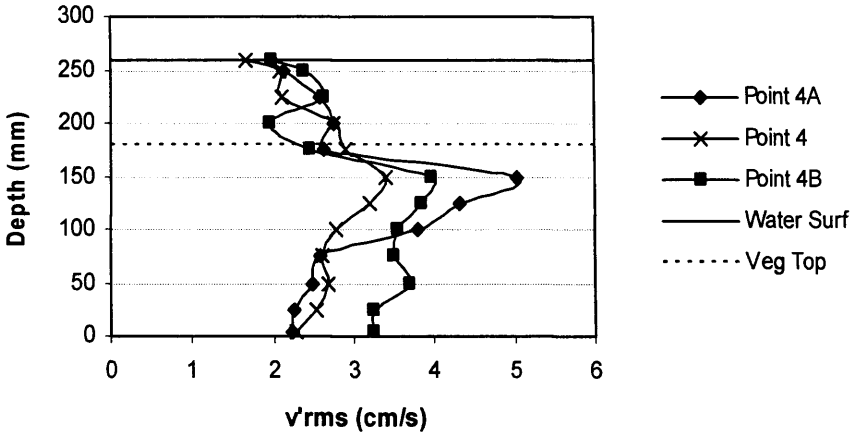

(c)

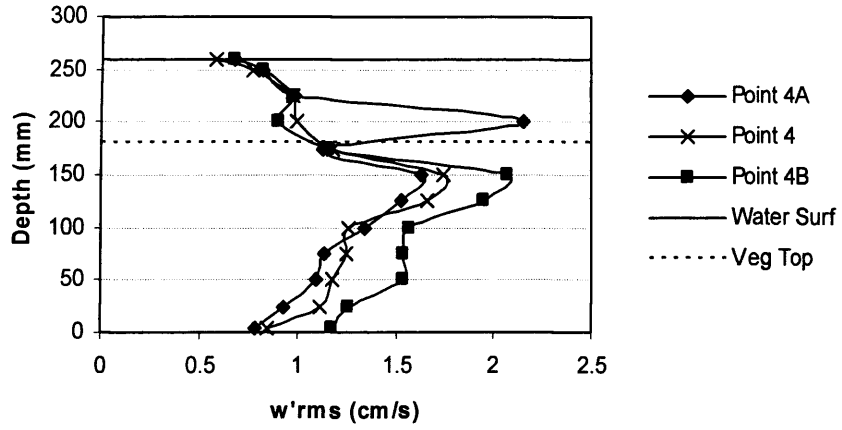

Fig. 5.13 Time-averaged *rms* velocity components [cms^{-1}] for low density configuration: (a) longitudinal $u'rms$, (b) transverse $v'rms$, and (c) vertical $w'rms$.

(a)

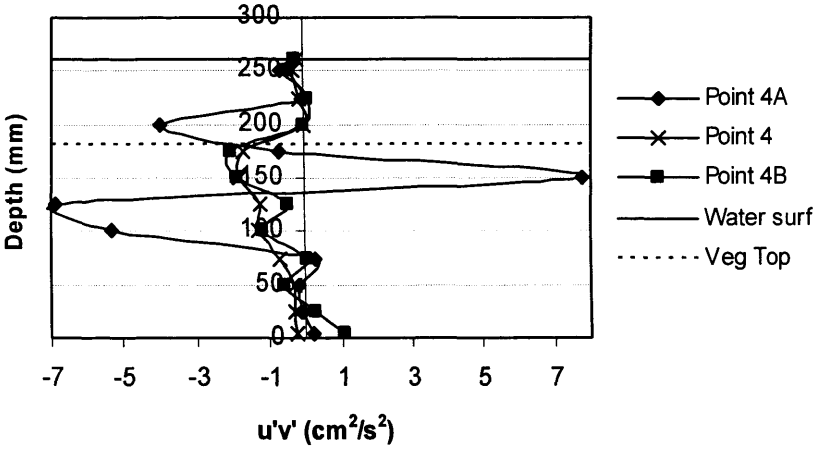

(b)

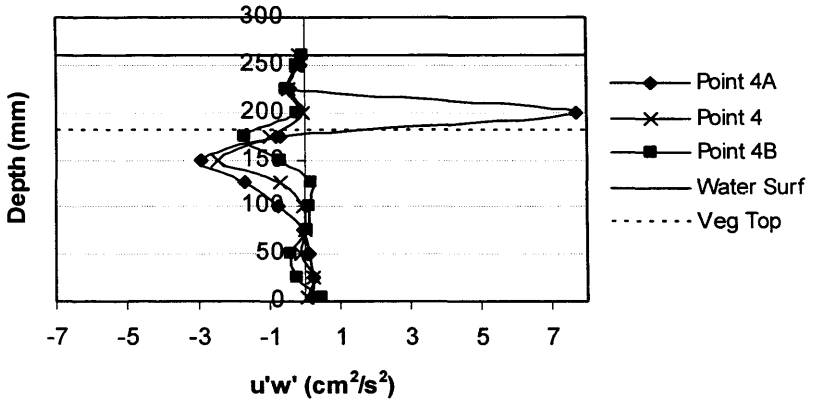

(c)

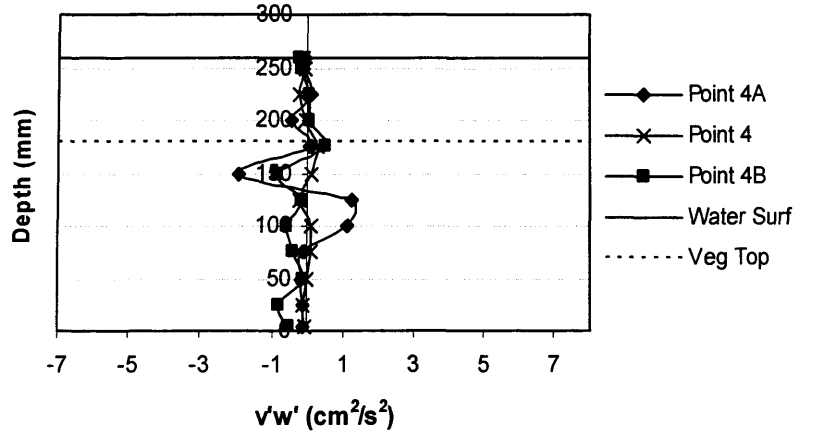

Fig. 5.14 Reynolds stress components [cm^2s^{-2}] for low density configuration: (a) longitudinal $\overline{u'v'}$, (b) transverse $\overline{u'w'}$, and (c) vertical $\overline{v'w'}$.

5.3 Fully emergent rigid vegetation flow (rod height = 300 mm)

As outlined in section 5.2, the same tests were undertaken for the same densities, but emergent vegetation condition where rod height was 300 mm.(Fig. 5.15). Firstly, it was found that the impact of the emergent rods on the water elevation relative to the partially depth rods was negligible. The velocity measuring sites for the high density rods were 5 mm above the bed and then 25 mm increments to the water surface (i.e. at 5, 25, 50, 75, 100, 125, 150, 175, 200, 225, 250 and 260 mm). However, for the medium and low density configuration, the measurements were taken at 5 mm above the bed and then at increments of 50 mm to the water surface (i.e. at 5, 50, 100, 150, 200 and 250 mm).

(a)

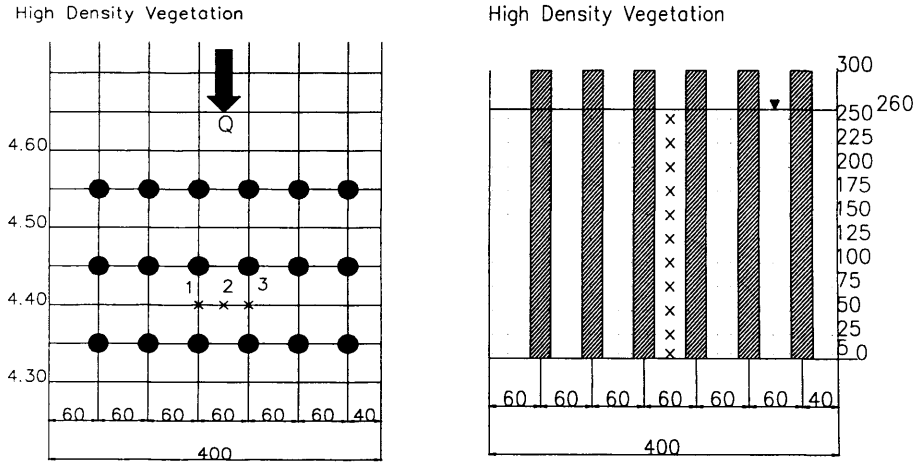

(b)

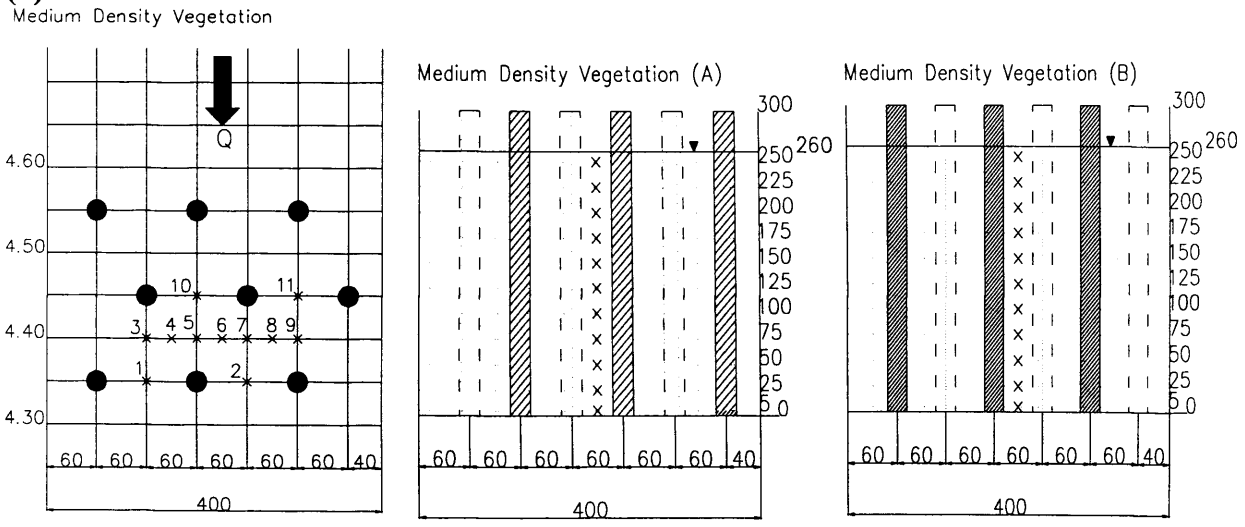

(c)

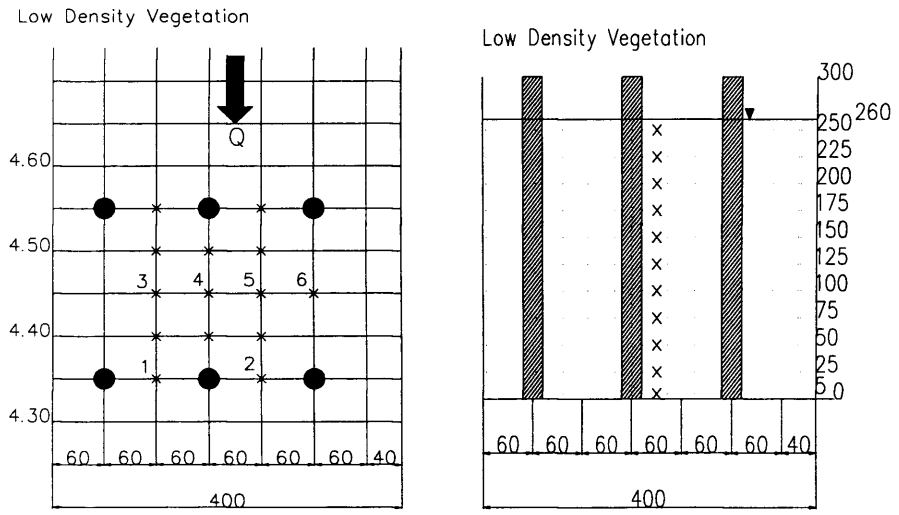

(d)

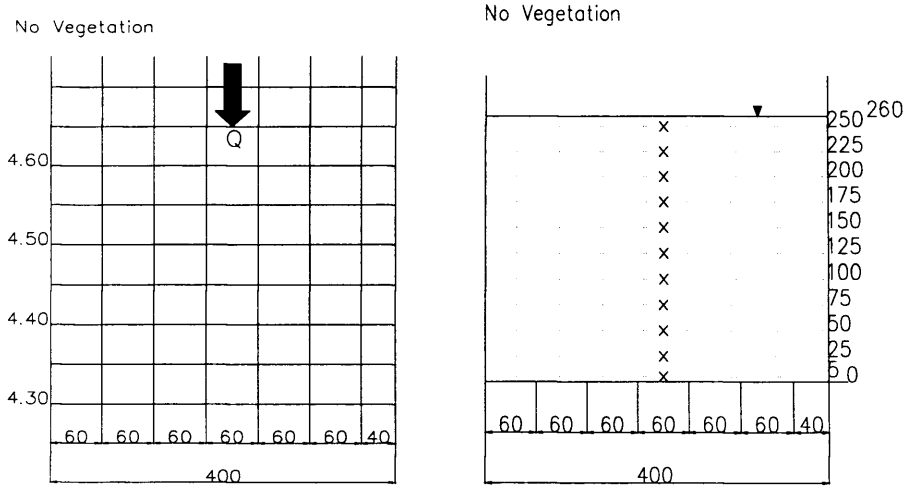

Fig. 5.15 Layout for the simple channel for the fully emergent rods, showing the location of the measuring points for the vertical velocity profiles at four configurations: (a) high, (b) medium, (c) low, and (d) no vegetation.

5.3.1 Time-averaged velocity components ($\overline{U}$, $\overline{V}$, $\overline{W}$)

The effects of the emergent vegetation for the various densities are outlined herein for the velocity components in the simple channel (see Figs. 5.16a-d to 5.18a-d).

a) Time-averaged longitudinal component of velocity ($\overline{U}$)

For the emergent vegetation state then, due to the vegetation penetrating from the bed to the water surface for all vegetation densities, the value parameters remained fairly constant or involved only small variations of the velocity components from the bed to the water surface at all measuring points (Fig. 5.16a-d). Also the effects of vortex shedding were observed for the submerged conditions near the vegetation tops, whereas for the emergent conditions the vorticity was only observed below the water surface. This effect was exacerbated by the staggered nature of the rods, and it was found that for a medium density and a water depth of 200 mm, then the velocity steeply reduced by 2 to 3 cm/s and for low density vegetation only a small reduction in the velocity, as seen in Fig. 5.16b-c. For the no vegetation case the velocity increased normally from the bed to the water surface.

The measured time-averaged velocities at the different measuring sites, for the different densities showed clear differences in the velocity. For the high density configuration, then the velocity for points behind the rods was about 3 cm/s, but for the points between the rods then the velocity were about 7 cm/s. For the medium density rods, the velocity was about 2.5 cm/s behind the rods and about 6 cm/s, in between the rods. For the low density configuration of the rods the velocity was about 4 cm/s and 7 cm/s behind and in between the rods respectively. For all densities the velocity profiles behind and in between the rods were found to be significantly different, as shown in Fig.5.16.

The velocity in all vegetation configurations for all points was almost constant from the bed to near the water surface except for the medium density configuration, where the staggering effect caused the velocity to decrease by about 2 to 3 cm/s from an elevation of about 200 mm above the bed and increase again to the surface and to approximately the same velocity near the bed (Fig. 5.16b). For the low density configuration, a small reduction in the velocity again occurred at

the same elevation (i.e. 200 mm) (Fig. 5.16c). For no vegetation, the velocity started at about 5.5 cm/s near the bed and increased steadily towards the water surface and reached to 8.5 cm/s near the surface (Fig. 5.16d).

(a)

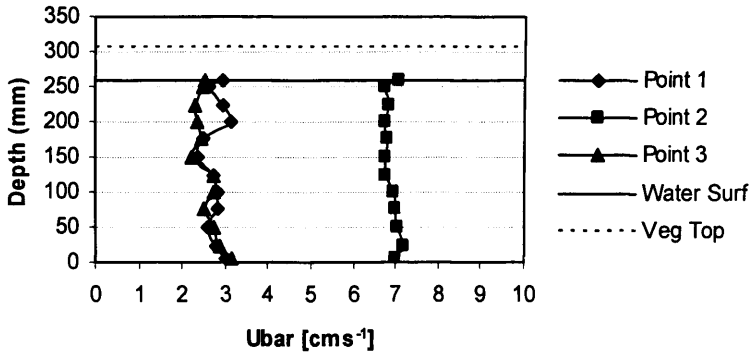

(b)

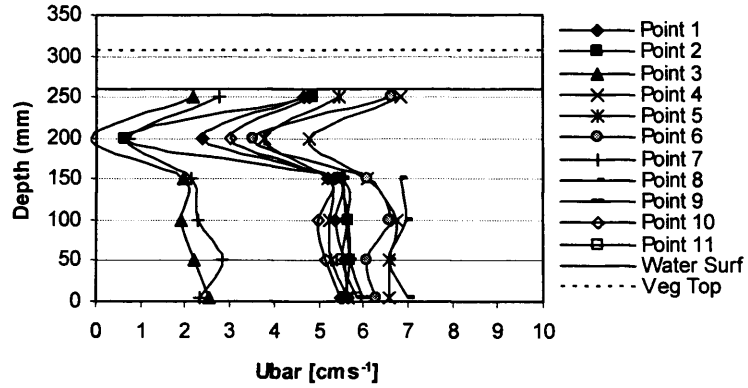

(c)

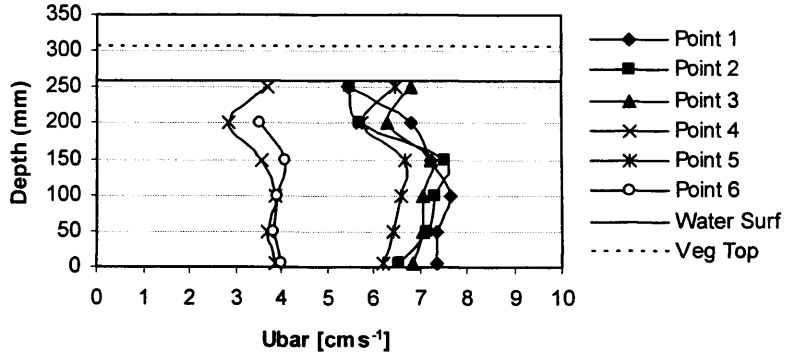

(d)

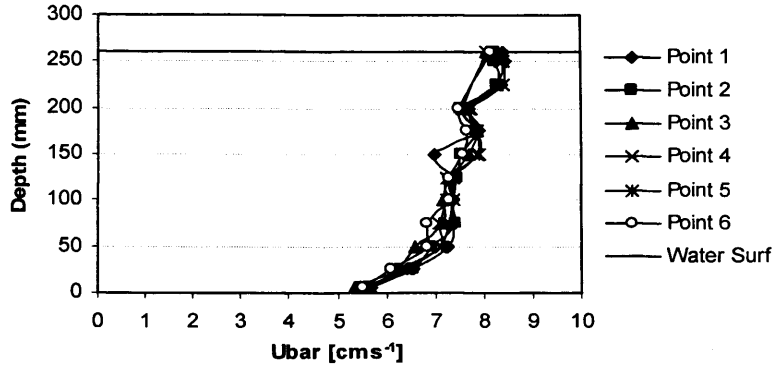

Fig. 5.16 Time-averaged longitudinal velocity ($\overline{U}$) [cms^{-1}] for four configurations: (a) high, (b) medium, (c) low, and (d) no vegetation.

b) Time-averaged transverse component of velocity ($\overline{V}$)

Figure 5.17a-d shows the transverse velocity components and profiles for all points in the vegetation zone. The transverse velocity component from close to the bed to the surface was almost constant or showed little variation, for all densities.

For the emergent state, it was observed that at the points in between the rods the longitudinal velocity ($\overline{U}$) was maximum and behind the rods the velocity was minimum. For $\overline{V}$ the opposite occurred, i.e. points with a high $\overline{U}$ had a low $\overline{V}$ and vice- versa (see Figs. 5.16a-b and 5.17a-b). Also the transverse velocity ($\overline{V}$) in no vegetation state at all points was close to zero with a minimal dispersion from bed to water surface (Fig. 5.17c-d).

(a)

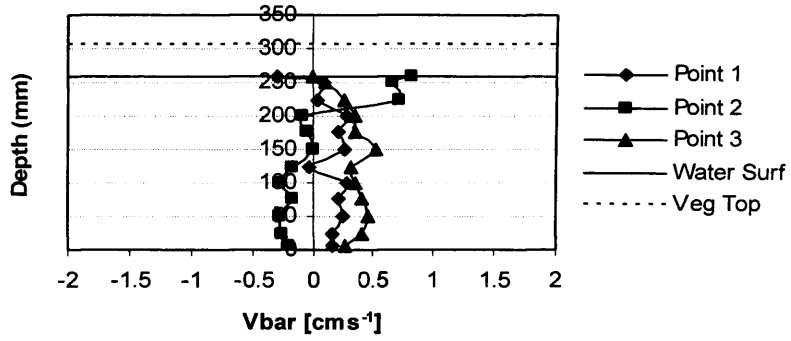

(b)

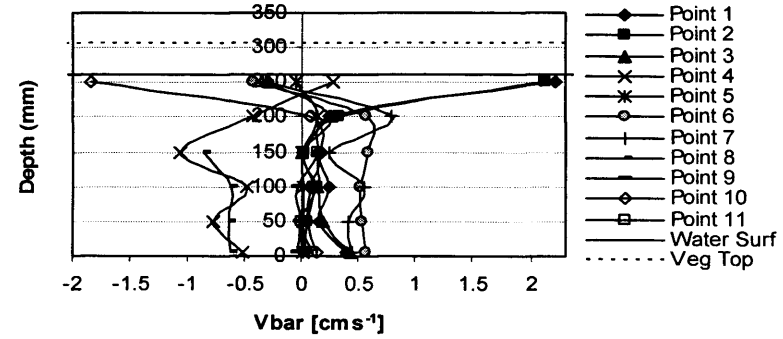

(c)

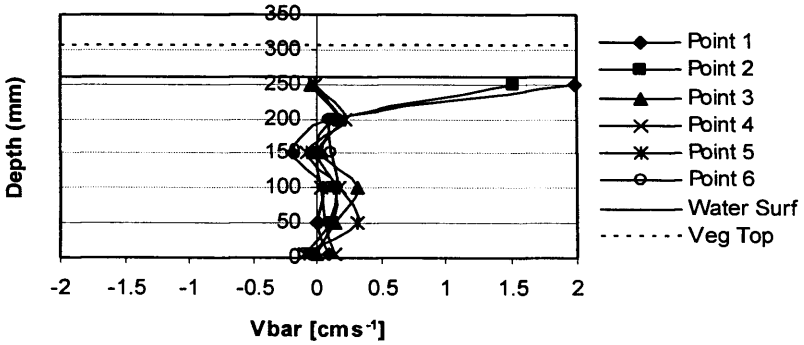

(d)

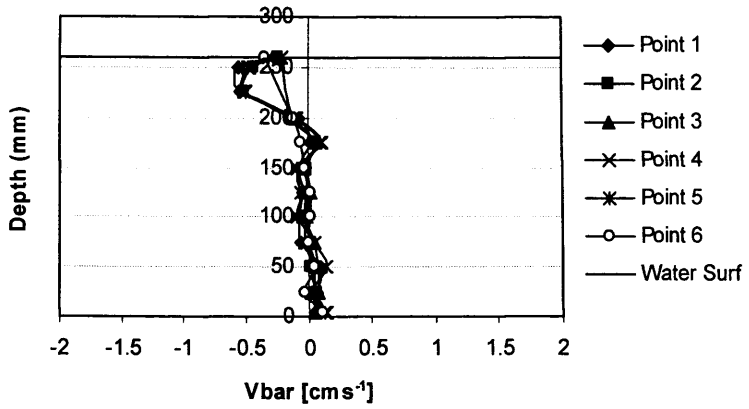

Fig. 5.17 Time-averaged transverse velocity ($\overline{V}$) [cms^{-1}] for four configurations: (a) high, (b) medium, (c) low, and (d) no vegetation.

c) Time-averaged vertical component of velocity ($\overline{W}$)

Fig. 5.18a-d shows the vertical velocity component for some of the point locations, in between and behind the rods, for the emergent configuration. As shown, vertical velocity is effectively zero or negative for the normal flow, but at critical locations, such as the transition regions or behind the rods, the velocity is positive. Also, for the vertical velocity at all locations from near the bed to the water surface the changes in magnitude were small, except near the bed and the water surface where the effects of bed roughness and vortex shedding respectively dominated. For the case with no vegetation, the vertical velocity decreased from bed to 100 mm and then increased towards the surface.

As for changes in $\overline{V}$, it was found that the vertical velocity $\overline{W}$ changed in a reverse manner with respect to $\overline{U}$, so that at points where $\overline{U}$ was a maximum then $\overline{W}$ was a minimum and voice-versa. These velocities can be seen in Figs. 5.16a-c and 5.18a-c at points 2 for the high density, 3 and 7 for medium density, and 4 and 6 for low density configurations.

(a)

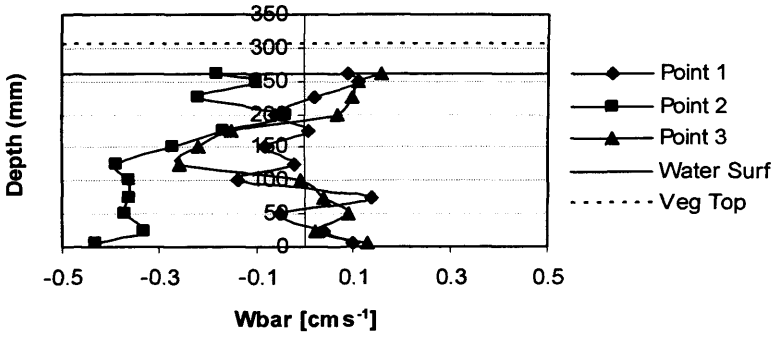

(b)

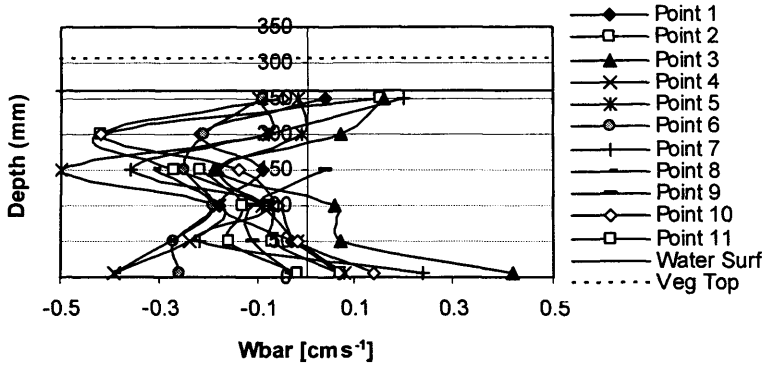

(c)

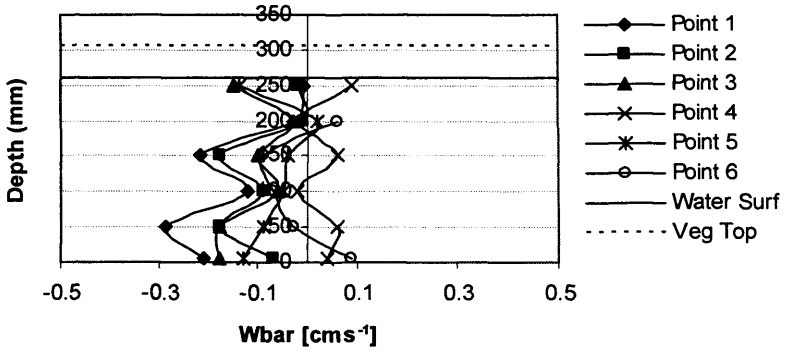

(d)

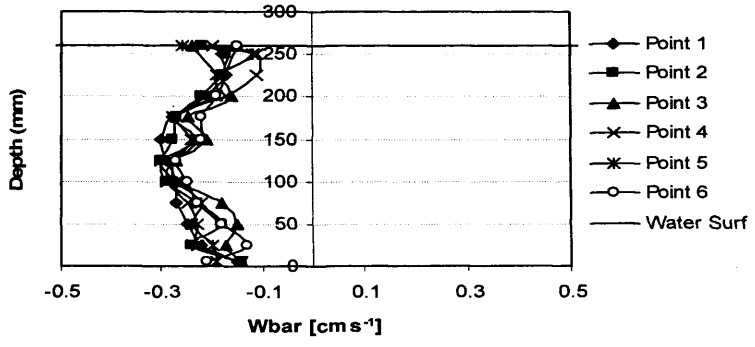

Fig. 5.18 Time-averaged vertical velocity ($\overline{W}$) [cms^{-1}] for four configurations: (a) high, (b) medium, (c) low, and (d) no vegetation.

5.3.2 Time-averaged *rms* velocity fluctuations component (*u'rms*, *v'rms* *w'rms*)

Figures 5.19a-d to 5.21a-d show the time-averaged velocity fluctuating components, where it can be seen that velocity fluctuations for the longitudinal, transverse and vertical components increase, with increasing rod density. However, due to the staggering effect for the medium density there was little difference in the velocity components as compared to these measured for the high density. For all densities, and all fluctuating components, it was found that for all points the velocity components were nearly constant from near the bed to the water surface, except for the medium and low density configurations where the velocity increased sharply from an elevation of 150 mm above the bed to reach at maximum value at an elevation of about 200 mm above the bed. The velocity then decreased sharply towards the water surface, reaching a velocity approximately equal to that at an elevation of 150 mm above the bed.

Also, for the time averaged *rms* velocity fluctuation (i.e. *u'rms*) at all points the velocity profiles were similar in form with the least dispersion occurring for all density configurations (Fig. 5.19a-d). For the *v'rms* and *w'rms* fluctuating velocity components, although the profiles were similar for all of the densities, the magnitudes were different for the velocity locations. The results showed that the points between the rods had minimum values and points behind the rods had maximum values for *v'rms* and *w'rms* . For the case of no vegetation, the fluctuating components at all points had almost the same profiles from the bed towards the water surface (Figs. 5.20a-d and 5.21a-d).

(a)

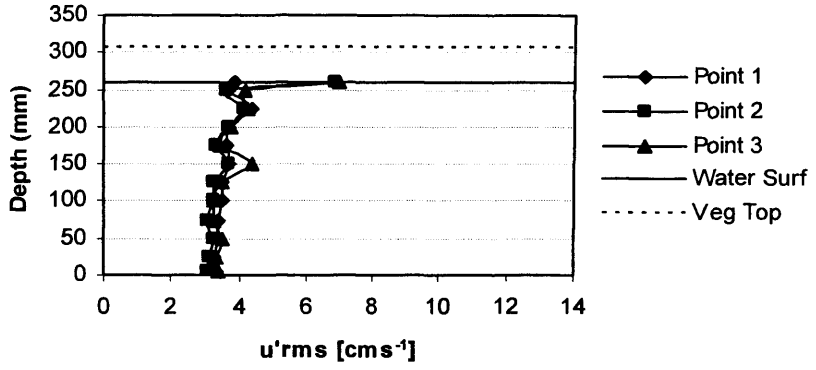

(b)

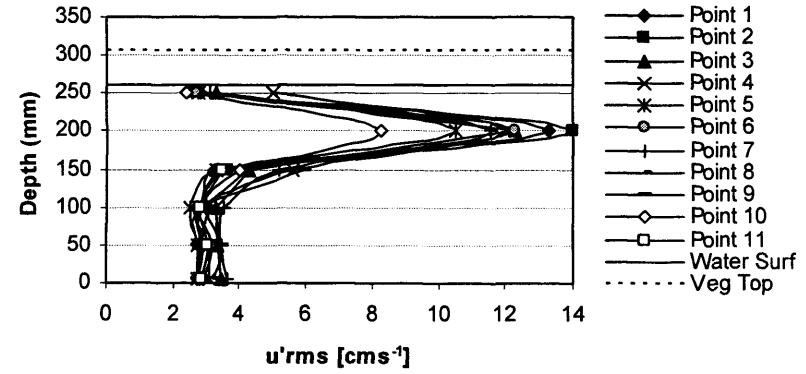

(c)

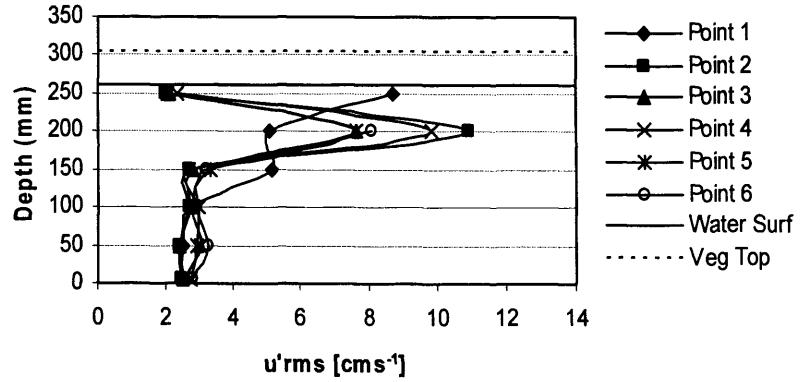

(d)

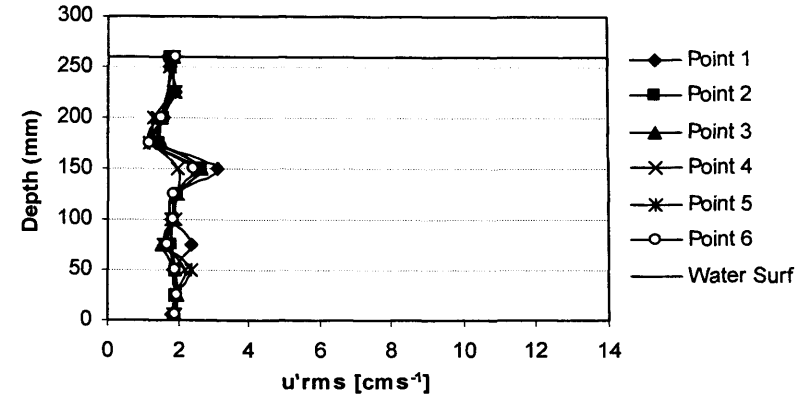

Fig. 5.19 Time-averaged *rms* velocity fluctuations (*u'rms*) [cms^{-1}] for four configurations: (a) high, (b) medium, (c) low, and (d) no vegetation.

(a)

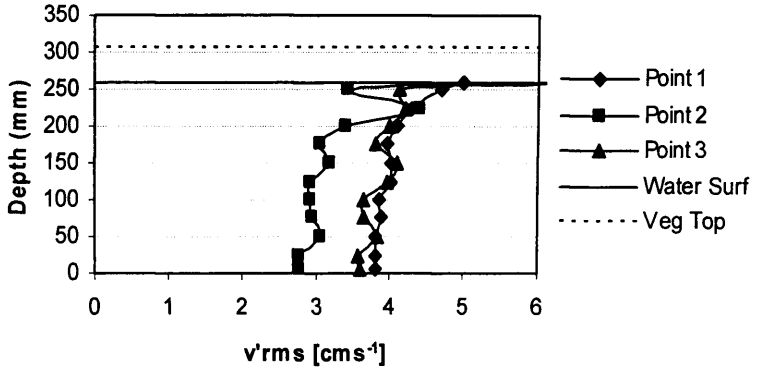

(b)

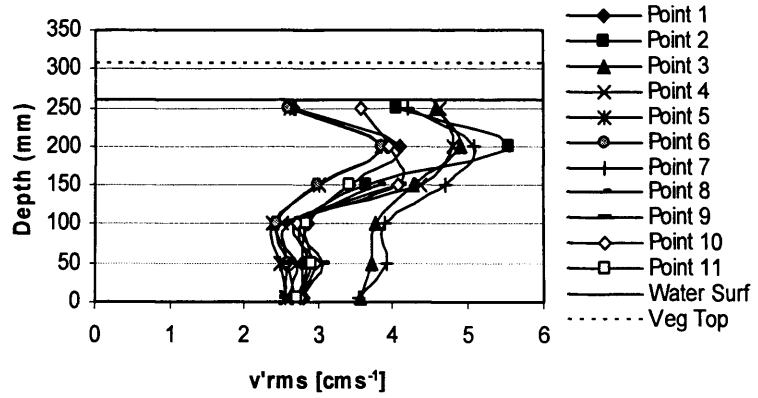

(c)

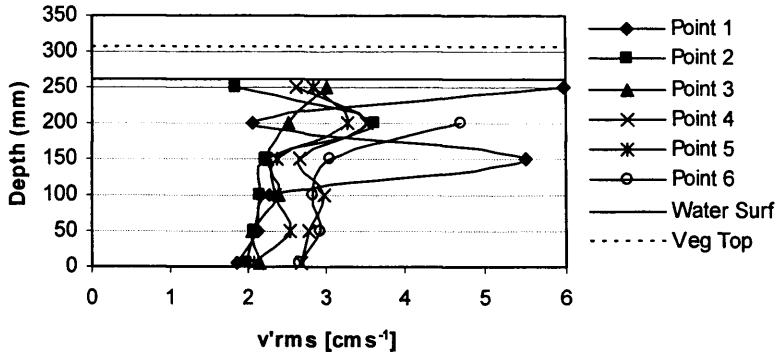

(d)

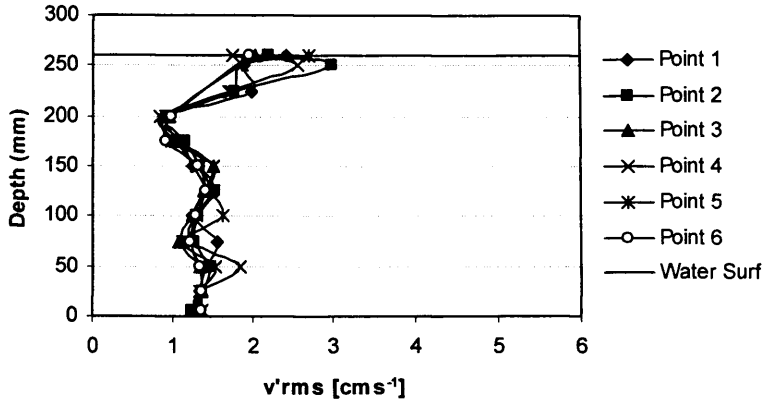

Fig. 5.20 Time-averaged *rms* velocity fluctuations ($v'rms$) [cms^{-1}] for four configurations: (a) high, (b) medium, (c) low, and (d) no vegetation.

(a)

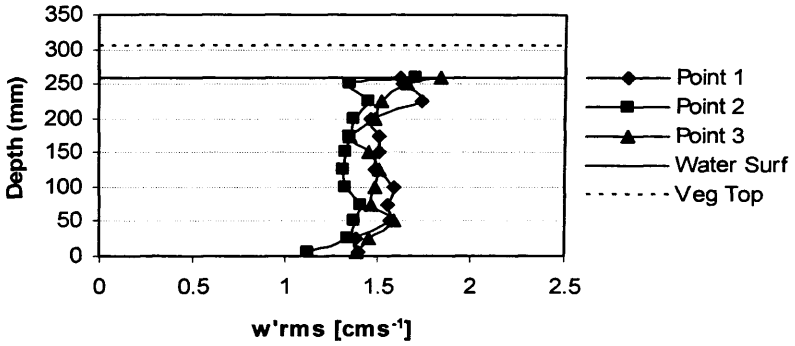

(b)

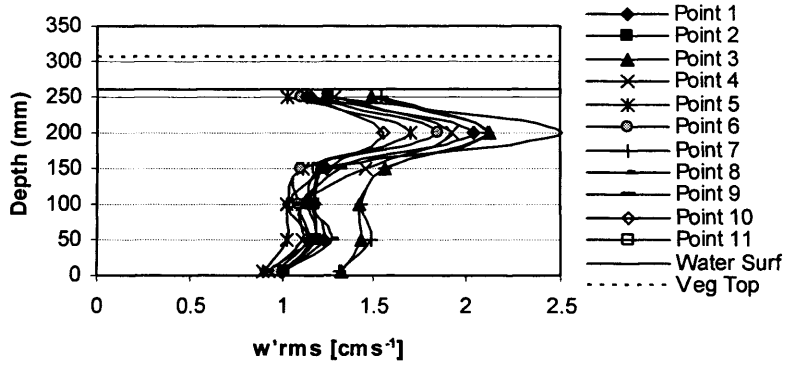

(c)

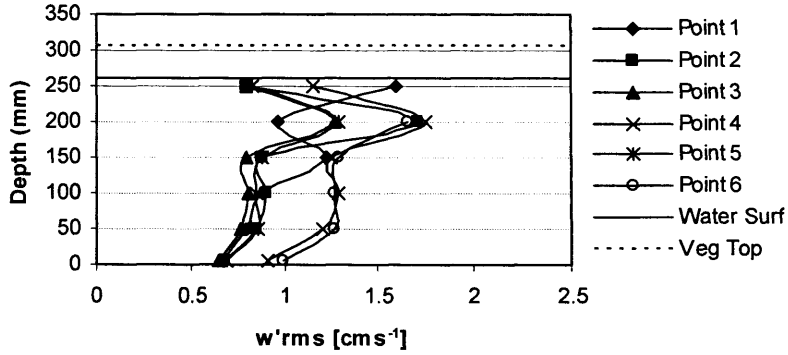

(d)

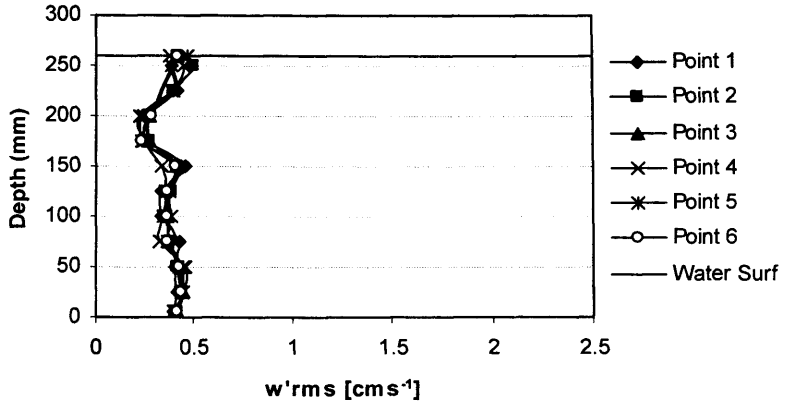

Fig. 5.21 Time-averaged *rms* velocity fluctuations ($w'rms$) [cms^{-1}] for four configurations: (a) high, (b) medium, (c) low, and (d) no vegetation.

5.3.3 Reynolds Stresses ($\overline{u'v'}$, $\overline{u'w'}$, $\overline{v'w'}$)

The Reynolds stress components in fully emergent vegetation flow for all densities and at all of the points where measurements were taken over the channel depth are considered (Figs. 5.22a-d to 5.24a-d). Thus the results showed that with an increase in density, the Reynolds stress components increased with negative sign at all of the points. As can be see in the figures from the bed to an elevation of about 150 mm they remained constant or had a very small rate of variations at all locations, but above an elevation of about 150 mm stress magnitudes increased or decreased steeply and reached a peak at about 200 mm elevation and then returned again to a similar stress magnitude near the surface as that near the bed. For the no vegetation case a minimum Reynolds stress component value occurs, as can be seen from the graphs, with a constant value occurred throughout the flow depth. Also the effect of staggering with high scattering is observed in the medium density vegetation configuration as variations are very high compared to other configurations.

In addition, the magnitude of the Reynolds stress components (i.e. $\overline{u'v'}$, $\overline{u'w'}$, $\overline{v'w'}$) at various measuring points, were approximately similar in profile to the velocity fluctuation components ($u'rms$, $v'rms$ $w'rms$). This means that for the points between the rods the stress magnitudes are a minimum and the Reynolds stresses behind the rods are maximum.

(a)

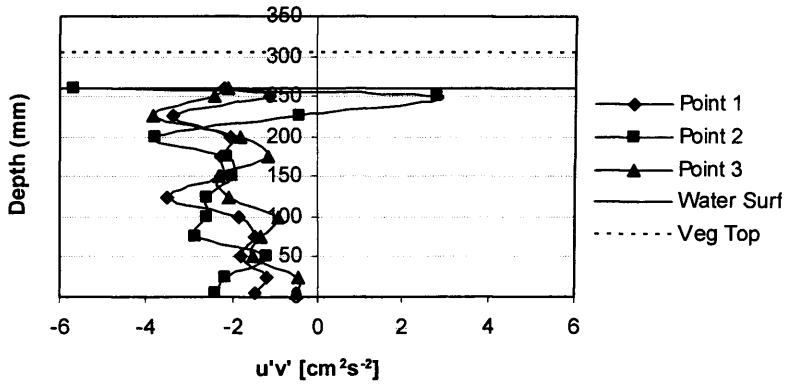

(b)

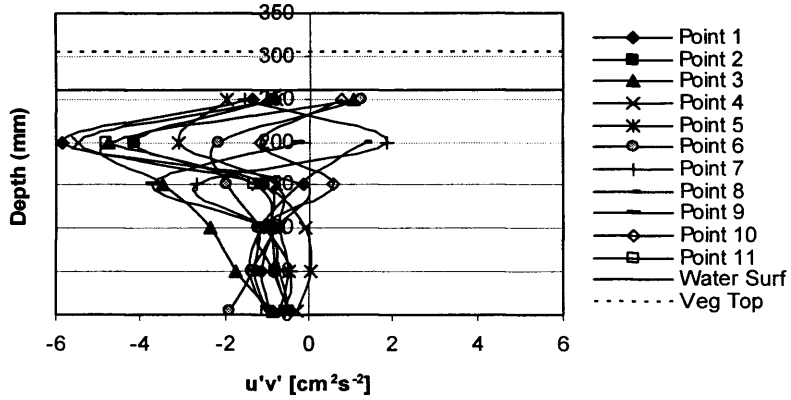

(c)

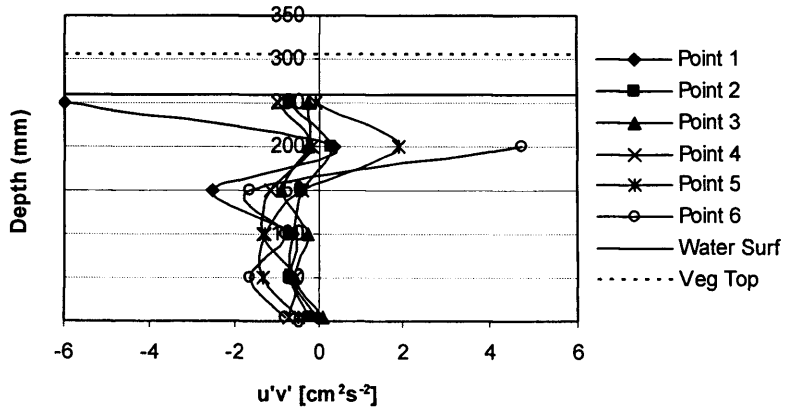

(d)

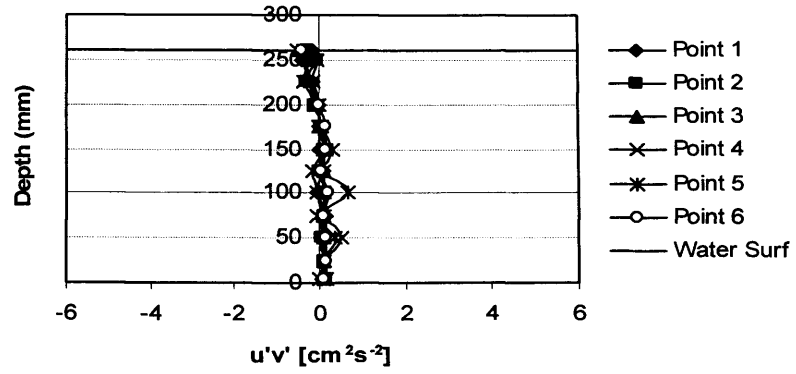

Fig. 5.22 Reynolds stress ($\overline{u'v'}$) [cm^2s^{-2}] for four configurations: (a) high, (b) medium, (c) low, and (d) no vegetation.

(a)

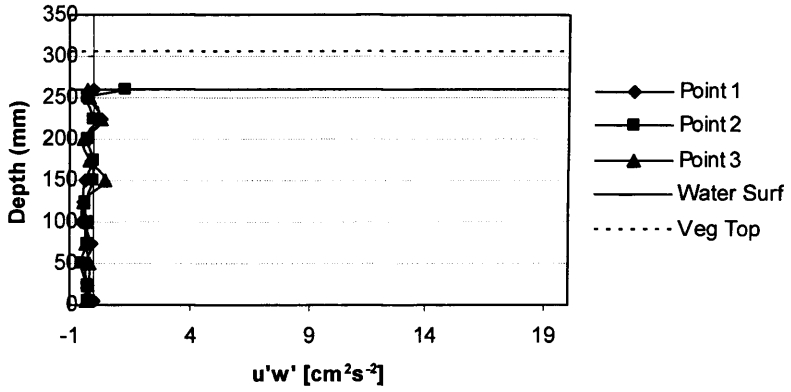

(b)

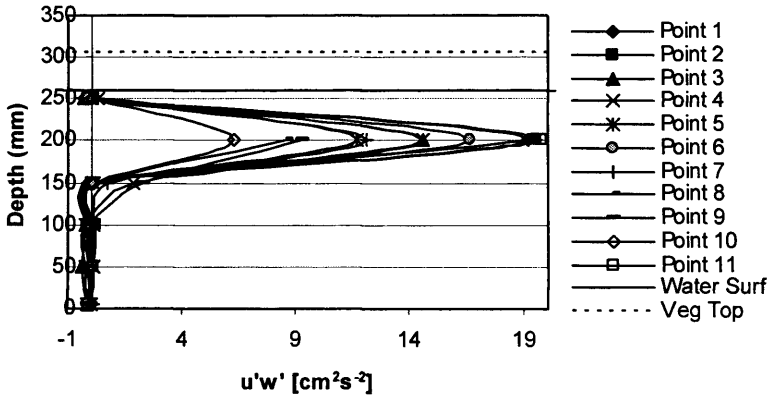

(c)

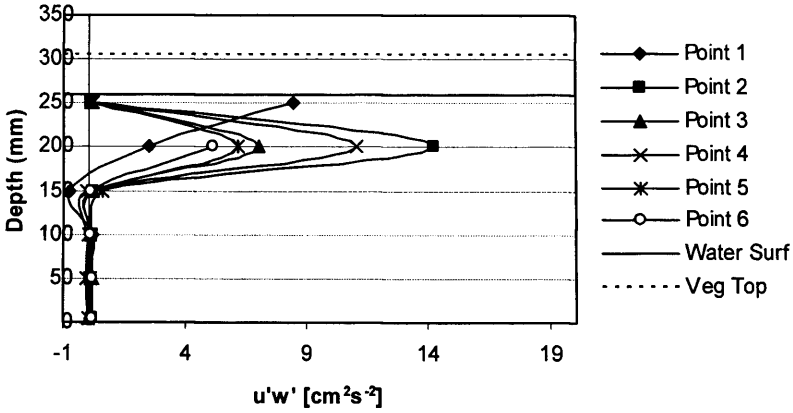

(d)

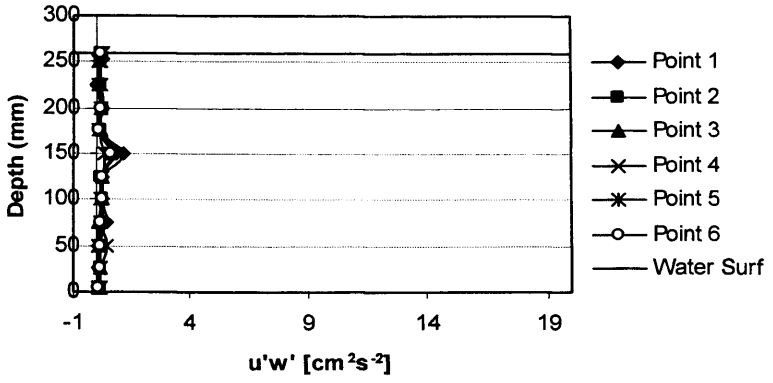

Fig. 5.23 Reynolds stress ($\overline{u'w'}$) [cm^2s^{-2}] for four configurations: (a) high, (b) medium, (c) low, and (d) no vegetation.

(a)

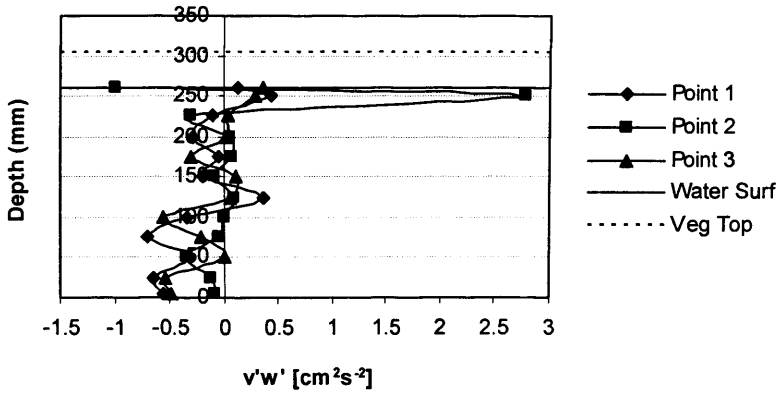

(b)

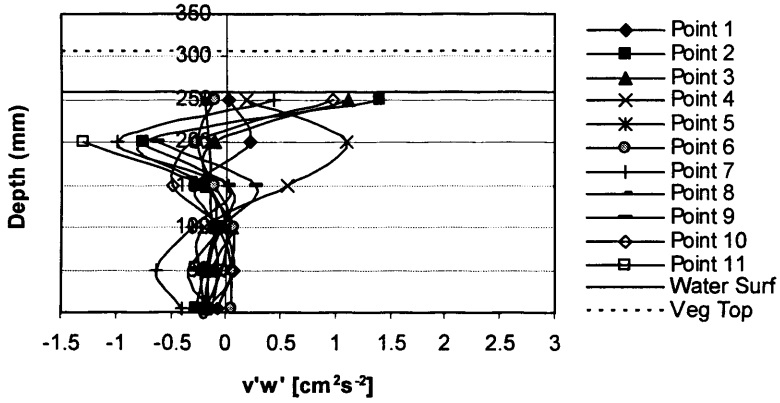

(c)

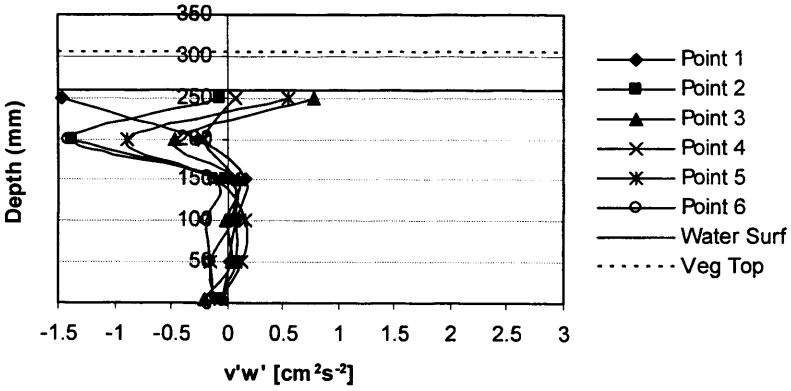

(d)

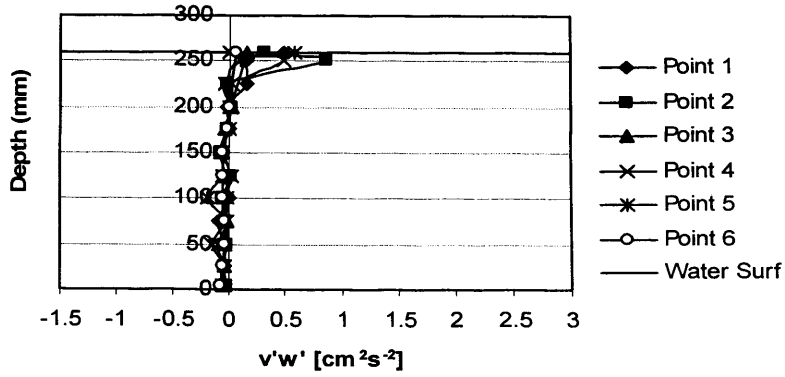

Fig. 5.24 Reynolds stress ($\overline{v'w'}$) [cm^2s^{-2}] for four configurations: (a) high, (b) medium, (c) low, and (d) no vegetation.

5.4 Further experiments

From the results shown herein it is observed that for the submerged condition there is a high variation in the velocity in the region near the top of the rods. This is due to the trailing vortex occurring in the region near the top of the rods, i.e. at an elevation of 150 mm. The effect of these variations at some locations, and for some densities, was not observed near the water surface. This phenomenon also significantly changes with different rod densities and at different locations. Although for the emergent rod scenarios no significant trailing vortex effect was identified near the top of the rods, in some cases the variation in the velocity magnitude near the water surface was observed to be high in comparison with the results for the submerged states and the higher depths (i.e. 200 mm elevation above the bed). These variations were observed more for the medium and low density configurations.

Despite the general trends outlined herein, there were still some velocity variations observed which required a large number of experiments to be undertaken, which was beyond the objectives of the current study. In analysing and discussing the reasons for these velocity variations, more information is needed of the variations, which again would require more experiments at different locations and densities.

In this chapter details are given of experiments undertaken in the narrow rectangular channel, with velocity measurements being taken in between and behind the rods for four density configurations, and for the submerged and emergent cases. Results show that for the submerged vegetation case, when the vegetation density increases, the velocity decreases within the vegetation zone, and the flow accelerated and diverted towards the upper region of the flow. The vegetation density controlled the magnitude of these effects. Thus, the flows were characterized by a highly turbulent region near the top of the rods. For the emergent vegetation state, due to the vegetation penetrating from the bed to the

water surface for all vegetation densities, the various velocity parameter values remained fairly constant or varied only slightly from the bed to the water surface and at all of the measurement points. It was observed that at the points in between the rods, the longitudinal velocity ($\overline{U}$) was at its maximum, and behind the rods the velocity was a minimum. For the $\overline{V}$ and $\overline{W}$ velocity components the reverse occurred. Also the velocity fluctuations and Reynolds stress components for the points in between and behind the rods were a minimum and maximum respectively.

CHAPTER 6
WIDE RECTANGULAR CHANNEL

6.1 Introduction

Determination of the relationship between the stage and discharge characteristics in channels is generally the most significant parameter in river engineering studies. This relationship enables the flow resistance and conveyance capacity to be understood, especially when vegetation affects these parameters. Although the bed resistance equations, such as the Darcy-Weisbach, Chézy, and Manning equations, have been used extensively for calculating flow resistance, these equations are not in their general form suitable for vegetated channels. In the original development of the Manning equation it was not regarded as directly applicable to vegetated flows as it was found to vary with velocity and depth. The effect of vegetation on channel flows is significant, since vegetation includes an additional drag resistance to the flow. Hence the vegetation normally causes a loss in the flow energy which can be several times larger than the bed resistance. Hence, significant limitations exist in applying conventional bed resistance formulae for vegetated channels.

In recent years, many investigations have been carried out on the effects of vegetation on the flow in natural vegetated channels. Most of these studies have involved solving the problem by extending the current bed resistance equations to account for the effects of vegetation based on including new or empirically determined resistance coefficients. Unfortunately, due to their empirical nature, these studies have not provided suitable resistance formulae applicable for a wide range of vegetation characteristics. Recently, an increase in the awareness of the importance of the ecological and environmental effects of aquatic vegetation has encouraged additional investigations to be undertaken. Most of these studies have

focused on the velocity profiles and the turbulence characteristics of vegetated channels instead of extending existing bed resistance laws.

In this chapter some experiments have been undertaken in a wide channel to investigate effects of vegetation for fully vegetation, partial one-sided vegetation, and partial two-sided vegetation in two states of submerged and emergent vegetation with four density configurations based on empirical measurements.

6.2 Flow in a fully vegetated channel

6.2.1 Submerged vegetation (rods height = 180 mm)

A set of experimental investigations were undertaken for a relatively wide channel. The details of the fully submerged vegetation experimental set up for the wide channel are illustrated in Fig. 6.1 for the high, medium and low vegetation densities respectively. The changes in the velocity profiles in various directions will then be discussed.

(a)

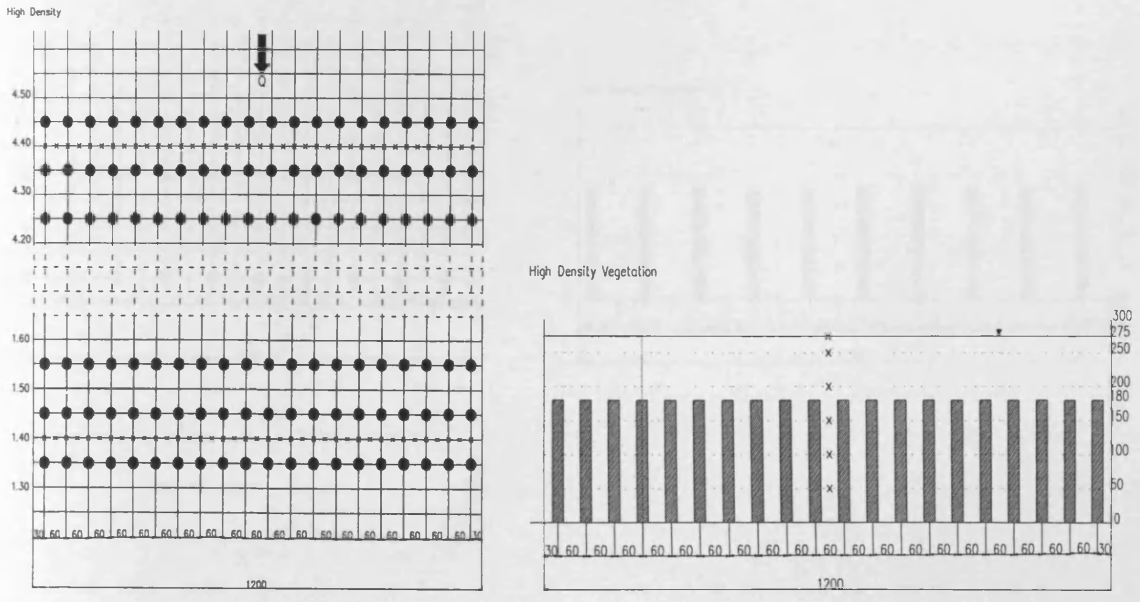

(b)

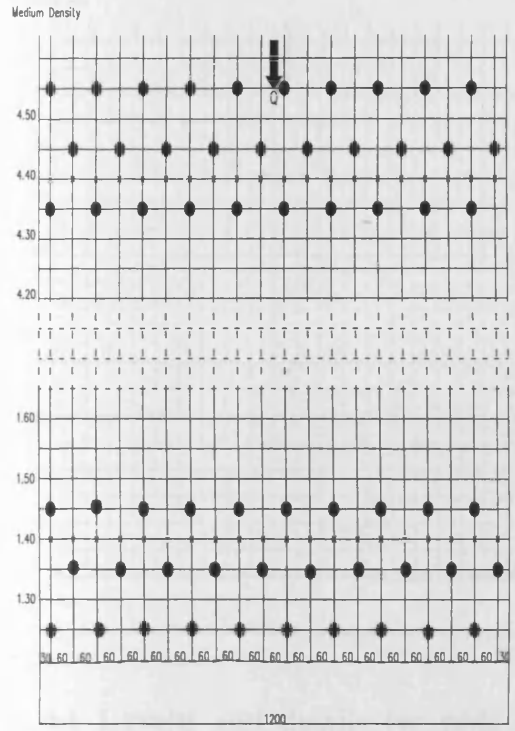
Medium Density
Q
4.50
4.40
4.30
4.20
1.60
1.50
1.40
1.30
1200

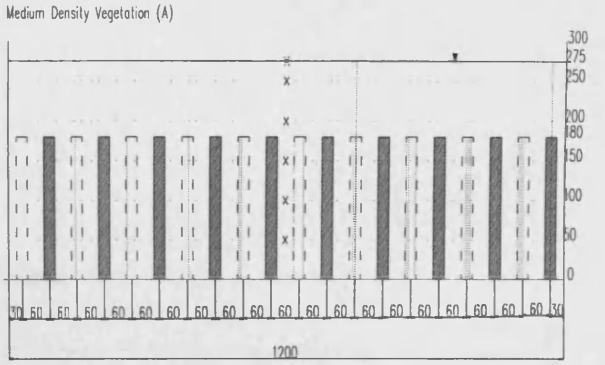
Medium Density Vegetation (A)
300
275
250
200
180
150
100
50
0
1200

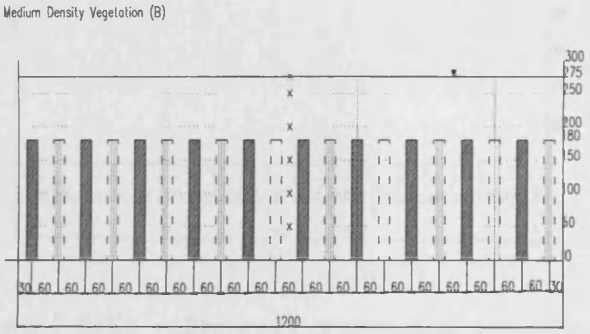
Medium Density Vegetation (B)
300
275
250
200
180
150
100
50
0
1200

(c)

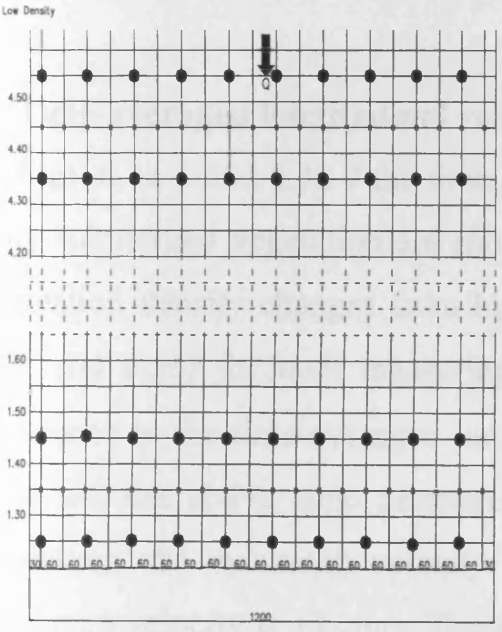
Low Density
Q
4.50
4.40
4.30
4.20
1.60
1.50
1.40
1.30
1200

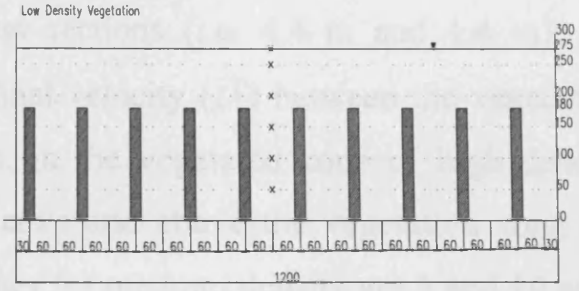
Low Density Vegetation
300
275
250
200
180
150
100
50
0
1200

(d)

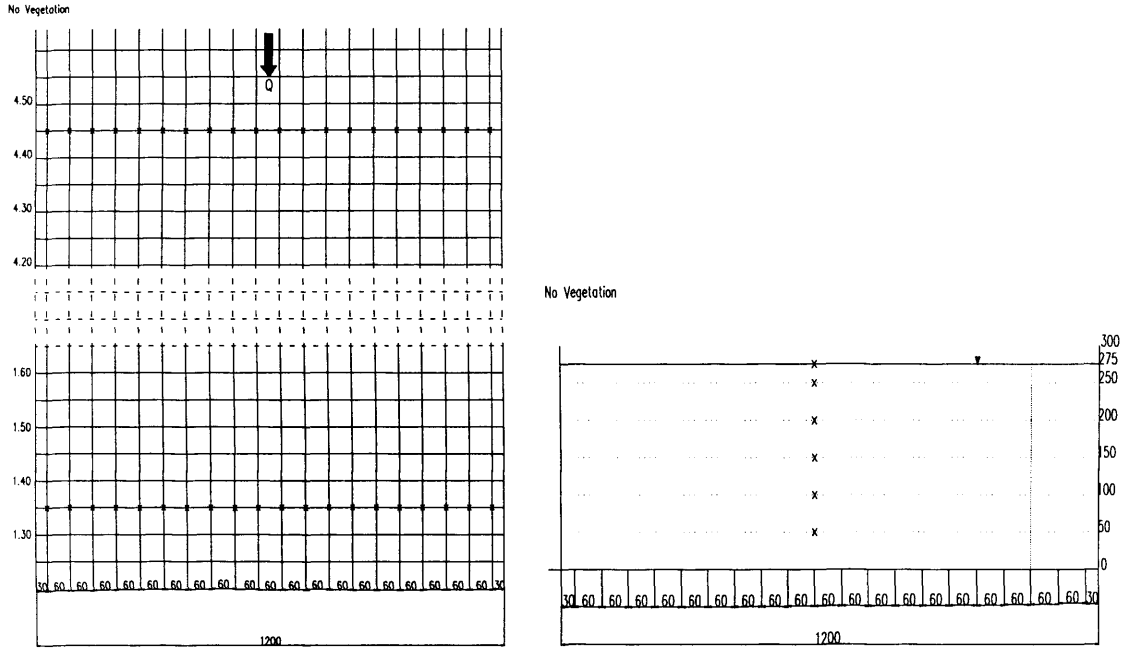

Fig. 6.1 Layout and details for wide channel fully submerged vegetation experiments showing measuring point locations and vertical velocity profile sets at 4.4 and 1.4 and for four configurations: (a) high, (b) medium, (c) low, and (d) no vegetation.

a) Time-averaged longitudinal velocity component ($\overline{U}$)

In Figs. 6.2a-d and 6.3a-d the time-averaged longitudinal velocity components for fully submerged vegetation are shown. From the figures it is evident that, as the vegetation density changes from high (Figs. 6.2a and 6.3a) to low density (Figs. 6.2c and 6.3c) for both measuring cross sections (i.e. 4.4 m and 1.4 m), the difference in the time-averaged longitudinal velocity ($\overline{U}$) between the vegetation zone and the above zone decreases. So, in the vegetated zone of high density vegetation, the maximum velocity is 5 cm/s and above the vegetation zone the maximum velocity is 13 cm/s. These values for medium density are 5 and 10 cm/s and for low density are 6 and 9 cm/s respectively. For no vegetation, except within the thin layers near the bed and the side walls, where the velocity contours are parallel and very close together (from 0-4 cm/s), for more than 50% of the overall area the velocity is in the range of 4-5 cm/s (see Figs. 6.2d. and 6.3d).

Although for all configurations the maximum velocity is located in the near water surface, the maximum non-uniformity is for the high density vegetation, decreasing towards low density and no vegetation states. Hence, the maximum uniformity can be seen in the no vegetation configuration as expected (Figs. 6.2 and 6.3). Therefore, with the rods in existence and based on the density, the velocity profile differs significantly, with the rods causing pronounced non-uniformity in the velocity profile. Because of the drag force due to the rods and the effect of vortex shading, the velocity profiles behind and in between the rods are very different. The results show that for the high density situation within the vegetated zone, the velocity profile is much smaller than that of the above vegetation zone. However, as it changes towards medium and low densities the velocity effectively increases in the vegetated zone and decreases above the vegetation zone. From high to low density configurations and then no vegetation, the uniformity of the longitudinal velocity also increases. In other words, the obstruction of the flow by the rods creates a drag force opposite to the direction of flow, with vortex shedding occurring behind the rods and secondary currents being observed above the vegetation.

The depth-averaged longitudinal velocity profiles for all the rod densities are illustrated across the cross-section in Figs. 6.2e and 6.3e. The results show that as the vegetation density increases the velocity variations behind and in between the rods also increases. Again for the high density a high variation in the maximum and minimum points occurs which is higher than for medium and low densities. With a density reduction from high to medium and low the variations decrease and as a result, for the no vegetation case a horizontal line with no considerable variations is observed. Also for the no vegetation case at cross-sections 4.4 and 1.4 there was some disparity in the evaluated discharges from the measured velocity data.

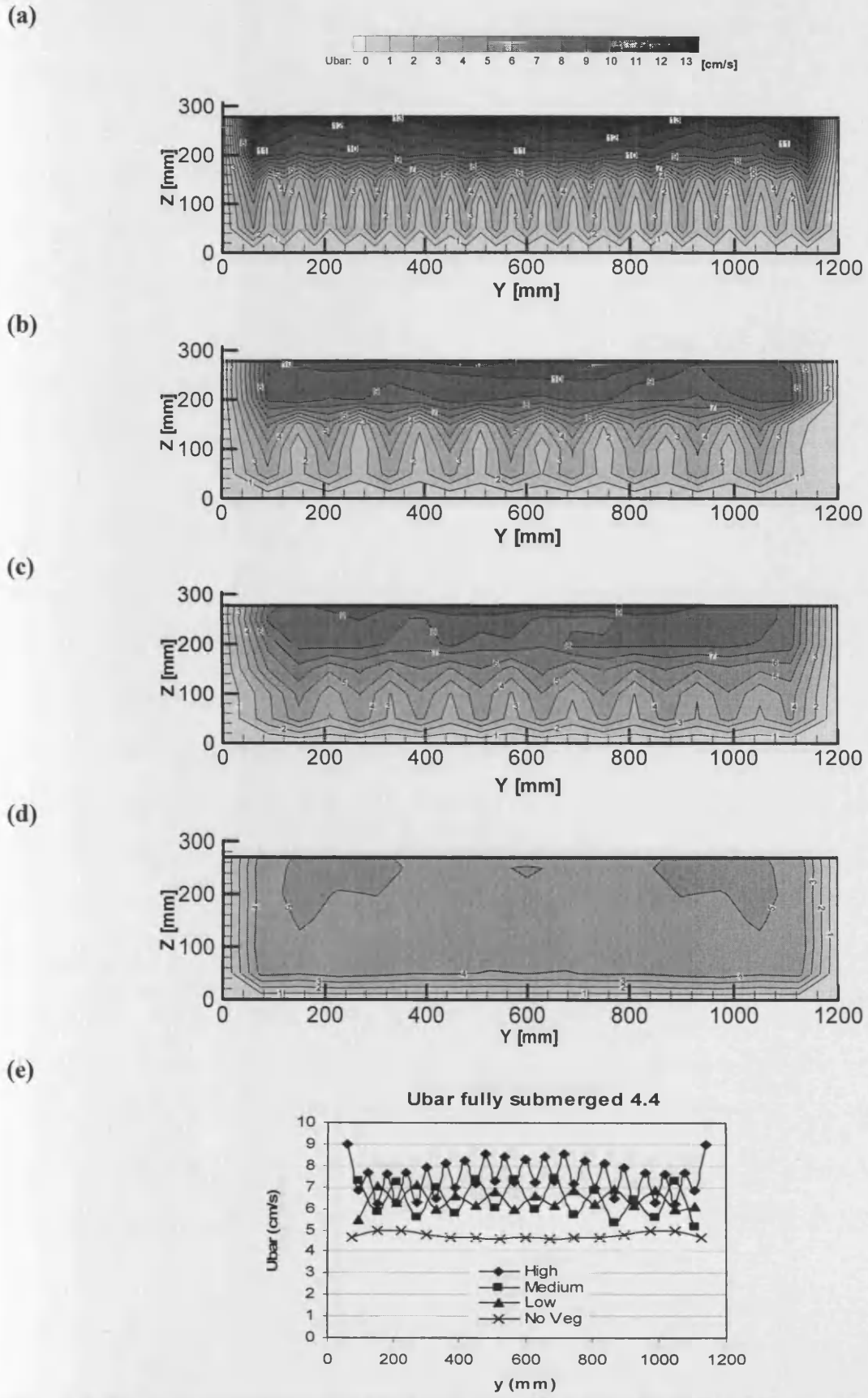

Fig. 6.2 Time-averaged longitudinal velocity ($\overline{U}$) [cms^{-1}] fully submerged vegetation at cross-section 4.4 for four configurations: (a) high, (b) medium, (c) low, and (d) no vegetation; (e) depth-averaged longitudinal velocity profiles.

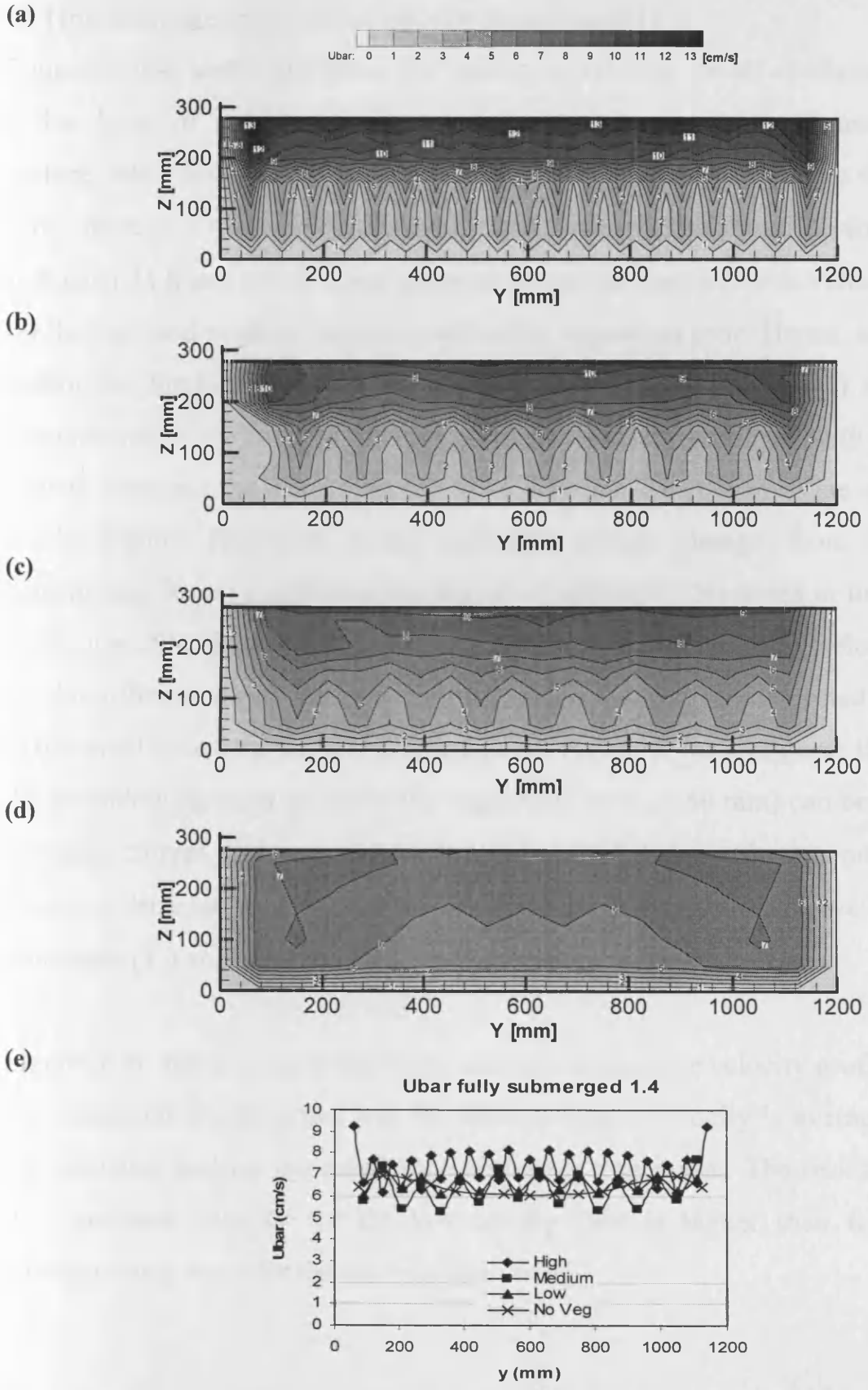

Fig. 6.3 Time-averaged longitudinal velocity ($\overline{U}$) [cms^{-1}] fully submerged vegetation at cross-section 1.4 for four configurations: (a) high, (b) medium, (c) low, and (d) no vegetation; (e) depth-averaged longitudinal velocity profiles.

b) Time-averaged transverse velocity component ($\overline{V}$)

Figures 6.4a-d and 6.5a-d show the transverse velocity for all configurations, with a thin layer of negative transverse velocity $\overline{V}$ being observed near the water surface. Also, between the top of vegetation (180 mm depth) and the thin negative layer, there is a transverse velocity $\overline{V}$ layer, with the maximum positive velocity. In Figs. 6.4a-b and 6.5a-b some negative values for the transverse velocity $\overline{V}$ occur for the high and medium densities within the vegetation zone. Hence, as mentioned before, for the high and medium densities (Figs.6.4a-b and 6.5a-b) the effective compression of the flow by the rods gives rise to the negative velocity for the high density state and the staggering of rods for the medium density state also leads to similar results. Therefore, as the vegetation density changes from high to low density, and for no vegetation, the degree of uniformity increases in the transverse velocity profile. With regard to the various diffusion effects of the velocity profiles for the different vegetation densities, the results can not be interpreted exactly due to the small variations for the different states. However for all figures the effects of the secondary currents on top of the vegetation zone ($\geq$180 mm) can be seen. In the previous, current, and next sections it will be concluded that the secondary currents causes a decrease in the longitudinal velocity ($\overline{U}$) and an increase in both the transverse ($\overline{V}$) and vertical velocity ($\overline{W}$) components.

Figures 6.4e and 6.5e show the depth-averaged transverse velocity profiles. Herein, the vegetation is submerged and the depth-averaged velocity is averaged between the vegetated and no vegetated zone above the vegetation. The results show that the transverse velocity for the low density case is higher than for the other configurations, even for the no vegetation case.

(a)

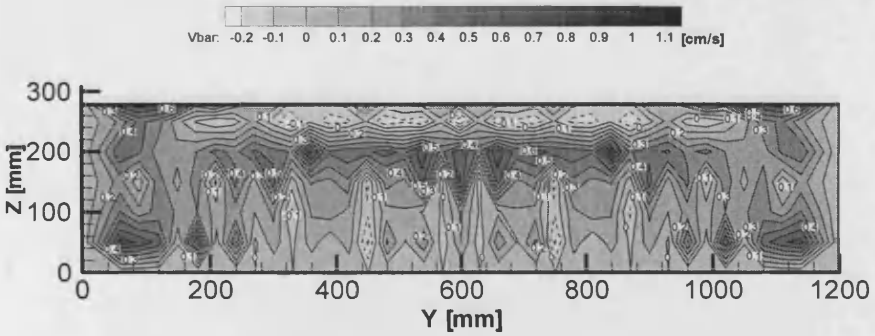

(b)

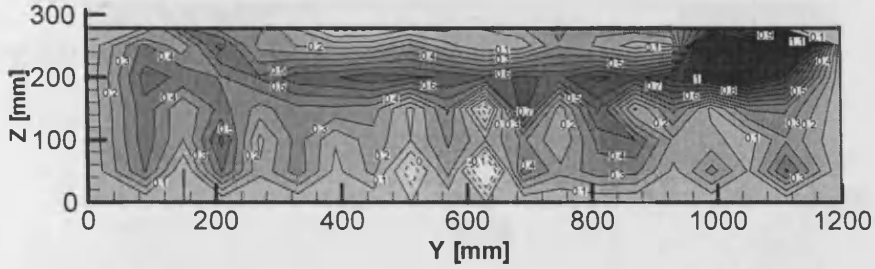

(c)

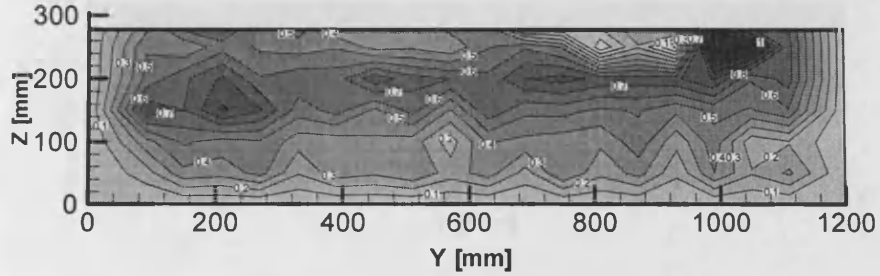

(d)

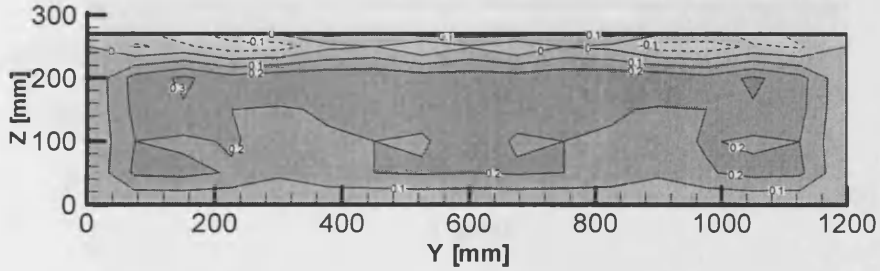

(e)

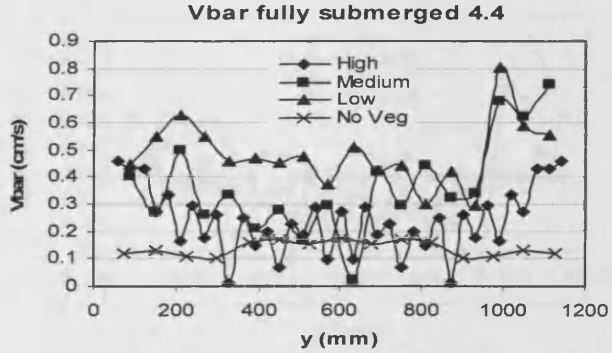

Fig. 6.4 Time-averaged transverse velocity ($\overline{V}$) [cms^{-1}] fully submerged vegetation at cross-section 4.4 for four configurations: (a) high, (b) medium, (c) low, and (d) no vegetation; (e) depth-averaged transverse velocity profiles.

(a)

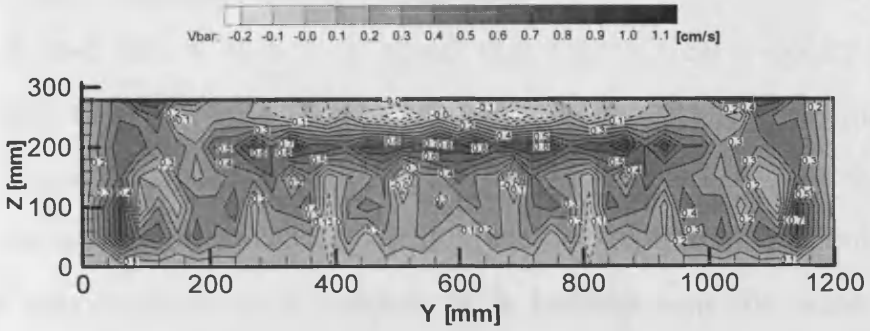

(b)

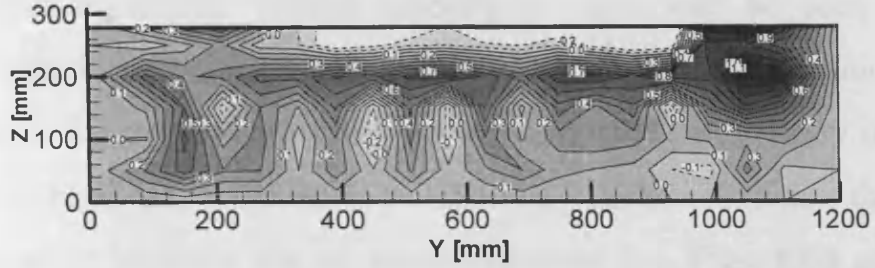

(c)

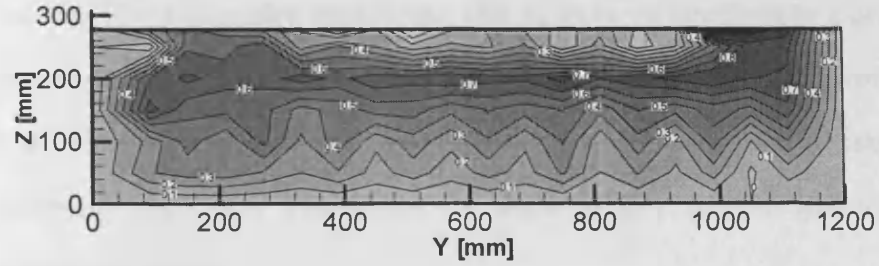

(d)

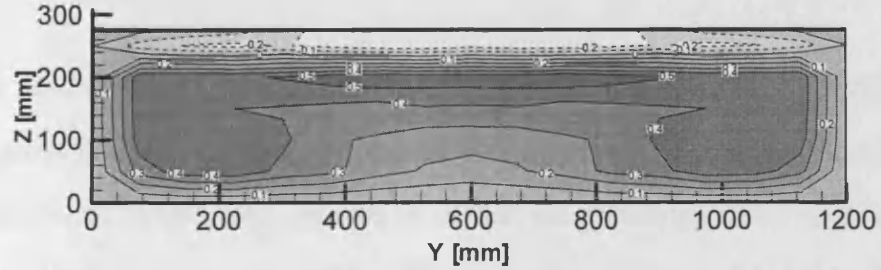

(e)

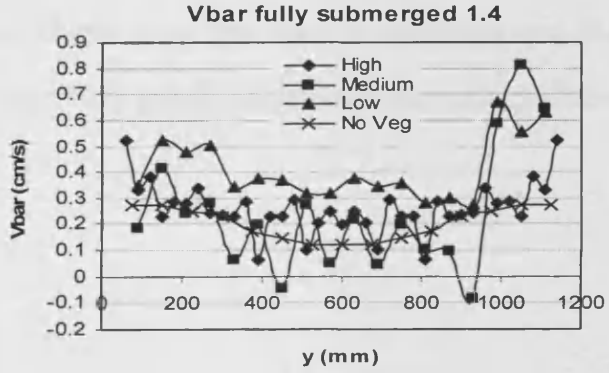

Fig. 6.5 Time-averaged transverse velocity ($\overline{V}$) [cms^{-1}] fully submerged vegetation at cross-section 1.4 for four configurations: (a) high, (b) medium, (c) low, and (d) no vegetation; (e) depth-averaged transverse velocity profiles.

c) Time-averaged vertical velocity component ($\overline{W}$)

From Figs. 6.6a-d and 6.7a-d it is noted that the vertical velocity profiles are almost opposite to the results for the transverse velocity profiles shown in Figs. 6.4a-d and 6.5a-d. This means that a negative layer occurs on top of the vegetation area (i.e. at elevation 180 mm) due to the effects of secondary currents and then a thin positive maximum vertical velocity $\overline{W}$ is located near the water surface. In addition, some maximum vertical velocity $\overline{W}$ value can be seen within the vegetated zone. Herein some similarities arise between the medium and high densities due to the staggering of the vegetation. Also the uniformity in the profile increases from high to low densities, and then no vegetation. Hence, the maximum uniformity can be seen for the no vegetation case (i.e. Figs. 6.6d and 6.7d). In looking at the results with more attention, the effects of secondary currents on top of the vegetation zone ($\geq$180 mm) are more obvious for the transverse velocity. Also, on top of the vegetation zone ($\geq$180 mm) vice-versa $\overline{V}$ is maximum positive and $\overline{W}$ is minimum negative. These results show that $\overline{V}$ and $\overline{W}$ are vice-versa on top of the vegetation zone.

Figures 6.6e and 6.7e show the depth-averaged vertical velocity profile. For this case all the graphs show similar variations for all the densities. For the high density a higher magnitude in the oscillations is observed in comparison with medium and low densities. This is to be expected with the higher degree of local turbulence. For the no vegetation case, there is no resistance variation and the results show a near horizontal line with only very small variations across the channel width.

(a)

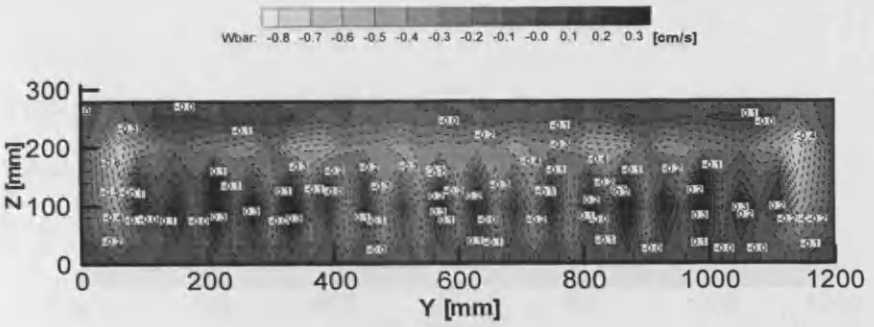

(b)

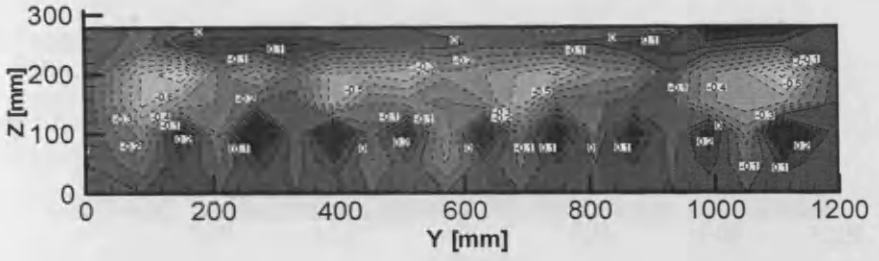

(c)

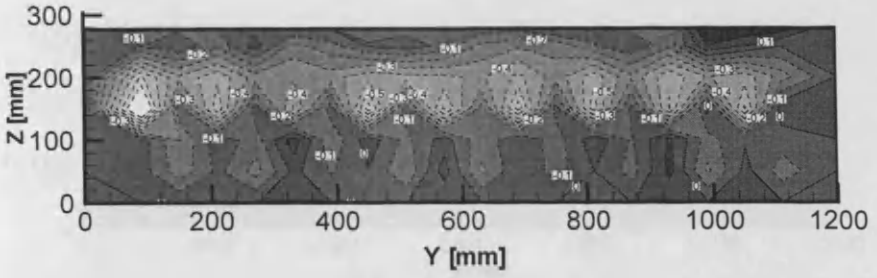

(d)

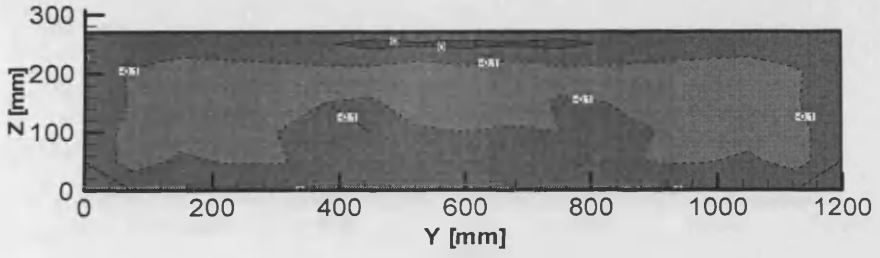

(e)

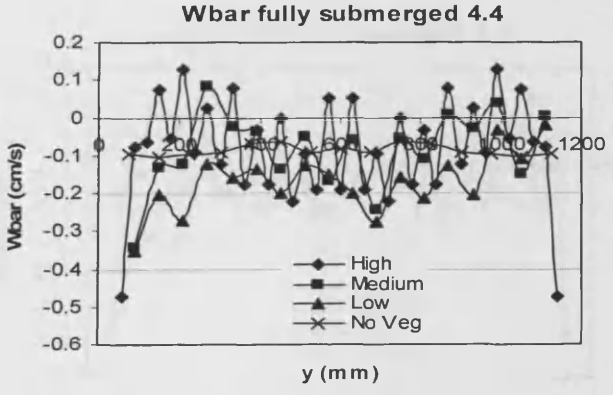

Fig. 6.6 Time-averaged vertical velocity ($\overline{W}$) [cms^{-1}] fully submerged vegetation at cross-section 4.4 for four configurations: (a) high, (b) medium, (c) low, and (d) no vegetation; (e) depth-averaged vertical velocity profiles.

(a)

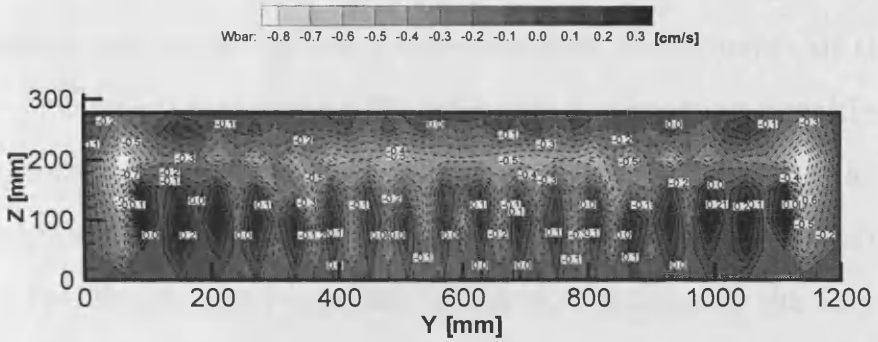

(b)

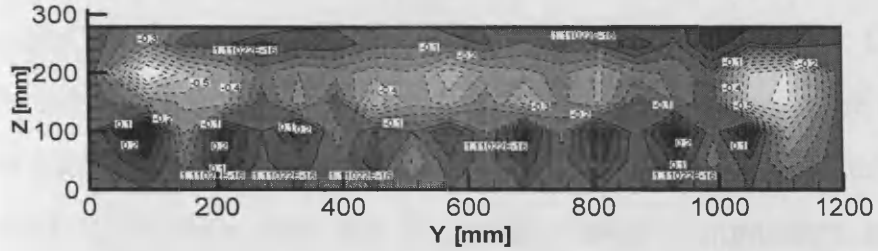

(c)

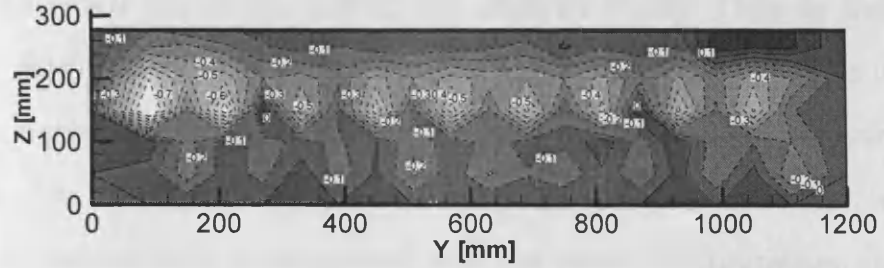

(d)

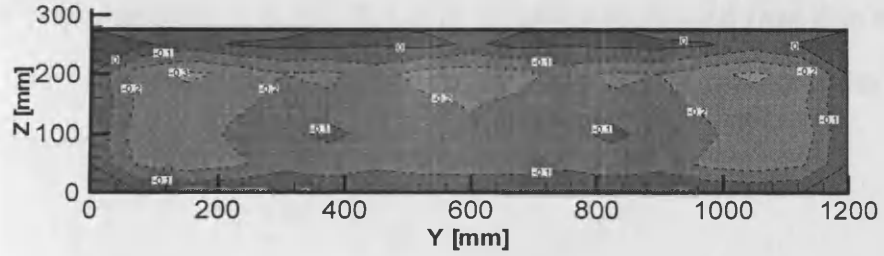

(e)

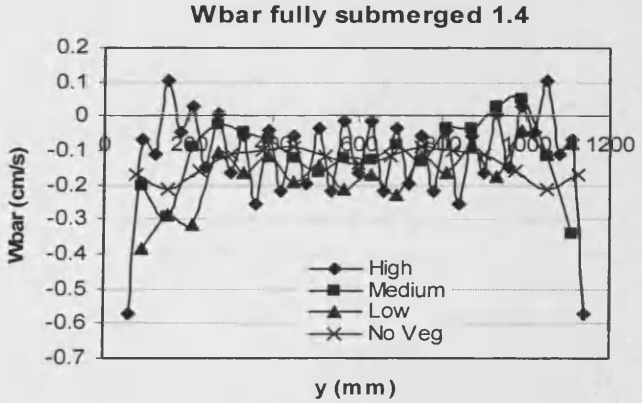

Fig. 6.7 Time-averaged vertical velocity ($\overline{W}$) [cms^{-1}] fully submerged vegetation at cross-section 1.4 for four configurations: (a) high, (b) medium, (c) low, and (d) no vegetation; (e) depth-averaged vertical velocity profiles.

d) Depth-averaged Reynolds stress components ($\overline{u'v'}$, $\overline{u'w'}$, $\overline{v'w'}$)

Figure 6.8 shows the results of the depth-averaged components of the Reynolds stresses ($\overline{u'v'}$, $\overline{u'w'}$, $\overline{v'w'}$) for all the fully submerged vegetation densities. As can be seen, the Reynolds stress components for the no vegetation case, for all graphs and both cross-sections (4.4 and 1.4), are constant or show little variation. Also in cross-section 1.4, due to the proximity to the weir (tailgate), the Reynolds stress components are very small (near zero) and almost constant at a horizontal elevation across the channel width. Since, at both cross-sections for the high density configuration, the velocity components in the vegetated zone are close to zero, the flow transfers to the top of the vegetation zone, as longitudinal velocity is high. Therefore it is clear that the Reynolds stress components are low and constant, with small variations across the channel width. Thus as the vegetation decreases to medium and low densities, then the velocity components increase and therefore the variations in the Reynolds stress components also increase. So, a high variation in the Reynolds stress components occurs for the low density configuration, particularly as compared with the other configuration. In comparing the results of cross-section 4.4 and 1.4 it is clearly concluded that due to proximity of the weir, the variations in the Reynolds stress components at cross-section 1.4 are less than those for cross-section 4.4.

(a)

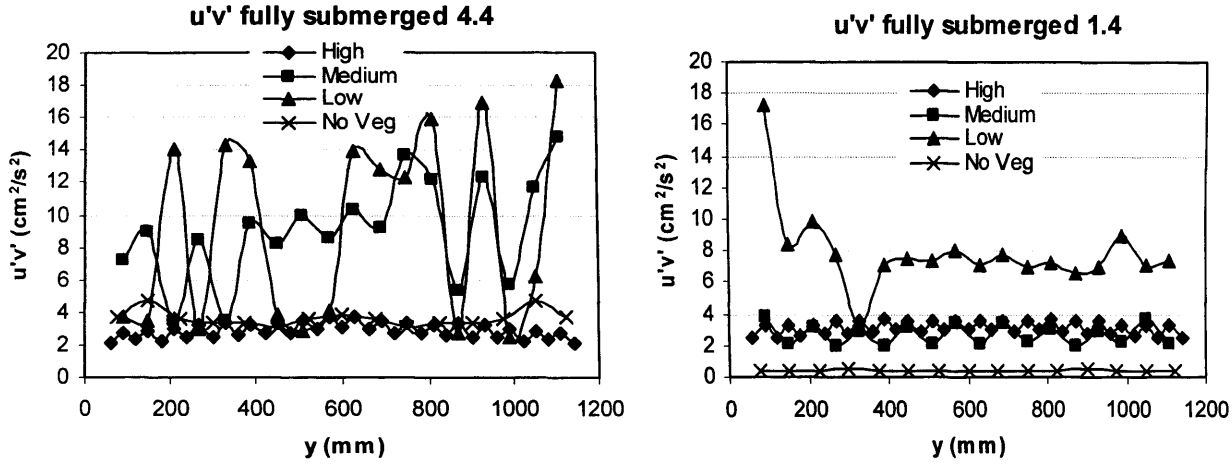

(b)

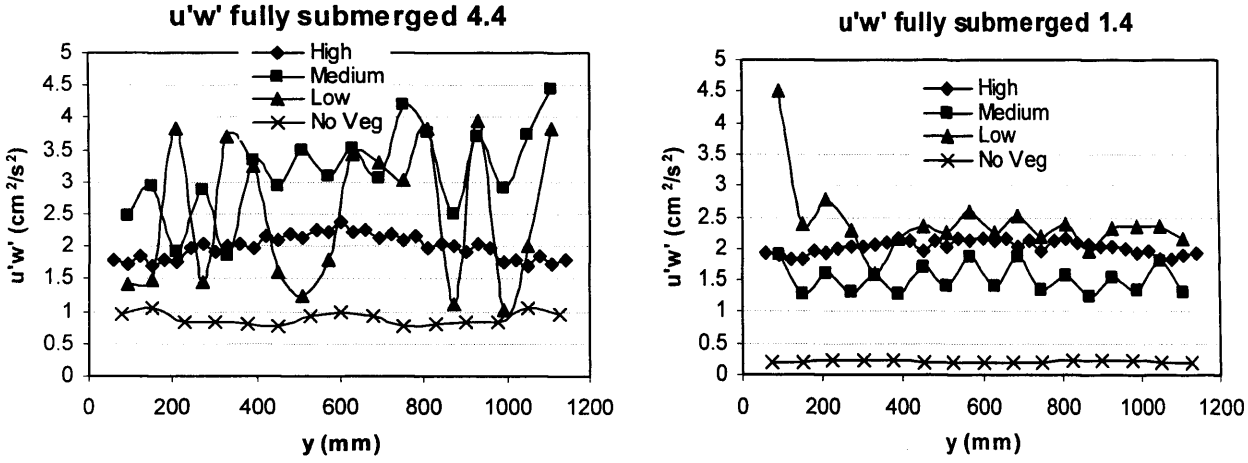

(c)

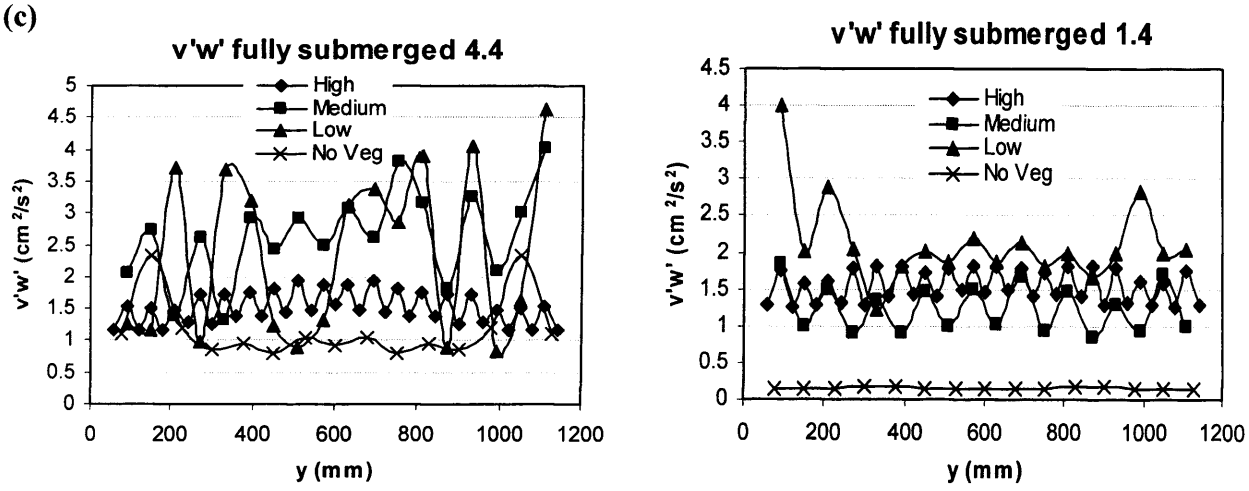

Fig. 6.8 Depth-averaged Reynolds stresses components ($\overline{u'v'}$, $\overline{u'w'}$, $\overline{v'w'}$) [cm^2/s^2] for four configurations in fully submerged vegetation at cross-sections 4.4 and 1.4; (a) $\overline{u'v'}$, (b) $\overline{u'w'}$, and (c) $\overline{v'w'}$.

6.2.2 Emergent vegetation (rods height = 300 mm)

An emergent vegetation case has been explored in this section. The experimental setup of the fully emergent vegetation for different vegetation densities is illustrated in Fig. 6.9. Also the velocity component profiles in various densities are discussed in the next sections.

(a)

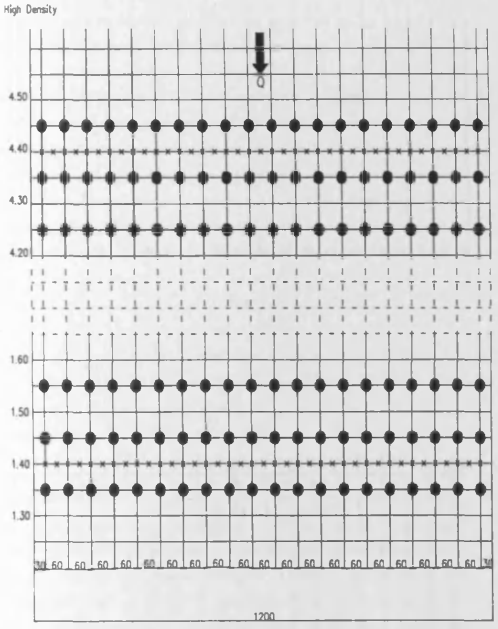

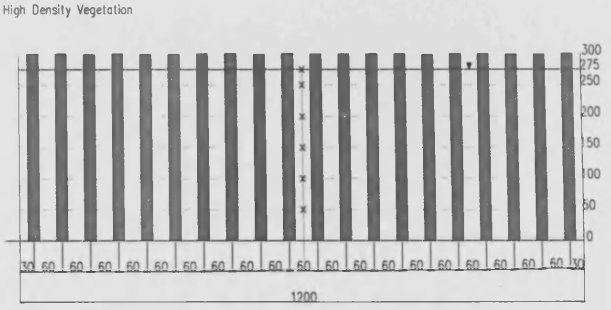

(b)

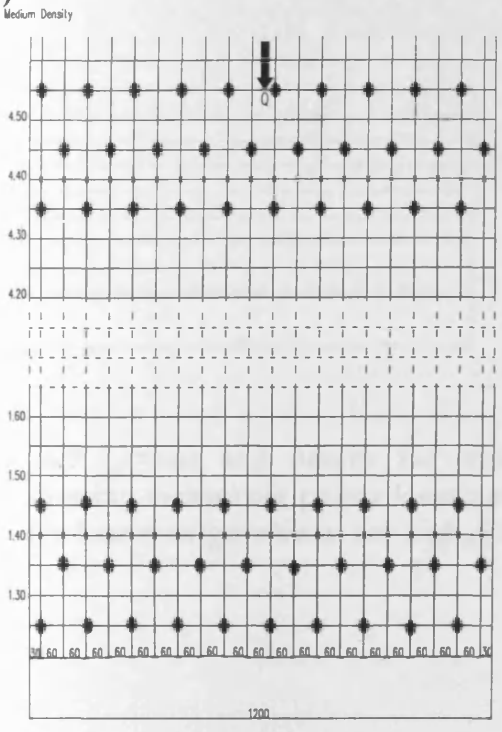

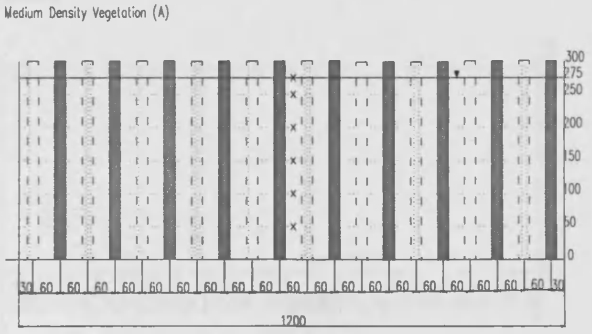

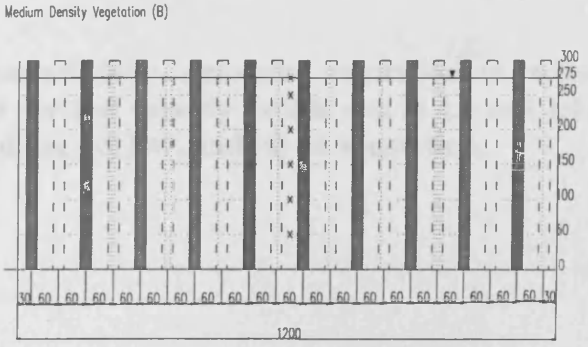

(c)

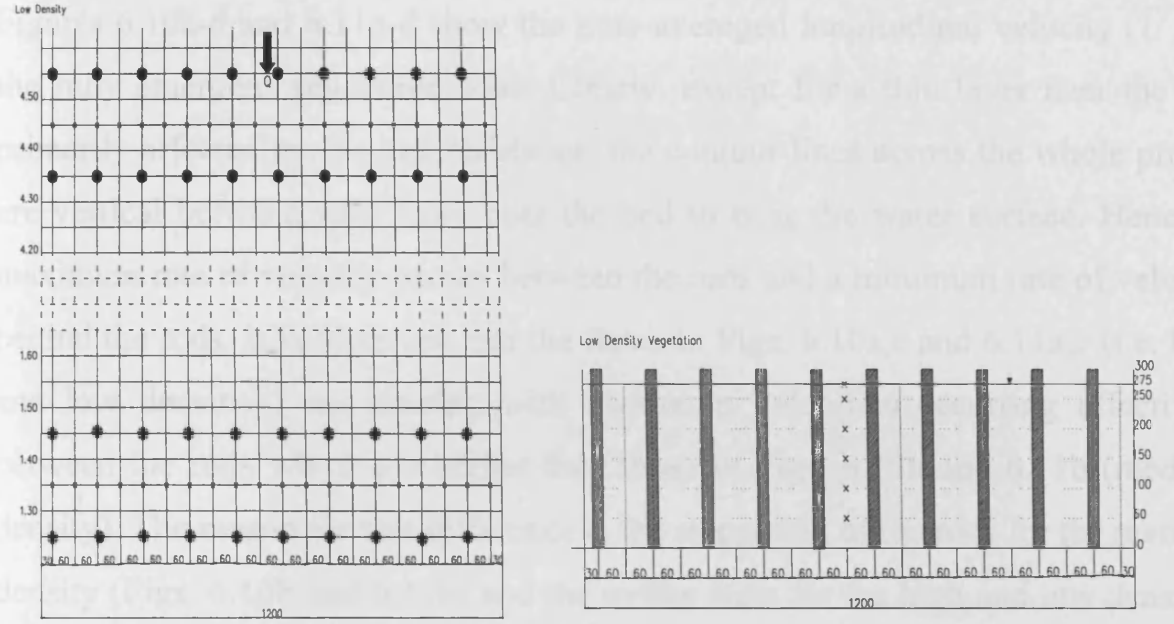

(d)

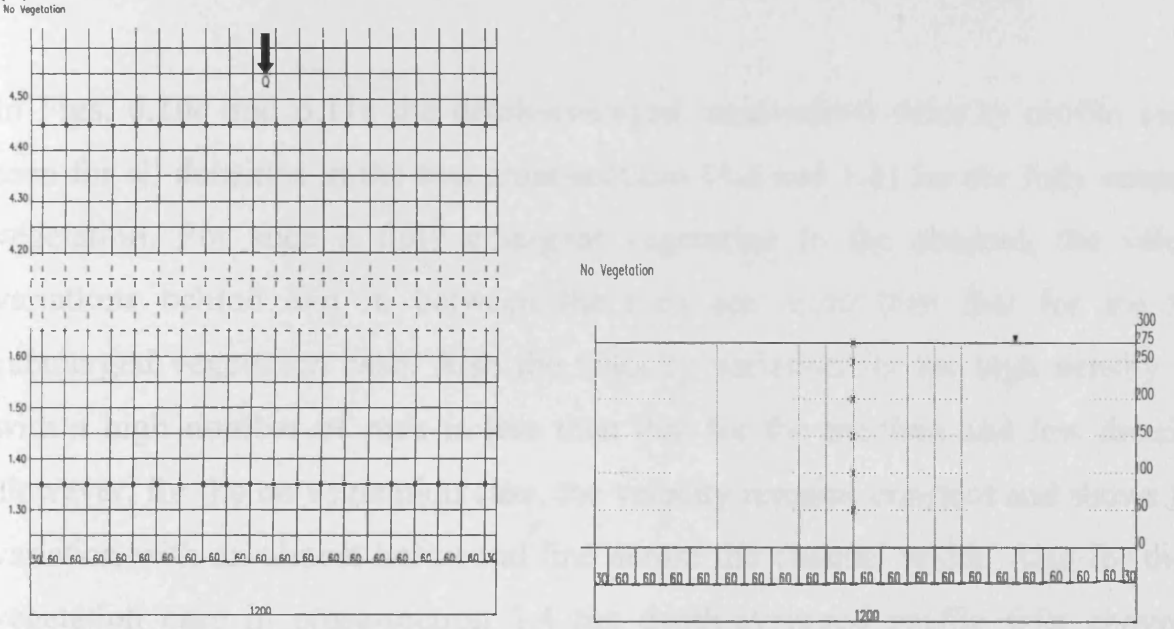

Fig. 6.9 Layout and details for wide channel fully emergent vegetation experiments showing measuring points locations and vertical velocity profile sets at 4.4 and 1.4 and for four configurations: (a) high, (b) medium, (c) low, and (d) no vegetation.

a) Time-averaged longitudinal velocity ($\overline{U}$)

Figures 6.10a-d and 6.11a-d show the time-averaged longitudinal velocity ($\overline{U}$) for the fully emergent vegetation state. Clearly, except for a thin layer near the bed primarily affected by the bed resistance, the contour lines across the whole profile are vertical between rods from near the bed to near the water surface. Hence, a maximum rate of velocity occurs between the rods and a minimum rate of velocity behind the rods. It is observed that the flows in Figs. 6.10a,c and 6.11a,c (i.e. high and low densities) are similar, with maximum velocities occurring effectively between the rods which are higher than those in Figs. 6.10b and 6.11b (medium density). The reason for this difference is the staggering of the rods for the medium density (Figs. 6.10b and 6.11b) and the in-line state for the high and low densities (Figs. 6.10a,c and 6.11a,c). No significant difference in the profiles of Figs. 6.10a,c and 6.11a,c can be noticed.

In Figs. 6.10e and 6.11e the depth-averaged longitudinal velocity profile can be seen for all densities in the two cross-sections (4.4 and 1.4) for the fully emergent vegetation. For such a fully emergent vegetation in the channel, the velocity variations behind and in between the rods are more than that for the fully submerged vegetation case. Also the velocity variation for the high density case with a high number of rods is less than that for the medium and low densities. However, for the no vegetation case, the velocity remains constant and shows little variation with an almost horizontal line across the channel width. Also for the no vegetation case in cross-section 1.4 the depth-averaged profile falls above the normal case as happened for cross-section 4.4.

(a)

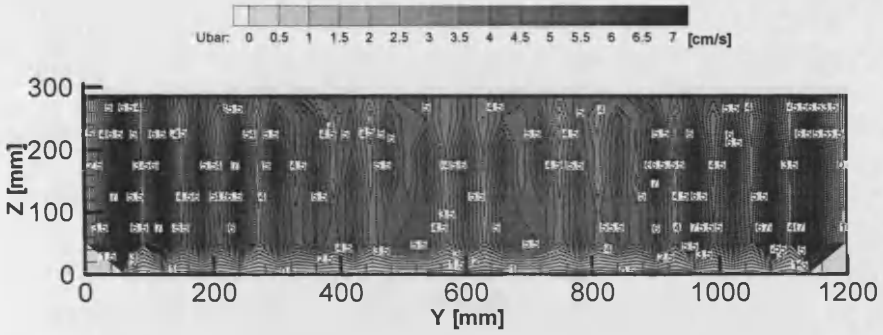

(b)

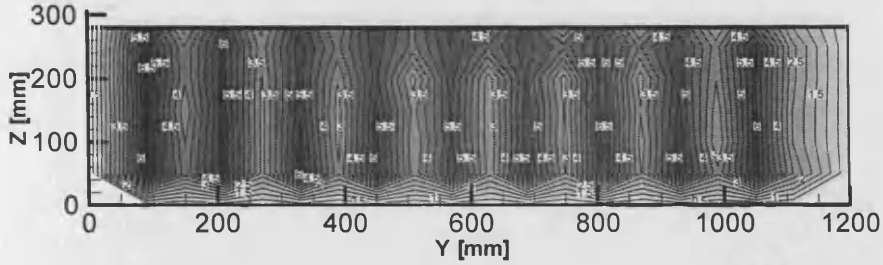

(c)

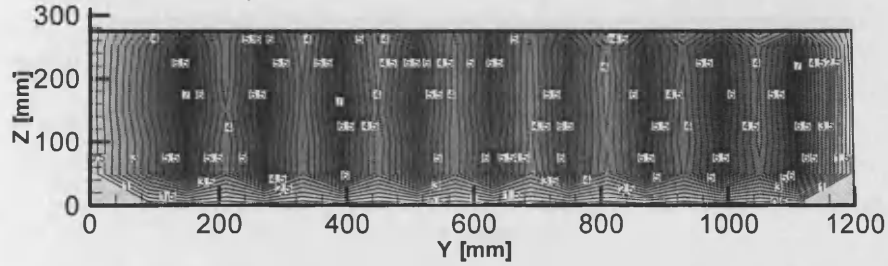

(d)

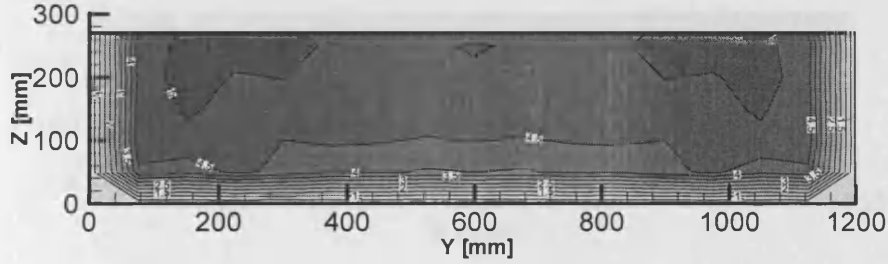

(e)

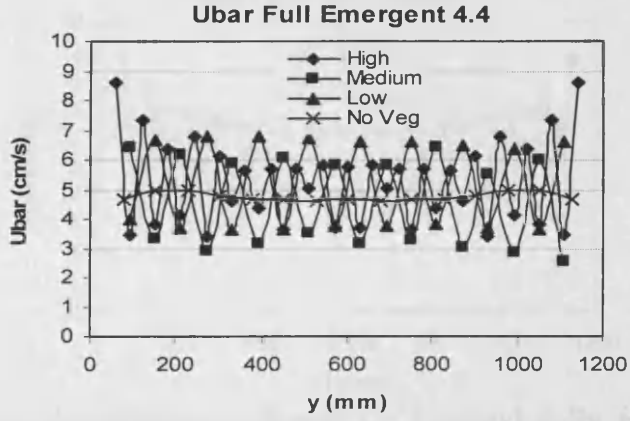

Fig. 6.10 Time-averaged longitudinal velocity ($\overline{U}$) [cms^{-1}] fully emergent vegetation at cross-section 4.4 for four configurations: (a) high, (b) medium, (c) low, and (d) no vegetation; (e) depth-averaged longitudinal velocity profiles.

(a)

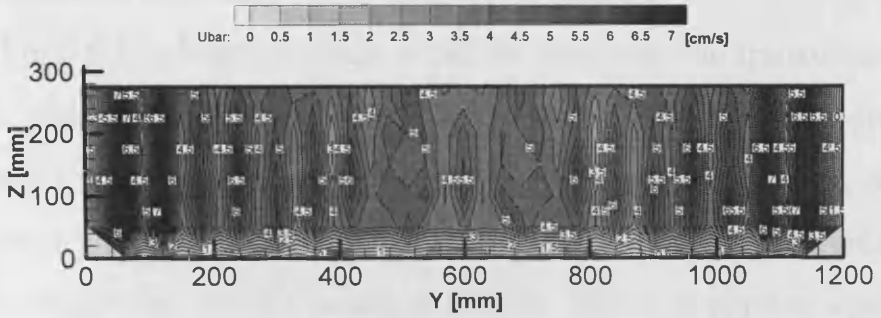

(b)

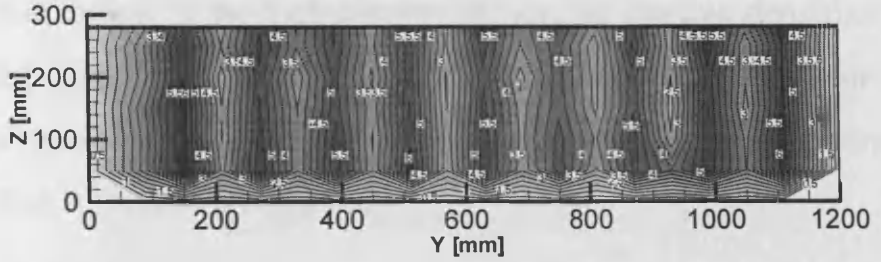

(c)

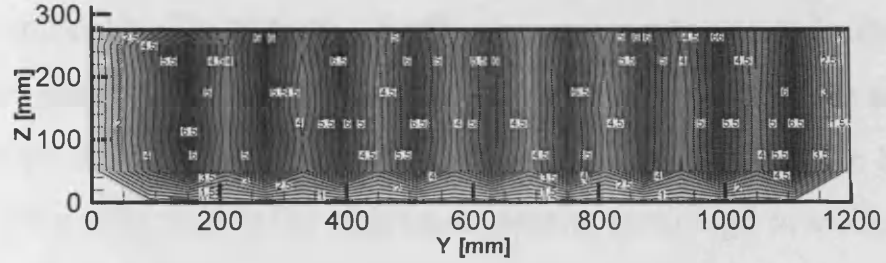

(d)

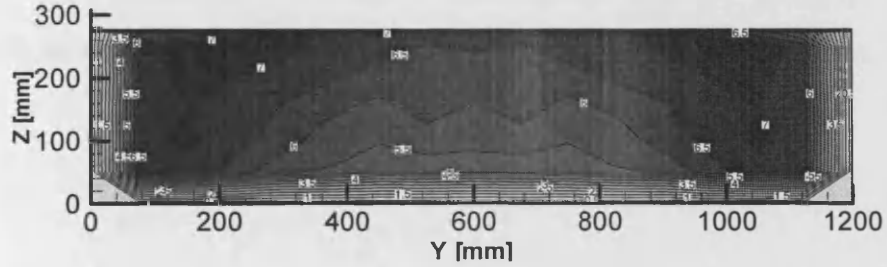

(e)

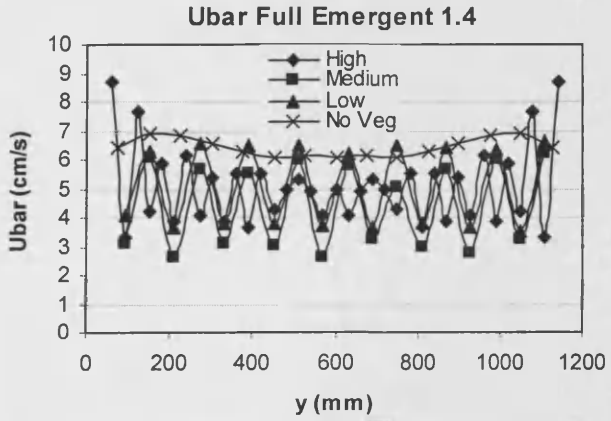

Fig. 6.11 Time-averaged longitudinal velocity ($\overline{U}$) [cm/s] fully emergent vegetation at cross-section 1.4 for four configurations: (a) high, (b) medium, (c) low, and (d) no vegetation; (e) depth-averaged longitudinal velocity profiles.

b) Time-averaged transverse velocity component ($\overline{V}$)

In studying Figs. 6.12a,b and 6.13a,b it can be seen that the transverse velocity $\overline{V}$ for the high and medium densities has a similar range of variation between a maximum and a minimum. As mentioned in the previous sections, although the vegetation density for the high density state is double that for the medium density, the effect of staggering for the medium density causes a similar variation in the velocity profile to that of the high density. Hence, for the low densities (Figs. 6.12c and 6.13c) the range of transverse velocity variations is far less than for the high and medium densities. For the low density state a high rate of uniformity in the velocity profile is therefore observed.

Figs. 6.12e and 6.13e illustrate the depth-averaged transverse velocity profile for the fully emergent vegetation at cross-sections 4.4 and 1.4. As can be seen, there is a high variation in the velocity between and behind the rods for the high density case. Then, for a reduction in the vegetation density from high to medium and low, the velocity variation decreases. A minimum variation in the velocity for the cases of low density and no vegetation can be seen across the channel width.

(a)

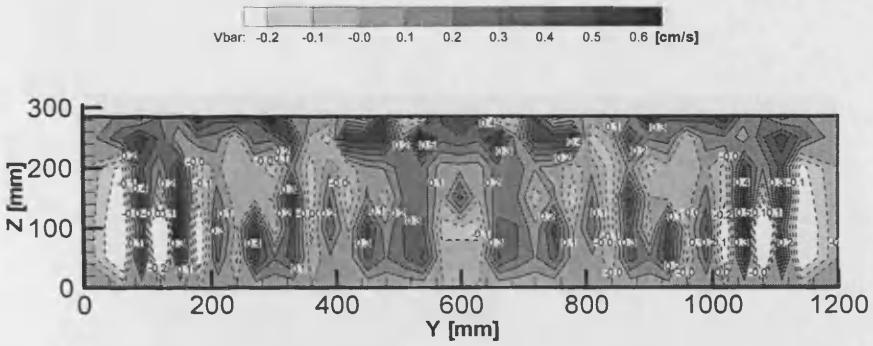

(b)

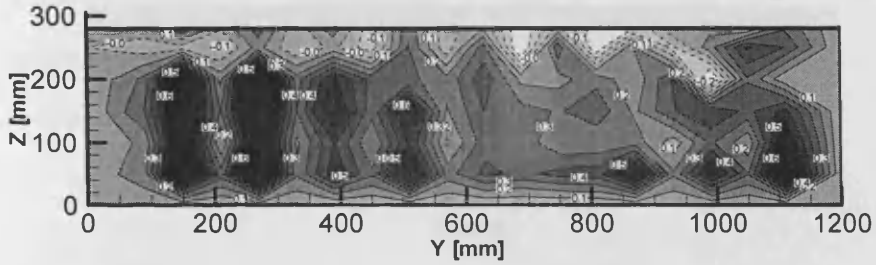

(c)

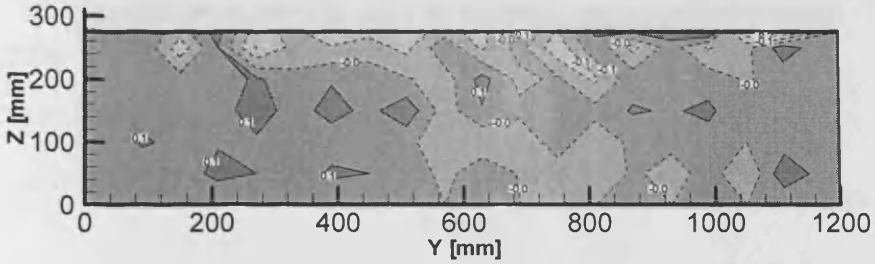

(d)

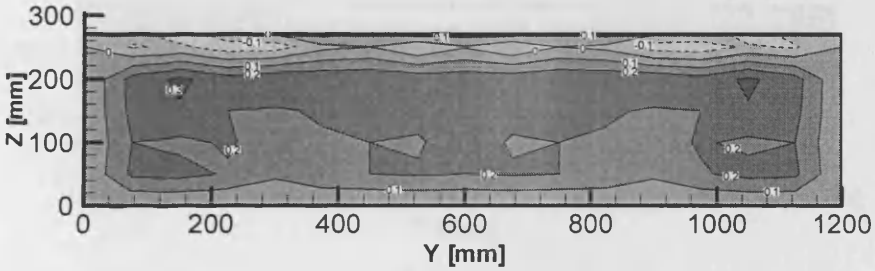

(e)

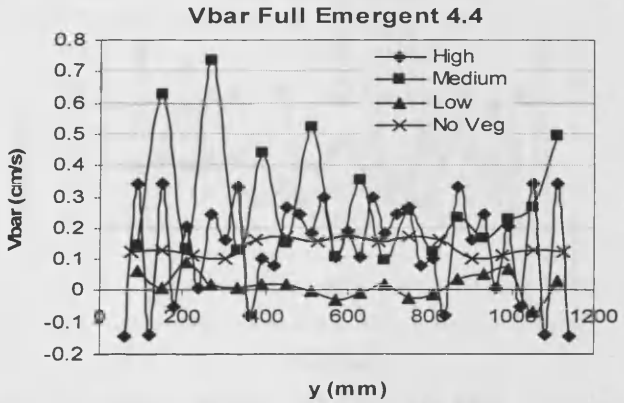

Fig. 6.12 Time-averaged transverse velocity ($\overline{V}$) [cms^{-1}] fully emergent vegetation at cross-section 4.4 for four configurations: (a) high, (b) medium, (c) low, and (d) no vegetation; (e) depth-averaged transverse velocity profiles.

(a)

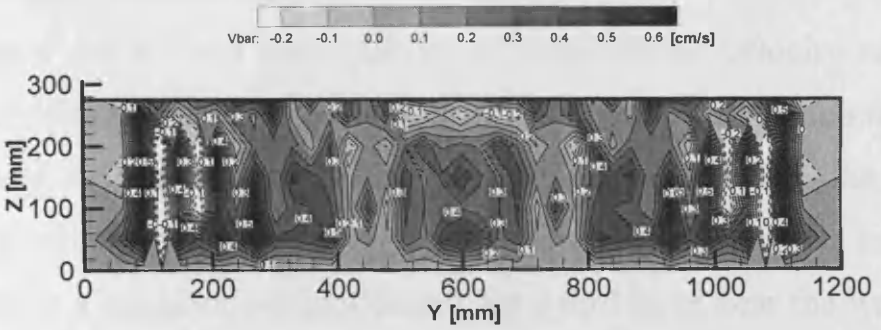

(b)

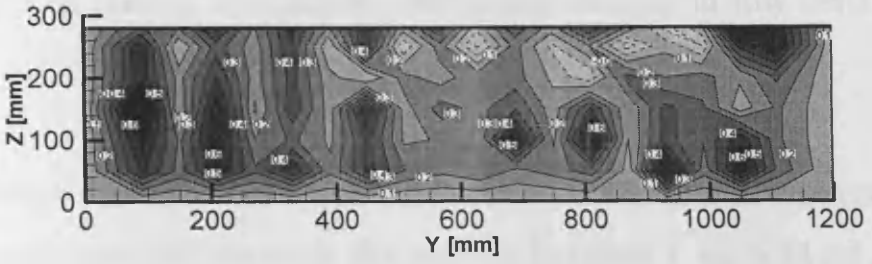

(c)

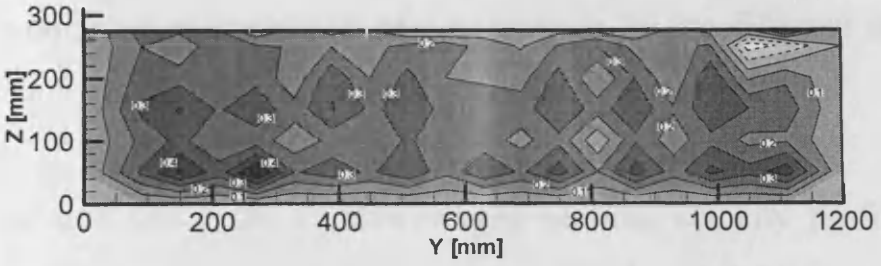

(d)

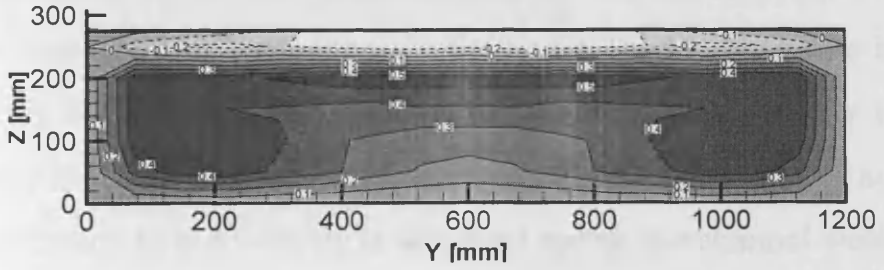

(e)

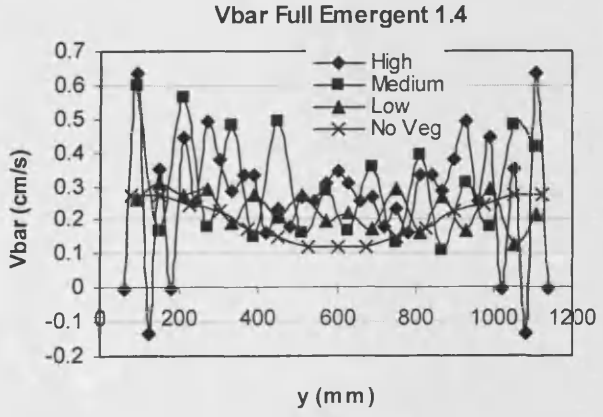

Fig. 6.13 Time-averaged transverse velocity ($\overline{V}$) [cms^{-1}] fully emergent vegetation at cross-section 1.4 for four configurations: (a) high, (b) medium, (c) low, and (d) no vegetation; (e) depth-averaged transverse velocity profiles.

c) Time-averaged vertical velocity component ($\overline{W}$)

Figures 6.14a-d and 6.15a-d show that for all densities the velocity variations are approximately similar, with the same range of maximum and minimum velocities being observed. Unlike the case for the high density state, where the majority of areas have positive vertical velocity, values, for the medium and low densities most areas have a negative velocity except for a thin layer near the water surface. Therefore for this reason, similarities between medium and low densities can be seen.

For the different diffusion effects on the velocity structure in different densities, there is no significant difference in the profiles between Figs. 6.14a-d and 6.15a-d and therefore an exact interpretation of the variation for the different states is also hard to achieve.

In Figs. 6.14e and 6.15e the depth-averaged vertical velocity profile for fully emergent vegetation at the two cross-sections of 4.4 and 1.4 can be seen. It is evident from these figures that, although the vertical velocity for the high density configuration is higher than for the other configurations, the velocity variation for the low density is more than for the other cases. Also, for the case of no vegetation a minimum variation in the velocity is observed across the channel width.

(a)

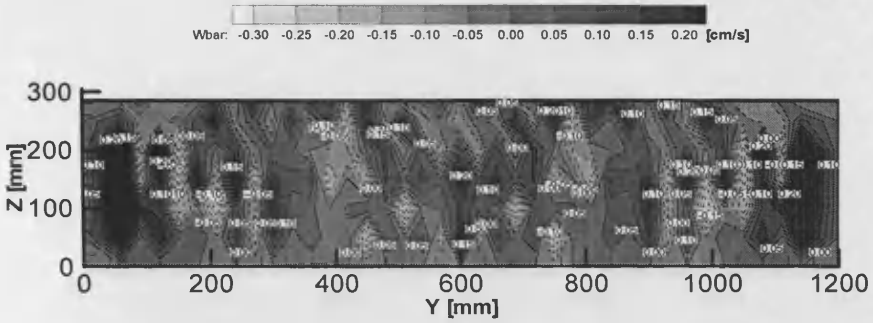

(b)

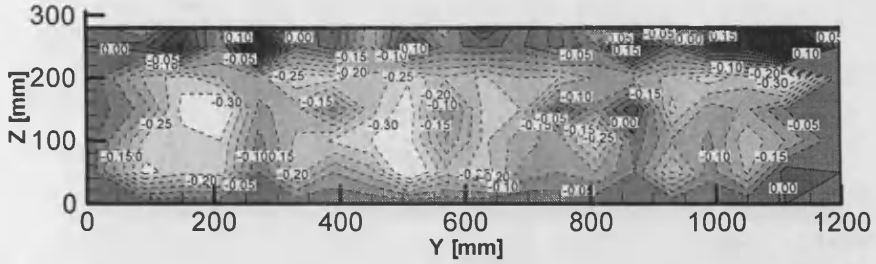

(c)

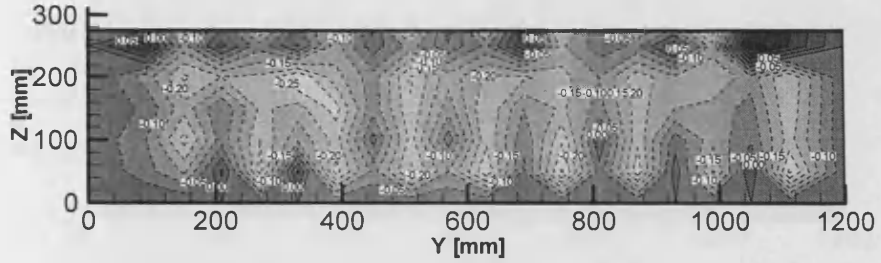

(d)

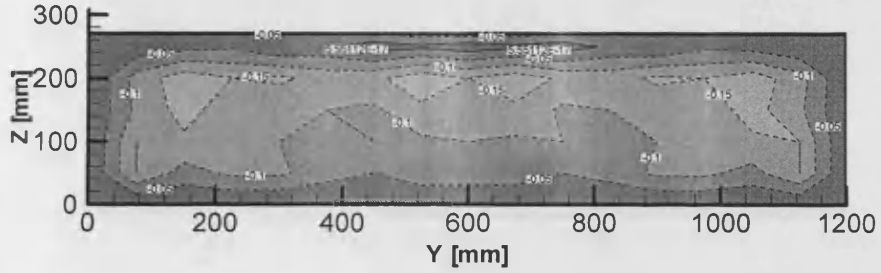

(e)

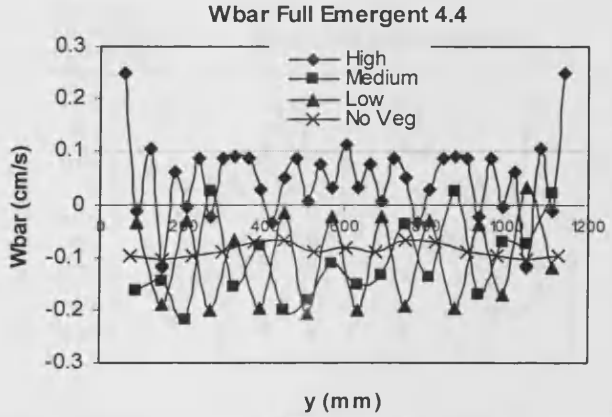

Fig. 6.14 Time-averaged vertical velocity ($\overline{W}$) [cms^{-1}] fully emergent vegetation at cross-section 4.4 for four configurations: (a) high, (b) medium, (c) low, and (d) no vegetation; (e) depth-averaged vertical velocity profiles.

(a)

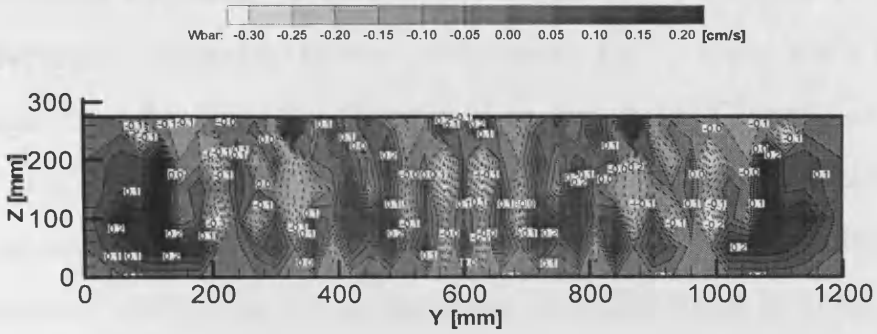

(b)

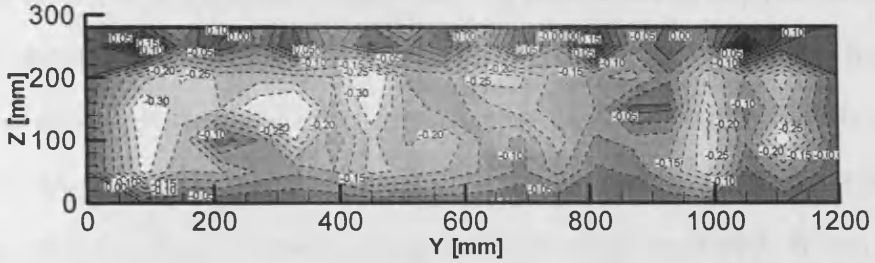

(c)

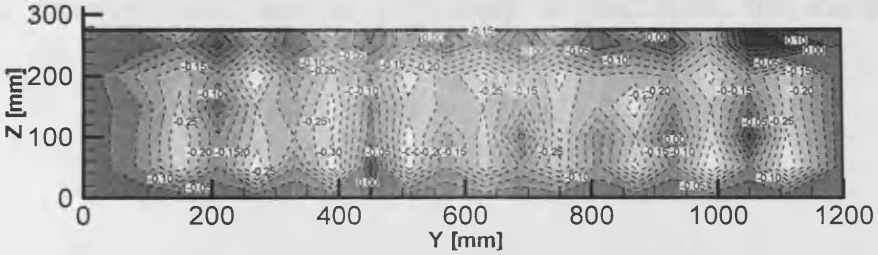

(d)

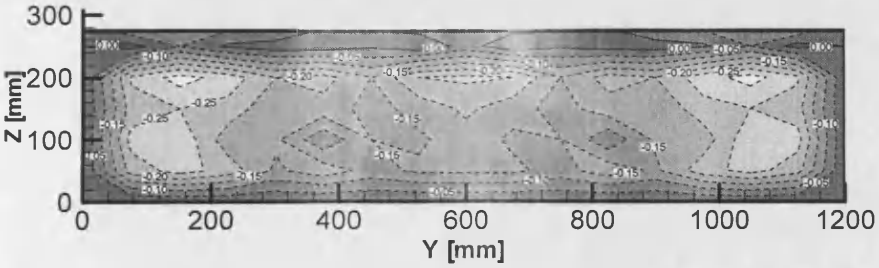

(e)

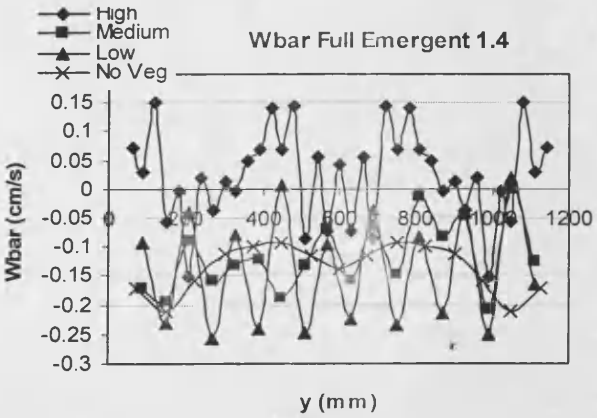

Fig. 6.15 Time-averaged vertical velocity ($\overline{W}$) [cms^{-1}] fully emergent vegetation at cross-section 1.4 for four configurations: (a) high, (b) medium, (c) low, and (d) no vegetation; (e) depth-averaged vertical velocity profiles.

d) Depth-averaged Reynolds stresses components ($\overline{u'v'}$, $\overline{u'w'}$, $\overline{v'w'}$)

The depth-averaged Reynolds stress components ($\overline{u'v'}$, $\overline{u'w'}$, $\overline{v'w'}$) for all fully emergent vegetation densities are illustrated in Fig. 6.16. Clearly, except for the high density configuration, for all configurations across both cross-sections 4.4 and 1.4, the components have small values (close to zero) and with little variation across the channel width. For the no vegetation configuration in cross-section 1.4, due to the close proximity to the weir, the Reynolds stress components are almost zero, with almost a horizontal line and no variation across the channel width. Therefore for the high density configuration, higher Reynolds stress components are measured, together with higher variations been found in comparison with the other configurations. Also, in comparing the two cross-sections, it can be seen that for the high density case, due to proximity to the weir, the variations in all Reynolds stress components across cross-section 1.4 are less than those for cross-section 4.4.

(a)

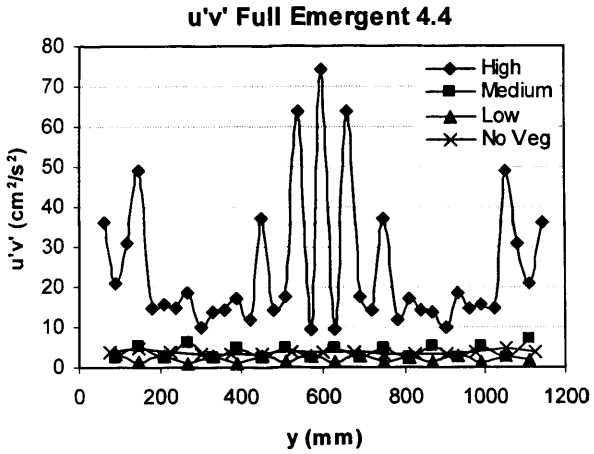

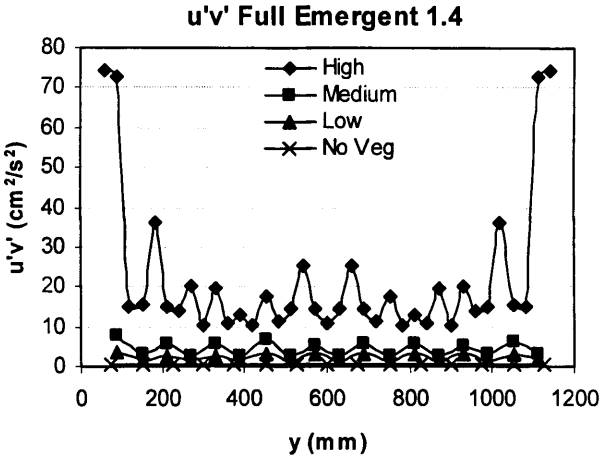

(b)

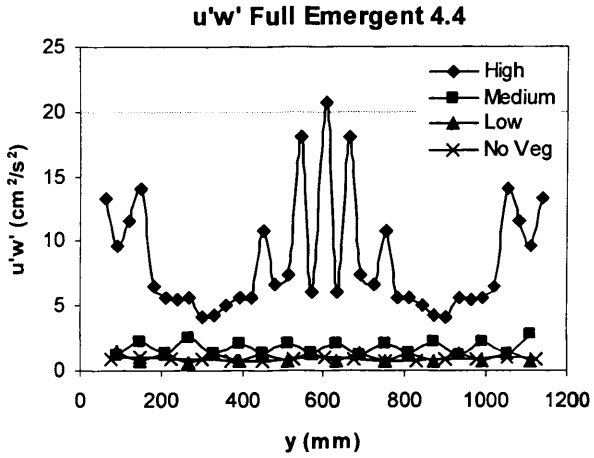

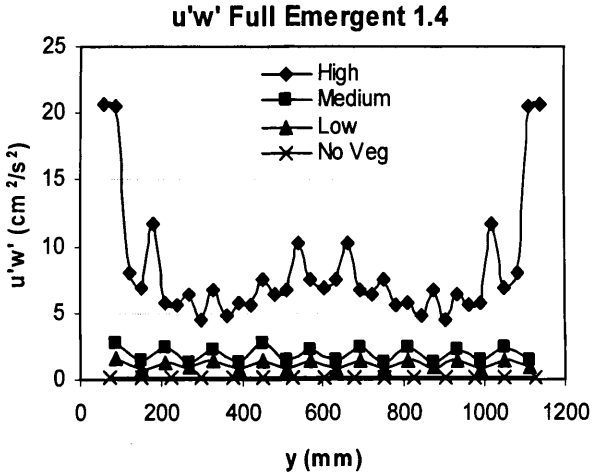

(c)

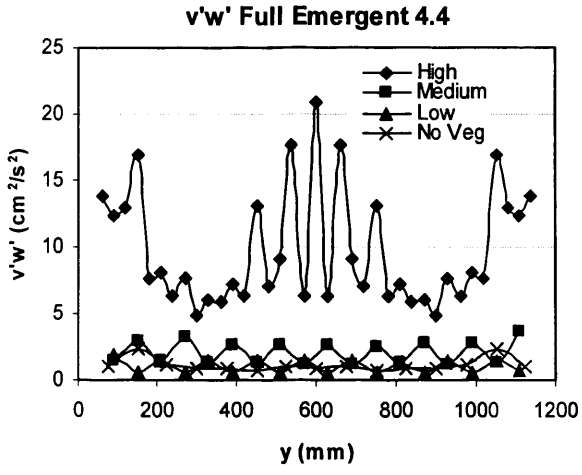

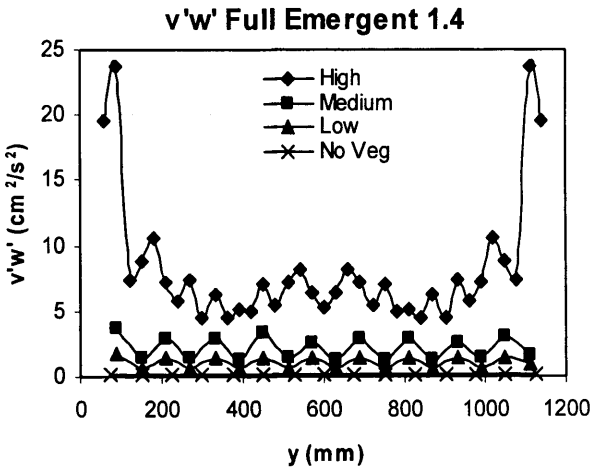

Fig. 6.16 Depth-averaged Reynolds stresses components ($\overline{u'v'}$, $\overline{u'w'}$, $\overline{v'w'}$) [cm^2/s^2] for four configurations in fully emergent vegetation at cross-sections 4.4 and 1.4; (a) $\overline{u'v'}$, (b) $\overline{u'w'}$, and (c) $\overline{v'w'}$.

6.3 Flow in a partial one-sided vegetated flow

6.3.1 Submerged vegetation (rods height = 180 mm)

A number of experiments have been carried out in this part to investigate the effect of submerged partial one-sided vegetations on the velocity profiles in different directions. The layout of the setup is illustrated in Fig. 6.17.

(a)

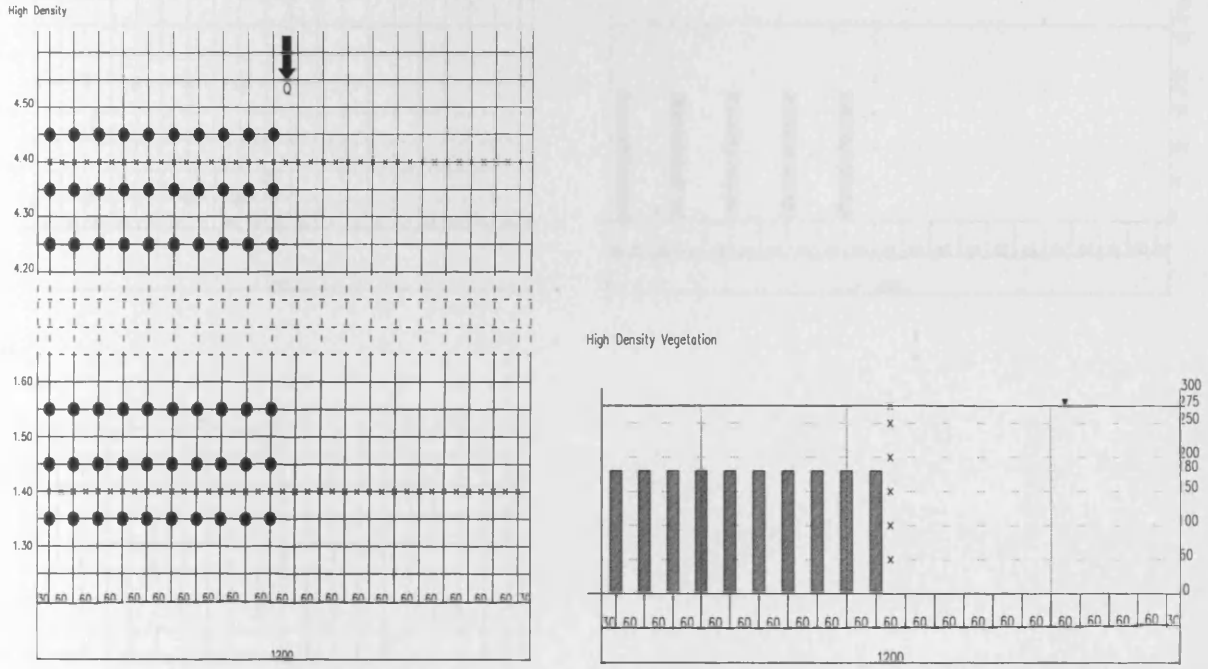

(b)

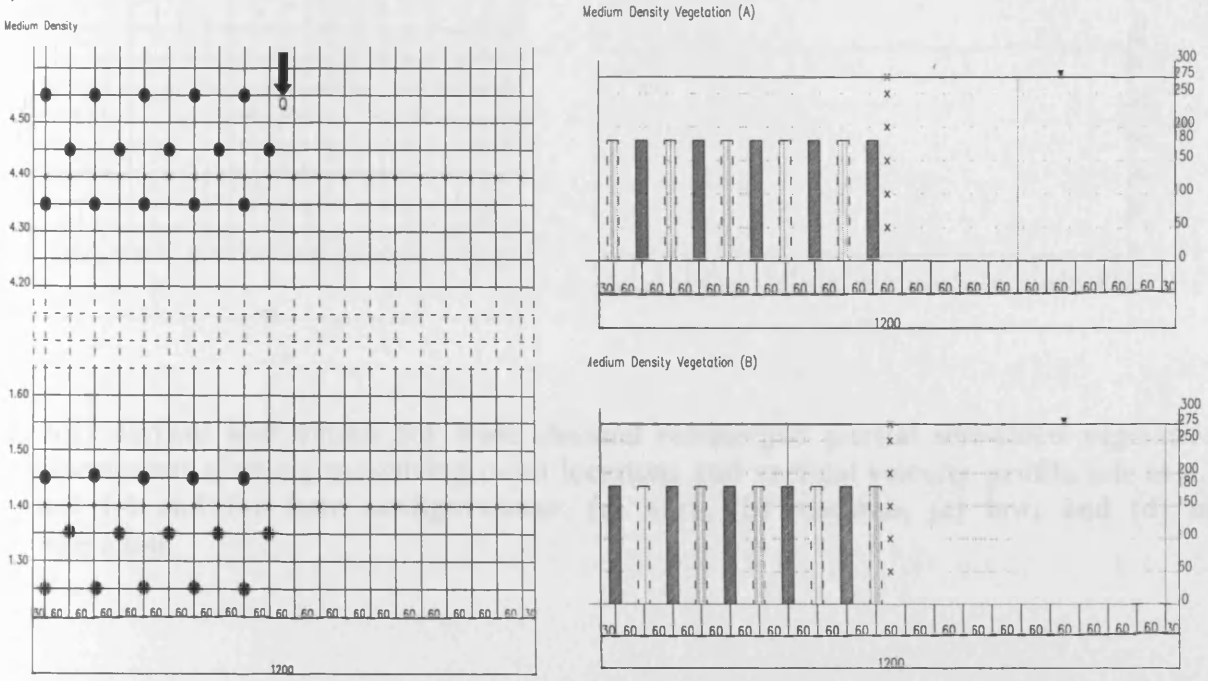

(c)

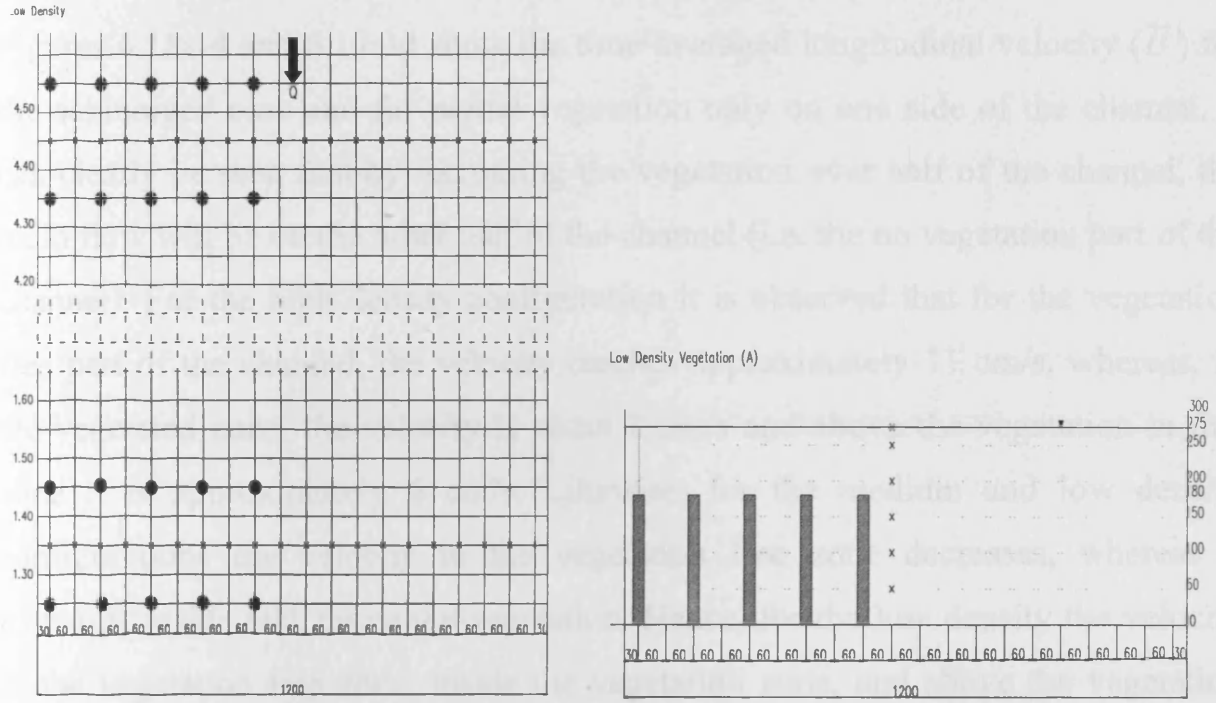

(d)

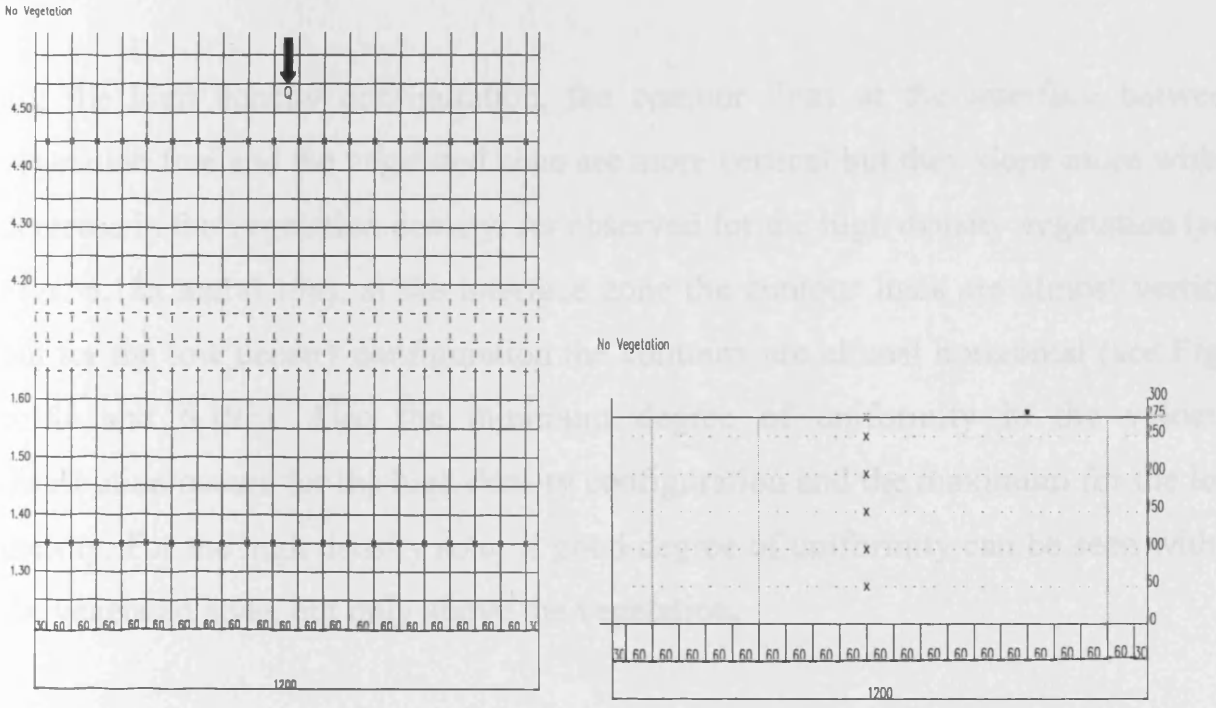

Fig. 6.17 Layout and details for wide channel submerged partial one-sided vegetation experiments showing measuring point locations and vertical velocity profile sets at 4.4 and 1.4 and for four configurations: (a) high, (b) medium, (c) low, and (d) no vegetation.

a) Time-averaged longitudinal velocity ($\overline{U}$)

Figures 6.18a-d and 6.19a-d show the time-averaged longitudinal velocity ($\overline{U}$) for the submerged case and for partial vegetation only on one side of the channel. It can clearly be seen that by increasing the vegetation over half of the channel, the main flow will be on the other half of the channel (i.e. the no vegetation part of the channel). For the high density configuration it is observed that for the vegetation free part of the channel, the velocity reaches approximately 11 cm/s, whereas, in the vegetated zone, the velocity is about 2 cm/s and above the vegetation in this zone it is approximately 6 cm/s. Likewise, for the medium and low density configurations the velocity in the vegetation free zone decreases, whereas it increases inside and above the vegetation. Hence, for the low density the velocity in the vegetation free zone, inside the vegetation zone, and above the vegetation zone peaks at about 9, 5, and 7 cm/s respectively.

For the high density configuration, the contour lines at the interface between vegetation free and the vegetated zone are more vertical but they slope more with a decrease in the vegetation density. As observed for the high density vegetation (see Figs. 6.18a and 6.19a), at the interface zone the contour lines are almost vertical but for the low density configuration the contours are almost horizontal (see Figs. 6.18c and 6.19c). Also the minimum degree of uniformity in the velocity distribution occurs for the high density configuration and the maximum for the low density. For the high density setup a good degree of uniformity can be seen within the vegetated zone, but only above the vegetation.

The depth-averaged longitudinal velocity profiles across the section for the submerged vegetation are shown for all densities at the cross-sections 4.4 and 1.4 in Figs. 6.18e and 6.19e. As mentioned previously, and also clearly demonstrated in the figures, due to existence of vegetation along half of the channel, the main flow advects to the non-vegetated part of the channel. For the high density

configuration it is observed that the lowest velocity is about 3 cm/s with little variation and is almost constant across the vegetated half of channel. In contrast, in the vegetation free half of channel, the velocity increases sharply to reach a maximum of nearly 12 cm/s i.e. a four fold increase. With the vegetation reduction, the velocity profile changes in the vegetated and vegetation free halves of the channel. This means that for the low density configuration, the velocity in the vegetated half of the channel remains at a maximum value with little variation and with the velocity being typically 4 cm/s. For the vegetation free half of the channel, however, the minimum velocity is about 8 cm/s (as compared to 12 cm/s for the high density case). For the no vegetation case the velocity is approximately 5 cm/s, with little variation across the section.

(a)

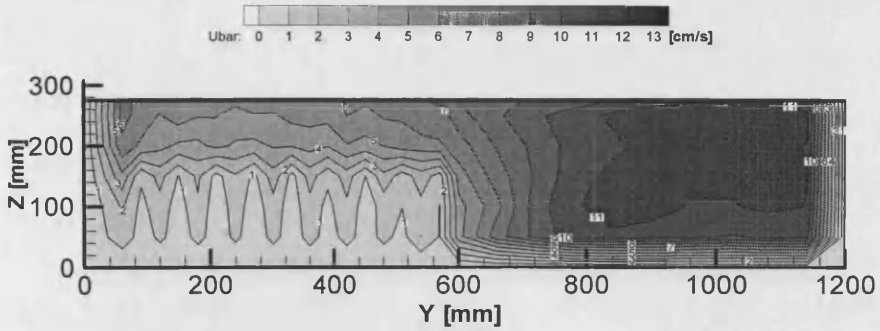

(b)

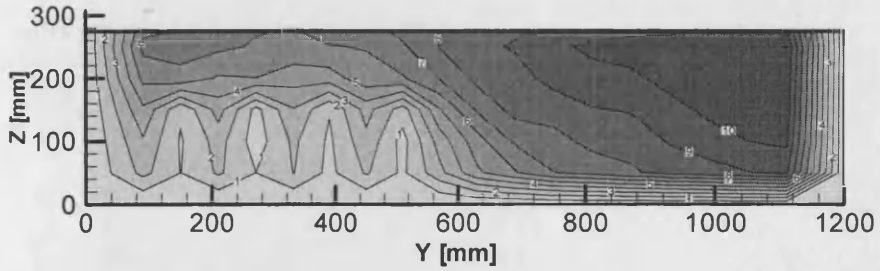

(c)

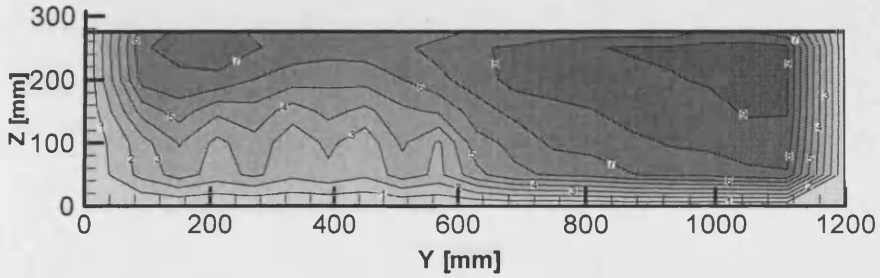

(d)

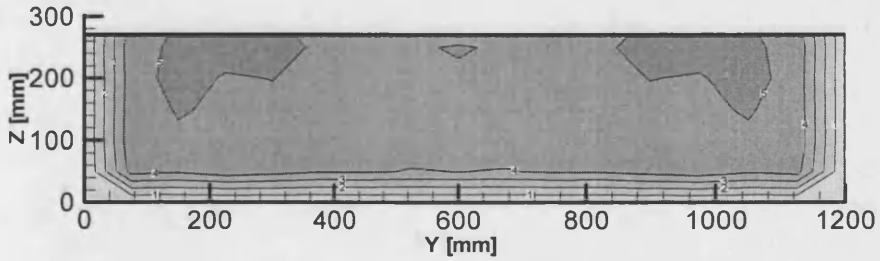

(e)

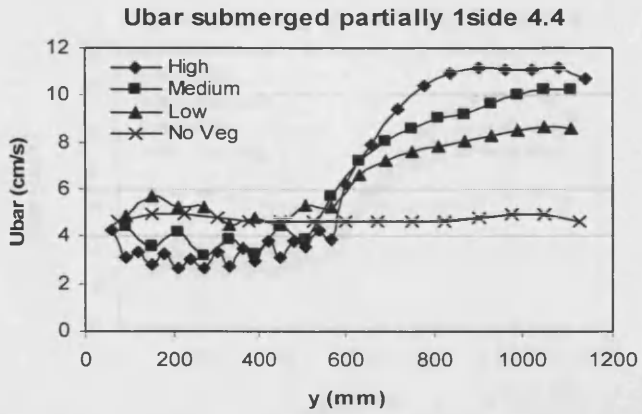

Fig. 6.18 Time-averaged longitudinal velocity ($\overline{U}$) [cm/s] submerged partial one-sided vegetation at cross-section 4.4 for four configurations: (a)high, (b) medium, (c) low, and (d) no vegetation; (e) depth-averaged vertical velocity profiles.

(a)

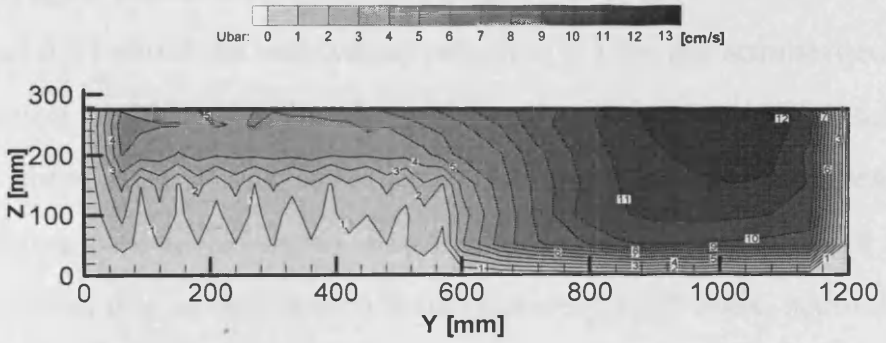

(b)

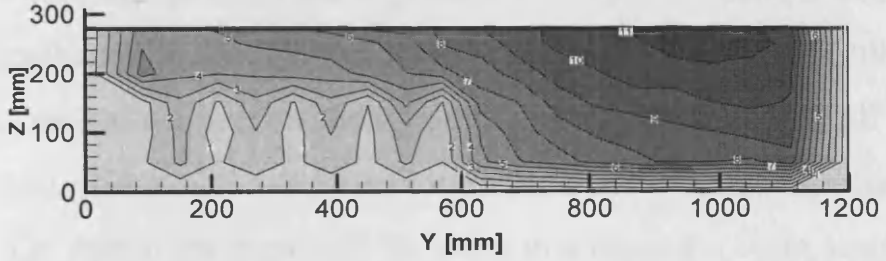

(c)

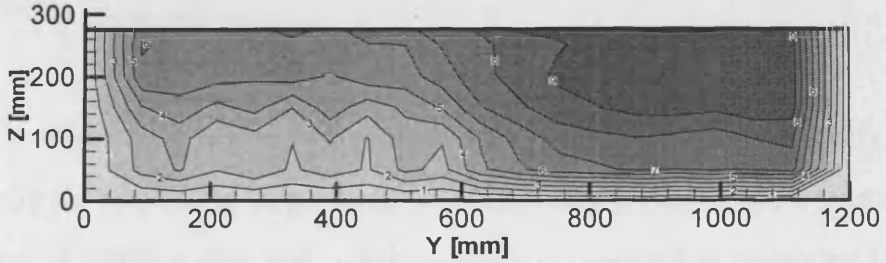

(d)

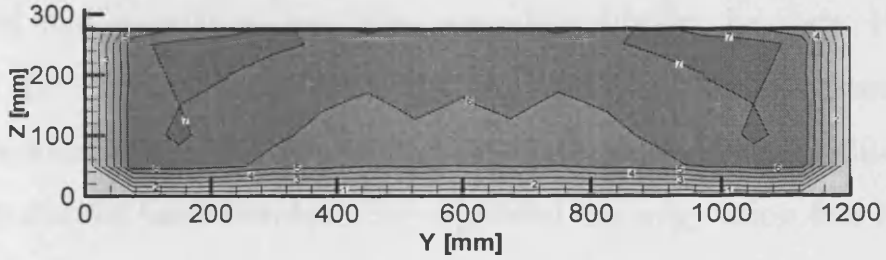

(e)

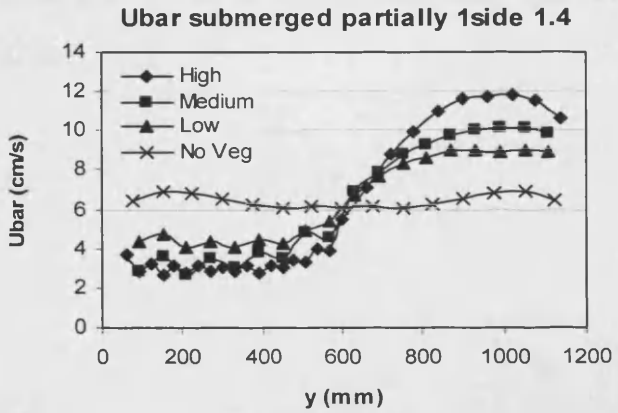

Fig. 6.19 Time-averaged longitudinal velocity ($\overline{U}$) [cm/s] submerged partial one-sided vegetation at cross-section 1.4 for four configurations: (a) high, (b) medium, (c) low, and (d) no vegetation; (e) depth-averaged vertical velocity profiles.

b) Time-averaged transverse velocity component ($\overline{V}$)

Figs. 6.20 and 6.21 show the transverse velocity ($\overline{V}$) for the submerged partial one-sided vegetation and the results show the velocities to be very scattered. The results also show that in the layer near the water surface the peak velocities sometimes move to a lower depth. Regarding Figs. 6.20a and 6.21a for the high density vegetation due to the existence of relatively high rods, secondary currents are not formed. However when the vegetation density is reduced a weak secondary current is established in the surface layer of the flow (see Figs. 6.20b,c). For the case with no vegetation, the secondary current completely covers all parts of the channel. Due to effects of wave formation in the wide channel especially at cross-section 1.4 (i.e. due to the proximity to weir) this caused a wide scattering in the velocity profiles.

Figures 6.20e and 6.21e show the depth-averaged transverse velocity profiles for submerged partial one-sided vegetation for four states. Since the vegetation for half of the channel is submerged, the depth-averaged transverse velocity is the sum of the vegetated and vegetation free zone velocities above the rods. Hence, some diffusion of the velocity profile is visible. Although for the low density case the velocity is a minimum over all areas compared to the high and medium densities, they have almost the same trends in the vegetated and vegetation free halves of the channel. The no vegetation case, as expected, has almost horizontal contours across the channel width.

(a)

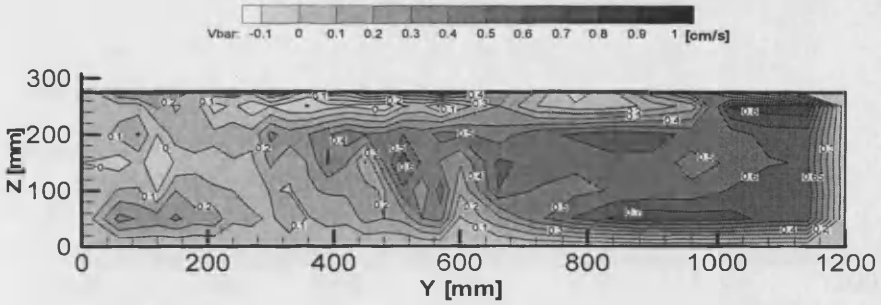

(b)

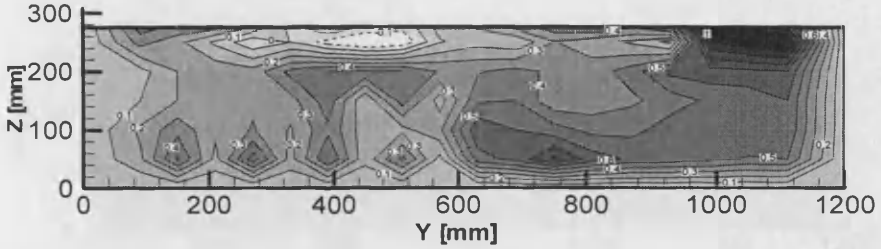

(c)

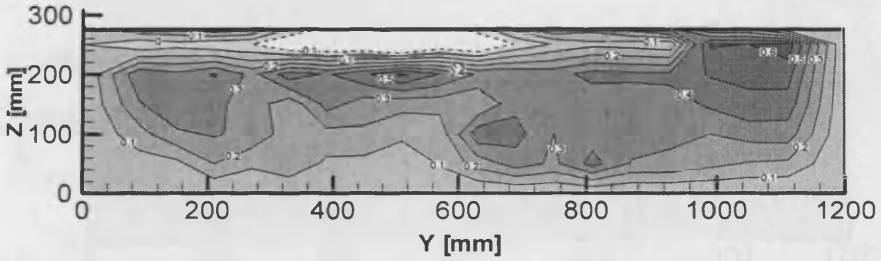

(d)

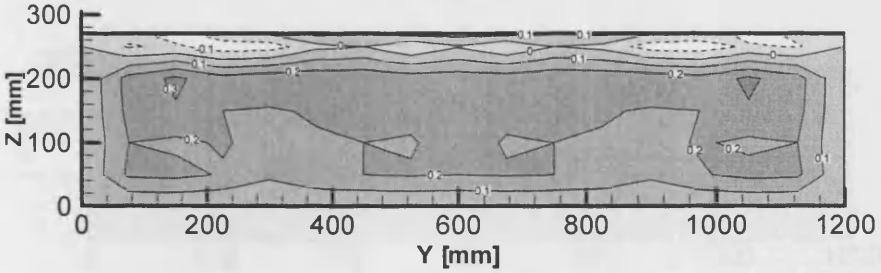

(e)

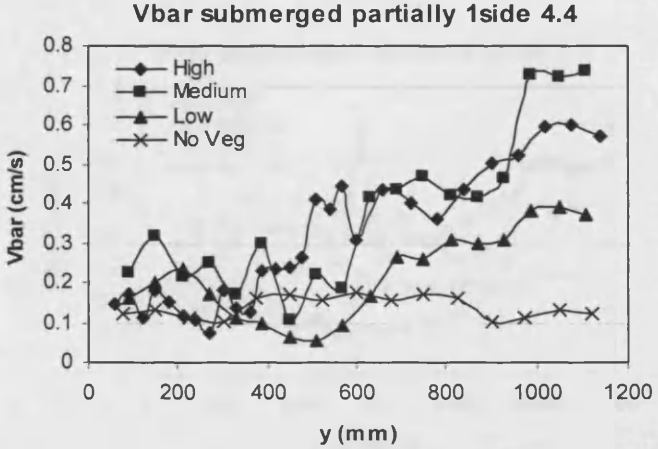

Fig. 6.20 Time-averaged transverse velocity ($\overline{V}$) [cms^{-1}] submerged partial one-sided vegetation at cross-section 4.4 for four configurations: (a) high, (b) medium, (c) low, and (d) no vegetation; (e) depth-averaged vertical velocity profiles.

(a)

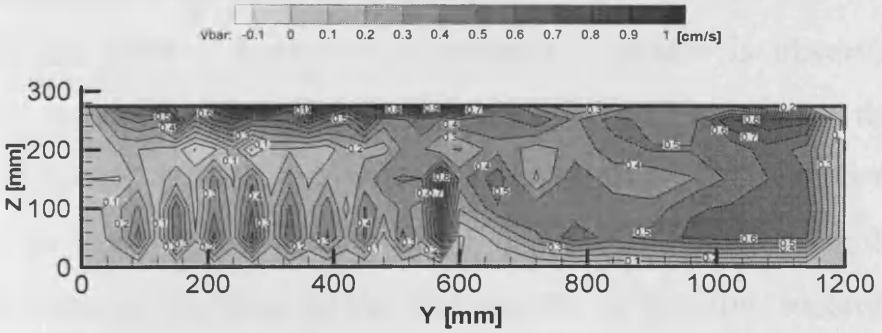

(b)

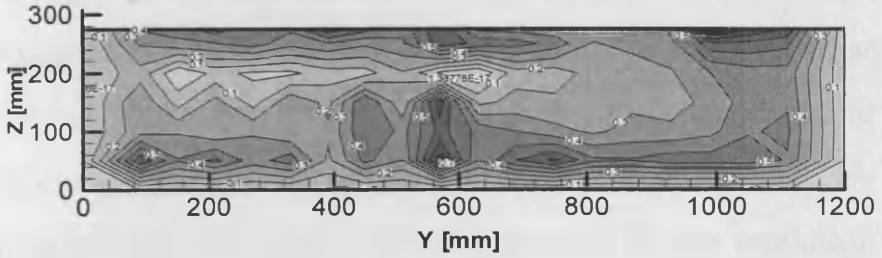

(c)

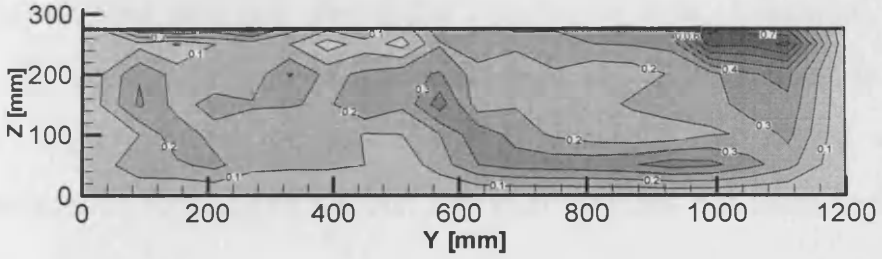

(d)

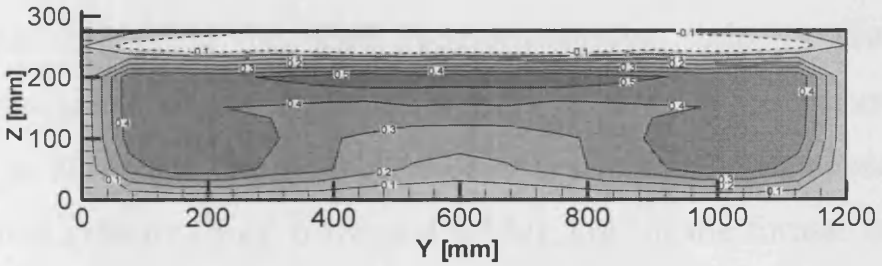

(e)

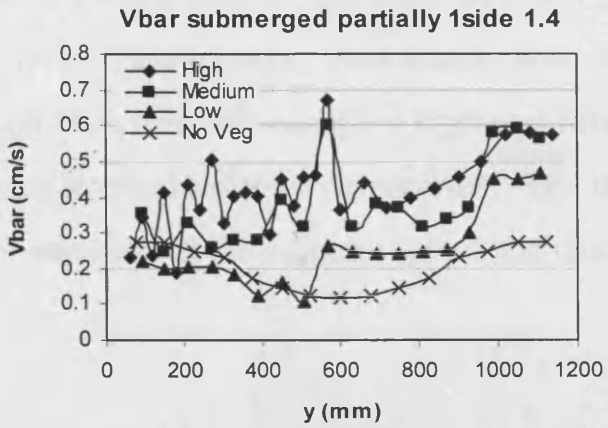

Fig. 6.21 Time-averaged transverse velocity ($\overline{V}$) [cms^{-1}] submerged partial one-sided vegetation at cross-section 1.4 for four configurations: (a) high, (b) medium, (c) low, and (d) no vegetation; (e) depth-averaged vertical velocity profiles.

c) Time-averaged vertical velocity component ($\overline{W}$)

In Figs. 6.22 and 6.23 a downward momentum transfer is observable for the vegetation free zone and above the vegetation zone for all vegetation densities. The maximum downward trend in the velocity is generally observed to occur in the area between the vegetation and vegetation free zones. In considering the figures in more detail it is considered that for the high density vegetation, secondary currents are formed strongly in the vegetation free zone of the channel and weakly above the vegetation part of the channel (see Figs. 6.22a and 6.23a). Also, sometimes for the high density configuration under the influence of vortex shedding of the rods, the secondary current is not visible. However, with the reduction in the velocity with the vegetation, the secondary current is formed in the transition zone in the middle of channel and also just above the vegetation zone. Likewise, for the low density case, the secondary current is formed fully in the transition zone (see Figs. 6.22c and 6.23c). However, because of the effects of a transversal wave on the velocity components, sometimes a secondary current does not form in the channel.

In Figs. 6.22e and 6.23e the depth-averaged vertical velocity profile for the submerged partial one-sided vegetation for the four cases, at the two cross-sections 4.4 and 1.4, is observed. The vertical velocity generally has an opposite trend to the longitudinal velocity (Figs. 6.18e and 6.19e), but for the former there is some diffusion in the profile. It can be seen for the vegetated half zone that the high and low density cases have respectively maximum and minimum velocities. Conversely, in the vegetation free half zone, the high and low density cases have a minimum and maximum vertical velocity respectively. For the no vegetation case there is also a minimal variation in the velocity across the channel width.

(a)

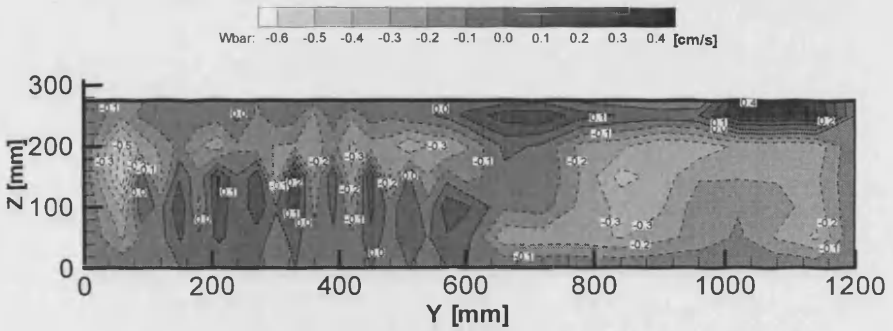

(b)

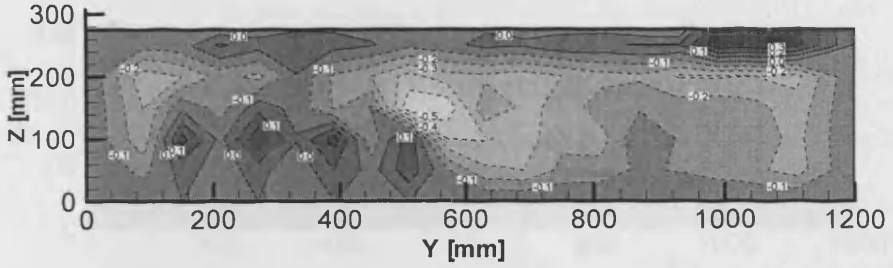

(c)

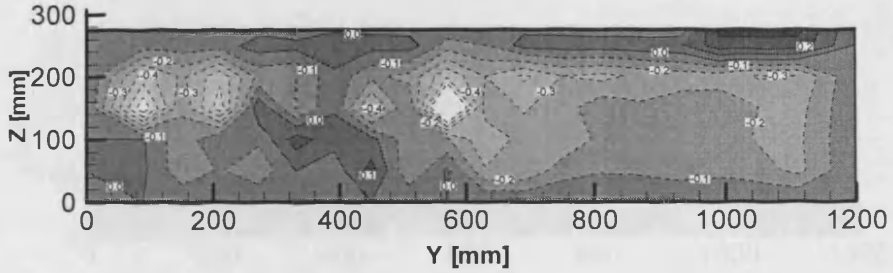

(d)

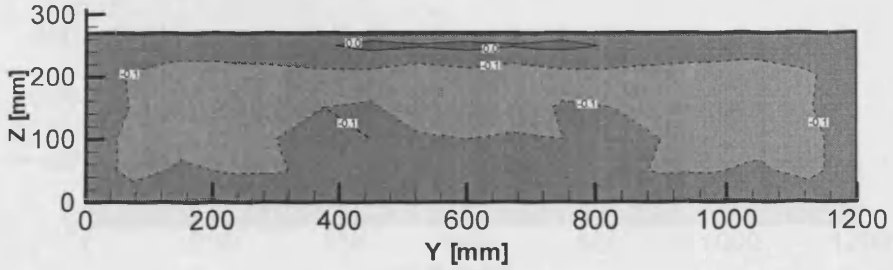

(e)

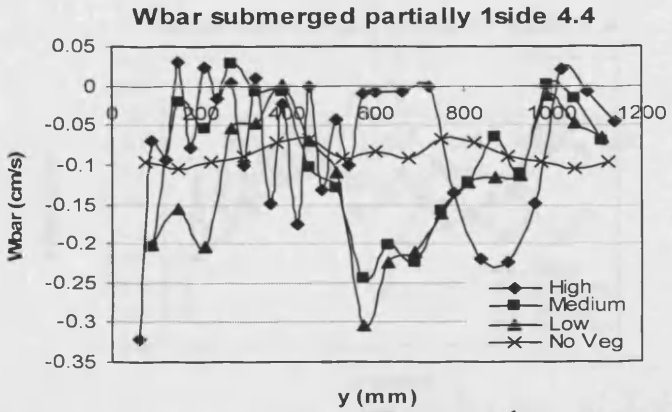

Fig. 6.22 Time-averaged vertical velocity ($\overline{W}$) [cms^{-1}] submerged partial one-sided vegetation at cross-section 4.4 for four configurations: (a) high, (b) medium, (c) low, and (d) no vegetation; (e) depth-averaged vertical velocity profiles.

(a)

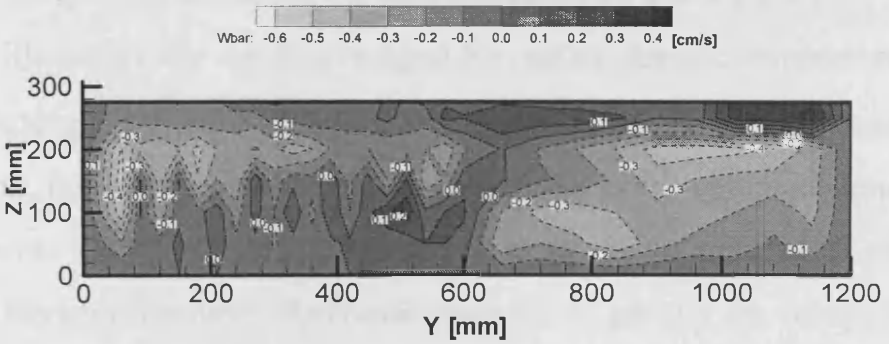

(b)

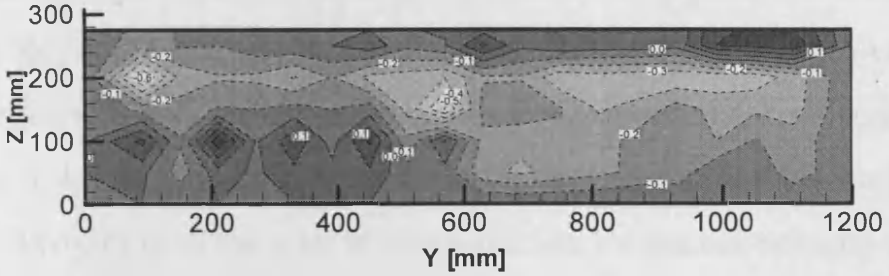

(c)

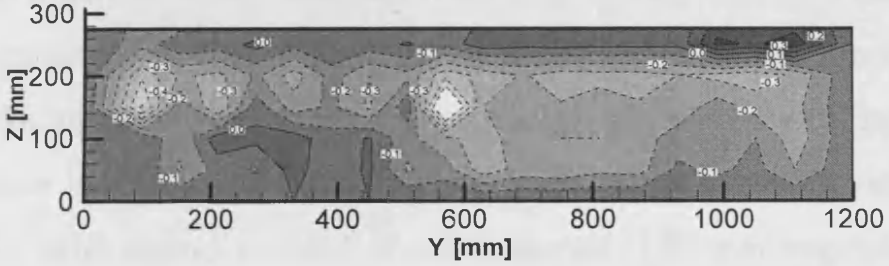

(d)

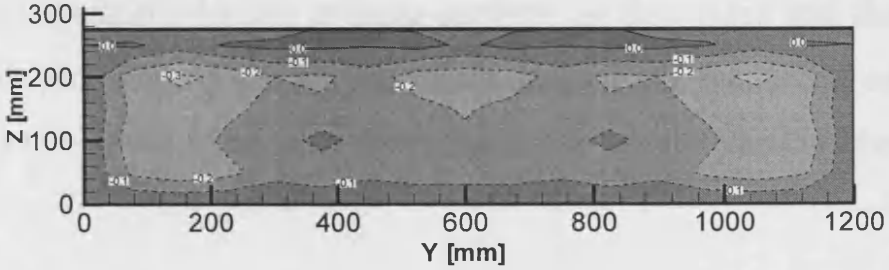

(e)

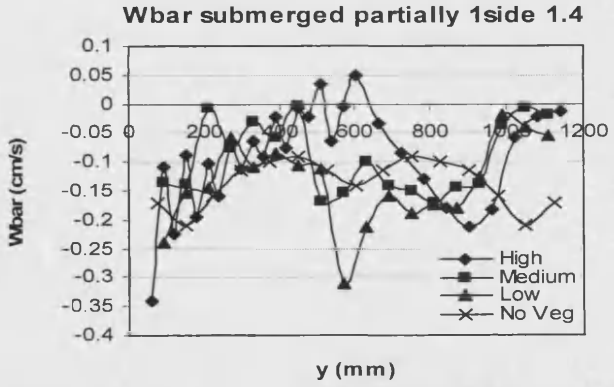

Fig. 6.23 Time-averaged vertical velocity ($\overline{W}$) [cms^{-1}] submerged partial one-sided vegetation at cross-section 1.4 for four configurations: (a) high, (b) medium, (c) low, and (d) no vegetation; (e) depth-averaged vertical velocity profiles.

d) Depth-averaged Reynolds stress components ($\overline{u'v'}$, $\overline{u'w'}$, $\overline{v'w'}$)

Figure 6.24 illustrates the depth-averaged Reynolds stress components ($\overline{u'v'}$, $\overline{u'w'}$, $\overline{v'w'}$) for submerged partial one-sided vegetation. As in the results demonstrated in all the graphs, the area between the vegetated and non-vegetated zones gives the maximum value for the Reynolds stress components. In general in the vegetated zone, the difference between Reynolds stresses is greater in compared with the differences in the non-vegetated zone. On the other hand, there is a clear difference between the Reynolds stresses at the cross-sections 4.4 and 1.4. In cross-section 4.4 of the vegetated half, the Reynolds stress is a minimum for all components. In cross-section 1.4, however, due to the proximity to the weir (tailgate) the results are different. Proximity to the weir in cross-section 1.4 causes velocity decreases in lower depth which is lower than the weir (i.e. lower than 250 mm), and all velocities decrease and then almost remain constant. Therefore the overall flow transfers to the upper layers (above the weir edge) and the longitudinal Reynolds stress increases more than the other Reynolds stresses (transverse and vertical). Consequently, with regard to level of submergence (180 mm vegetation height), the effect of vegetation density at cross-section 1.4 decreases and the staggering effect is more pronounced. Hence, the results for the no vegetation case at cross-section 1.4 are observed to be too small and with little variation compared to cross-section 4.4.

(a)

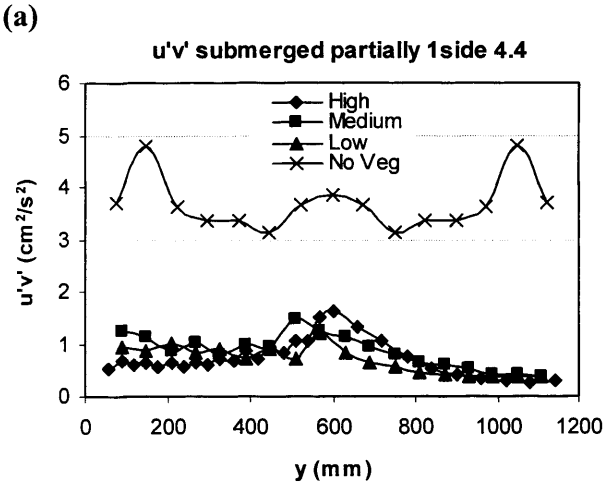

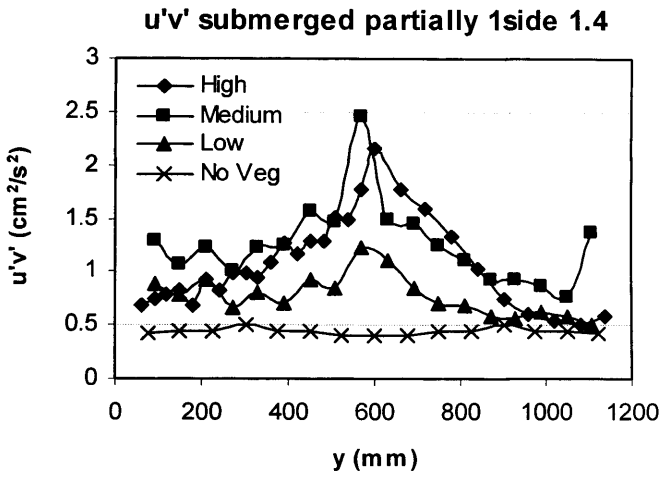

(b)

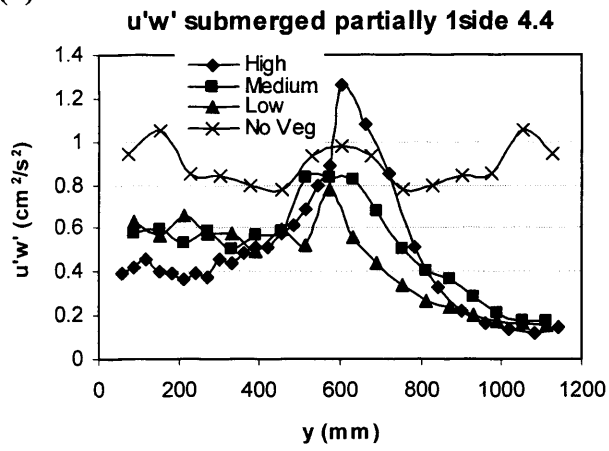

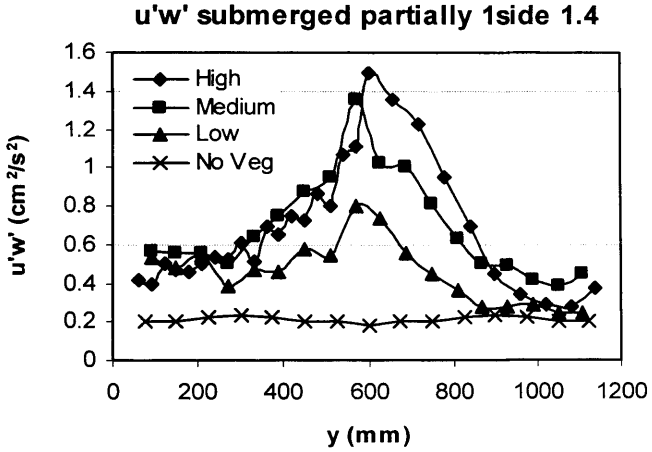

(c)

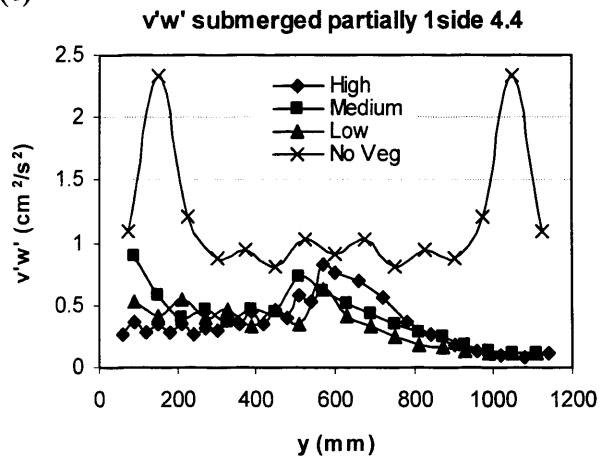

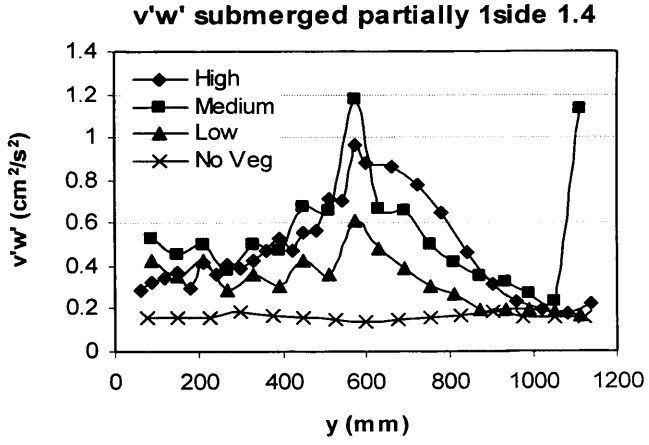

Fig. 6.24 Depth-averaged Reynolds stresses components ($\overline{u'v'}$, $\overline{u'w'}$, $\overline{v'w'}$) [cm^2/s^2] for four configurations in submerged partial one-sided vegetation at cross-sections 4.4 and 1.4; (a) $\overline{u'v'}$, (b) $\overline{u'w'}$, and (c) $\overline{v'w'}$.

6.3.2 Emergent vegetation (rods height = 300 mm)

A set of experiments was carried out to investigate the effect of partial one-sided emergent vegetation on the velocity profiles. As illustrated in Fig. 6.25 the rods have heights of 300 mm and the rods protrude above the water surface.

(a)

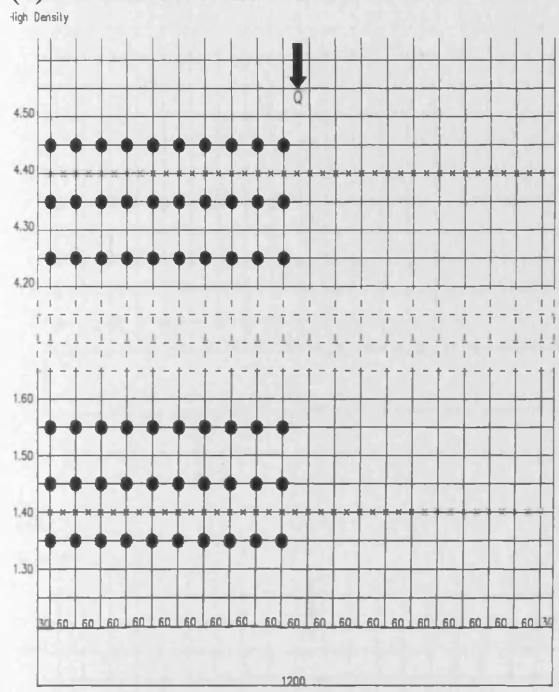

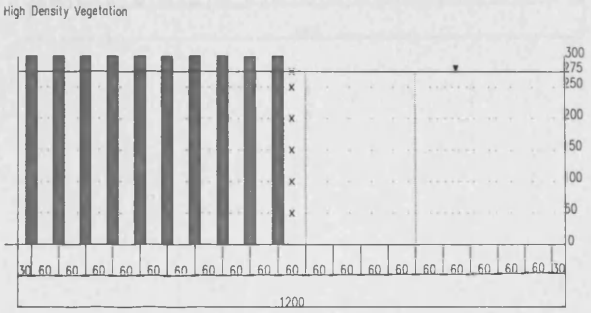

(b)

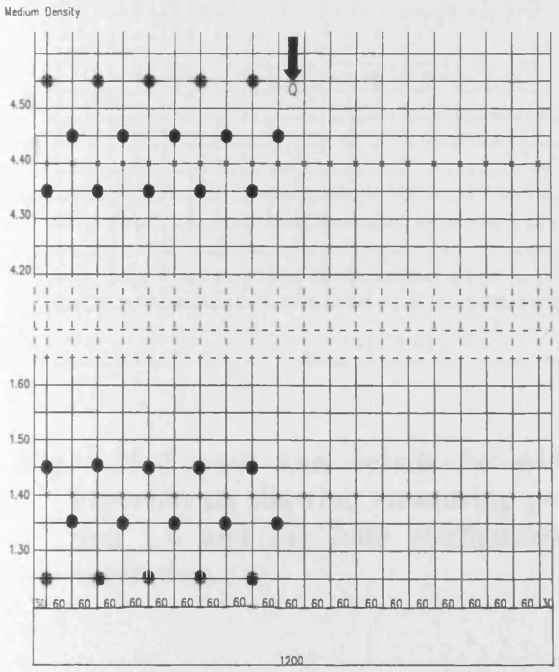

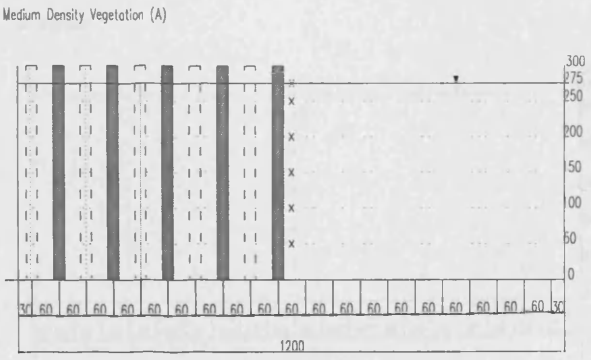

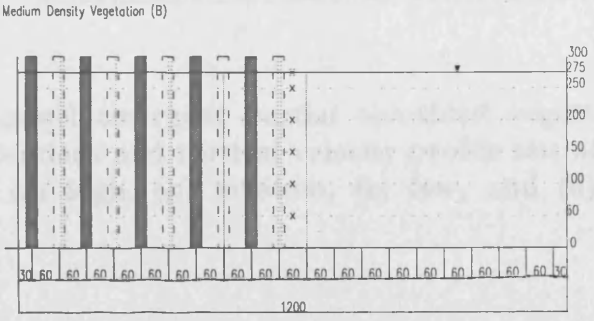

(c)

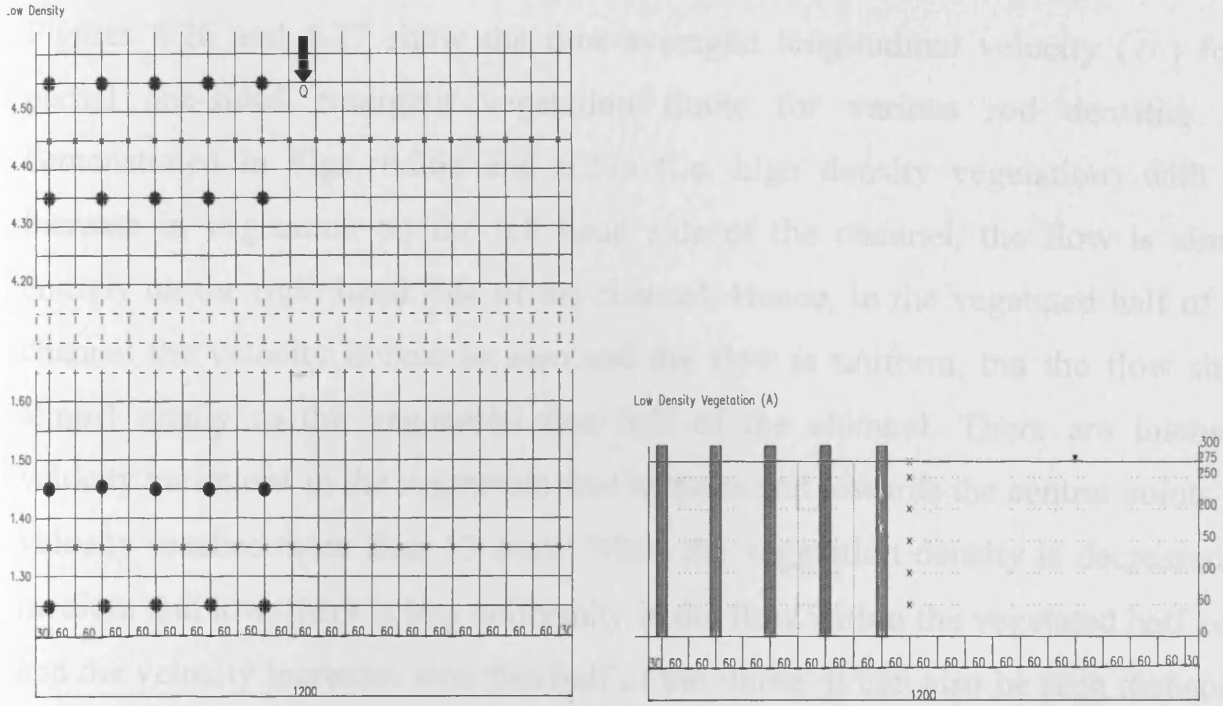

(d)

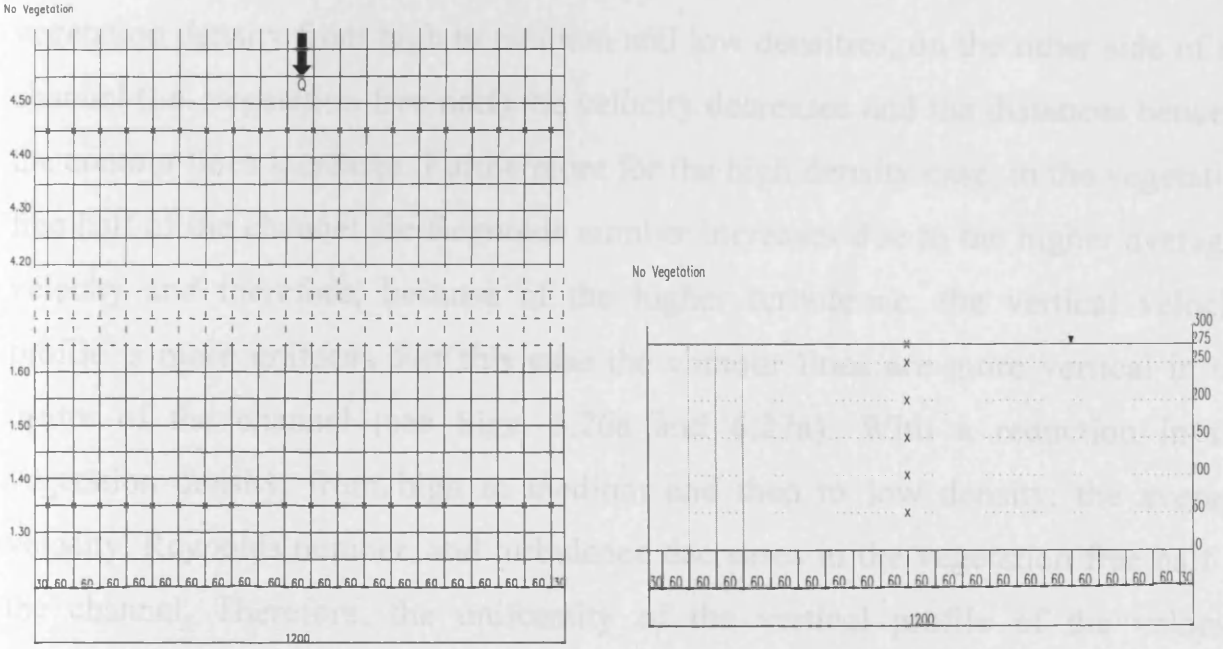

Fig. 6.25 Layout and details for wide channel emergent partial one-sided vegetation experiments showing measuring point locations and vertical velocity profile sets at 4.4 and 1.4 and for four configurations: (a) high, (b) medium, (c) low, and (d) no vegetation.

a) Time-averaged longitudinal velocity ($\overline{U}$)

Figures 6.26 and 6.27 show the time-averaged longitudinal velocity ($\overline{U}$) for a partial one-sided emergent vegetation flume for various rod densities. As demonstrated in Figs. 6.26a and 6.27a (i.e. high density vegetation) with the increase in vegetation on the left hand side of the channel, the flow is almost entirely on the right hand side of the channel. Hence, in the vegetated half of the channel the velocity is near to zero and the flow is uniform, but the flow shifts almost totally to the vegetation free half of the channel. There are intensive velocity variations in the vegetation free sections and towards the central points the velocity reaches more than 13 cm/s. When the vegetation density is decreased to medium and low, there is less uniformity in the flow within the vegetated half zone and the velocity increases over this half of the flume. It can also be seen that some vertical contour lines appear between the rods. For the low density the velocity reaches up to 3 cm/s between the rods. On the contrary, with a decrease in the vegetation density from high to medium and low densities, on the other side of the channel (i.e. vegetation free half) the velocity decreases and the distances between the contour lines increases. Furthermore for the high density case, in the vegetation free half of the channel the Reynolds number increases due to the higher averaged velocity and therefore, because of the higher turbulence, the vertical velocity profile is more uniform. For this case the contour lines are more vertical in the centre of the channel (see Figs. 6.26a and 6.27a). With a reduction in the vegetation density, from high to medium and then to low density, the average velocity, Reynolds number, and turbulence decreases in the vegetation free half of the channel. Therefore, the uniformity of the vertical profile of the velocity decreases and the contour lines change from near vertical to more circular. The distance between the contour lines also increases, confirming less variation across the flume (see Figs. 6.26c and 6.27c).

Figures 6.26e and 6.27e show the depth-averaged longitudinal velocity profile for the emergent partial one-sided vegetation for the cross-sections 4.4 and 1.4. From the results it is evident that, due to the existence of the emergent vegetation over half of the channel, the main flow transfers to the vegetation free half zone of channel. Hence, the velocity difference between the two halves is very pronounced, with the velocities being even higher than for the submerged partially one-sided configuration. For example, the velocity in vegetated half of the channel is less than 2 cm/s and almost constant with a similar trend for all densities. However, this sharply increases in the vegetation free half of the channel and reaches about 12 cm/s at the centre of the zone. Also, for the high density case, due to the small velocity in vegetated half of the channel (i.e. behind and in between the rods) the velocity variation is much smaller in comparison with that for the medium and low densities. With a reduction in the vegetation density in the vegetated half of the channel, the velocity difference between the two halves of the channel decreases. Hence, the velocity in the vegetated half of the channel is observed to be approximately 0.5 cm/s for the high density, whereas for the low density case, the velocity is seen to be approximately 2 cm/s. In contrast, in the vegetation free half of the channel, the velocity is higher than for the medium and low densities. For cross-section 1.4, for some parts of the section there is little diffusion in the velocity profile due to the proximity to the weir. The velocity profile, as before, in the no vegetation configuration is nearly constant with horizontal contour lines across the channel width.

(a)

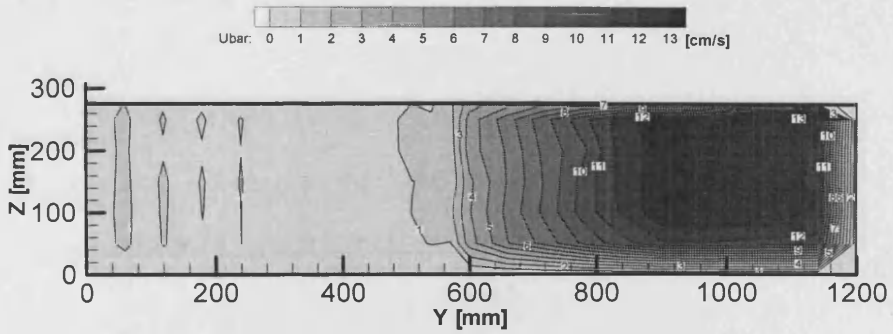

(b)

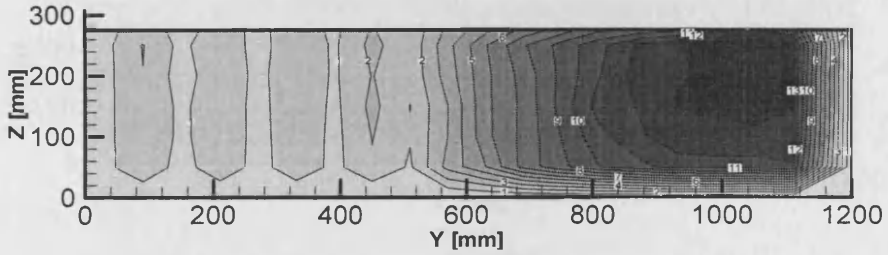

(c)

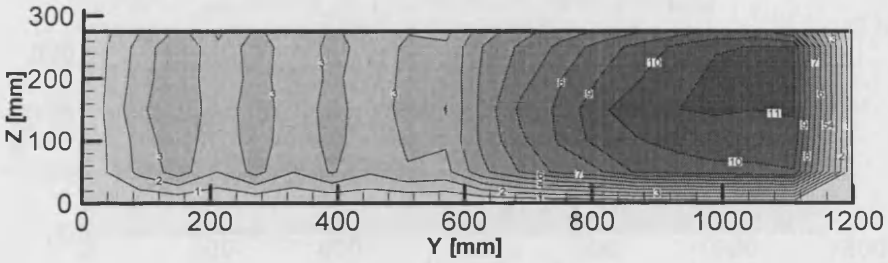

(d)

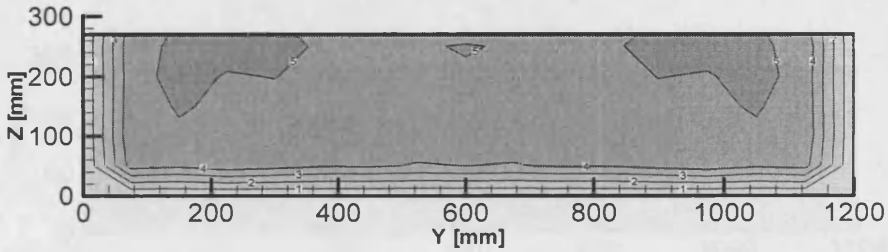

(e)

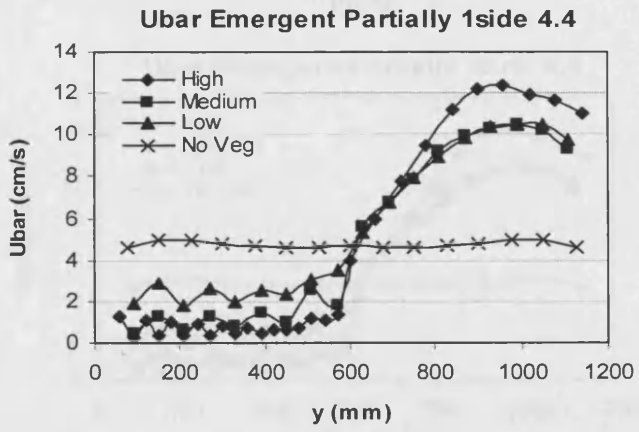

Fig. 6.26 Time-averaged longitudinal velocity ($\overline{U}$) [cms^{-1}] emergent partial one-sided vegetation at cross-section 4.4 for four configurations: (a) high, (b) medium, (c) low, and (d) no vegetation; (e) depth-averaged vertical velocity profiles.

(a)

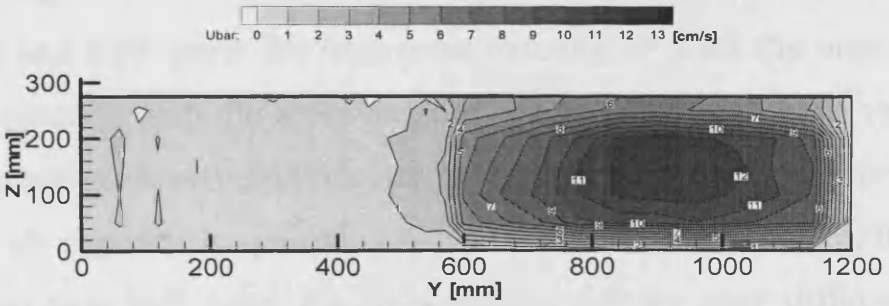

(b)

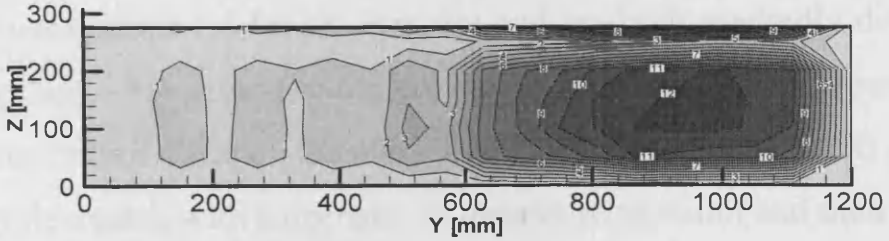

(c)

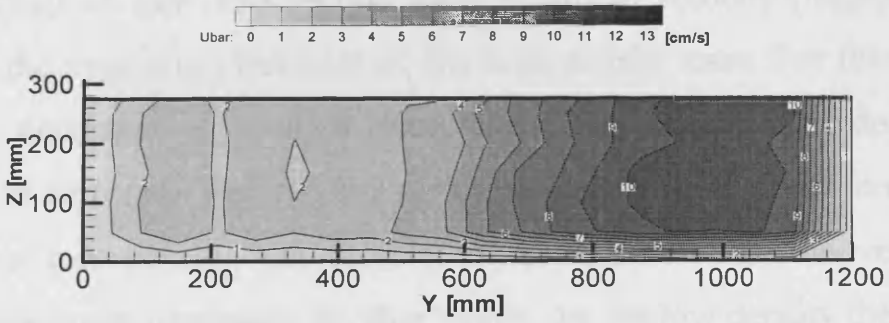

(d)

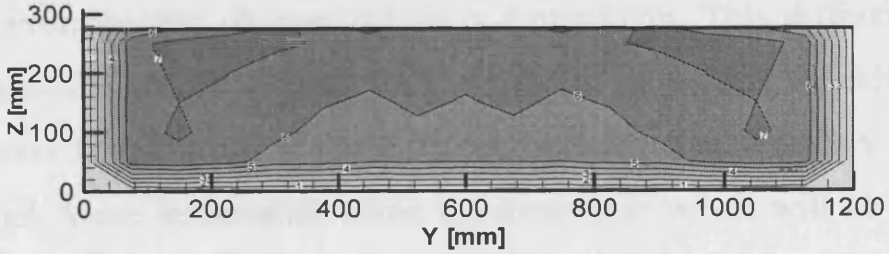

(e)

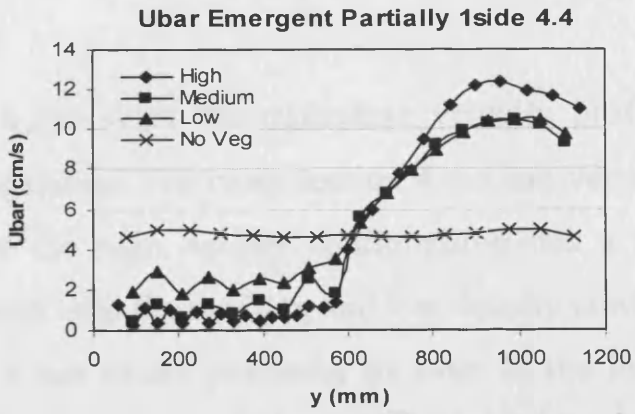

Fig. 6.27 Time-averaged longitudinal velocity ($\overline{U}$) [cms^{-1}] emergent partial one-sided vegetation at cross-section 1.4 for four configurations: (a) high, (b) medium, (c) low, and (d) no vegetation; (e) depth-averaged vertical velocity profiles.

b) Time-averaged transverse velocity ($\overline{V}$)

Figures 6.28 and 6.29 show the transverse velocity ($\overline{V}$) for the emergent partial one-sided vegetation with the cross-sections 4.4 and 1.4 again have very different results. Although the transverse velocity in the vegetated half zone for both cross-sections and all densities is approximately uniform and close to zero, the results in the vegetation free half zone, for cross-section 4.4 are very different from the results for cross-section 1.4 for all densities and are both markedly different from the vegetated half . For cross-section 4.4 with a high density configuration in the vegetation free half of channel, the maximum velocity (positive point) can be seen. This velocity decreases with a decrease in density to medium and then low density (see Fig. 6.28a,b,c). For cross-section 1.4 a minimum velocity (negative point) is observed in the vegetation free half for the high density case. For this case, when the density decreases to medium and low, the velocity also decreases and approaches to zero (see Fig. 6.29a,b,c). This means that for both cross-sections, from high to low density, the velocity difference between the vegetated and vegetation free zones decreases. In other words, for the low density the variation in velocity between the two channel halves is a minimum. This difference between the two cross-sections is caused by the effects of vortex shedding and the transverse wave in the channel, which sometimes prevents secondary current flow in the channel. More information about the transverse waves will be presented in Chapter 7.

Figures 6.28e and 6.29e show the transverse velocity profile for the emergent partial one-sided vegetation. For cross-section 4.4 some variation in the vegetated half is observed, as the high density configuration has a maximum transverse velocity in comparison with the medium and low density configurations. However, for cross-section 1.4 due to the proximity to weir, in the lower depth below the weir height (i.e. under 250 mm height from the bed), the velocity is almost constant and extremely small (near zero). Therefore, the effect of the vegetation

density is less pronounced in cross-section 1.4, unlike cross-section 4.4. Hence, in cross-section 1.4 the transverse velocity for the high density case is smaller than that for the medium and low densities. For the non-vegetated half of channel due to extensive diffusion in the velocity profile no assessment of the velocity structure can be readily made. For no vegetation case, due to effects of the weir proximity, no variation in the transverse velocity across the channel width is observed.

(a)

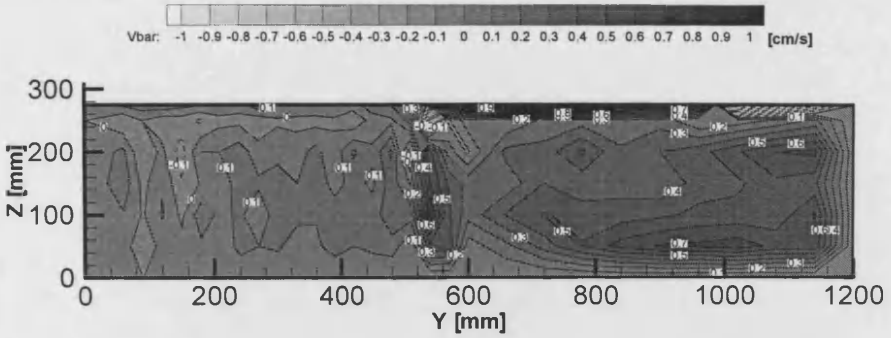

(b)

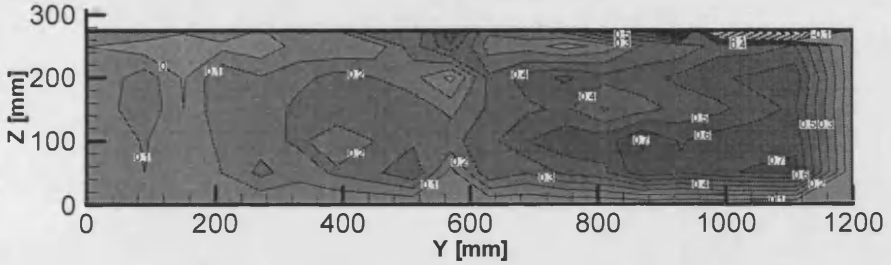

(c)

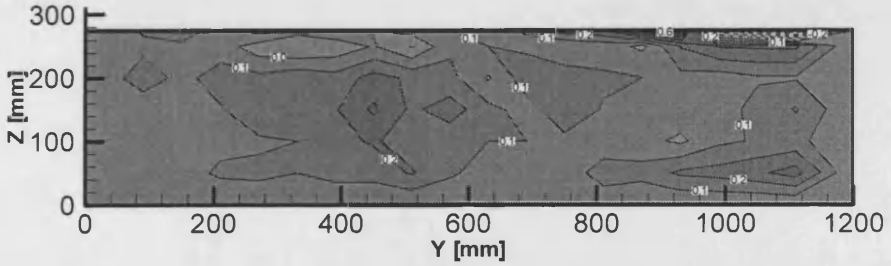

(d)

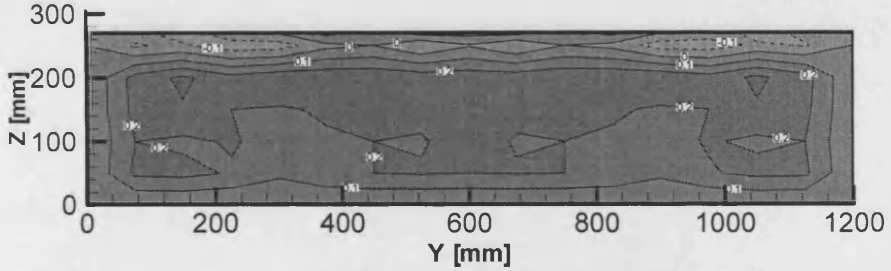

(e)

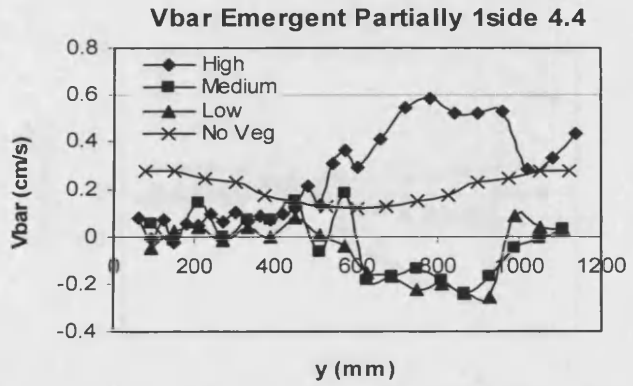

Fig. 6.28 Time-averaged transverse velocity ($\overline{V}$) [cms^{-1}] emergent partial one-sided vegetation at cross-section 4.4 for four configurations: (a) high, (b) medium, (c) low, and (d) no vegetation; (e) depth-averaged vertical velocity profiles.

(a)

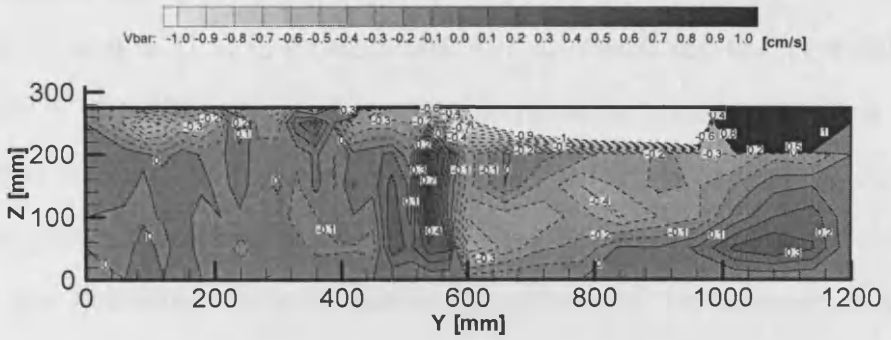

(b)

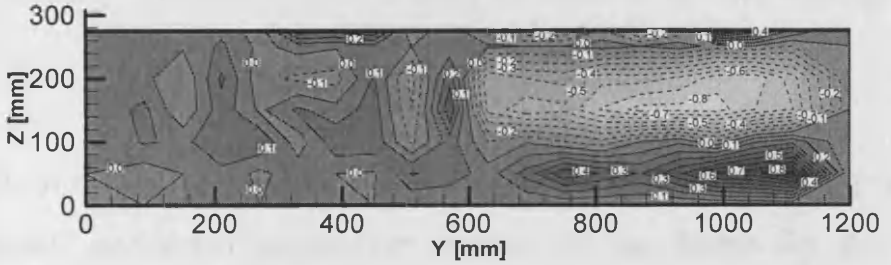

(c)

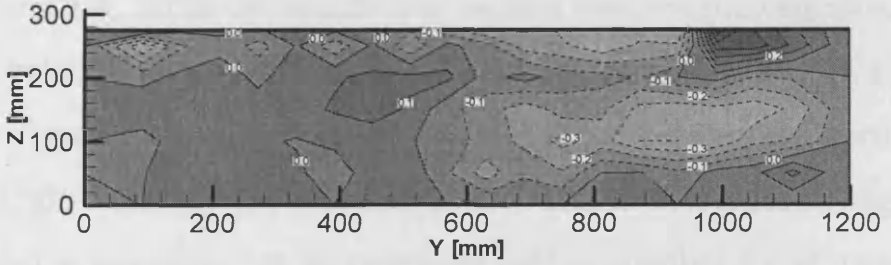

(d)

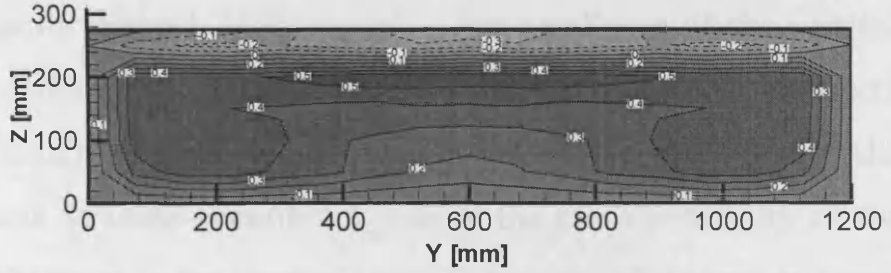

(e)

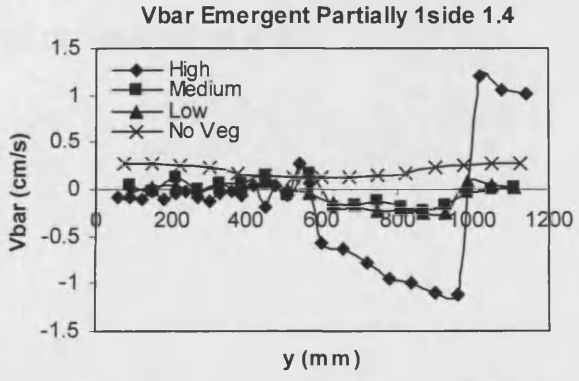

Fig. 6.29 Time-averaged transverse velocity ($\overline{V}$) [cms^{-1}] emergent partial one-sided vegetation at cross-section 1.4 for four configurations: (a) high, (b) medium, (c) low, and (d) no vegetation; (e) depth-averaged vertical velocity profiles.

c) Time-averaged vertical velocity component ($\overline{W}$)

From Figs. 6.30 and 6.31 it is evident that for all densities the vertical velocity in vegetated half of the channel is almost uniform with a velocity close to zero, but across the other half of the channel (i.e. vegetation free zone) the velocity structure forms a strong secondary current, with a downward-trend in the velocity core. As discussed in the previous section, due to the effect of the transverse wave on the flow, the secondary currents cannot always be formed or they change location in the channel.

Figures 6.30e and 6.31e show the depth-averaged vertical velocity profiles in the emergent partial one-sided vegetation section of the flume for the two cross-sections 4.4 and 1.4. From the results it is evident that, for the vegetated half of the channel, the velocity is too small to be measured accurately for all of the densities, but over the vegetation free half of the channel it can be seen the vertical velocity is relatively high. Also, the greatest part of the vertical velocities in vegetation free half of channel is negative, but in vegetated half is positive for all cases and both cross-sections of channel. With regard to the smallness of the vertical velocities, and also the diffusion for the different configurations in both cross-sections 4.4 and 1.4, it is difficult to analyse the results with any degree of certainty. Also for the no vegetation case in cross-section 1.4, due to the close proximity of the weir little variation is observed in the vertical velocity in wide of channel in comparison with the velocity variations at cross-section 4.4.

(a)

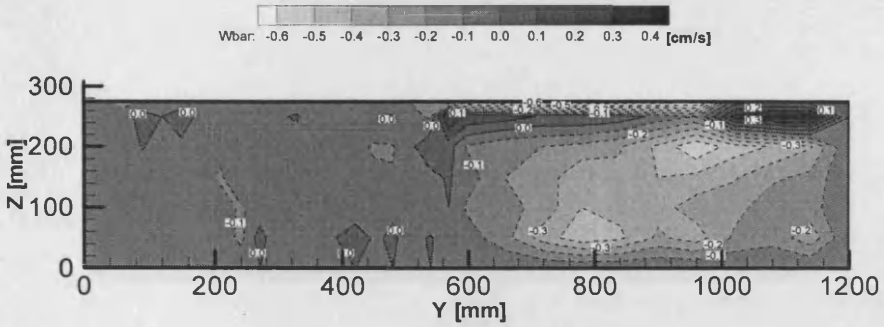

(b)

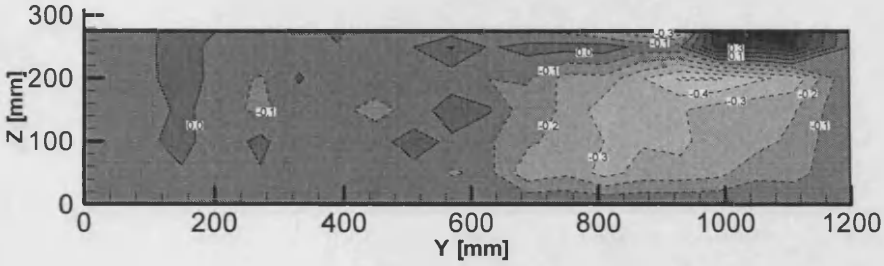

(c)

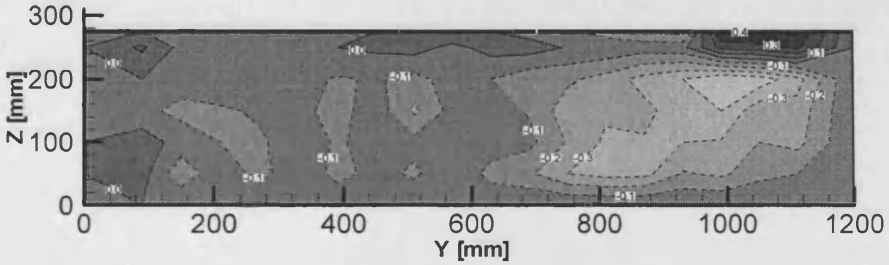

(d)

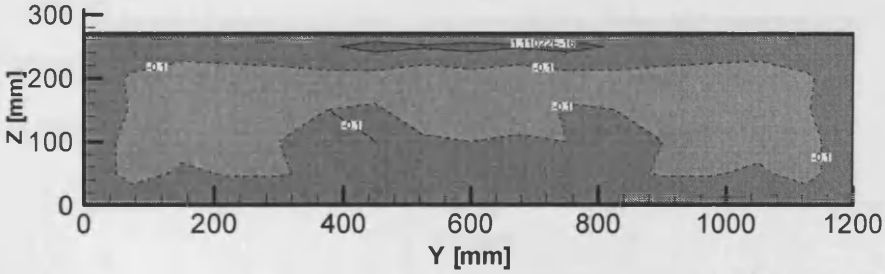

(e)

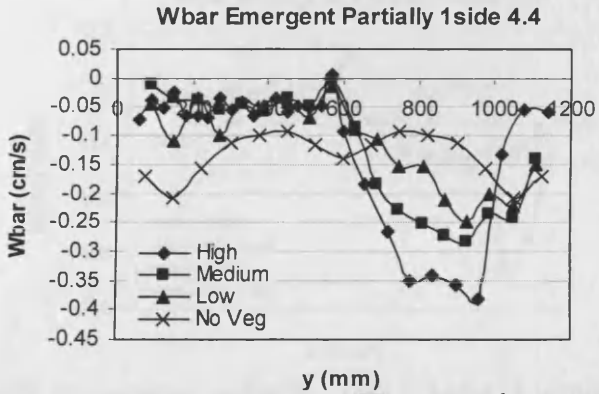

Fig. 6.30 Time-averaged transverse velocity ($\overline{W}$) [cms^{-1}] emergent partial one-sided vegetation at cross-section 4.4 for four configurations: (a) high, (b) medium, (c) low, and (d) no vegetation; (e) depth-averaged vertical velocity profiles.

(a)

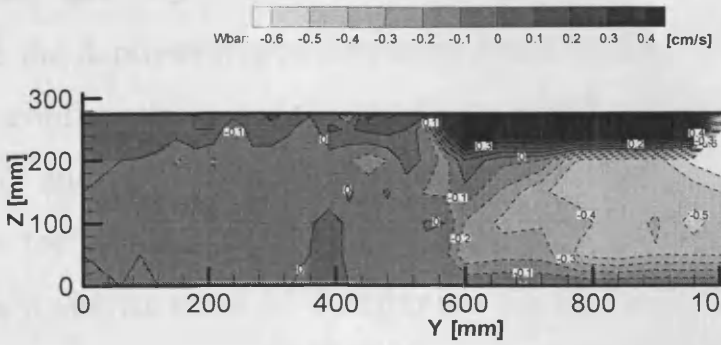

(b)

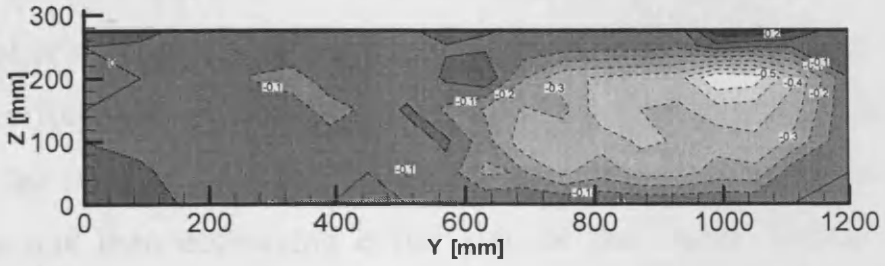

(c)

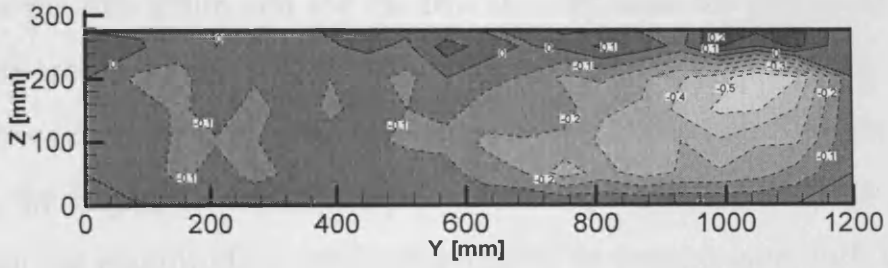

(d)

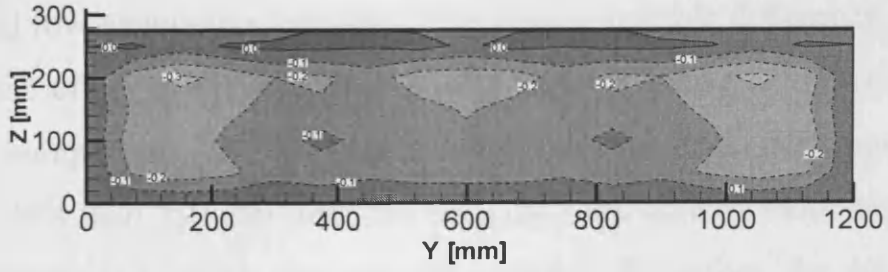

(e)

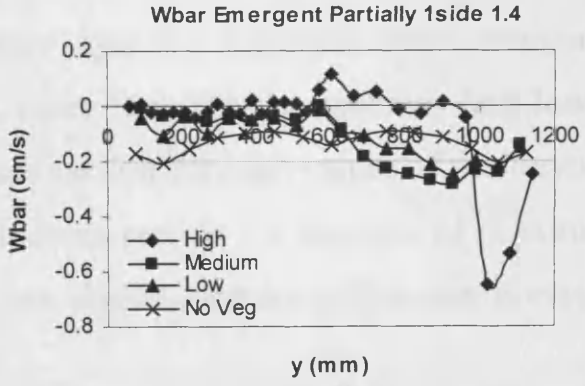

Fig. 6.31 Time-averaged transverse velocity ($\overline{W}$) [cms^{-1}] emergent partial one-sided vegetation at cross-section 1.4 for four configurations: (a) high, (b) medium, (c) low, and (d) no vegetation; (e) depth-averaged vertical velocity profiles.

d) Depth-averaged Reynolds stress components ($\overline{u'v'}$, $\overline{u'w'}$, $\overline{v'w'}$)

In Fig. 6.32 the depth-averaged Reynolds stress components ($\overline{u'v'}$, $\overline{u'w'}$, $\overline{v'w'}$) are given for 4 configurations for the emergent partial one-sided vegetation at cross-sections 4.4 and 1.4. From the results it is clear that all Reynolds stress components for all vegetation densities and for both cross-sections 4.4 and 1.4 almost have a similar trend of distribution for the wide channel. Also for cross-section 4.4 for the vegetated half of channel, the Reynolds stress components are almost equal or show little difference. However, for the vegetation free half of the channel, the Reynolds stress components for all configurations have a similar trend, with the stress sharply increasing and reaching a maximum value in middle of the zone and then decreasing either side of the centre. Hence, for the high density case the maximum and for the low density case the minimum stresses can be seen. For cross-section 1.4, and for all configurations except the high density case, the stress across the flume does not vary significantly. For the high density vegetation, the Reynolds stress components have a similar trend as for the other densities, but the magnitude is noticeably higher in comparison with the results for medium and low vegetation densities. The reason for this difference is thought to be due to the effect of the proximity to the weir. Because of the relatively small velocity in comparison with the medium and low vegetation densities in the lower depths (i.e. less than 250 mm from the bed) the high density velocities transfers to the upper depths (i.e. above 250 mm sill surface). Therefore, for the high density vegetation, in the upper layer the Reynolds stress components increase for both halves of the flume, more than for the medium and low densities. For the no vegetation case in cross section 4.4 high values of the Reynolds stress components were observed, but in cross-section 1.4 because of proximity to the weir it gives minimal stresses and are almost constant with a near horizontal contour across the width of the channel.

`a)

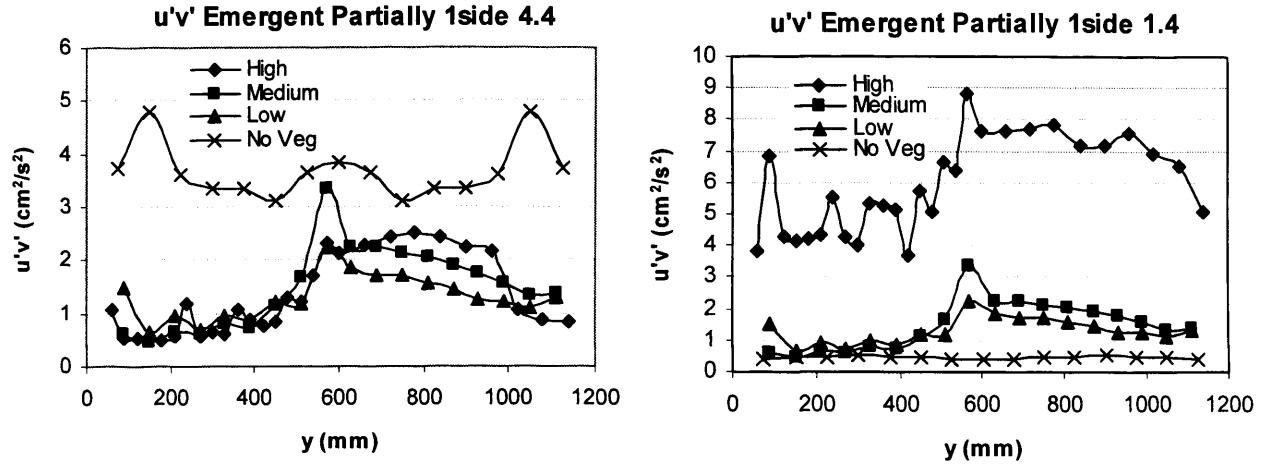

(b)

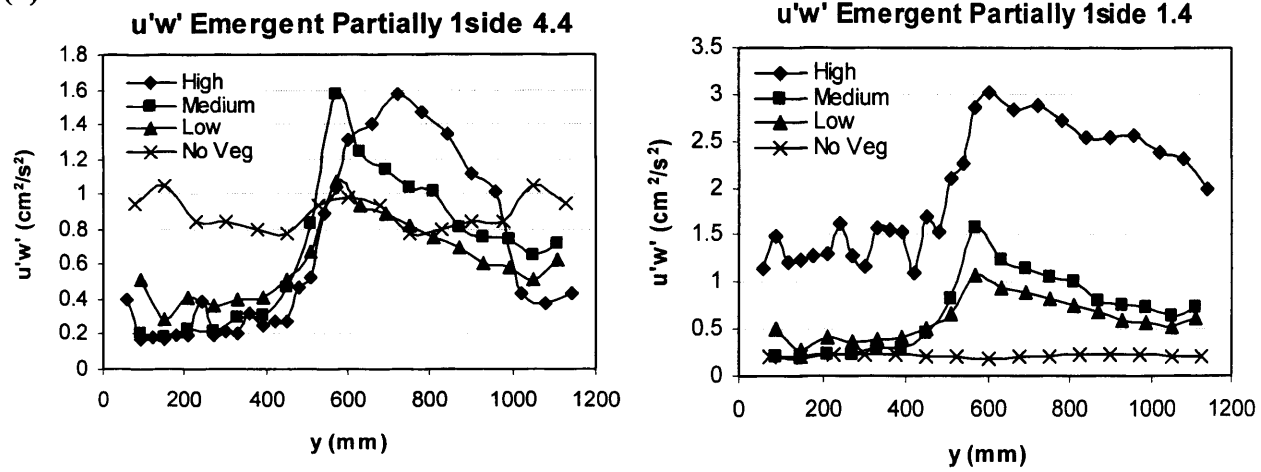

(c)

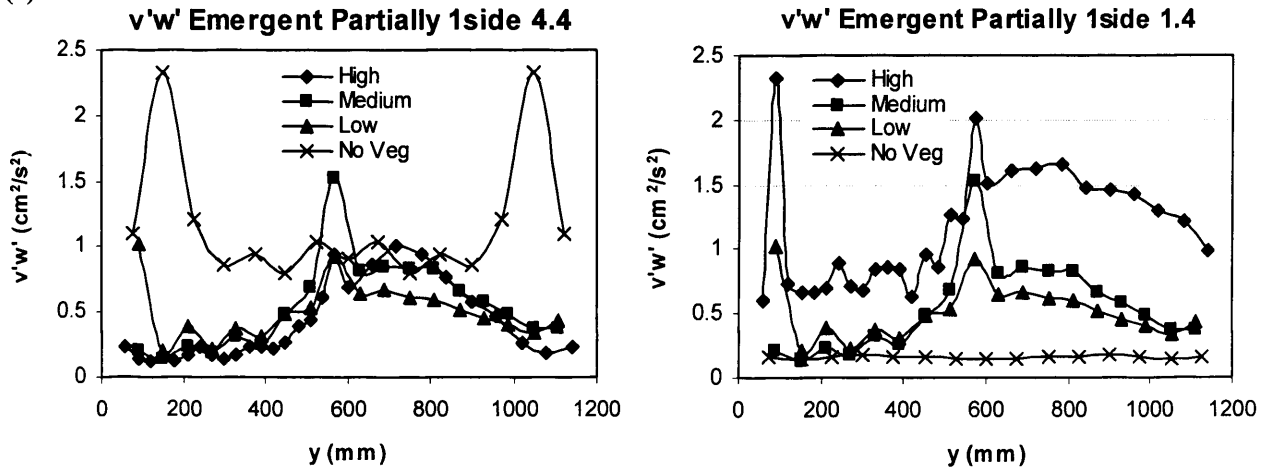

Fig. 6.32 Depth-averaged Reynolds stress components ($\overline{u'v'}$, $\overline{u'w'}$, $\overline{v'w'}$) [cm²/s²] for four configurations in emergent partial one-sided vegetation at cross-sections 4.4 and 1.4; (a) $\overline{u'v'}$, (b) $\overline{u'w'}$, and (c) $\overline{v'w'}$.

6.4 Flow in a partial two-sided vegetated channel

6.4.1 Submerged vegetation (rods height = 180 mm)

In the next set of vegetation configurations, the channel had partial two-sided submerged vegetation sections as shown in Fig. 6.33 with the various densities being illustrated. The measurement points and the profiles are also demonstrated.

(a) High Density

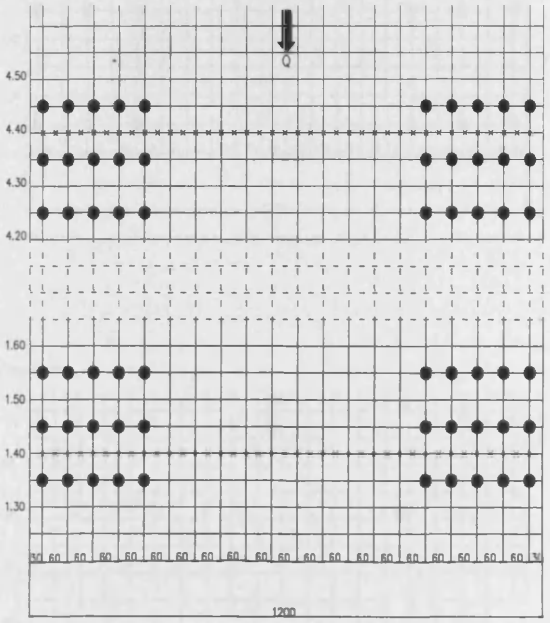

High Density Vegetation

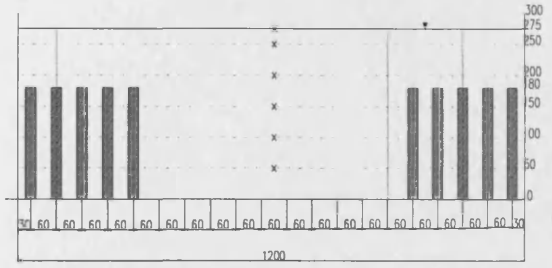

(b) Medium Density

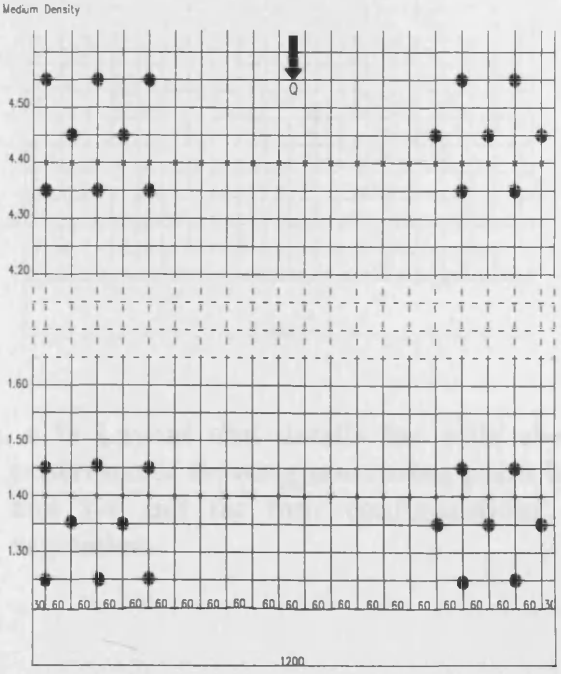

Medium Density Vegetation (A)

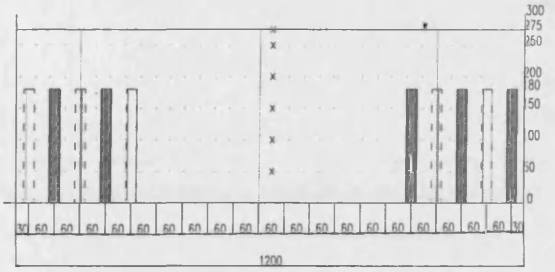

Medium Density Vegetation (B)

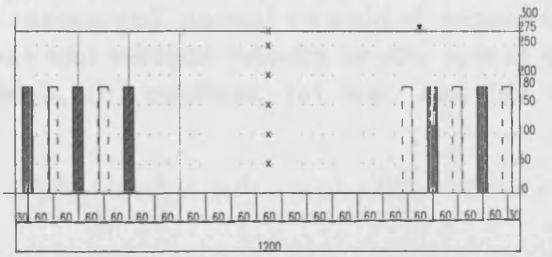

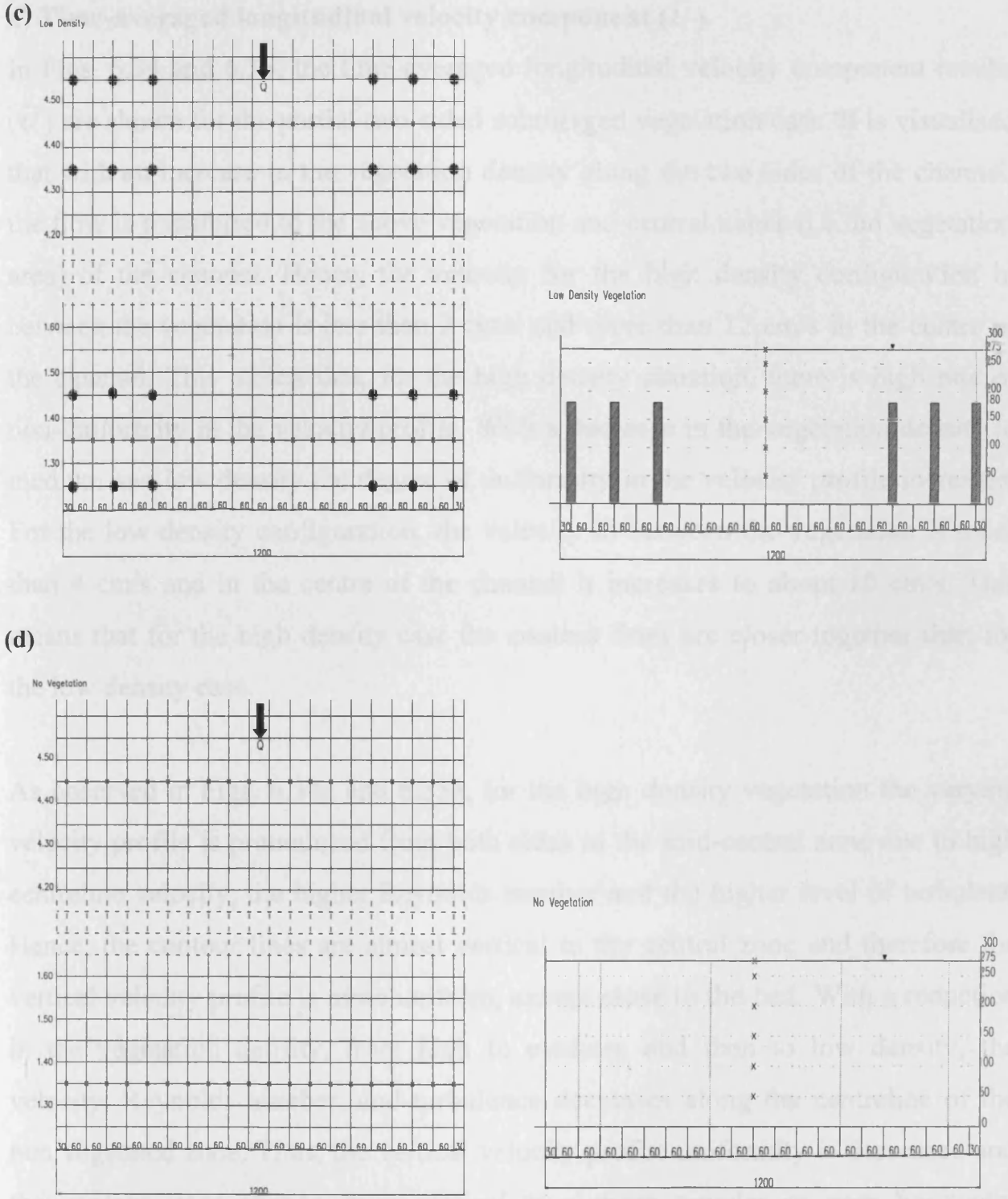

Fig. 6.33 Layout and details for wide channel submerged partial two-sided vegetation experiments showing measuring point locations and vertical velocity profile sets at 4.4 and 1.4 and for four configurations: (a) high, (b) medium, (c) low, and (d) no vegetation.

a) Time-averaged longitudinal velocity component ($\overline{U}$)

In Figs. 6.34 and 6.35, the time-averaged longitudinal velocity component results ($\overline{U}$) are shown for the partial two-sided submerged vegetation case. It is visualised that with an increase in the vegetation density along the two sides of the channel, the flow is transferred to the above vegetation and central zones (i.e. no vegetation area) of the channel. Hence, the velocity for the high density configuration in between the vegetation is less than 2 cm/s and more than 12 cm/s in the centre of the channel. This means that, for the high density situation, there is high rate of non-uniformity in the velocity profile. With a decrease in the vegetation density to medium and low density the degree of uniformity in the velocity profile increases. For the low density configuration, the velocity in between the vegetation is more than 4 cm/s and in the centre of the channel it increases to about 10 cm/s. This means that for the high density case the contour lines are closer together than for the low density case.

As observed in Figs. 6.34a and 6.35a, for the high density vegetation the varying velocity profile is pronounced from both sides to the mid-central zone due to high centreline velocity, the higher Reynolds number and the higher level of turbulent. Hence, the contour lines are almost vertical in the central zone and therefore the vertical velocity profile is more uniform, except close to the bed. With a reduction in the vegetation density, from high to medium and then to low density, the velocity, Reynolds number, and turbulence decreases along the centreline of the non vegetated zone. Thus, the vertical velocity profile uniformity is decreased and the contour lines change from vertical to a more circular or near horizontal structure, and the distances between the contour lines increases (see Figs. 6.34c and 6.35c).

Figures 6.34e and 6.35e show the depth-averaged longitudinal velocity profiles in the submerged partial two-sided vegetation structure for the four configurations

and across the two cross-sections 4.4 and 1.4. As clearly demonstrated in the graphs, in the vegetated area of two sides of the channel the high and low density cases have a minimum and maximum longitudinal velocity respectively. However, for the non-vegetated reach along the centre of the channel the velocity profiles change. For the high density case the velocity increases sharply and peaks at about 11 cm/s along the centreline. For the medium and the low density cases and for the lower surface slopes, the velocities peak at about 10 and 9 cm/s respectively along the centreline. For the non-vegetation, the velocity is much more constant across the channel section.

(a)

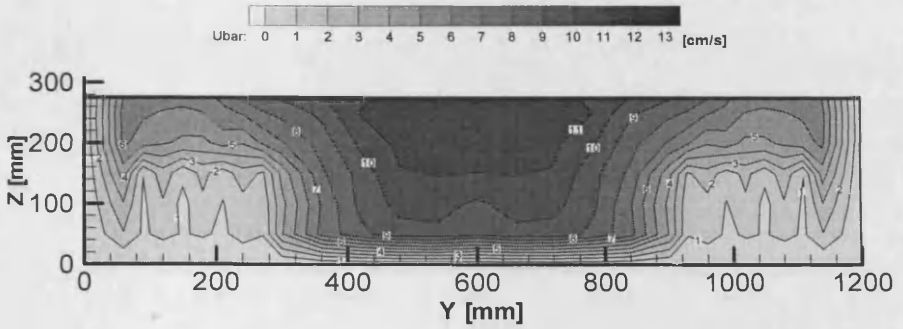

(b)

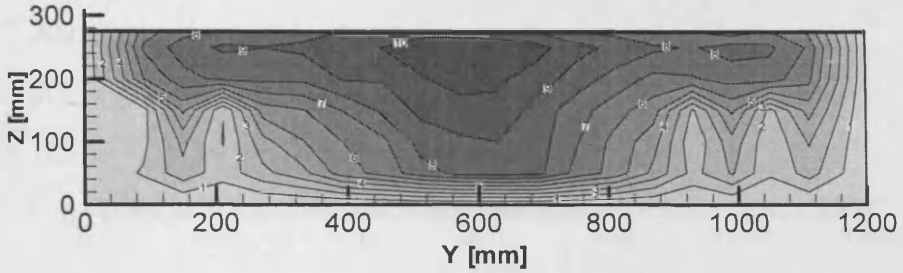

(c)

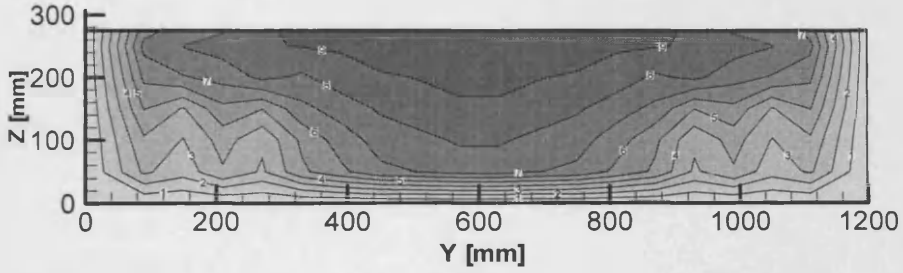

(d)

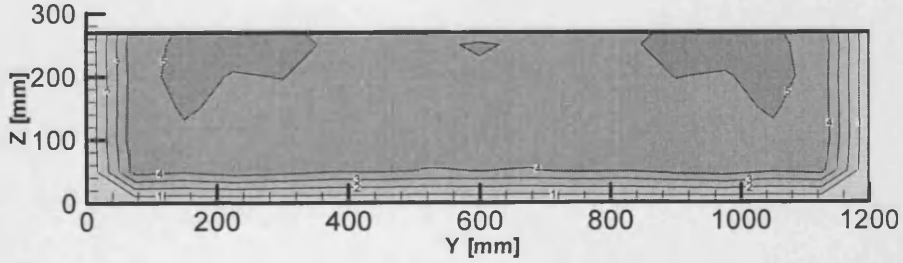

(e)

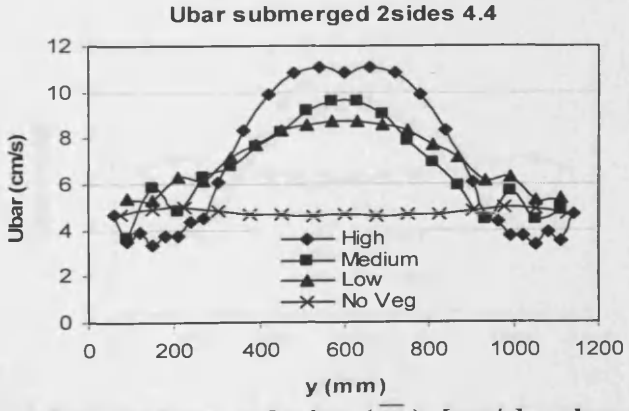

Fig. 6.34 Time-averaged longitudinal velocity ($\overline{U}$) [cm/s] submerged partial two-sided vegetation at cross-section 4.4 for four configurations: (a) high, (b) medium, (c) low, and (d) no vegetation; (e) depth-averaged vertical velocity profiles.

(a)

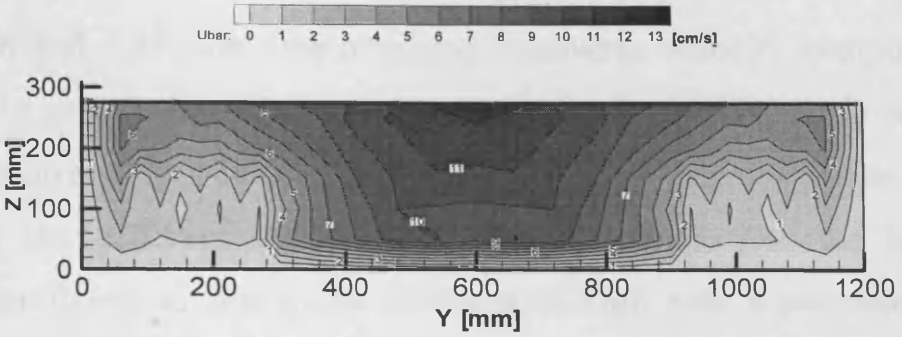

(b)

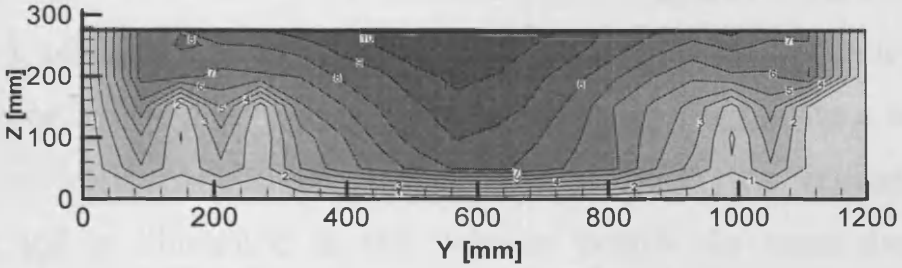

(c)

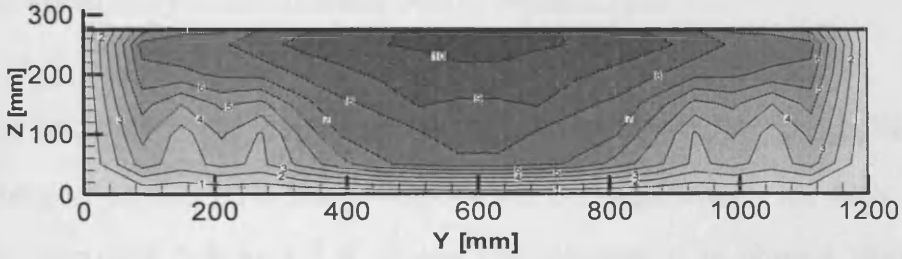

(d)

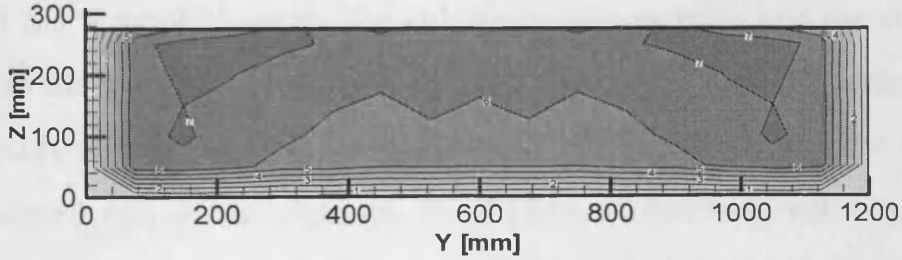

(e)

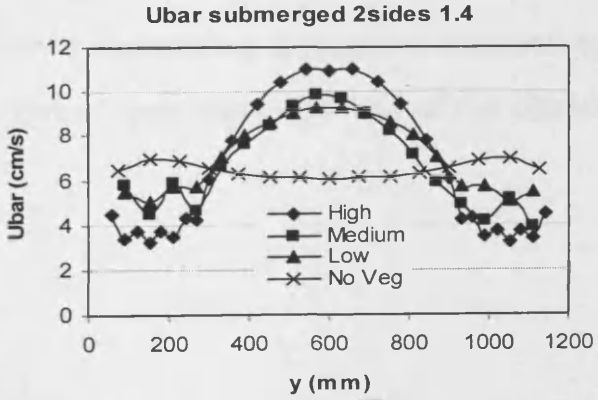

Fig. 6.35 Time-averaged longitudinal velocity ($\overline{U}$) [cm/s] submerged partial two-sided vegetation at cross-section 1.4 for four configurations: (a) high, (b) medium, (c) low, and (d) no vegetation; (e) depth-averaged vertical velocity profiles.

b) Time-averaged transverse velocity component ($\overline{V}$)

In Figs. 6.36 and 6.37, the time-averaged transverse velocity component ($\overline{V}$) is shown for the partial two-sided submerged vegetation scenario. As mentioned in previous section and as is evident from the figures, the velocity profile is very non-uniform for the different densities and cross-sections. For the high density vegetation configuration, due to the existence of high rods, a secondary current is not formed or is very weak. For a decrease in the vegetation density to the low density case a secondary current forms in a very small layer close the surface and the central zone, particularly along water surface (see Figs. 6.36a,c and 6.37a,c). The effect of vortex shedding in the channel from two vegetated sides is pronounced and is illustrated in the velocity profile. In some cases this has prevented the secondary current from being established.

In Figs. 6.36e and 6.37e the depth-averaged transverse velocity profiles are shown for the submerged partial two-sided vegetation configuration, for four states and at the two cross-sections 4.4 and 1.4. From the figures it is shown that, due to the small size of the vegetated zones, the submerged vegetation and the summation of the velocity in the vegetated zone and the non-vegetated zone, the velocity profiles differ noticeably above the rods. Also for cross section 4.4, along the centreline of the non-vegetated part of the channel, the difference between velocity profiles for the different densities is high. However, for cross-section 1.4, due to proximity to the weir, the results show a decreasing difference between velocity profiles for the different cases for the central non-vegetated half of the channel.

(a)

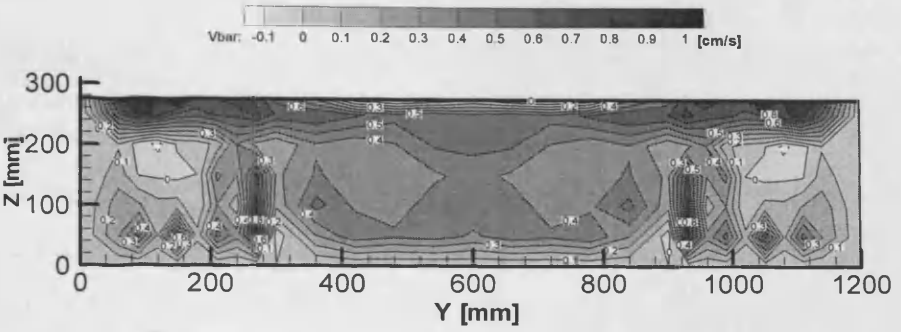

(b)

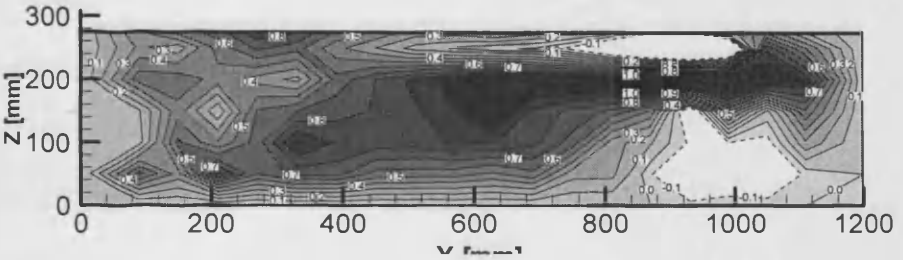

(c)

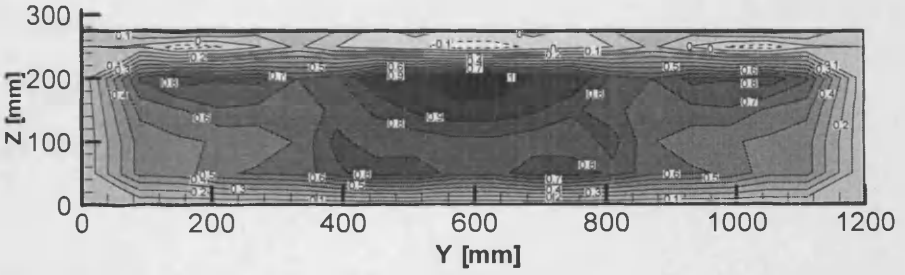

(d)

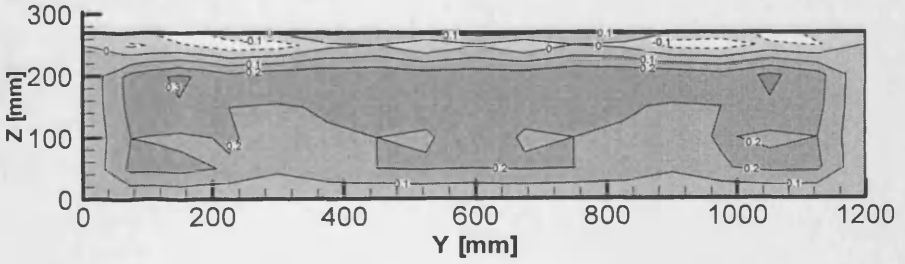

(e)

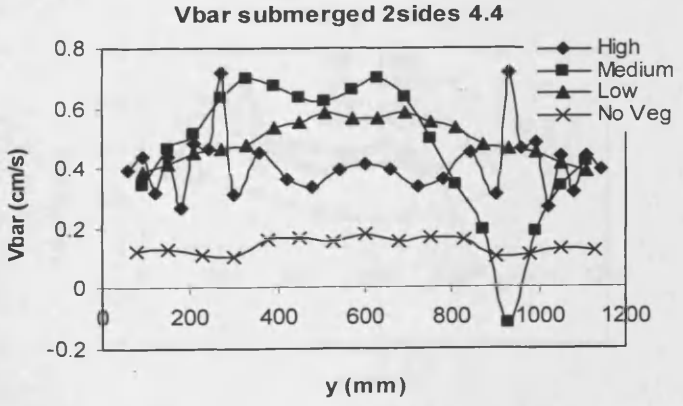

Fig. 6.36 Time-averaged transverse velocity ($\overline{V}$) [cms^{-1}] submerged partial two-sided vegetation at cross-section 4.4 for four configurations: (a) high, (b) medium, (c) low, and (d) no vegetation; (e) depth-averaged vertical velocity profiles.

(a)

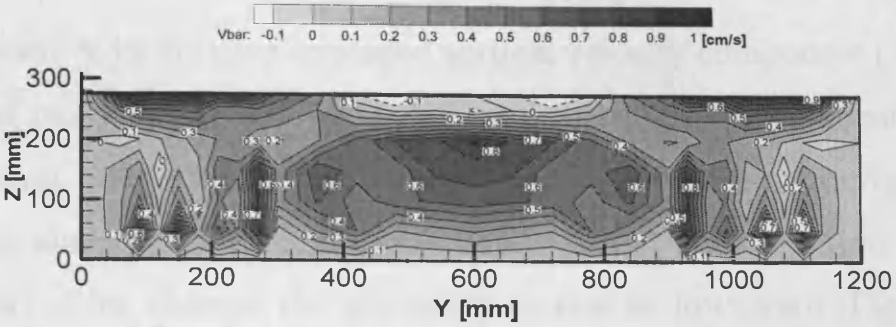

(b)

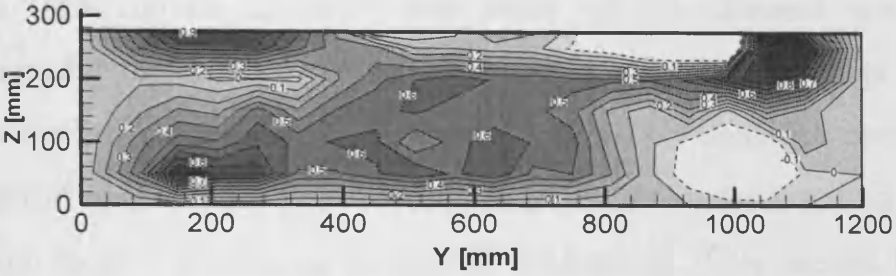

(c)

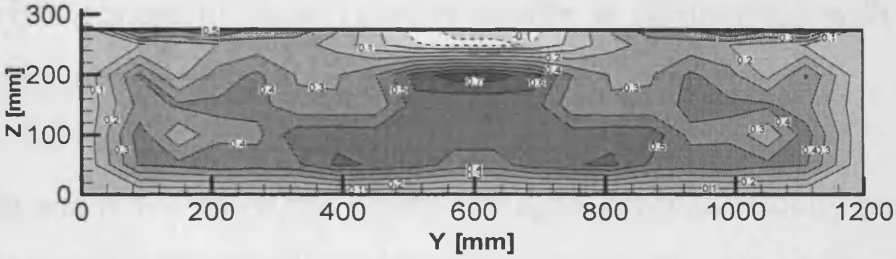

(d)

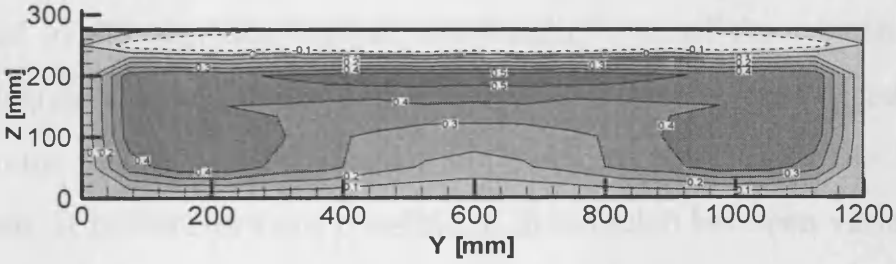

(e)

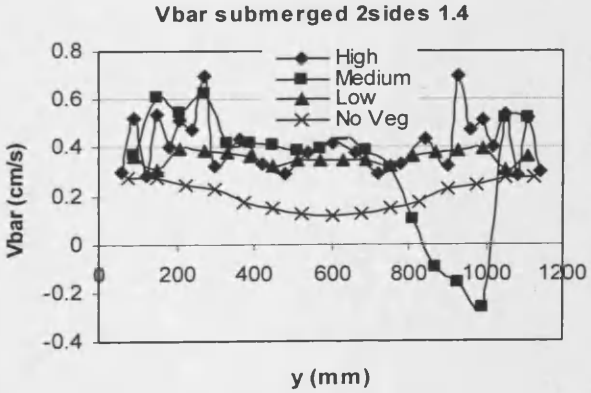

Fig. 6.37 Time-averaged transverse velocity ($\overline{V}$) [cms^{-1}] submerged partial two-sided vegetation at cross-section 1.4 for four configurations: (a) high, (b) medium, (c) low, and (d) no vegetation; (e) depth-averaged vertical velocity profiles.

c) Time-averaged vertical velocity component ($\overline{W}$)

In Figs. 6.38 and 6.39 the time-averaged vertical velocity component ($\overline{W}$) is shown for the partial two-sided submerged vegetation configuration. As mentioned in the previous section, due to the numerous rods for the high density configuration then the secondary currents are pronounced with distinct velocity profiles. Although in the centre part of the channel the secondary current is downward (Figs. 6.38a and 6.395a), the flow moves towards both sides of the channel and above the vegetation zone for the medium and low density configurations (Figs. 6.38b,c and 6.39b,c). On the other hand, although for all vegetation densities over the central half zone a positive thin layer is observed on the water surface, with a reduction in the vegetation density producing increased uniformity. This means that the low density case has a more uniform velocity profile in comparison with the medium and high density rod configurations.

Figures 6.38e and 6.39e show the depth-averaged vertical velocity profiles for the various states of the submerged two-sided vegetation, at cross-sections 4.4 and 1.4. As mentioned in the previous section, the smaller size of the vegetated zone, the submerged vegetation, and summation of the velocities in the vegetated and non-vegetated zones results in diffusion of the velocity profiles in the flow section above the rods. It is therefore not possible to distinguish between variations for the different configurations across the channel width at both cross-sections 4.4 and 1.4.

(a)

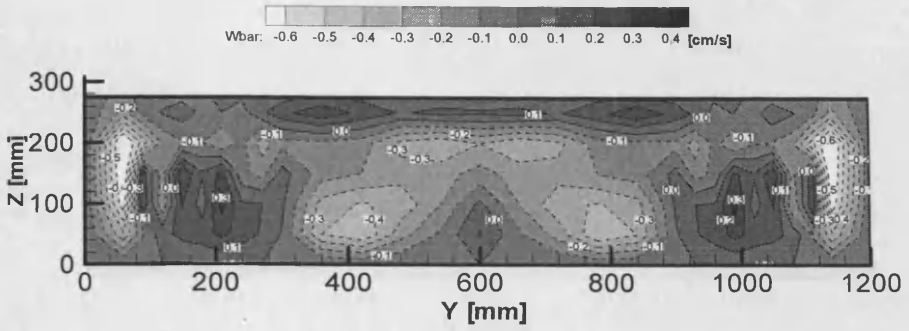

(b)

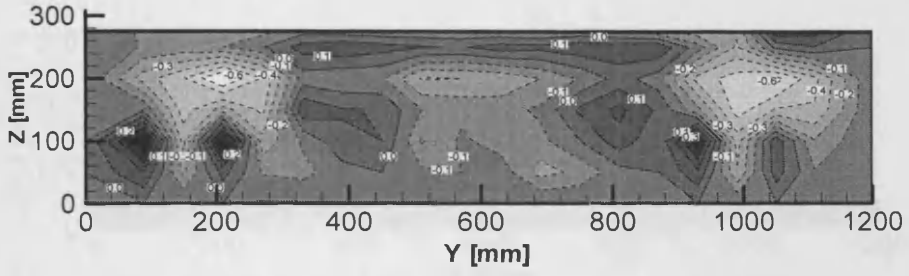

(c)

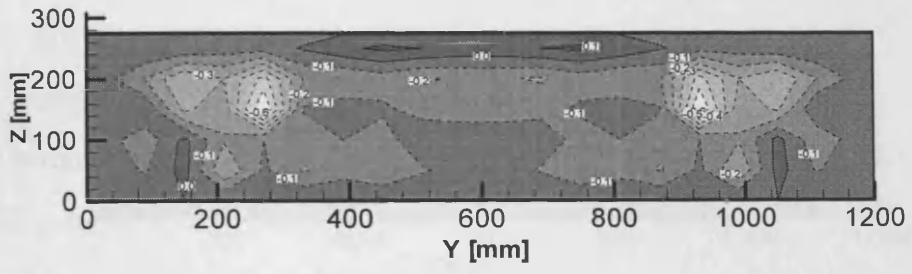

(d)

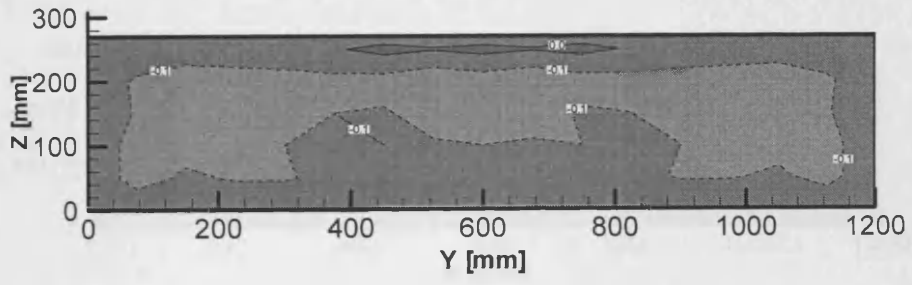

(e)

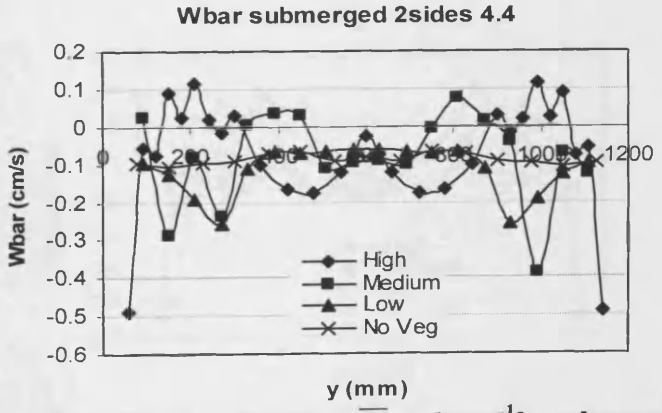

Fig. 6.38 Time-averaged vertical velocity ($\overline{W}$) [cms^{-1}] submerged partial two-sided vegetation at cross-section 4.4 for four configurations: (a) high, (b) medium, (c) low, and (d) no vegetation; (e) depth-averaged vertical velocity profiles.

(a)

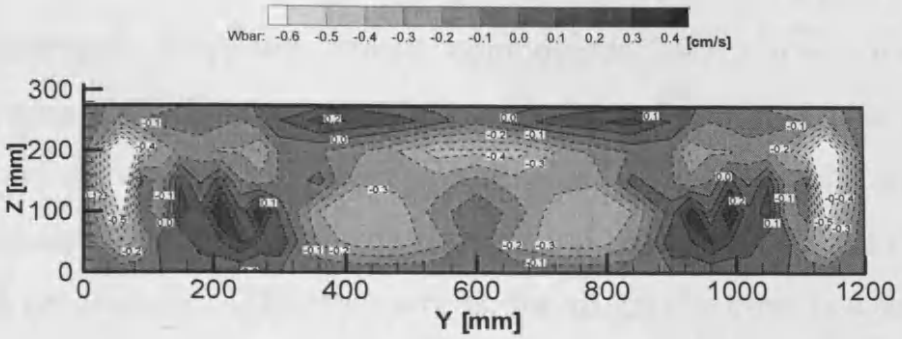

(b)

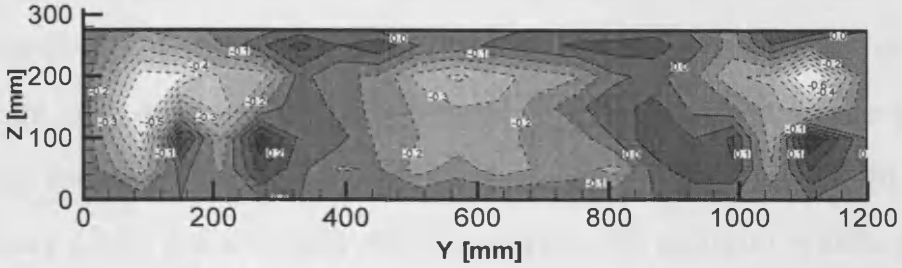

(c)

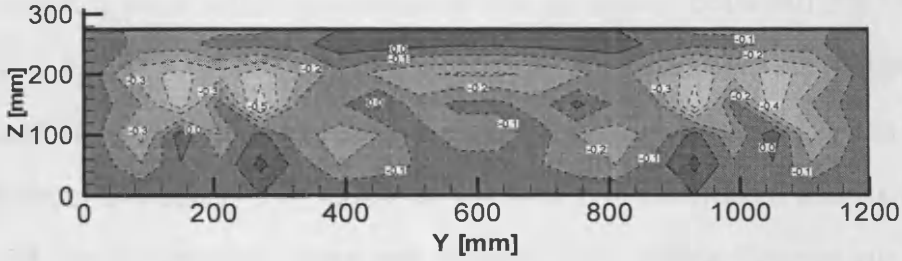

(d)

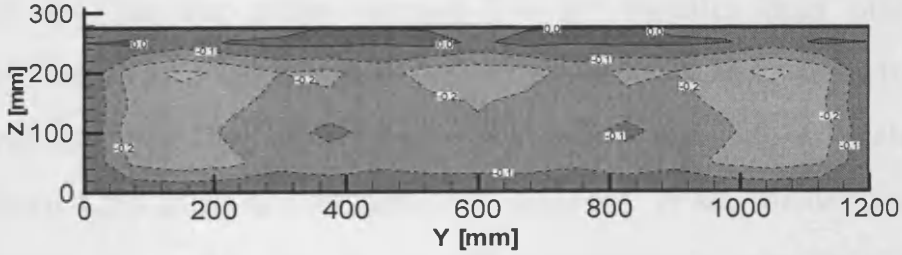

(e)

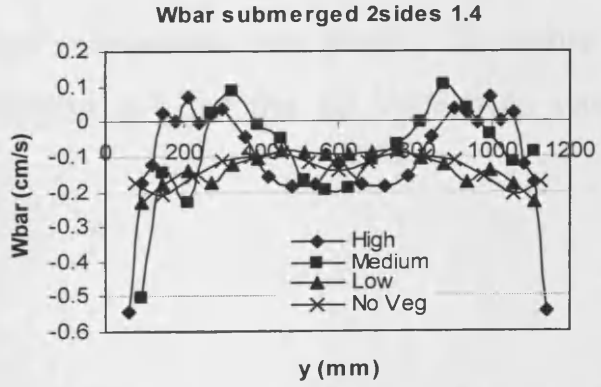

Fig. 6.39 Time-averaged vertical velocity ($\overline{W}$) [cms^{-1}] submerged partial two-sided vegetation at cross-section 1.4 for four configurations: (a) high, (b) medium, (c) low, and (d) no vegetation; (e) depth-averaged vertical velocity profiles.

d) Depth-averaged Reynolds stress components ($\overline{u'v'}$, $\overline{u'w'}$, $\overline{v'w'}$)

The depth-averaged Reynolds stress components ($\overline{u'v'}$, $\overline{u'w'}$, $\overline{v'w'}$) for the submerged partial two-sided vegetation for the four cases and across the sections 4.4 and 1.4 are shown in Fig. 6.40. As can be seen for all graphs, the Reynolds stress components for all configurations show the same trends across the channel width at both cross-sections. In other words, for all graphs there is a small velocity variation in the vegetated zone on both sides of the channel. The stresses then decrease towards the centre of the non-vegetated half of the channel and reach to a minimum point at the centre of the channel. For all configurations and for both cross-sections, the low density configuration always gives a minimum stresses and the high density gives a maximum stresses across the channel width. Also, for the high density case, a peak stress occurred at the interface between the vegetated and vegetation free zones and on the two sides of the channel. As expected, the no vegetation case also has the minimum variation in the Reynolds stress components across the channel at both cross-sections 4.4 and 1.4. Although the Reynolds stress components in no vegetation case are bigger than other vegetation densities in cross section 4.4 but for cross section 1.4 are smaller than other densities. However, as mentioned previously for cross-section 1.4, due to effects of proximity with the weir, the velocity and variations in depth at levels lower than the edge of weir (250 mm) are too small to measure. Also, for depths higher than 250 mm up to water surface the longitudinal velocity is extremely high and the transverse and vertical variations are small. Therefore the Reynolds stress components across section 1.4 for the no vegetation case are very small and without any change.

(a)

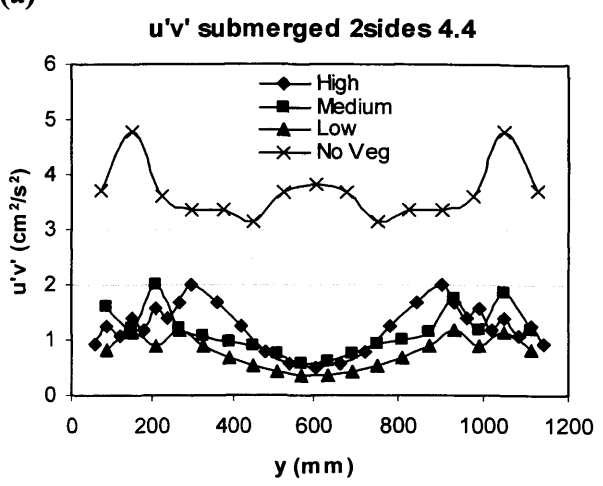

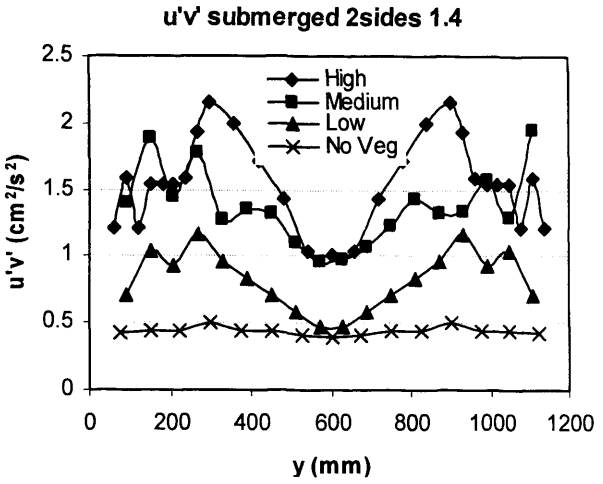

(b)

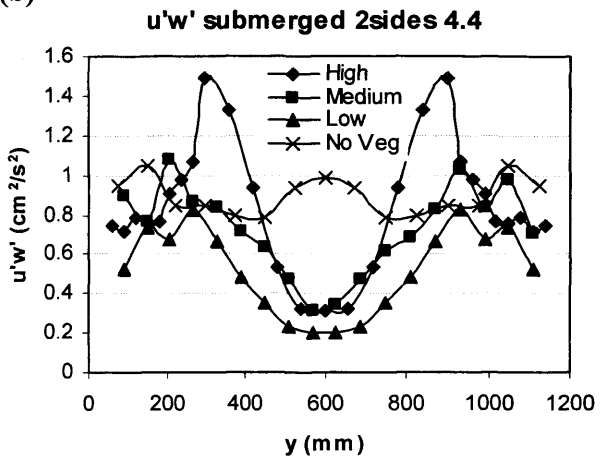

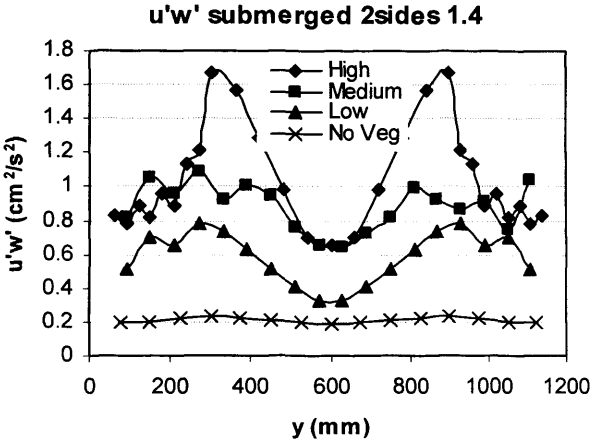

(c)

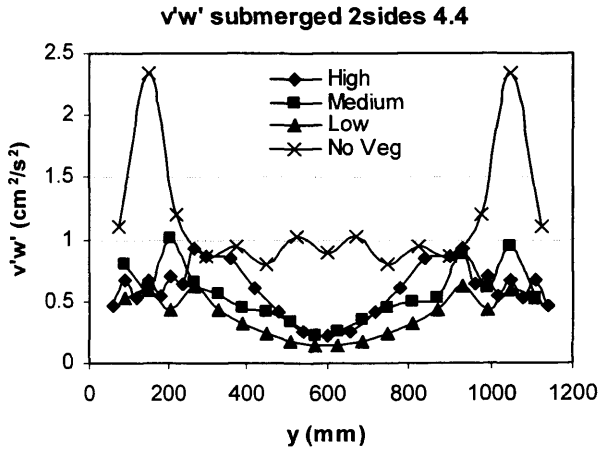

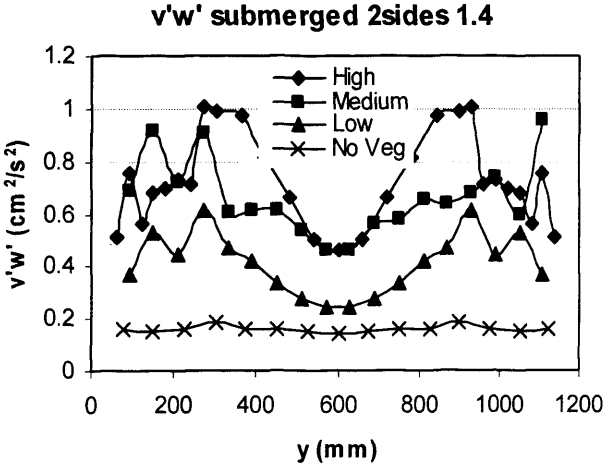

Fig. 6.40 Depth-averaged Reynolds stress components ($\overline{u'v'}$, $\overline{u'w'}$, $\overline{v'w'}$) [cm^2/s^2] for four configurations in submerged partial two-sided vegetation at cross-sections 4.4 and 1.4; (a) $\overline{u'v'}$, (b) $\overline{u'w'}$, and (c) $\overline{v'w'}$.

6.4.2 Emergent vegetation (rods height = 300 mm)

The experimental setup and details of the measurement location points of the partial two-sided emergent vegetation for different densities are illustrated in Fig. 6.41.

(a)

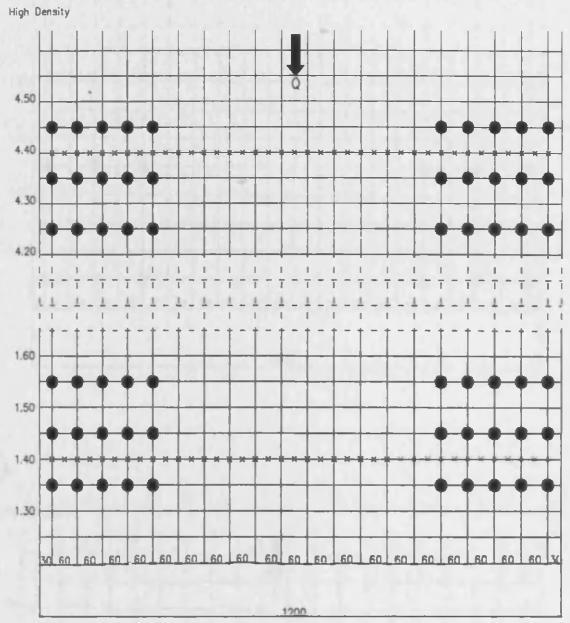

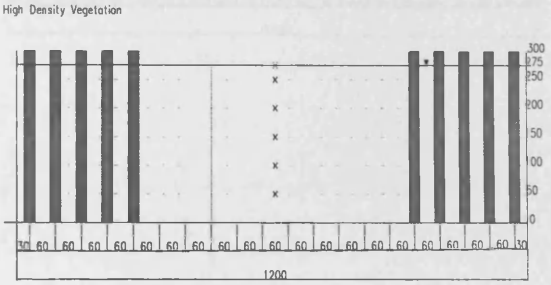

(b)

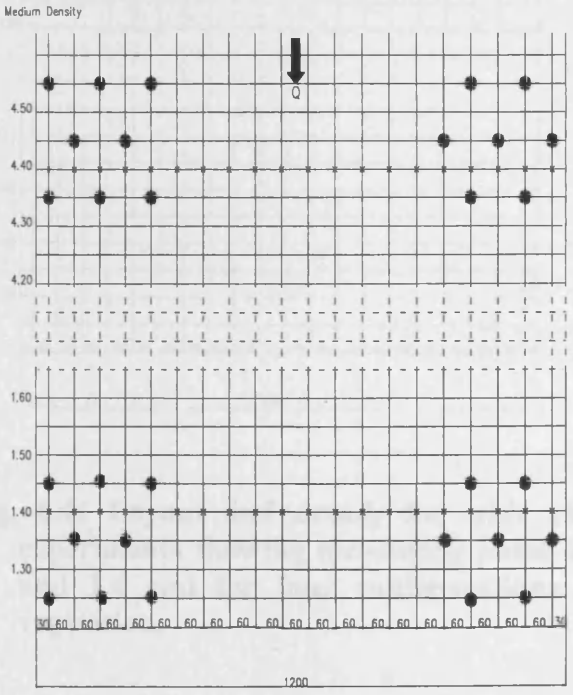

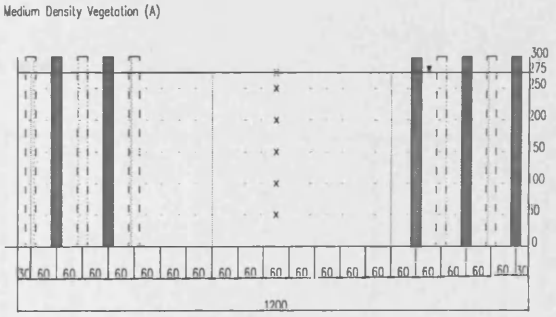

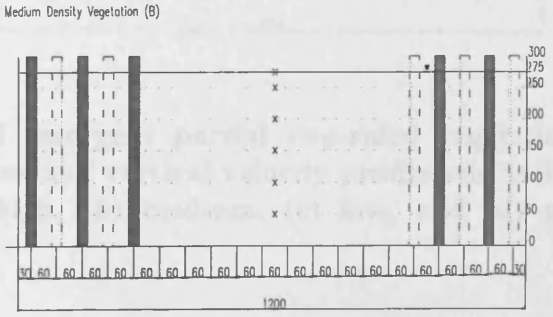

(c)

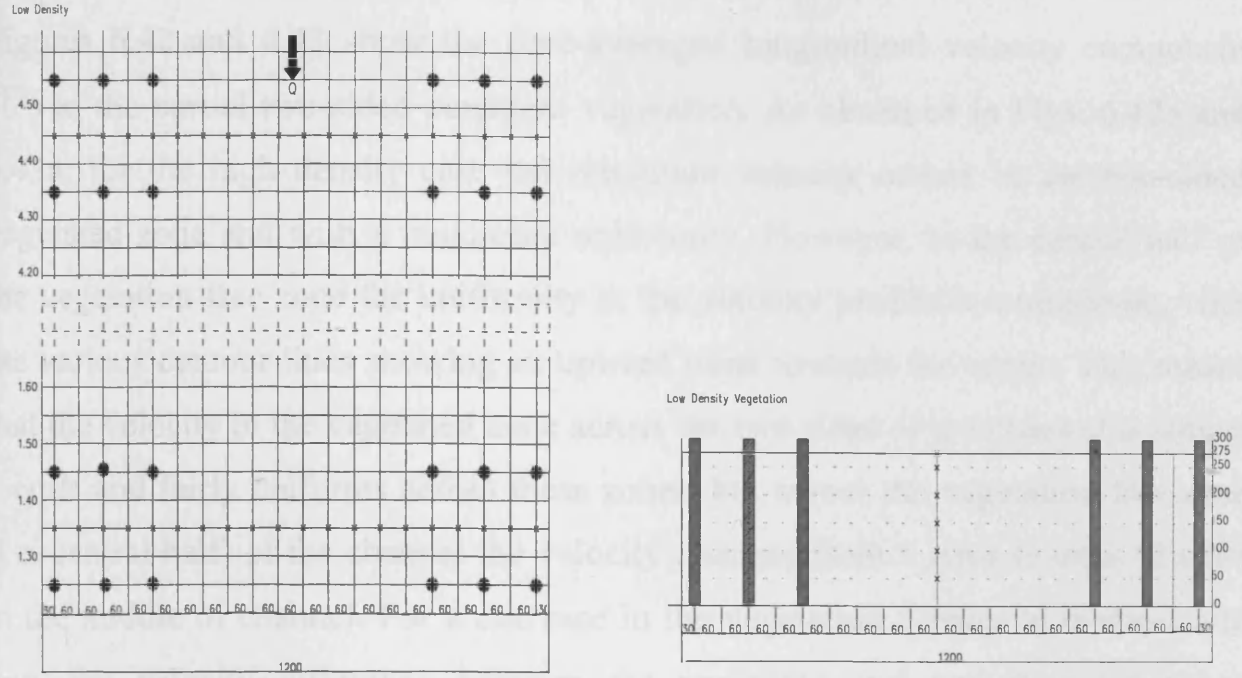

(d)

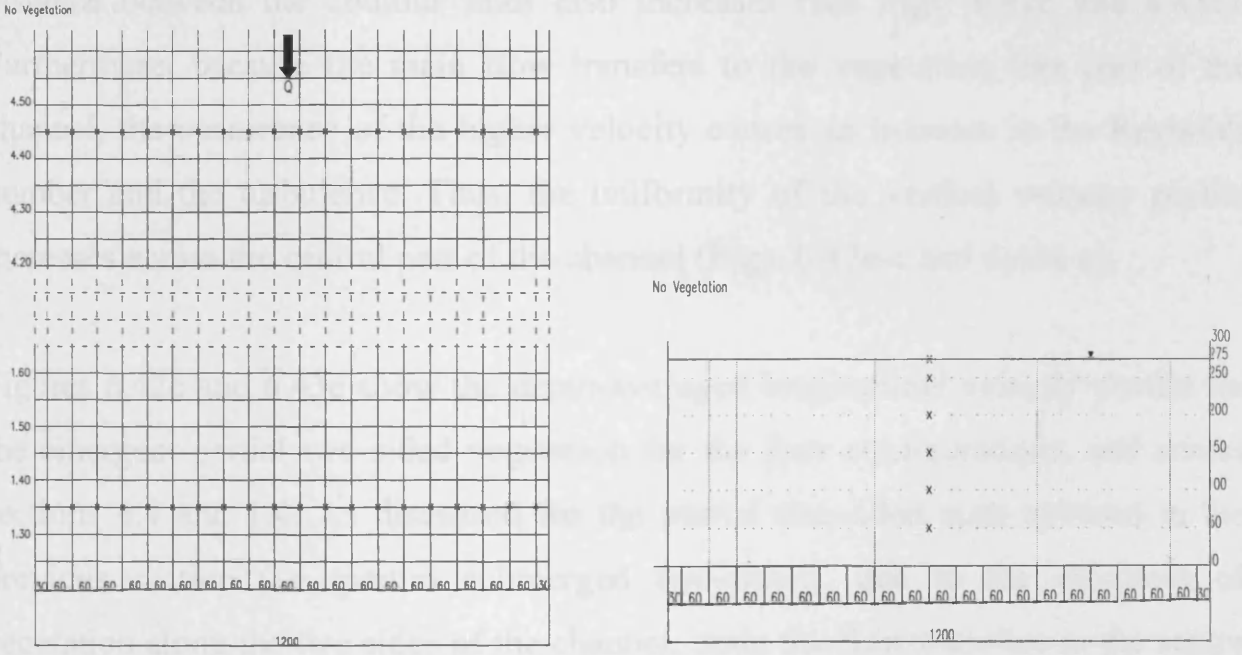

Fig. 6.41 Layout and details for wide channel emergent partial two-sided vegetation experiments showing measuring point locations and vertical velocity profile sets at 4.4 and 1.4 and for four configurations: (a) high, (b) medium, (c) low, and (d) no vegetation.

a) Time-averaged longitudinal velocity component ($\overline{U}$)

Figures 6.42 and 6.43 show the time-averaged longitudinal velocity component ($\overline{U}$) in the partial two-sided emergent vegetation. As observed in Figs. 6.42a and 6.43a, for the high density case the minimum velocity occurs in the two-sided vegetated zone and with a maximum uniformity. However, in the central half of the vegetation free zone the uniformity in the velocity profile is a minimum, with the various contour lines showing an upward trend towards the centre. This means that the velocity in the vegetated zone across the two sides of the channel is almost 1 cm/s and fairly uniforms across these zones, but across the vegetation free zone (i.e. central half) of the channel the velocity changes from 1 cm/s to over 12 cm/s in the middle of channel. For a decrease in the vegetation density to medium and low, the velocity difference between the vegetated and non-vegetated zones decreases. In other words, the uniformity in the velocity profile increases and the distance between the contour lines also increases (see Figs. 6.42c and 6.43c). Furthermore, because the main flow transfers to the vegetation free part of the channel, the occurrence of the higher velocity causes an increase in the Reynolds number and the turbulence. Thus, the uniformity of the vertical velocity profile increases across the central part of the channel (Figs. 6.42a-c and 6.43a-c).

Figures 6.42e and 6.43e show the depth-averaged longitudinal velocity profile for the emergent partial two-sided vegetation for the four configurations, and across sections 4.4 and 1.4. As discussed for the partial one-sided state covered in the previous section (i.e. partial submerged two-sided), due to the existence of vegetation along the two sides of the channel, main the flow transfers to the centre of the vegetation free zone of the channel, even more than for the partially submerged state. Although all of the density states have similar trends across the channel width, they exhibit very different velocities. As can be seen in the graphs for the vegetation zones, the velocity for the high and low density cases have minimum values of about 1 cm/s and a maximum value of about 3 cm/s. For all the

vegetation densities the velocity along both sides of the channel increases sharply towards the central part of the vegetation free zone and reaches a maximum value along the central line of the channel. Hence, the maximum velocity for the high density case is more than 12 cm/s whereas for the low density case it is about 11 cm/s. Also, as before, for the no vegetation case the velocity has a constant value of about 6 cm/s with very small variation across the channel width, for both sections 4.4 and 1.4.

(a)

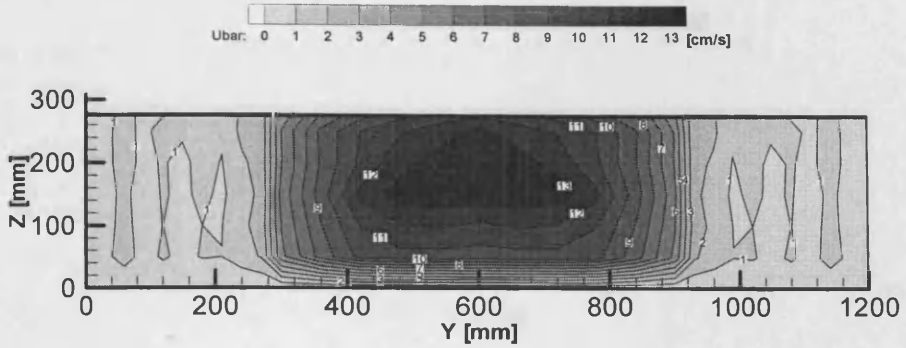

(b)

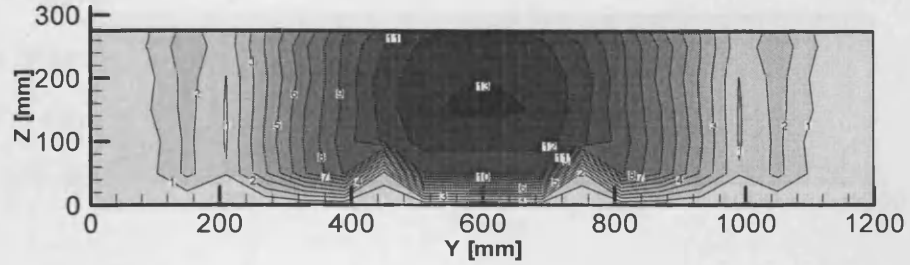

(c)

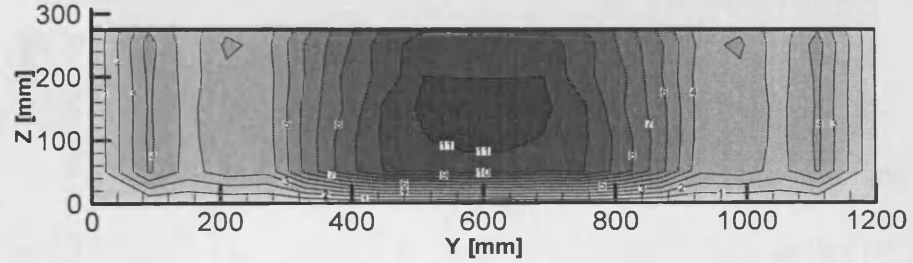

(d)

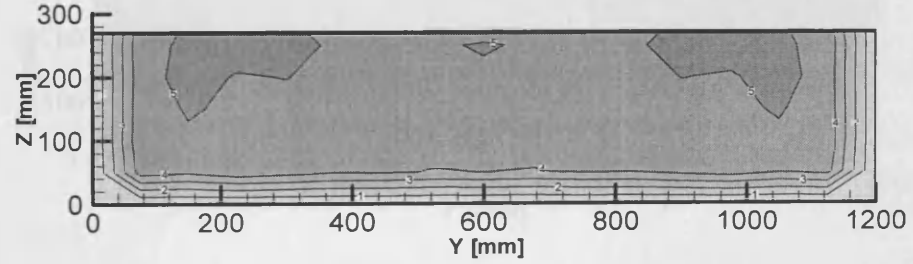

(e)

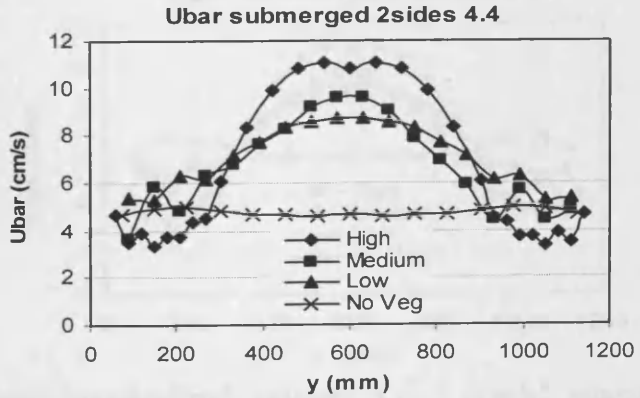

Fig. 6.42 Time-averaged longitudinal velocity ($\overline{U}$) [cm/s] emergent partial two-sided vegetation at cross-section 4.4 for four configurations: (a) high, (b) medium, (c) low, and (d) no vegetation; (e) depth-averaged vertical velocity profiles.

(a)

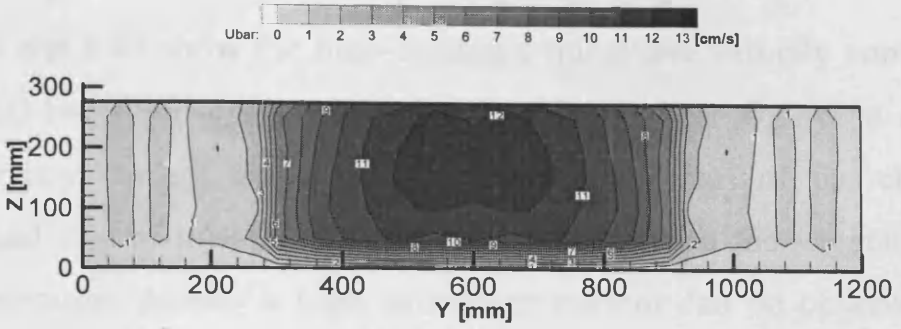

(b)

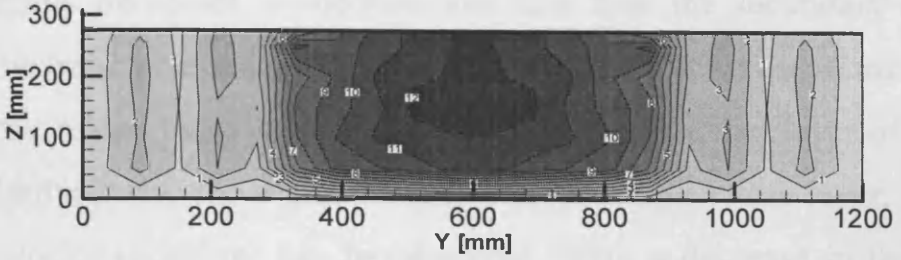

(c)

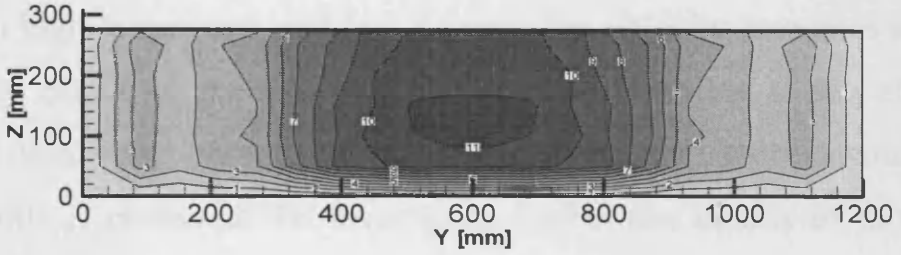

(d)

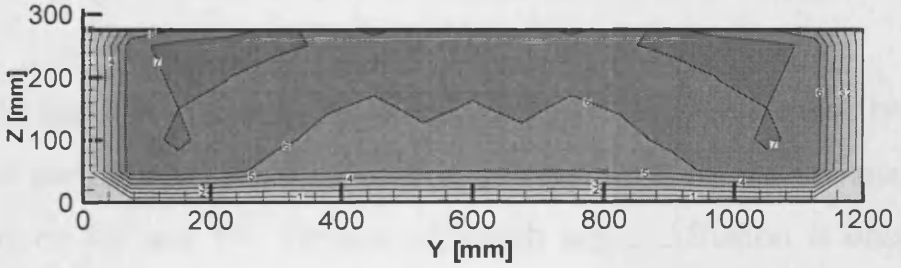

(e)

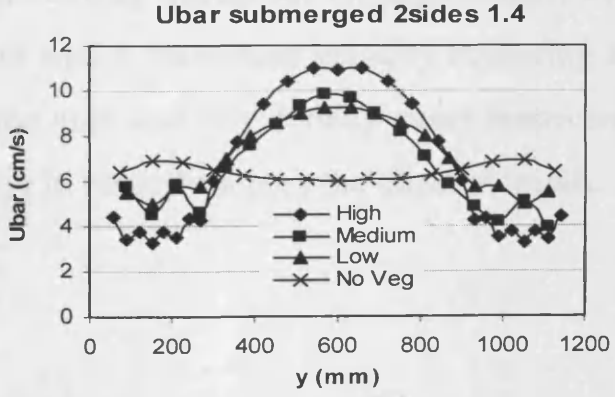

Fig. 6.43 Time-averaged longitudinal velocity ($\overline{U}$) [cm/s] emergent partial two-sided vegetation at cross-section 1.4 for four configurations: (a) high, (b) medium, (c) low, and (d) no vegetation; (e) depth-averaged vertical velocity profiles.

b) Time-averaged transverse velocity component ($\overline{V}$)

Figures 6.44 and 6.45 show the time-averaged transverse velocity component ($\overline{V}$) for the partial two-sided emergent vegetation. From these figures it can be seen that a secondary current has formed in the central part of the channel. The magnitude and size of this secondary current depends on the vegetation density. For high vegetation density a high secondary current can be observed, whereas when the density decreases to medium and low then the secondary current also decreases. The transverse velocities have similar trends across sections 4.4 and 1.4. In other words, as can be seen in all the figures, there is a thin layer of a minimum velocity (negative) near the water surface and then under this layer, a zone of a maximum velocity (positive) can be observed. With a decrease in the vegetation density from high to medium and low density, the velocity increases and a degree of uniformity occurs in the velocity profile. However, due to the effects of the trailing and transverse wave across the water surface, some scattering in the velocity profile is observed. To investigate further the details of this wave, this requires further experimental studies as outlined in the next chapter.

Figures 6.44e and 6.45e show the depth-averaged transverse velocity profiles for the emergent partial two-sided vegetation for the four configurations, and across the two sections 4.4 and 1.4. Herein, although some diffusion is observed in the profiles, the minimum velocity occurs for the high density case along both sides of the vegetated zone and with a maximum velocity occurring along the centreline of the channel. Hence, the high and low density cases respectively have a maximum and minimum variation in velocity across the channel width.

(a)

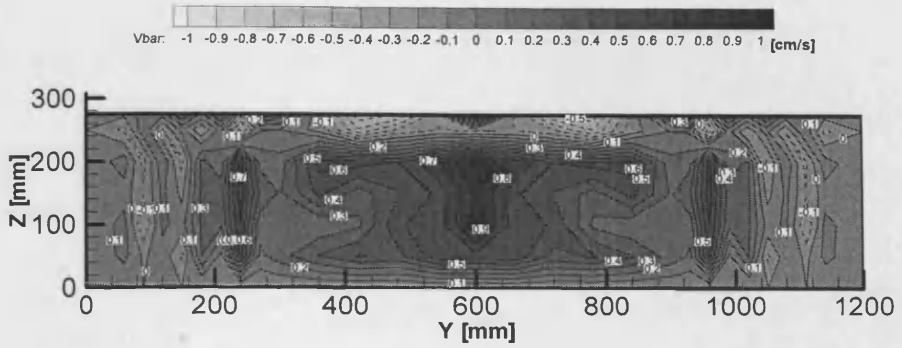

(b)

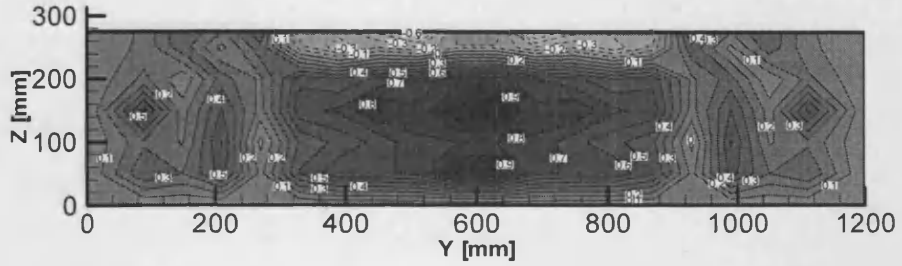

(c)

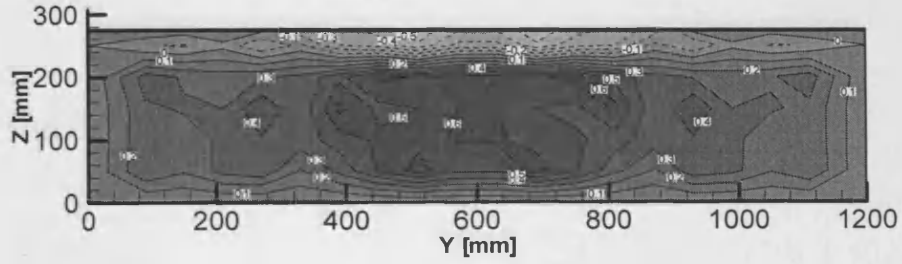

(d)

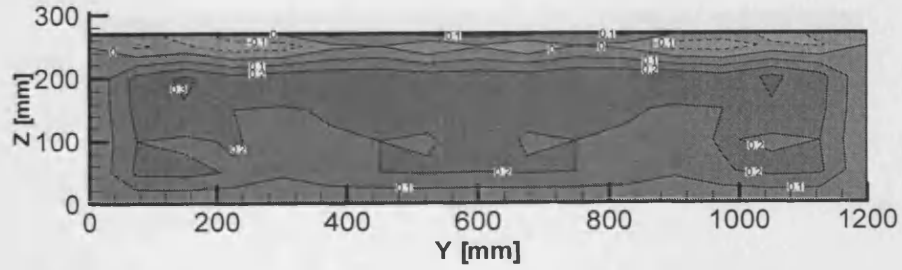

(e)

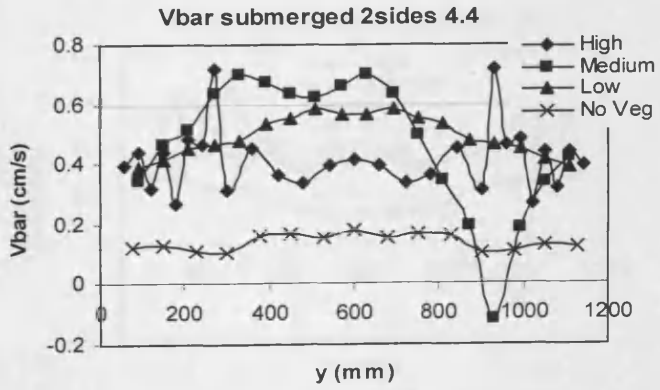

Fig. 6.44 Time-averaged transverse velocity ($\overline{V}$) [cms^{-1}] emergent partial two-sided vegetation at cross-section 4.4 for four configurations: (a) high, (b) medium, (c) low, and (d) no vegetation; (e) depth-averaged vertical velocity profiles.

(a)

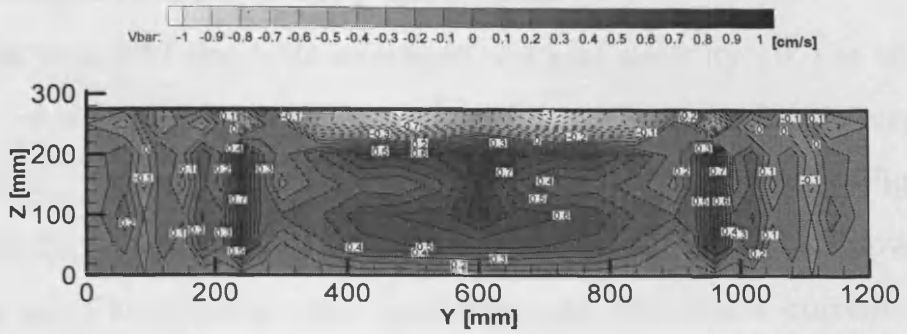

(b)

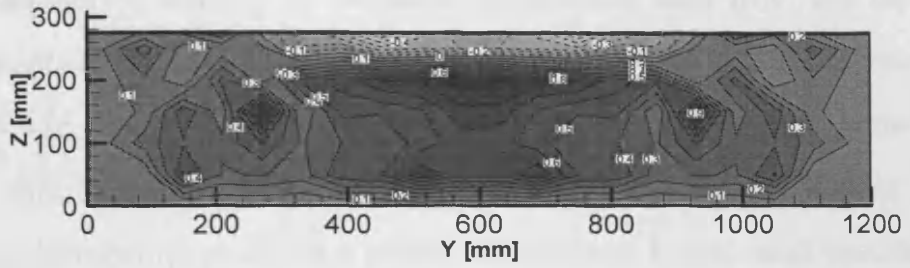

(c)

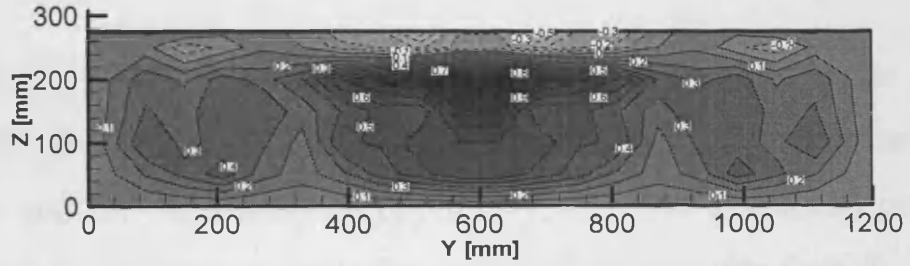

(d)

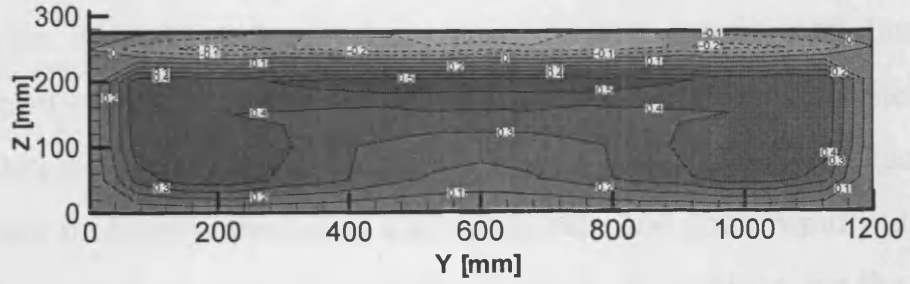

(e)

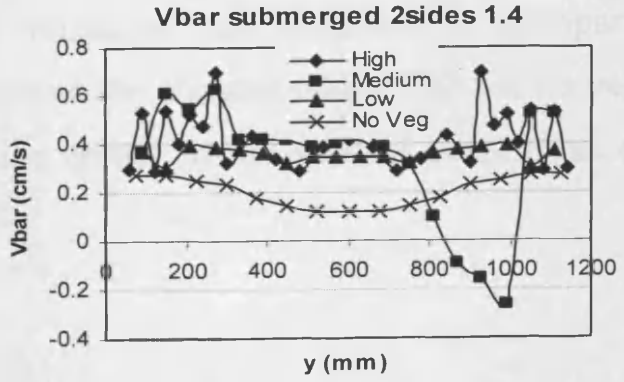

Fig. 6.45 Time-averaged transverse velocity ($\overline{V}$) [cms^{-1}] emergent partial two-sided vegetation at cross-section 1.4 for four configurations: (a) high, (b) medium, (c) low, and (d) no vegetation; (e) depth-averaged vertical velocity profiles.

c) Time-averaged vertical velocity ($\overline{W}$)

In Figs. 6.46 and 6.47 the time-averaged vertical velocity ($\overline{W}$) is shown for the partial two-sided emergent vegetation. It can be seen that, for the vegetation free half of channel, secondary currents are formed at several sites. In Figs. 6.46a and 6.47a for the high density configuration, several downward and upward velocity components are illustrated giving minimum and maximum current respectively. When the vegetation density is reduced to medium and low, the downward and upward currents decrease and the uniformity in velocity profile increases (see Figs. 6.46c and 6.47c). Also due to the effects of the trailing vortex, transverse waves arise again due to the rods interacting with the flow. Again, further experiments have been undertaken to study this effect, as outlined in the next section.

In Figs. 6.46e and 6.47e the depth-averaged vertical velocity profile is shown for various configurations of the emergent partial two-sided vegetation and for the two sections 4.4 and 1.4. As mentioned previously, the vertical velocity generally has a reverse trend in comparison with the longitudinal velocity (see Figs. 6.46a and 6.47a). Herein, for the two vegetated zones, the low density case has a minimum rate velocity in comparison with the other densities. Then, towards the centre of the non-vegetated half, the velocity increases for all densities and in adjacent points of the two zones it sharply reaches a maximum rate and then rapidly decreases to a minimum towards the central line of the channel. As is clear, for the high density configuration more variations are observed in comparison with the other configurations and across the channel width. For the no vegetation case, there is the minimum variation across in the vertical velocity as can be seen from the results.

(a)

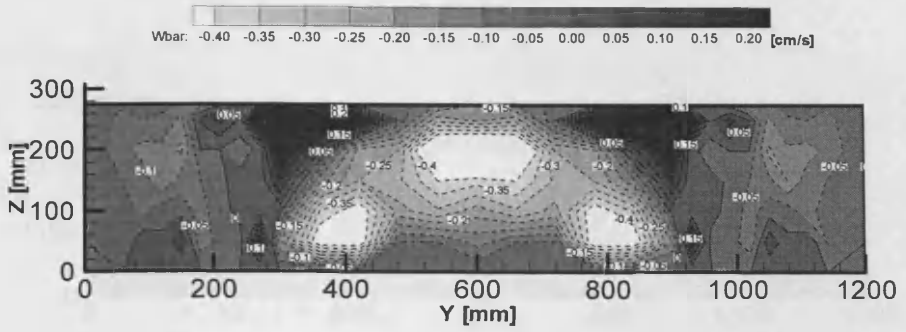

(b)

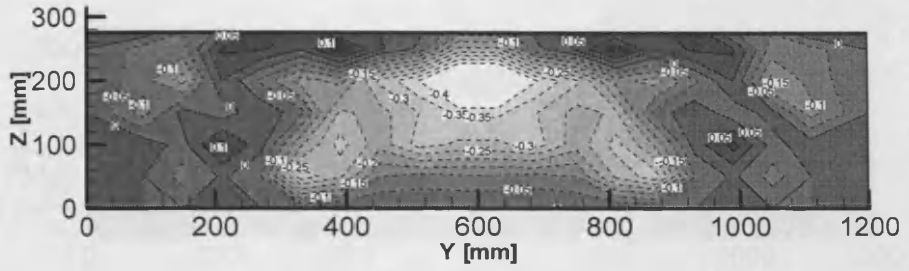

(c)

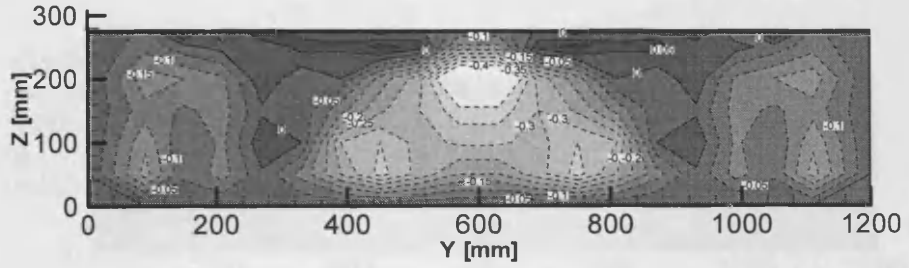

(d)

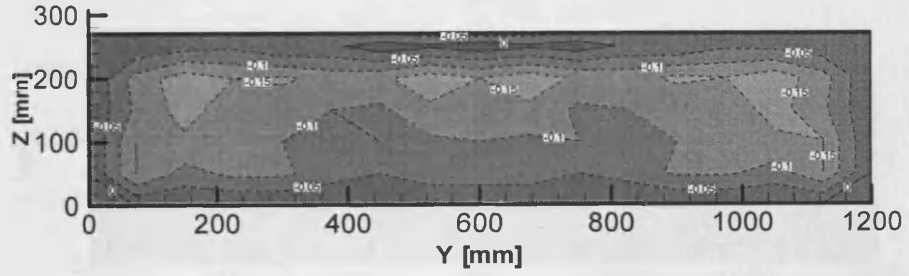

(e)

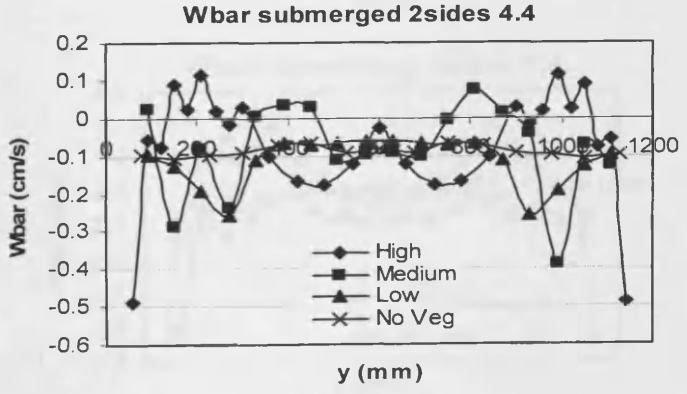

Fig. 6.46 Time-averaged vertical velocity ($\overline{W}$) [cms^{-1}] emergent partial two-sided vegetation at cross-section 4.4 for four configurations: (a) high, (b) medium, (c) low, and (d) no vegetation; (e) depth-averaged vertical velocity profiles.

(a)

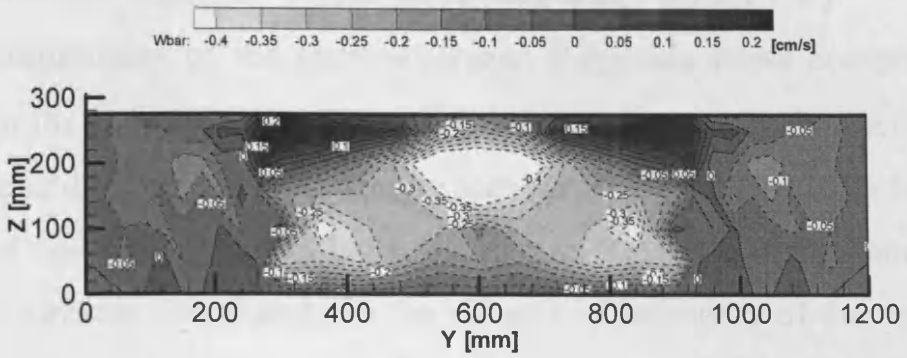

(b)

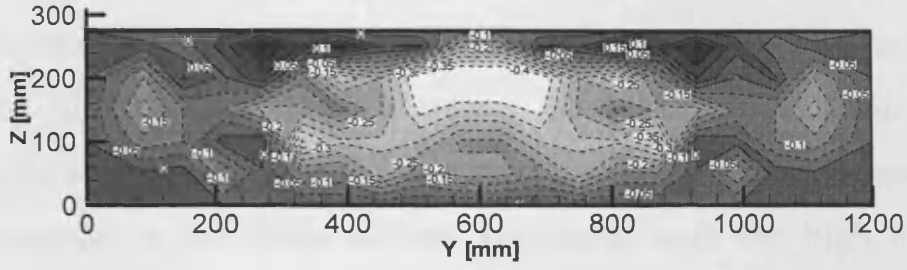

(c)

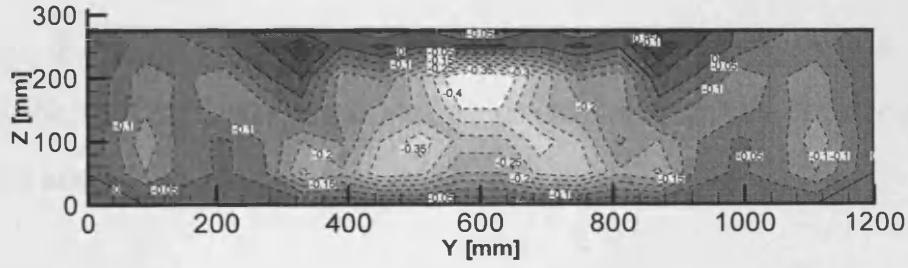

(d)

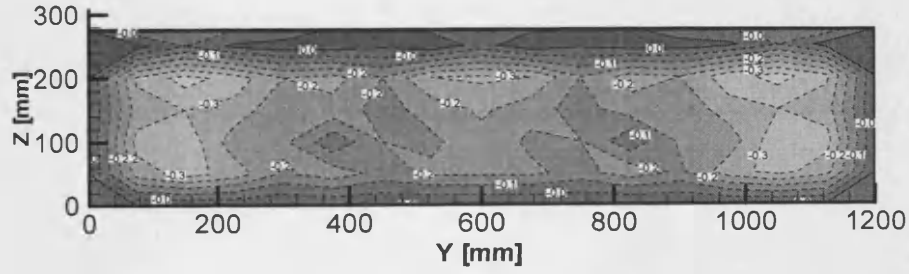

(e)

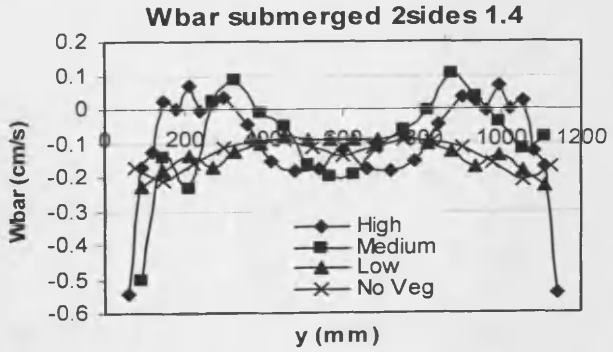

Fig. 6.47 Time-averaged vertical velocity ($\overline{W}$) [cms^{-1}] emergent partial two-sided vegetation at cross-section 1.4 for four configurations: (a) high, (b) medium, (c) low, and (d) no vegetation; (e) depth-averaged vertical velocity profiles.

d) Depth-averaged Reynolds stress components ($\overline{u'v'}$, $\overline{u'w'}$, $\overline{v'w'}$)

Various configurations of the depth-averaged Reynolds stress components ($\overline{u'v'}$, $\overline{u'w'}$, $\overline{v'w'}$) for the emergent partial two-sided vegetation across the sections 4.4 and 1.4 are illustrated in Fig. 6.48. As can be seen, in all of the graphs for both sides of the vegetated zones, all densities have a minimum Reynolds stress component. For all cases, the stresses rise sharply in the vicinity of boundary of the vegetated and vegetation free zones, reaching a peak and then decreasing to a minimum in the centre of the channel. At the transition from the vegetated to the non-vegetated zones for the high and low density cases, the maximum and minimum peak Reynolds stress components occur at these locations. For the low density case, the minimum variation in the stress occurs, compared with the high density case, across the channel width. For the no vegetation case in cross-section 4.4 high values of the Reynolds stress are observed, but in cross-section 1.4 due to proximity to the weir the minimum Reynolds stress components occur across the channel width and for all densities.

(a)

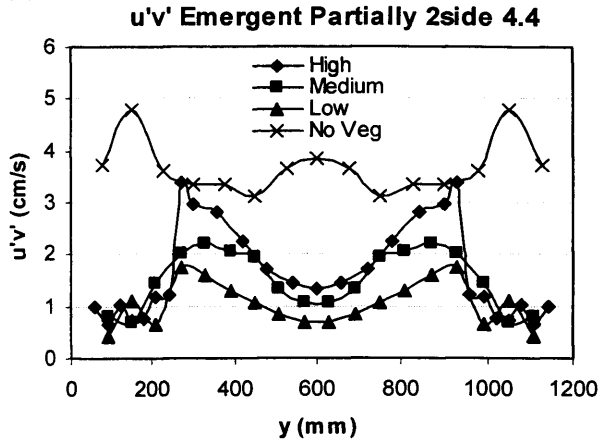

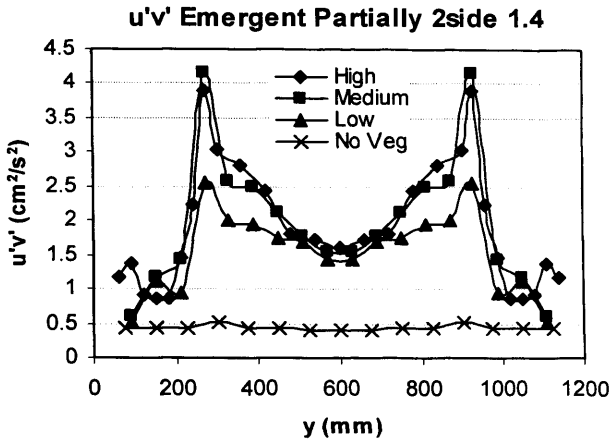

(b)

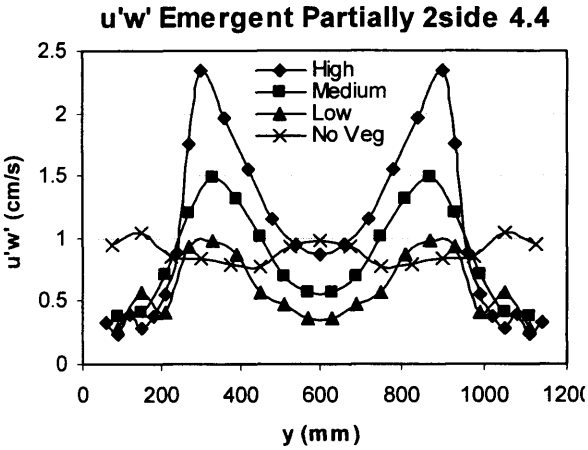

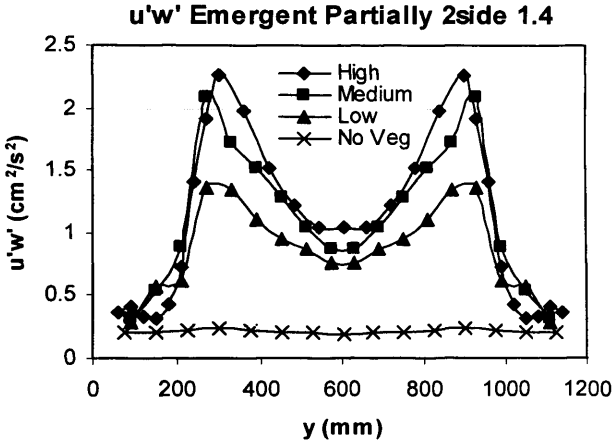

(c)

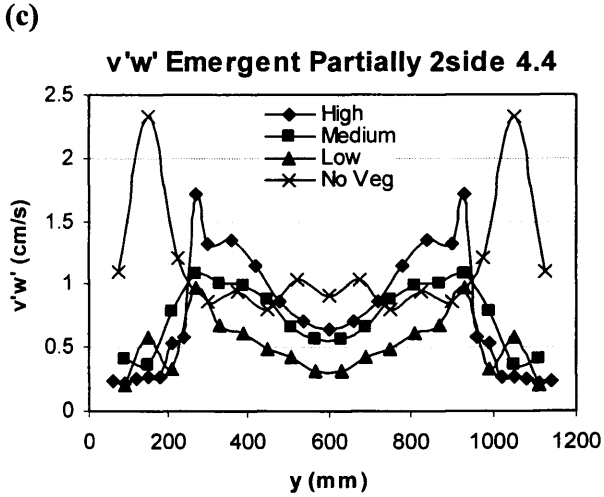

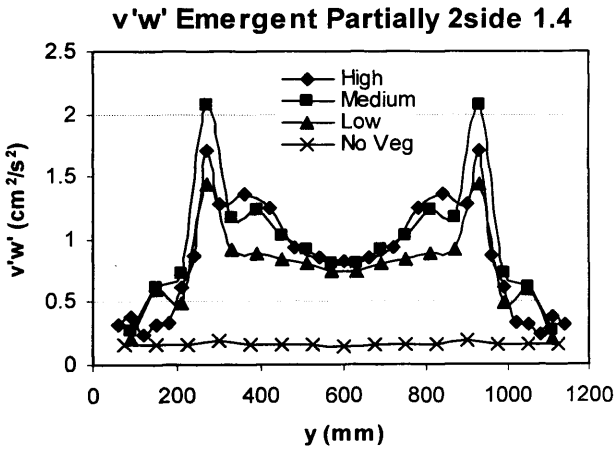

Fig. 6.48 Depth-averaged Reynolds stress components ($\overline{u'v'}$, $\overline{u'w'}$, $\overline{v'w'}$) [cm^2/s^2] for four configurations in emergent partial two-sided vegetation at cross-sections 4.4 and 1.4; (a) $\overline{u'v'}$, (b) $\overline{u'w'}$, and (c) $\overline{v'w'}$.

In this chapter experiments reported in a laboratory flume with 10 m length and 1.2 m width for four density configurations and two states of submerged and emergent in full vegetation, partial one-sided vegetation, and partial two-sided vegetation. For all states the velocity components were measured and the time-averaged velocity components ($\overline{U}$, $\overline{V}$, $\overline{W}$) were calculated from the data. The depth-averaged velocity profiles, and depth-averaged Reynolds stresses components ($\overline{u'v'}$, $\overline{u'w'}$, $\overline{v'w'}$) for four density configuration and for three locations of vegetation (i.e. fully, partial one-sided and partial two-sided vegetation) were later calculated, for the two states of submerged and emergent vegetation. The changes in the velocity profiles for the different configurations were then discussed.

CHAPTER 7
WAVE GENERATION IN VEGETATED OPEN CHANNEL

7.1 Introduction

Traditionally, it has been known that wind may cause vortex induced vibration of pylon wires, etc. (Blevins, 1977). Strouhal (1878) found that the Aeolian tones generated by a wire in the wind were proportional to the wind speed divided by the wire thickness. It was noted that the sound greatly increased when the natural tones of the wire coincided with the Aeolian tones. The periodicity of the wake of a cylinder with the formation of a stable vortex street was subsequently explained and presented by Von Karman (Karman, 1912).

Much research can be found in the literature about vortex shedding and related phenomena. Subsequent research on vortex shedding has been focused mainly on the acoustic resonant noise generated from heat exchangers when a gas flows through a bank of tubes. The results for this kind of vortex shedding can be found in the published works of Fitz-hugh (1973), Blevins (1985), Žukauskas and Katinas (1979), Weaver et al. (1986), Ziada et al. (1989), and Hamakawa et al. (2001). Also, further research on this topic can be found in the book edited by Naudascher and Rockwell (1980).

In contrast, research on the vortex shedding and related phenomena for water as the medium, is very limited. When a solid body obstructs a flowing fluid, vortex shedding may occur and this can cause vibration in the flow. There are many situations where the steady flow of water passes around a cluster of rigid vertical cylinders. These rigid cylinders may represent bridge piers, jetties or vegetation on the floodplains of rivers. This situation of rigid cylinders may produce transverse waves created by vortex shedding.

In 1939, Crausse reported his findings on wave oscillations in open channels and this is thought to be the first time that such phenomena were reported and analysed (Crausse, 1939). Schuster (1967) subsequently studied oscillations produced by two sets of bridge piers. Wave amplitude of 600 mm with a frequency of 0.38 Hz was observed in his study. Clays and Tison (1968) observed oscillations in a canal with only one bridge pier spanning the cross section. Falvey (1980) presented a summary of wave generation in a trapezoidal canal section with piers and Rohde et al. (1980) studied oscillations caused by non-circular cylinders in a canal and went on to discuss the implications of the Strouhal number for this specific situation.

The latest study reported in the literature was carried out by Zima and Ackermann (2002). They used two flumes, of widths 150 mm and 450 mm and two types of wooden cylinders, of diameter 12.7 mm and 25.4 mm, for the small and large flume respectively. The lengths of flumes were 2.75 m and 12 m respectively. They obtained the following results:

- The maximum amplitude (A) of the waves was 35% of the mean flow depth,
- The maximum dimensionless wave amplitudes occurred when the frequency ratio of vortex shedding and wave (f_s/f) was between 0.7 and 1.3,
- The maximum dimensionless wave amplitudes were estimated using their proposed formula.

They proposed the following equation for simulating the maximum values of the dimensionless amplitude (A/h) that may occur in a canal:

$$\frac{A}{h} = \frac{N}{S^2}\frac{D}{b}\left(\frac{D}{l}\right)^2 k \qquad (7.1)$$

where: k = constant equal to 2.255

A = maximum amplitude

h = depth of flow

N =.number of the rods in each row

S = Strouhal number

D = cylinder diameter

b = distance between rows of the rods

l = width of channel

7.2 Vortex wake and Strouhal number

As a particle flows towards the leading edge of a rigid cylinder, boundary layers will develop on both sides of the cylinder. Near the widest section of the cylinder, the boundary layers may separate from each side of the cylinder surface and form vortices and a wake. A regular pattern of vortices may form in the wake that interact with the cylinder motion and can be the source of the effects called vortex-induced vibration (Blevins, 1977). This process is schematically shown in Fig. 7.1. Based on the studies of Lienhard (1966), vortex shedding occurs downstream of a cylinder when the cylinder Reynolds number, i.e. UD/ν , is in the range $40 \le R_e < 3\times10^5$ and for $3.5\times10^6 \le R_e$ where U is the free stream velocity, D is the diameter (widest) of the cylinder, and ν is the kinematic viscosity of the fluid.

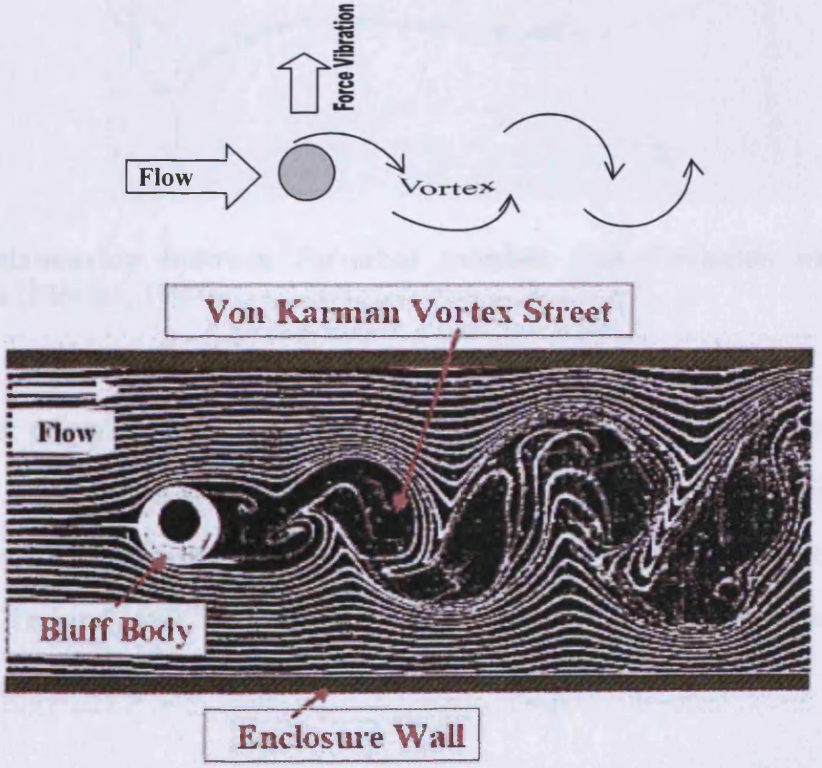

Fig. 7.1. Schematic view of vortex shedding formation from one cylinder.

The Strouhal number (S) is the proportionality constant between the predominant frequency of the vortex shedding (f_s) and the free stream velocity (U) divided by the cylinder diameter (D).

$$f_s = \frac{SU}{D} \qquad \text{Or} \qquad S = \frac{f_s D}{U} \qquad (7.2)$$

The Strouhal number is a function of the geometry and Reynolds number for low Mach number flows. For a circular cylinder and based on experimental data, Lienhard (1966) presented a graph for estimating the Strouhal number for the corresponding Reynolds number of a cylinder. This graph is shown in Fig. 7.2 and, although there is a variation in S with Re, the Strouhal number for a single cylinder is typically equal to 0.2 in the range of Reynolds number flows for vortex shedding. Also, the cylinder Reynolds number can be between approximately 300 and 300,000. This graph is shown in Fig. 7.2.

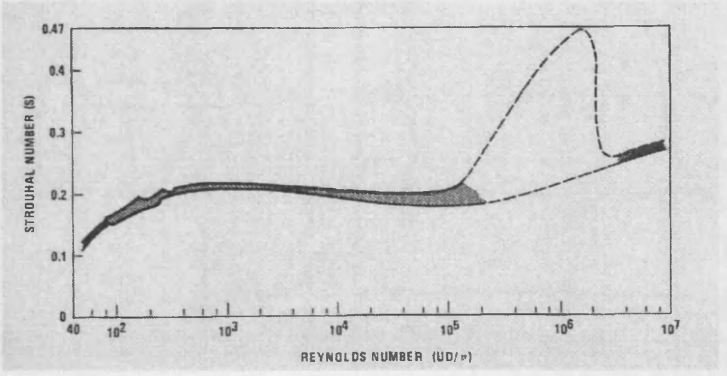

Fig. 7.2. Relationship between Strouhal number and Reynolds number for circular cylinders (Blevins, 1977).

For a cluster of cylinders arranged in staggered rows, or in in-line rows, and when the fluid is a gas, then the Strouhal number is based on the cylinder diameter and the distance between cylinders in a row (T) and the distance between the cylinder rows (P). Fitz-hugh (1973) presented two maps for these cases which are shown in Figs. 7.3 and 7.4 respectively.

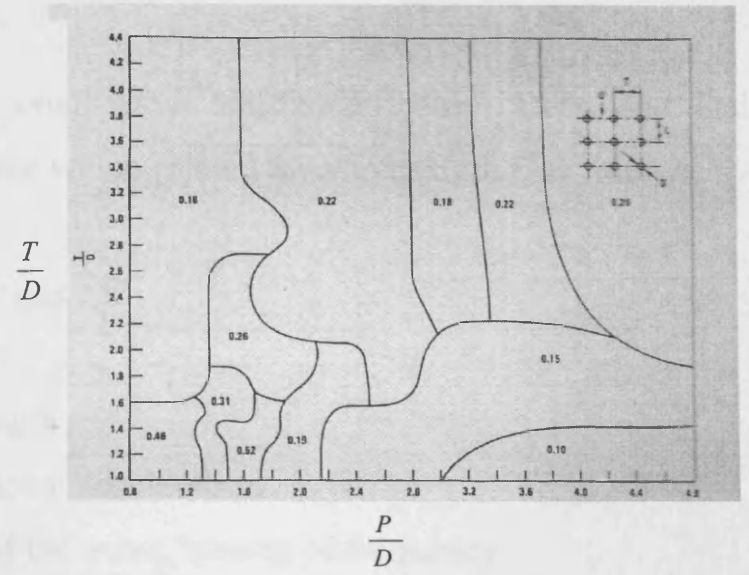

Fig. 7.3. Fitz-hugh's Strouhal number map for in-line cylinders (Blevins 1977).

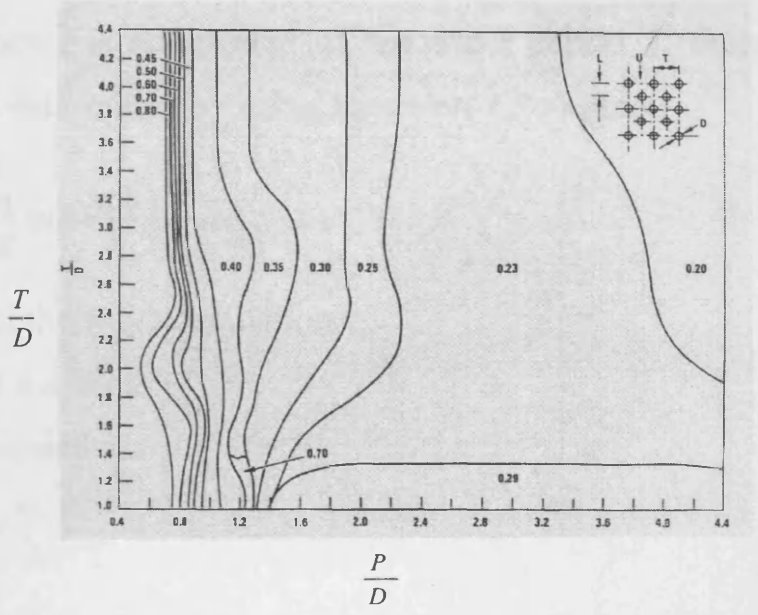

Fig. 7.4. Fitz-hugh's Strouhal number map for staggered cylinders (Blevins 1977).

Zukauskas et al. (1988) presented the following two equations for Strouhal number estimation for air or water and where the cylinders are arranged in a single row:

For staggered bundles $S_t = 0.2 + \exp\left[-0.44\left(T/D\right)^{1.8}\right]$ when $T/D \geq 1.15$ (7.3)

For in-line bundles $S_t = 0.2 + \exp\left[-1.2\left(T/D\right)^{1.8}\right]$ when $T/D \geq 1.15$ (7.4)

7.3 Wavelength

Using Stokesi or small-wave amplitude theory, Dean and Dalrymple (1984) presented an equation which related the wavelength L as follows:

$$L = \frac{g}{2\pi} T^2 \tanh \frac{2\pi h}{L} \tag{7.5}$$

where: L = wavelength

g = gravitational acceleration

T = period of the wave, inverse of frequency

h = flow depth

The wave frequency f is an inverse of the wave period T, therefore, the wave frequency f can be determined by using Equation 7.5 to give:

$$f = \left(\frac{gn}{4\pi l} \tanh \frac{n\pi h}{l} \right)^{1/2} \tag{7.6}$$

where: n = mode of the wave oscillation

l = width of the channel

Also, l can be calculated as:

$$l = \frac{nL}{2} \tag{7.7}$$

When the amplitude (A) is at the maximum rate, then f_s should be equal to f (i.e. $f_s = f$), and the combination of Equations 7.2 and 7.6 as:

$$\frac{SU}{D} = \left(\frac{gn}{4\pi l} \tanh \frac{n\pi h}{l} \right)^{1/2} \tag{7.8}$$

$$S = \frac{D\left(\frac{gn}{4\pi l} \tanh \frac{n\pi h}{l} \right)^{1/2}}{U} \tag{7.9}$$

Equation 7.9 is used to calculate the Strouhal number S.

7.4 Experimental set-up

In the current study, the effects and characteristics of vortex shedding were investigated around idealised tree vegetation. Measurements were taken in a wide flume, of width 1200 mm, length 10 m, and depth 360 mm (see Fig. 7.5). A wooden pallet was employed to separate the flume into two sections (or channels) of varying width (see Fig. 7.6). The slope of the flume was constant and set equal to 0.001. The rods consisted of wooden cylinders with a diameter of 24 mm and a height of 300 mm. The rigid rods were screwed into the bed of the flume at different distances and spacings (i.e. different T and P) and for different arrangements (i.e. staggered and in-line), as shown in Fig. 7.6.

Fig. 7.5. Experimental flume configuration.

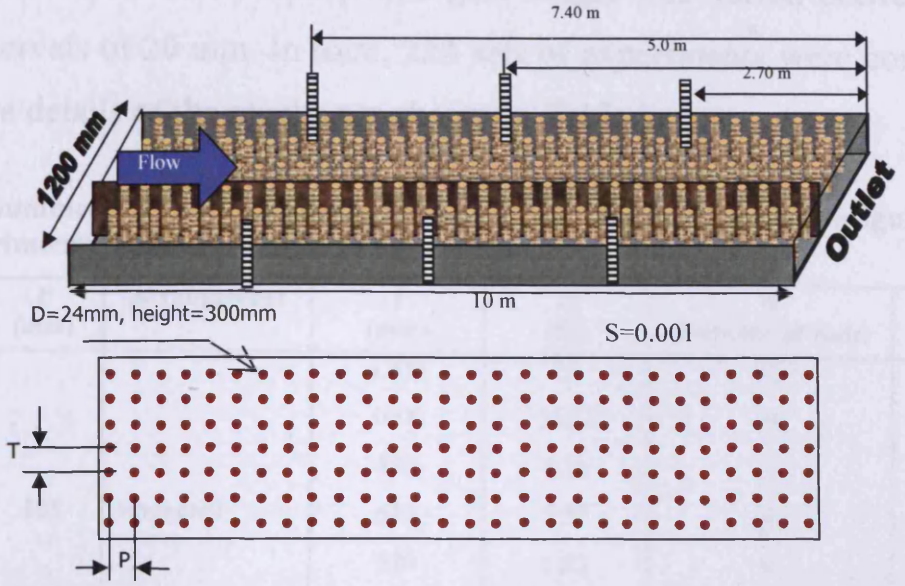

Fig. 7.6. Schematic view of the experimental set-up.

The section used for measuring the mean flow was located along the centre reach of the flume. The wave displacements were measured at three stations located at 2.70 m, 5 m, and 7.40 m from outlet of the flume (Fig. 7.6). Both parameters were measured by markers against rulers in millimetre scales, fixed at the side and centre of the flume. With the aid of the wooden pallet the flume was separated into two channel sections, thereby enabling different channel widths to be studied. The experiments were carried out in two stages, namely the first and second stages.

7.4.1 First stage of experiments

In the first stage of the experiments, and with the aid of the wooden pallet, the flume was separated into two different channel thereby enabling seven different channel widths to be investigated. The effective widths of the flumes were 1200, 1000, 855, 680, 520, 345, and 200 mm respectively. The flow discharge to the main flume was constant and equal to 13 *l/s* and, for the case where the flume was divided, then the discharge was also divided into two portions, based on the width ratio of each part of the flume. A controllable weir gate was located at the outlet of the flume, as before, with the weir again being used to set different depth and

velocity conditions in the flume. The gate height was varied between 0 and 300 mm at intervals of 20 mm. In total, 224 sets of experiments were conducted in the flume. The details of the results are shown in Table 1.

Table 7.1 Summery of flume characteristics and data measurements configurations for experimental studies (first stage experiments).

T (mm)	P (mm)	Arrangement	l (mm)	Q (l/s)	N (Number of rods)	No. of experiments
120	105	Staggered	1200	13	10	14
			1000	10.83	9	10
			855	9.26	7	9
			680	7.37	6	6
			520	5.63	4	6
			345	3.74	3	9
			200	2.17	1	10
60	105	In-line	1200	13	20	13
			1000	10.83	17	6
			855	9.26	14	6
			680	7.37	11	6
			520	5.63	9	6
			345	3.74	6	6
			200	2.17	3	6
120	105	In-line	1200	13	10	13
			1000	10.83	9	6
			855	9.26	7	6
			680	7.37	6	6
			520	5.63	4	6
			345	3.74	3	6
			200	2.17	1	6
120	210	In-line	1200	13	10	13
			1000	10.83	9	6
			855	9.26	7	6
			680	7.37	6	6
			520	5.63	4	6
			345	3.74	3	6
			200	2.17	1	6
240	210	In-line	1200	13	10	13
Total number of experiments						**224**

The flow water temperature was constant and measured at 17° C. For each experimental study, the data were collected for four parameters, namely: mode of waves, average depth of flow, water displacement in the centre and water displacement in the side of flume.

7.4.2 Second stage of experiments

From the results of the first stage of the experiments, it was found that there was no particular relationship between the amplitude and the longitudinal and transverse distances between the rods (i.e. inside and between the rows-T and P respectively). Hence, in a second stage of the experiments were carried out with a denser configuration of the rods, smaller interval changes in the tailgate (i.e. 5 mm) and with a higher level accuracy in the measurements. With the aid of the wooden pallet the flume was again separated into two different width channels, with three different flume widths being considered. The widths of the channels were 1200, 800 and 400mm. The flow discharge in the main flume was constant and equal to 18.33 *l/s* and, in the case of flume separation; this value was divided into two portions equal to 12.22 *l/s* and 6.11 *l/s*. Again, there was a controllable weir gate at the outlet of the flume and this weir was used to make set conditions in the experimental programme. The gate height was changed between 280 and 30 mm, with an interval of 5 mm.

Details of the experimental set up are shown in Table 7.2. The water temperature was constant and equal to 17° C. For each experiment a value of four parameters was recorded, i.e. the mode of the waves, average depth of flow, and water displacement at the sides of the flume and at three pre-determined stations.

Table 7.2. Summery of flume characteristics and data measurement configurations in the experimental studies (second stage experiments).

T (mm)	P (mm)	Arrangement	l (mm)	Q (L/s)	N (Number of rods)	Exp. No.
60	105	In-line	1200	18.33	20	1
			800	12.22	13	2
			400	6.11	7	3
	210	In-line	1200	18.33	20	4
			800	12.22	13	5
			400	6.11	7	6
	315	In-line	1200	18.33	20	7
			800	12.22	13	8
			400	6.11	7	9
	420	In-line	1200	18.33	20	10
			800	12.22	13	11
			400	6.11	7	12
120	105	In-line	1200	18.33	10	13
			800	12.22	6	14
			400	6.11	3	15
	420	In-line	1200	18.33	10	16
			800	12.22	6	17
			400	6.11	3	18
240	105	In-line	1200	18.33	5	19
			800	12.22	3	20
			400	6.11	2	21
	420	In-line	1200	18.33	5	22
120	105	Staggered	1200	18.33	10	23
			800	12.22	6.5	24
			400	6.11	3	25
	315	Staggered	1200	18.33	10	26
			800	12.22	6.5	27
			400	6.11	3	28
240	105	Staggered	1200	18.33	5	29
			800	12.22	3	30
			400	6.11	1.5	31
	210	Staggered	1200	18.33	5	32
			800	12.22	3	33
			400	6.11	1.5	34
360	105	Staggered	1200	18.33	3.5	35
			800	12.22	2	36
			400	6.11	1	37
	315	Staggered	1200	18.33	3.5	38

7.5 Experimental observations

For most of the studied cases, the height of the outlet weir was reduced from the highest to the lowest levels, with three or four modes of vibration occurring for each sequence. These modes are shown in Fig. 7.7 and introduced by n=1, 2, 3, and 4. The amplitude of a wave (A) was defined as the maximum water displacement. The maximum wave amplitude observed in the experiments was equal to 40% of the mean flow depth, with this result having profound potential implications for flooding.

As mentioned before, the amplitude was measured at three sections along the flume. For each individual experiment the difference between the measured amplitude for these three stations was found to be small. The average of these three measured values was then used for data analyses.

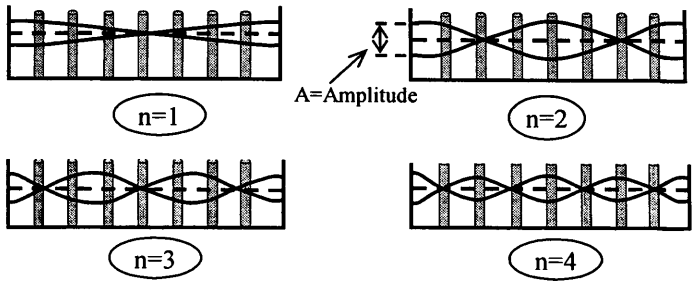

Fig. 7.7. Modes of waves appeared in the laboratory flume.

7.5.1 First stage experiments

Table 7.3 shows the measured and calculated parameters related to the points of maximum amplitude and the transverse wave modes.

Table 7.3 Measured parameters related to the points of maximum amplitude of first stage of the experimental studies.

Staggered

T (mm)	P (mm)	Q (l/s)	N	l (mm)	h (mm)	n	A(sides) (mm)	V (m/s)	Re (cylinder)
120	105	13	10	1200	272	1	20	0.0398	883.44
		13	10	1200	148	2	40	0.0732	1623.62
		13	10	1200	125	3	40	0.0867	1922.37
		10.8	9	1000	287	1	10	0.0377	837.267
		10.8	9	1000	175	2	35	0.0619	1373.12
		10.8	9	1000	140	3	30	0.0774	1716.4
		9.26	7	855	170	2	10	0.0637	1413.5
		9.26	7	855	145	3	20	0.0747	1657.21
		7.37	6	680	163	2	5	0.0665	1474.21
		7.37	6	680	145	3	30	0.0747	1657.21
		5.63	4	520	163	2	5	0.0665	1474.21
		5.63	4	520	145	3	25	0.0747	1657.21
		3.74	3	345	145	3	15	0.0747	1657.21

In-line

T (mm)	P (mm)	Q (l/s)	N	l (mm)	h (mm)	n	A(sides) (mm)	V (m/s)	Re (cylinder)
		13	20	1200	300	1	40	0.0361	800.986
		13	20	1200	190	2	45	0.057	1264.71
		13	20	1200	160	3	50	0.0677	1501.85
		10.8	17	1000	260	1	30	0.0417	924.214
		10.8	17	1000	160	2	40	0.0677	1501.85
60	105	9.26	14	855	260	1	30	0.0417	924.214
		9.26	14	855	160	3	45	0.0677	1501.85
		7.37	11	680	215	1	20	0.0504	1117.65
		7.37	11	680	160	2	30	0.0677	1501.85
		5.63	9	520	175	1	40	0.0619	1373.12
		3.74	6	345	160	2	40	0.0677	1501.85
		13	10	1200	250	1	30	0.0433	961.183
		13	10	1200	160	2	40	0.0677	1501.85
		13	10	1200	115	3	45	0.0942	2089.53
		10.8	9	1000	145	2	40	0.0747	1657.21
120	105	10.8	9	1000	115	3	40	0.0942	2089.53
		9.26	7	855	120	3	15	0.0903	2002.46
		7.37	6	680	115	3	15	0.0942	2089.53
		5.63	4	520	115	3	15	0.0942	2089.53
		3.74	3	345	120	2	10	0.0903	2002.46
		13	10	1200	270	1	15	0.0401	889.984
		13	10	1200	175	2	30	0.0619	1373.12
		13	10	1200	140	3	40	0.0774	1716.4
		13	10	1200	105	4	35	0.1032	2288.53
		10.8	9	1000	250	1	5	0.0433	961.183
		10.8	9	1000	105	4	20	0.1032	2288.53
		9.26	7	855	135	2	10	0.0802	1779.97
		9.26	7	855	100	3	10	0.1083	2402.96
120	210	7.37	6	680	190	1	5	0.057	1264.71
		7.37	6	680	135	2	5	0.0802	1779.97
		7.37	6	680	105	3	10	0.1032	2288.53
		5.63	4	520	105	3	10	0.1032	2288.53
		3.74	3	345	135	1	5	0.0802	1779.97
		3.74	3	345	100	3	10	0.1083	2402.96
		13	5	1200	165	2	5	0.0657	1456.34
		13	5	1200	130	3	10	0.0833	1848.43
		13	5	1200	95	4	10	0.114	2529.43

In Fig. 7.8 the relationship between the wave amplitude, the transverse wave modes, and the depth of flow are shown for two sets of experiments, and for different channel widths. As can be seen, when the water level is near to the highest depth (i.e. 300 mm) no wave oscillations occur.

When the water level is reduced slowly, the first mode of the transverse wave appears. This mode is defined by n=1 as shown in Figs. 7.7 and 7.8 in first step experiments. For this mode when the water depth is gradually reduced it can be seen that the water displacement is increased slowly until it reaches its maximum value. At the point of maximum lateral displacement, it can be seen that the width of the flume is exactly half of the vortex shedding wave length. Beyond this point, the water displacement reduces again until the wave is completely diminished. As the depth is further reduced then the second mode of the wave occurs, as determined by n=2 in Figs. 7.7 and 7.8. This wave also reaches a maximum level displacement and then reduces to a minimum at approximately half the flume width. For the peak point of this mode it can be seen that the width of the flume is again equal to the vortex shedding wave length. The third and fourth modes appear as the depth is further reduced giving the 3rd and 4th modes, and defined respectively by n=3 and n=4 in Figs. 7.7 and 7.8 respectively.

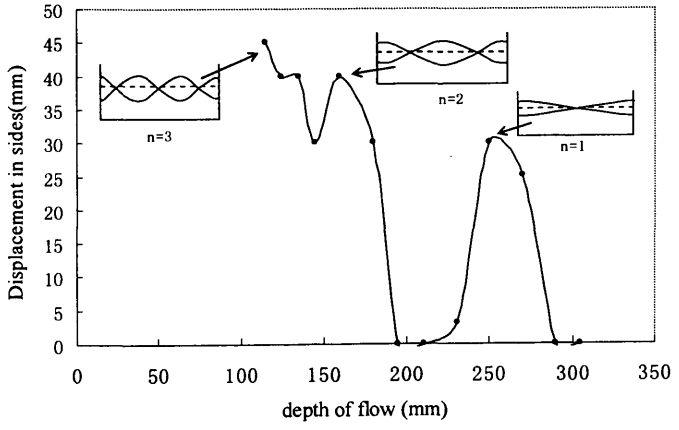

Rods are in-line arrangement, l=1200 mm, Q=13 l/s, T=120,. P=105.

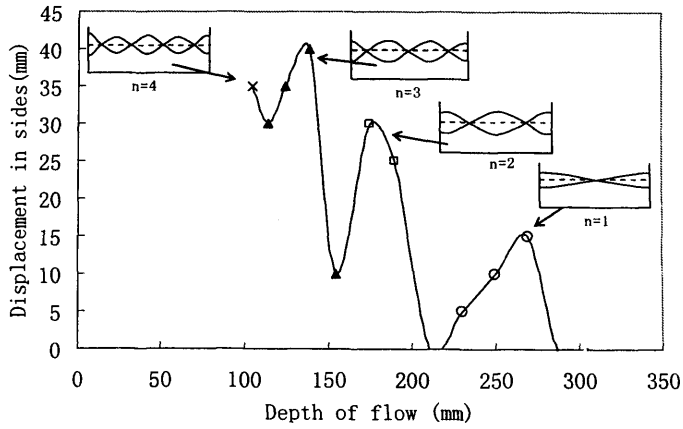

Rods are in-line arrangement, l=1200 mm, Q=13 l/s, T=120, P=210.

Fig. 7.8 Relationship between water displacements, transverse wave modes, and depth of flow for two experimental rod arrangements.

7.5.2 Second stage experiments

For the second stage experiments, the relationship between the relative wave amplitude, the transverse waves modes, and depth of flow are shown in Fig. 7.9 for six sets of experiments with different channel widths. As can be seen, for most of the experimental situations, the modes of vibration appeared in sequence and the maximum relative amplitudes (A/h) increased when the modes were increased. Only for experiments numbered 1 and 2 (Table 7.2), where T and P were both at their minimum values, the sequence was slightly different. In these experiments after the first mode of waves (n=1) the third mode of waves (n=3) then appeared (Fig. 7.10).

The maximum relative amplitudes for each mode of the experiments are separated and used for further analyses. These data are shown in Table 7.4. The Reynolds numbers of the experiments were in the range: 1000 to 4400 and the maximum wave amplitudes observed in the experiments were 40% of the mean flow depth.

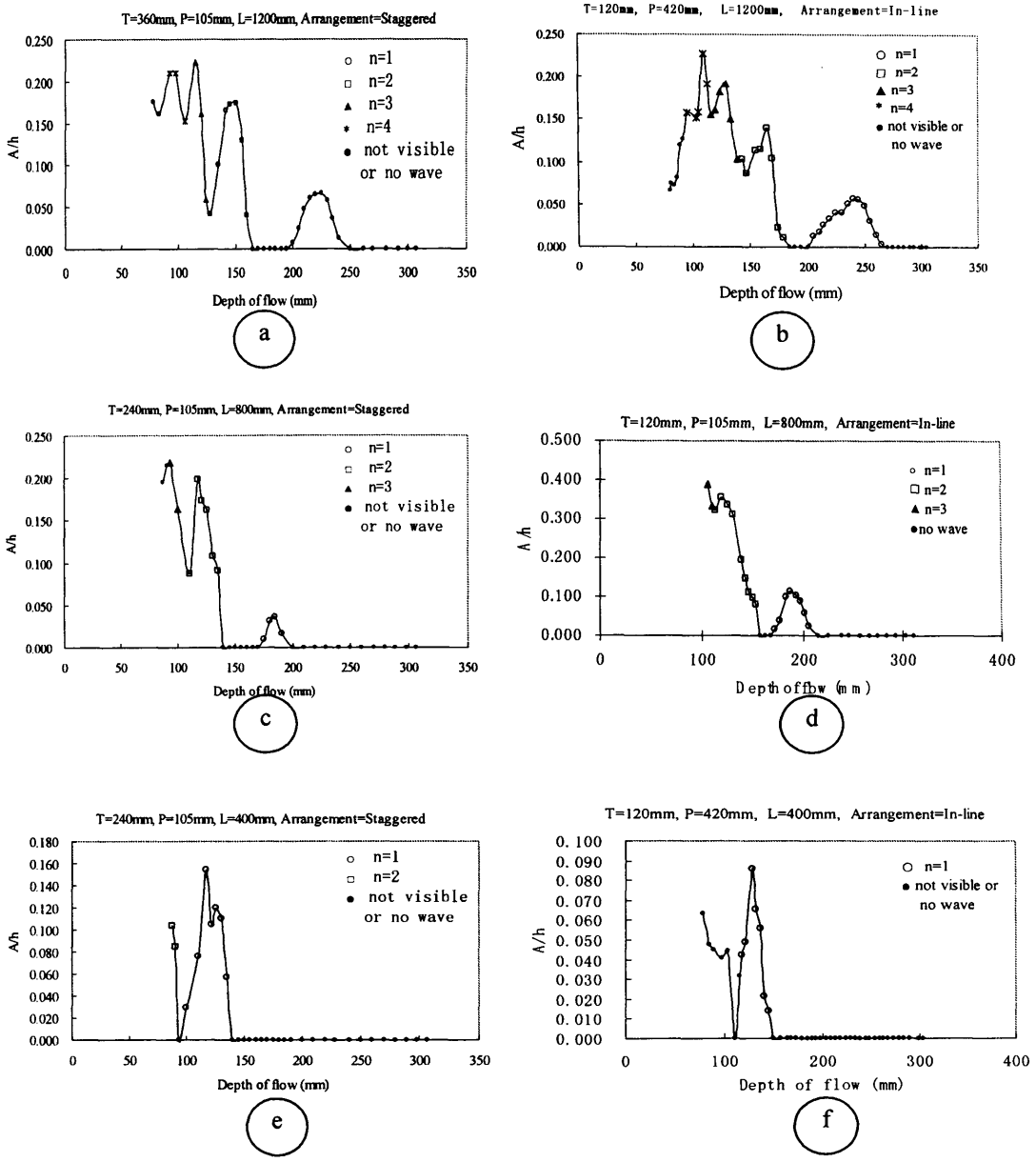

Fig. 7.9 Relationship between water amplitude, transverse wave modes, and depth of flow for six sets of experiments.

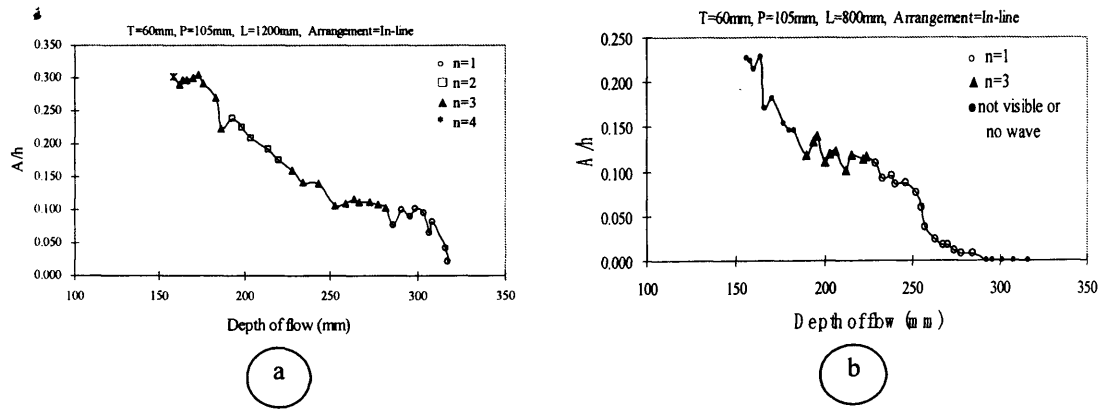

Fig. 7.10 Relationship between water amplitude, transverse wave modes, and depth of flow for the experiments number 1 and 2.

Table 7.4 Measured parameters related to the points of maximum relative amplitude of the second stage of the experimental studies.

Exp. No.	h (mm)	n	A (mm)	Exp. No.	h (mm)	n	A (mm)	Exp. No.	h (mm)	n	A (mm)
22	204	1	1.3	11	230	1	2.0	26	170	2	22.0
16	240	1	13.7	8	230	1	5.7	29	158	2	28.7
19	199	1	15.7	5	251	1	10.0	38	140	2	5.7
1	299	1	30.3	17	128	2	10.0	35	150	2	26.0
13	242	1	26.0	14	120	2	42.7	32	125	3	28.3
10	304	1	19.0	11	175	2	28.3	23	134	3	32.0
7	291	1	18.0	8	144	2	29.0	26	129	3	21.7
4	309	1	23.7	5	203	2	24.7	29	120	3	31.7
22	140	2	12.0	20	110	2	17.3	38	118	3	8.3
16	165	2	23.0	17	104	3	9.0	35	114	3	25.3
19	143	2	27.3	2	196	3	27.3	32	81	4	10.0
1	193	2	46.0	14	106	3	41.3	23	115	4	41.7
13	166	2	37.0	11	150	3	15.7	26	95	4	18.0
10	234	2	31.0	8	127	3	23.3	29	95	4	28.3
7	204	2	29.7	5	160	3	23.3	35	92	4	19.3
4	259	2	34.7	17	128	1	11.0	24	193	1	18.3
22	109	3	8.7	20	100	1	13.7	27	210	1	3.7
16	130	3	25.0	3	158	1	22.0	30	185	1	6.7
19	120	3	22.7	15	114	1	31.0	36	111	1	20.3
1	264	3	30.7	12	170	1	19.0	24	130	2	30.0
1	173	3	52.7	9	148	1	16.0	27	133	2	22.3
13	130	3	40.7	6	173	1	17.3	30	117	2	23.3
10	190	3	31.3	3	196	2	10.7	24	114	3	31.7
7	175	3	36.7	12	133	2	6.3	27	108	3	11.0
4	205	3	41.0	9	123	2	9.0	30	93	3	20.3
22	93	4	9.0	6	155	2	19.3	25	130	1	18.3
16	110	4	25.0	12	119	3	3.0	28	133	1	10.7
19	100	4	24.0	32	244	1	14.0	31	117	1	18.0
1	158	4	47.7	23	245	1	21.3	37	111	2	17.0
13	119	4	47.3	26	249	1	11.3	25	114	2	21.7
10	155	4	31.7	29	277	1	19.3	28	90	2	7.7
7	139	4	32.7	38	219	1	1.7	31	87	2	9.0
4	175	4	34.0	35	225	1	15.0	37	77	3	8.0
2	238	1	22.7	32	164	2	24.3				
14	187	1	21.3	23	163	2	34.0				

7.6 Analysis

From the experimental data, all points with the largest amplitudes for each mode have been selected and used for further analysis. Hence, the numbers of data sets extracted for further analysis in the first and second stage of the experiments were 49 and 103 respectively. The average velocity, U, was calculated by dividing the discharge by the cross sectional area of the flume. The Reynolds number, UD/ν, was calculated with respect to the rod diameter and the kinematic viscosity for water. In the first stage of the experiment analysis data, the wave frequency and then the new Strouhal number were calculated. In the second stage of the experiment analysis, the amplitude of the transverse waves was measured and then their relative amplitude (A/h) was calculated and is discussed herein.

7.6.1 Frequency and Strouhal number (the first stage experiments analysis)

When resonance is generated, the frequency of the vortex shedding (f_s) is obtained by Equation 7.2 (i.e. $f_s = \frac{SU}{D}$). In calculating f_s this needs to provide a good estimate of the Strouhal number. There are three methods regularly used to obtain the Strouhal number as indicated in the introduction. These include: Lienhard graphs, Fitz-hugh's map and by using Žukauskas et al.'s equations, which all enable the Strouhal number and the frequency of the vortex shedding to be determined. For all of the experimental conditions, and using these methods to calculate the Strouhal number, values of about 0.2 were obtained and therefore the frequencies of the vortex shedding from these three methods were the same.

The wave frequency was calculated based on small-wave amplitude theory, as given by Dean and Dalrymple (1984), and based on Equation 7.6. When the amplitude (A) is the maximum, then f_s (the frequencies of the vortex shedding) should be equal to f (the wave frequency). Therefore assuming that f_s is equal to f

when the amplitude (A) is a maximum, then S (the Strouhal number) can be calculated from the measured parameters using the following equations:

$$f_s = \frac{SU}{D} \qquad \text{and} \qquad f = \left(\frac{gn}{4\pi d} \tanh \frac{n\pi h}{l} \right)^{1/2}$$

Thus, if: $f = f_s$ then

$$S = \frac{D\left(\frac{gn}{4\pi d} \tanh \frac{n\pi h}{l} \right)^{1/2}}{U}$$

By using this equation, a new S is proposed from the results of the related experiments. The results of the corresponding calculations are presented in Table 7.5.

Table 7.5 Summary of the calculated parameters.

Staggered

T (mm)	P (mm)	Q (l/s)	N	l (mm)	h (mm)	n	A(sides) (mm)	V (m/s)	Re (cylinder)	T/D	P/D	fs	f	fs/f	S (computed)	A/h (measur)	A/h (Zima eq)
		13	10	1200	272	1	20	0.0398	883.44	5	4.38	0.3319	0.63084	0.52613	0.380137	0.0735	0.051543
		13	10	1200	148	2	40	0.0732	1623.62	5	4.38	0.60998	0.91929	0.66354	0.3014124	0.2703	0.051543
		13	10	1200	125	3	40	0.0867	1922.37	5	4.38	0.72222	1.21268	0.59556	0.3358184	0.32	0.051543
		10.8	9	1000	287	1	10	0.0377	837.267	5	4.38	0.31456	0.74805	0.4205	0.4756201	0.0348	0.0668
		10.8	9	1000	175	2	35	0.0619	1373.12	5	4.38	0.51587	1.11762	0.46158	0.4332919	0.2	0.0668
		10.8	9	1000	140	3	30	0.0774	1716.4	5	4.38	0.64484	1.42437	0.45272	0.4417751	0.2143	0.0668
120	105	9.26	7	855	170	2	10	0.0637	1413.5	5	4.38	0.53105	1.24421	0.42681	0.4685873	0.0588	0.071072
		9.26	7	855	145	3	20	0.0747	1657.21	5	4.38	0.62261	1.58836	0.39198	0.5102286	0.1379	0.071072
		7.37	6	680	163	2	5	0.0665	1474.21	5	4.38	0.55385	1.4422	0.38403	0.520789	0.0307	0.096308
		7.37	6	680	145	3	30	0.0747	1657.21	5	4.38	0.62261	1.8224	0.34164	0.5854125	0.2069	0.096308
		5.63	4	520	163	2	5	0.0665	1474.21	5	4.38	0.55385	1.69902	0.32598	0.6135304	0.0307	0.109795
		5.63	4	520	145	3	25	0.0747	1657.21	5	4.38	0.62261	2.11074	0.29497	0.6780352	0.1724	0.109795
		3.74	3	345	145	3	15	0.0747	1657.21	5	4.38	0.62261	2.60396	0.2391	0.836473	0.1034	0.187074

T (mm)	P (mm)	Q (l/s)	N	l (mm)	h (mm)	n	A(sides) (mm)	V (m/s)	Re (cylinder)	T/D	P/D	fs	f	fs/f	S (computed)	A/h (measur)	A/h (Zima eq)
		13	20	1200	300	1	40	0.0361	800.986	2.5	4.38	0.30093	0.65303	0.35283	0.4340149	0.1333	0.103086
		13	20	1200	190	2	45	0.057	1264.71	2.5	4.38	0.47515	0.99382	0.4781	0.4183199	0.2368	0.103086
		13	20	1200	160	3	50	0.0677	1501.85	2.5	4.38	0.56424	1.28782	0.43813	0.4564824	0.3125	0.103086
		10.8	17	1000	260	1	30	0.0417	924.214	2.5	4.38	0.34722	0.72486	0.47902	0.4175209	0.1154	0.126177
		10.8	17	1000	160	2	40	0.0677	1501.85	2.5	4.38	0.56424	1.09182	0.51679	0.3870074	0.25	0.126177
60	105	9.26	14	855	260	1	30	0.0417	924.214	2.5	4.38	0.34722	0.82303	0.42188	0.4740653	0.1154	0.142143
		9.26	14	855	160	3	45	0.0677	1501.85	2.5	4.38	0.56424	1.60677	0.35116	0.5695398	0.2813	0.142143
		7.37	11	680	215	1	20	0.0504	1117.65	2.5	4.38	0.4199	0.93313	0.44999	0.4444551	0.093	0.176565
		7.37	11	680	160	2	30	0.0677	1501.85	2.5	4.38	0.56424	1.43815	0.39233	0.5097691	0.1875	0.176565
		5.63	9	520	175	1	40	0.0619	1373.12	2.5	4.38	0.51587	1.0851	0.47542	0.4206831	0.2286	0.24704
		3.74	6	345	160	2	40	0.0677	1501.85	2.5	4.38	0.56424	2.12064	0.26607	0.751687	0.25	0.374149

In-line

T (mm)	P (mm)	Q (l/s)	N	l (mm)	h (mm)	n	A(sides) (mm)	V (m/s)	Re (cylinder)	T/D	P/D	fs	f	fs/f	S (computed)	A/h (measur)	A/h (Zima eq)
		13	10	1200	250	1	30	0.0433	961.183	5	4.38	0.36111	0.61132	0.59071	0.3385763	0.12	0.051543
		13	10	1200	160	2	40	0.0677	1501.85	5	4.38	0.56424	0.9436	0.59796	0.3344716	0.25	0.051543
		13	10	1200	115	3	45	0.0942	2089.53	5	4.38	0.78502	1.1834	0.66337	0.3014927	0.3913	0.051543
		10.8	9	1000	145	2	40	0.0747	1657.21	5	4.38	0.62261	1.06125	0.58667	0.3409055	0.2759	0.0668
120	105	10.8	9	1000	115	3	40	0.0942	2089.53	5	4.38	0.78502	1.3639	0.57557	0.3474794	0.3478	0.0668
		9.26	7	855	120	3	15	0.0903	2002.46	5	4.38	0.75231	1.54116	0.48815	0.4097104	0.125	0.071072
		7.37	6	680	115	3	15	0.0942	2089.53	5	4.38	0.78502	1.7804	0.44093	0.4535904	0.1304	0.096308
		5.63	4	520	115	3	15	0.0942	2089.53	5	4.38	0.78502	2.0892	0.37575	0.5322635	0.1304	0.109795
		3.74	3	345	120	2	10	0.0903	2002.46	5	4.38	0.75231	2.10018	0.35821	0.5583254	0.0833	0.187074

T (mm)	P (mm)	Q (l/s)	N	l (mm)	h (mm)	n	A(sides) (mm)	V (m/s)	Re (cylinder)	T/D	P/D	fs	f	fs/f	S (computed)	A/h (measur)	A/h (Zima eq)
		13	10	1200	270	1	15	0.0401	889.984	5	8.75	0.33436	0.62915	0.42236	0.3763276	0.0556	0.025771
		13	10	1200	175	2	30	0.0619	1373.12	5	8.75	0.51587	0.97046	0.53158	0.3762394	0.1714	0.025771
		13	10	1200	140	3	40	0.0774	1716.4	5	8.75	0.64484	1.24953	0.51607	0.387548	0.2857	0.025771
		13	10	1200	105	4	35	0.1032	2288.53	5	8.75	0.85979	1.44284	0.5959	0.3356264	0.3333	0.025771
		10.8	9	1000	250	1	5	0.0433	961.183	5	8.75	0.36111	0.71536	0.5048	0.3961996	0.02	0.0334
		10.8	9	1000	105	4	20	0.1032	2288.53	5	8.75	0.85979	1.64473	0.52275	0.3825885	0.1905	0.0334
120	210	9.26	7	855	135	2	10	0.0802	1779.97	5	8.75	0.66872	1.17646	0.56842	0.3518534	0.0741	0.035536
		9.26	7	855	100	3	10	0.1083	2402.96	5	8.75	0.90278	1.48123	0.60948	0.3281505	0.1	0.035536
		7.37	6	680	190	1	5	0.057	1264.71	5	8.75	0.47515	0.89966	0.52814	0.3786873	0.0263	0.048154
		7.37	6	680	135	2	5	0.0802	1779.97	5	8.75	0.66872	1.39471	0.47947	0.4171265	0.037	0.048154
		7.37	6	680	105	3	10	0.1032	2288.53	5	8.75	0.85979	1.75703	0.48934	0.4087124	0.0952	0.048154
		5.63	4	520	105	3	10	0.1032	2288.53	5	8.75	0.85979	2.07512	0.41433	0.4827043	0.0952	0.054898
		3.74	3	345	135	1	5	0.0802	1779.97	5	8.75	0.66872	1.38034	0.48446	0.4128278	0.037	0.093537
		3.74	3	345	100	3	10	0.1083	2402.96	5	8.75	0.90278	2.59389	0.34804	0.5746466	0.1	0.093537

In-line

T (mm)	P (mm)	Q (l/s)	N	l (mm)	h (mm)	n	A(sides) (mm)	V (m/s)	Re (cylinder)	T/D	P/D	fs	f	fs/f	S (computed)	A/h (measur)	A/h (Zima eq)
		13	5	1200	165	2	5	0.0657	1456.34	10	8.75	0.54714	0.95297	0.57414	0.3483483	0.0303	0.012886
240	210	13	5	1200	130	3	10	0.0833	1848.43	10	8.75	0.69444	1.22585	0.5665	0.3530434	0.0769	0.012886
		13	5	1200	95	4	10	0.114	2529.43	10	8.75	0.95029	1.40547	0.67614	0.2957968	0.1053	0.012886

***N*= number of the rods in each row, perpendicular to the flow direction**

The wave frequencies (f) related to the maximum amplitude (A_{max}), and the frequency of vortex shedding (f_s) obtained from the Strouhal number from Fitz-hugh's map (i.e. $S=0.2$), were computed and compared. The comparisons between all of the measured wave frequencies (f) and the calculated frequencies of vortex shedding (f_s) show that f is higher than f_s, as can be seen in Fig. 7.11. Hence, the difference between the frequencies for each situation is high and cannot be ignored. The reason for this discrepancy was thought to be the fact that the methods used for estimating the Strouhal number did not cover this specific situation and also did not match the condition of the present experimental work, in which a cluster of tubes were not considered, and the fluid was water. In other words, the differences should be related to the value of S as calculated from Fitz-hugh's map, which mainly has been used for heat exchanger vibrations. Attention was therefore focused on finding a formula for estimating the Strouhal number for the current experimental configuration and tests.

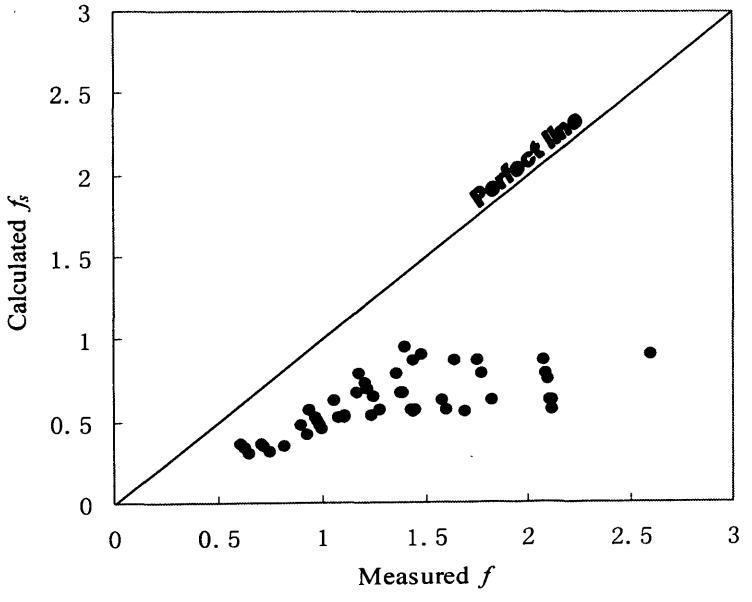

Fig. 7.11 Comparison between the measured frequency of the waves and calculated frequency of vortex shedding when S is estimated from Lienhard graphs, Fitz-hugh's map, and the equations of Žukauskas et al.

The actual Strouhal number can be calculated from the observed wave frequencies shown in Table 7.5 and given by the following equation:

$$S = \frac{fD}{U} \tag{7.10}$$

where S is the Strouhal number, f is the wave frequency, D is the cylinder diameter and U is the free stream velocity. From the data collected, a comparison was first made between the staggered and in-line arrangements. The Strouhal number for both cases, and for the same conditions, is shown in Fig. 7.12. As can be seen, for all widths of the channel the Strouhal numbers for the staggered rods were greater than those for the in-line rods. In Fig. 7.12 a linear regression representation is also shown for both cases. The difference between the two lines is nearly 22% or, in other words, for the same conditions the vortex shedding frequency for the staggered row arrangement is 22% higher than that for the in-line arrangement. Therefore, in the subsequent further analysis, only the data for the in-line row arrangement were used.

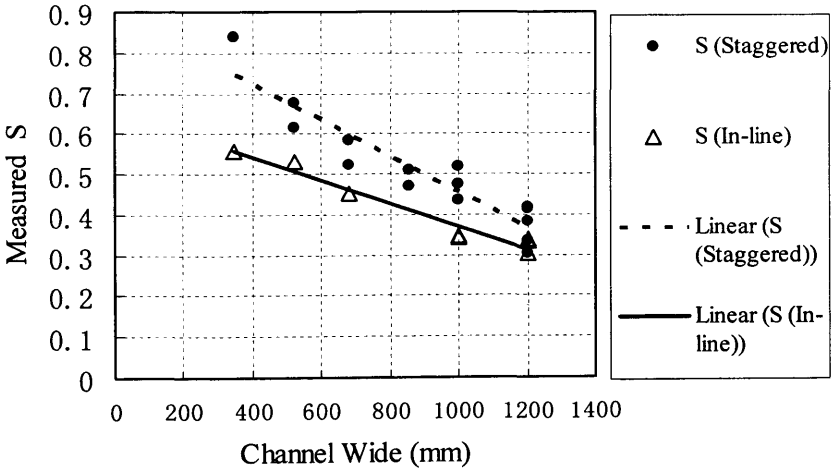

Fig. 7.12 Comparison of measured Strouhal number between in-line and staggered rod arrangements for different channel widths. For both cases T=120 *mm* and P=105 *mm*.

To find the relationship between S and the significant variables, dimensional analysis was used. Functional relationships that include the parameters that govern the Strouhal number is given as:

$$\Phi(S, D, P, T, N) = 0 \qquad (7.11)$$

Equation 7.11 can be expressed in terms of the non-dimensional variables giving:

$$S = \Phi\left(\frac{T}{D}, N, \frac{P}{D}\right) \qquad (7.12)$$

where S is the Strouhal number, T/D is the ratio of the distance between the cylinders in a single row to the cylinder diameter, N is the number of cylinders in a single row and P/D is the ratio of the distance between the cylinder rows and the cylinder diameters. To verify the relationship between each of the non-dimensional variables and S, the data for each variable was separated and analysed individually; while the other two variables were kept constant or nearly constant. In Fig. 7.13 the relationships between T/D, S, and the power regression curve are shown, where it can be seen from the existing relationship that as T/D increases, then S decreases.

In Fig. 7.14 the relationship between the number of rods N, S, and the P/D values relationship is illustrated in the form of curves. It can also be seen that as N increases, S decreases, although only limited T/D values were available.

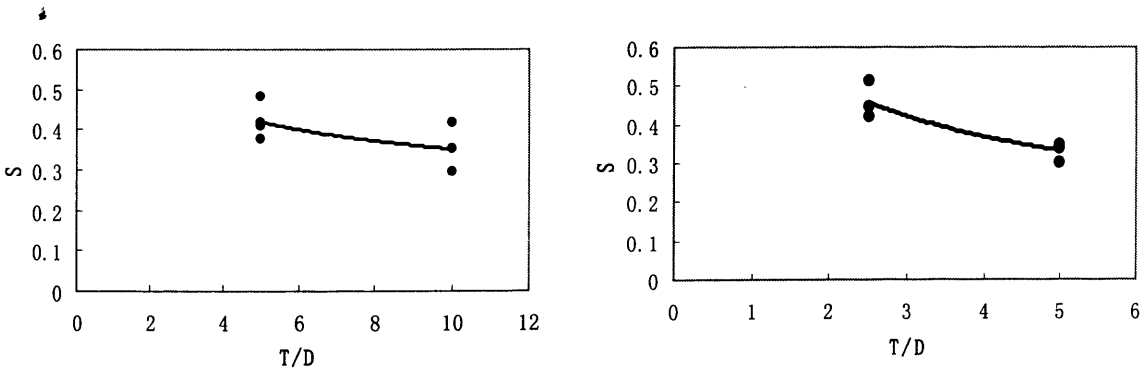

$P/D = 8.75$, $4 \leq N \geq 6$ $P/D = 4.375$, $9 \leq N \geq 11$

Fig. 7.13 Relationship between S and T/D for differing P/D values the power regression.

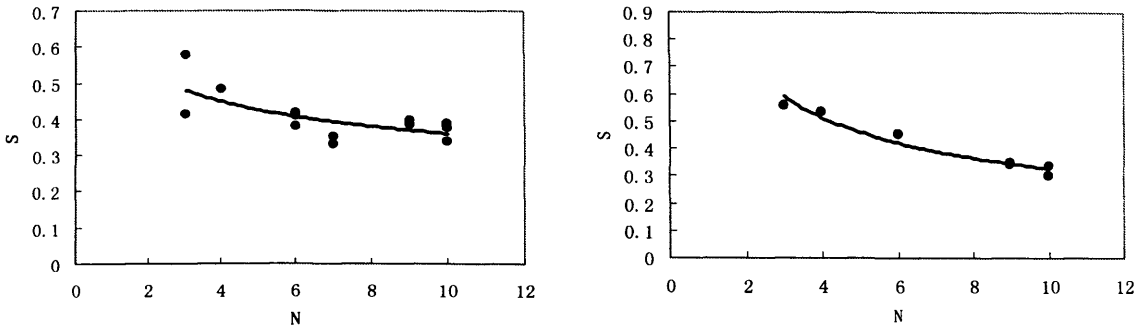

$T/D = 5$, $P/D = 8.75$ $T/D = 5$, $P/D = 4.375$

Fig. 7.14 Relationship between *S* and the number of rods, *N* for different *P/D* values.

The same analysis was then undertaken to find the possible relationship between *P/D* and *S*, but no relationship was found. Therefore, in the final analysis, the *P/D* term was omitted from Equation 7.12.

To find the best relationship between the remaining variables, the statistical software, SPSS, was used. The results of this analysis have lead to the following equation:

$$S_t = \frac{2.4}{\sqrt[3]{N(T/D)^2}} \tag{7.13}$$

where S_t = new Strouhal number. Equation 7.13 can be used for the in-line arrangement of rods. As mentioned previously, the frequency for the staggered arrangement was always 22% higher than that for the in-line arrangement. Therefore the equation for both arrangements (in-line and staggered) was given in the following form:

$$S_t = \frac{k}{\sqrt[3]{N(T/D)^2}} \tag{7.14}$$

where k is equal to 2.4 for the in-line arrangement, and 2.9 for the staggered arrangement.

In Fig. 7.15, the Strouhal numbers estimated by Equation 7.14 were compared with the measured values together with the perfect line also being shown. It can be seen that the Strouhal numbers calculated using the new equation have demonstrated the validity of this relationship.

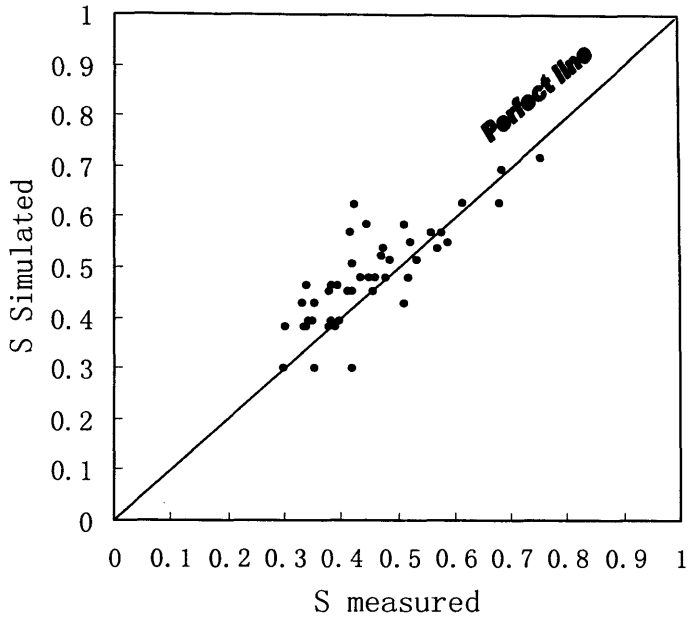

Fig. 7.15 Comparison between calculated Strouhal numbers of vortex shedding using the proposed equation and the measured values.

As can be seen in Table 7.5, in this set of experiments the wave displacement (A) was measured and the maximum displacement was 40% of the mean flow depth. Then, by analysing the measured data, the dimensionless displacement (A/h) was calculated. Also using the Zima and Ackermann equation (i.e. Equation 7.1) another dimensionless displacement (A/h) was calculated. The calculated values using the Zima equation and the measured values of A/h are compared in Fig. 7.16.

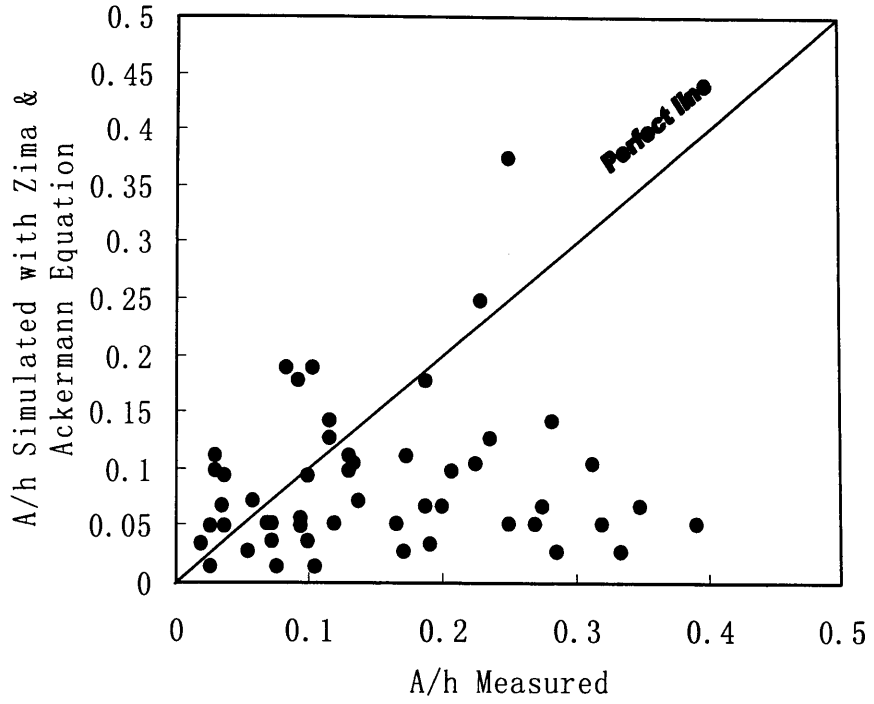

Fig. 7.16 Comparison between the calculated *A/h* from Zima and Ackermann equation (2002) and the measured data.

In comparing the measured and calculated values for (*A/h*), it is noted that the calculated values obtained from the Zima equation were significantly different from the measured values. Therefore, this equation cannot be used for this purpose. One of the differences between the results of the Zima equation and the measured data can be due to the use of the Fitz-hugh's map, and a Strouhal number of 0.2 (Equation 7.1) for water as the fluid medium.

In this study, further investigations were therefore undertaken using further analyses of the data to find a better relationship between *A/h* and the other parameters.

7.6.2 Wave amplitude (analysis of second stage experiments)

As for the previous section, from the experimental data for this study all points with the largest amplitude for each mode were selected and used for further analysis. Hence, the numbers of data sets extracted for further analysis were 103 and can be seen in Table 7.4.

The Zima and Ackermann equation (i.e. Equation 7.1) has been used to estimate the relative amplitude. In Fig. 7.17 the estimated *A/h* from Equation 7.1 and the measured data are shown and compared. As can be seen, the estimated values do not show a good match with the line of prefect agreement.

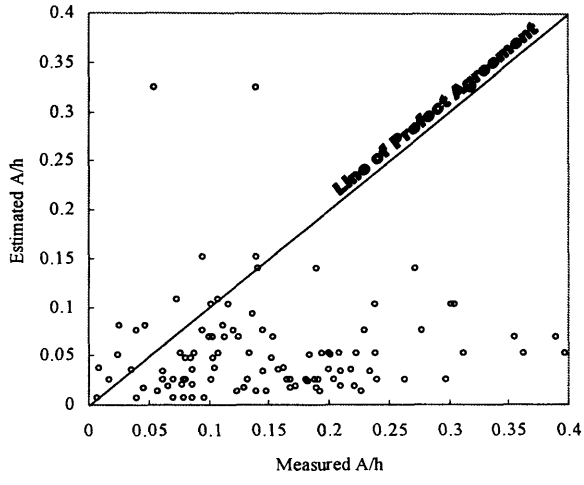

Fig. 7.17 Comparison between estimated *A/h* from the Zima and Ackermann equation (2002) and the measured data.

To find a relationship between *A/h* and the significant variables, dimensional analysis was again employed. A functional relationship that includes the parameters and may govern the wave amplitude is given as:

$$\Phi(A,h,T,D,P,l,\nu,V,N,n,S_t) = 0 \qquad (7.15)$$

In this equation V is the average velocity and is obtained by dividing the discharge by the area of the cross section of the flume and ν is the kinematics viscosity. The parameters can be expressed in terms of the dimensionless variable A/h (i.e. Equation 7.16) giving:

$$\frac{A}{h} = \Phi\left(\frac{T}{D}, \frac{l}{D}, \frac{P}{D}, S_t, R_e, N, n\right) \qquad (7.16)$$

where A/h is the relative amplitude, T/D is the ratio of the distance between the rods in a single row and the rod diameter, l/D is the ratio between the width of the channel and the rod diameter, P/D is the ratio of the distance between the rods rows and the cylinder diameter, and R_e is the Reynolds number (VD/ν), calculated with respect to the rod diameter and the kinematics viscosity of water. To determine the relationship between each of the non-dimensional variables and A/h, the data for each variable were separated and analysed, while the other variables were kept constant or nearly constant at each time. In Fig. 7.18a the relationship between P/D, the maximum of A/h, and the regression curve are shown. It is clear that when P/D is increased, A/h decreases. In Fig. 7.18b this relationship is shown for different widths of the flume and a similar result can be found.

In Figs. 7.19 the relationship between T/D and A/h is shown for different widths of the flume. In Fig. 7.19a the some variations are shown for values of T/D equal to or greater than 5 and for different widths of the flume. As can be seen when T/D is decreased, A/h increases. In Fig. 7.19b this relationship is shown for a situation when the values of T/D reach to 2.5. It can be seen that when the value of T/D decreases below 5, then the relationship changes in the reverse order. This means, for this part of the graph, when T/D decreases, then A/h also decreases. Therefore, it appears that the point $T/D=5$ is a critical point and the direction of the relationship changes at this point. The same analysis has been applied to find the possible relationship between R_e and A/h, but no clear relationship could be found.

Also, a comparison between the staggered and in-line rod arrangements has been made and no significant differences were distinguished.

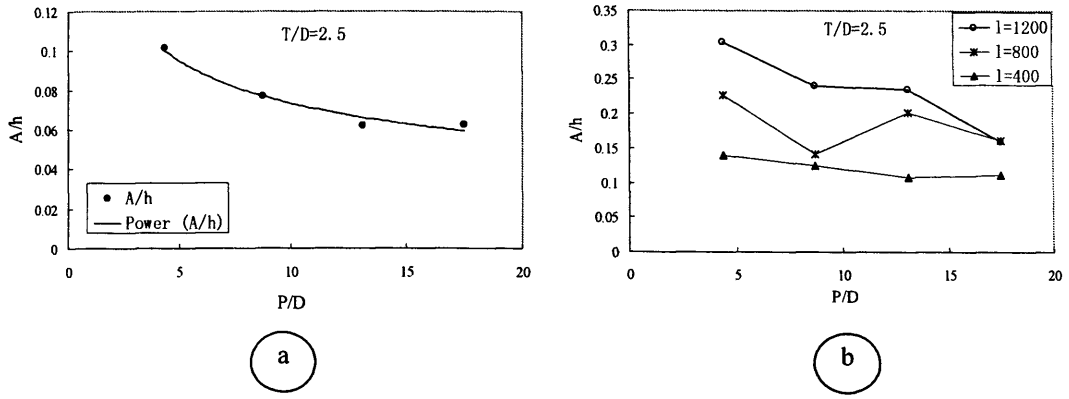

Fig. 7.18 Relationship between *P/D* and maximum *A/h*.

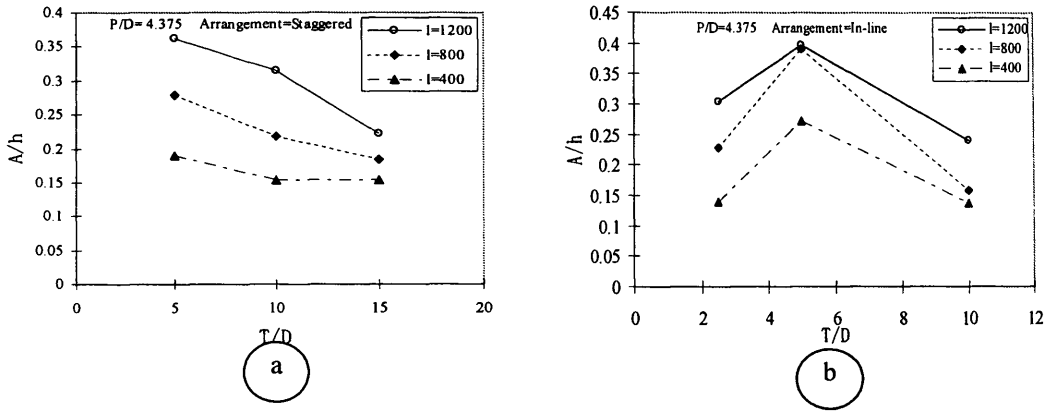

Fig. 7.19 Relationship between *T/D* and maximum *A/h*.

For the final analysis, the data were separated into two groups. The first group contained the data for *T/D* values equal to or greater than, 5 and the second group contained the data for *T/D* less than 5. The effects of the parameter *T/D* are include in the parameters *l/D* and *N* together and so there is no need to include *T/D* in the data analysis. Statistical analyses have been used to find the best relationship between the parameters. The results of the analysis have led to the following formulae.

For T/D≥5

$$\frac{A}{h} = 2\,N^{2/3}\left(\frac{D}{l}\right)\left(\frac{D}{P}\right)^{0.5} S_t^{-1/2}\, n^{2/3} \qquad (7.17)$$

For T/D<5

$$\frac{A}{h} = 0.12\,N^{-1/3}\left(\frac{D}{l}\right)^{-1/3}\left(\frac{D}{P}\right)^{0.5} S_t^{-1/2}\, n^{2/3} \qquad (7.18)$$

The Strouhal number (S_t) used in the analysis was calculated from Equation 7.14, but if the Fitz-hugh map is used to calculate the Strouhal number then the best curve fit is achieved when $T/D \geq 5$ and the constant factor should be 1.41, and for $T/D < 5$ the constant should be changed to 0.078. Table 7.6 shows the measured and calculated parameters related to the points of maximum amplitudes for the transverse wave modes.

Table 7.6 Measured and calculated parameters related to the points of maximum relative amplitude of second step of the experimental works.

In-line

T (mm)	P (mm)	Q (l/s)	N	l (mm)	h (mm)	n	A(sides) (mm)	V (m/s)	Re (cylinder)	T/D	P/D	T/l	l/D	A/h	St NewEq	A/h Zima Eq. S=0.2	A/h Zima Eq. S=New Eq.	A/h New Eq T/D<5
60	105	18.33	20	1200	299	1	30.333	0.051	1133.17	2.5	4.38	0.05	50	0.1014	0.4878	0.103086	0.0178968	0.11235
		18.33	20	1200	264	3	30.667	0.058	1283.4	2.5	4.38	0.05	50	0.1162	0.4878	0.103086	0.0178968	0.23353
		18.33	20	1200	193	2	46	0.079	1755.53	2.5	4.38	0.05	50	0.2383	0.4878	0.103086	0.0178968	0.17827
		18.33	20	1200	173	3	52.667	0.088	1958.48	2.5	4.38	0.05	50	0.3044	0.4878	0.103086	0.0178968	0.23353
		18.33	20	1200	158	4	47.667	0.097	2144.41	2.5	4.38	0.05	50	0.3017	0.4878	0.103086	0.0178968	0.28285
		12.22	13	800	238	1	22.667	0.064	1423.6	2.5	4.38	0.08	33.3	0.0952	0.5623	0.150763	0.0196403	0.10545
		12.22	13	800	196	3	27.333	0.078	1728.66	2.5	4.38	0.08	33.3	0.1395	0.5623	0.150763	0.0196403	0.21919
		6.11	7	400	196	2	10.667	0.078	1728.66	2.5	4.38	0.15	16.7	0.0544	0.6897	0.32472	0.0279983	0.14724
		6.11	7	400	158	1	22	0.097	2144.41	2.5	4.38	0.15	16.7	0.1392	0.6897	0.32472	0.0279983	0.0928

In-line

T (mm)	P (mm)	Q (l/s)	N	l (mm)	h (mm)	n	A(sides) (mm)	V (m/s)	Re (cylinder)	T/D	P/D	T/l	l/D	A/h	St NewEq	A/h Zima Eq. S=0.2	A/h Zima Eq. S=New Eq.	A/h New Eq T/D<5
60	210	18.33	20	1200	309	1	23.667	0.049	1096.5	2.5	8.75	0.05	50	0.0766	0.4878	0.051543	0.0089484	0.07945
		18.33	20	1200	259	2	34.667	0.059	1308.17	2.5	8.75	0.05	50	0.1338	0.4878	0.051543	0.0089484	0.12605
		18.33	20	1200	205	3	41	0.075	1652.77	2.5	8.75	0.05	50	0.2	0.4878	0.051543	0.0089484	0.16513
		18.33	20	1200	175	4	34	0.087	1936.1	2.5	8.75	0.05	50	0.1943	0.4878	0.051543	0.0089484	0.20001
		12.22	13	800	251	1	10	0.061	1349.87	2.5	8.75	0.08	33.3	0.0398	0.5623	0.075381	0.0098201	0.07457
		12.22	13	800	203	2	24.667	0.075	1669.05	2.5	8.75	0.08	33.3	0.1215	0.5623	0.075381	0.0098201	0.11831
		12.22	13	800	160	3	23.333	0.095	2117.61	2.5	8.75	0.08	33.3	0.1458	0.5623	0.075381	0.0098201	0.15499
		6.11	7	400	173	1	17.333	0.088	1958.48	2.5	8.75	0.15	16.7	0.1002	0.6897	0.16236	0.0139992	0.06562
		6.11	7	400	155	2	19.333	0.099	2185.92	2.5	8.75	0.15	16.7	0.1247	0.6897	0.16236	0.0139992	0.10411

In-line (continued)

T (mm)	P (mm)	Q (l/s)	N	l (mm)	h (mm)	n	A(sides) (mm)	V (m/s)	Re (cylinder)	T/D	P/D	T/l	l/D	A/h	St NewEq	A/h Zima Eq. S=0.2	A/h Zima Eq. S=New Eq.	A/h New Eq T/D<5
		18.33	20	1200	291	1	18	0.052	1164.32	2.5	13.1	0.05	50	0.0619	0.4878	0.034362	0.0059656	0.06487
		18.33	20	1200	204	2	29.667	0.075	1660.87	2.5	13.1	0.05	50	0.1454	0.4878	0.034362	0.0059656	0.10292
		18.33	20	1200	175	3	36.667	0.087	1936.1	2.5	13.1	0.05	50	0.2095	0.4878	0.034362	0.0059656	0.13483
		18.33	20	1200	139	4	32.667	0.11	2437.53	2.5	13.1	0.05	50	0.235	0.4878	0.034362	0.0059656	0.1633
60	315	12.22	13	800	230	1	5.6667	0.066	1473.12	2.5	13.1	0.08	33.3	0.0246	0.5623	0.050254	0.0065468	0.06088
		12.22	13	800	144	2	29	0.106	2352.9	2.5	13.1	0.08	33.3	0.2014	0.5623	0.050254	0.0065468	0.0966
		12.22	13	800	127	3	23.333	0.12	2667.85	2.5	13.1	0.08	33.3	0.1837	0.5623	0.050254	0.0065468	0.12655
		6.11	7	400	148	1	16	0.103	2289.3	2.5	13.1	0.15	16.7	0.1081	0.6897	0.10824	0.0093328	0.05358
		6.11	7	400	123	2	9	0.124	2754.61	2.5	13.1	0.15	16.7	0.0732	0.6897	0.10824	0.0093328	0.08501

In-line

T (mm)	P (mm)	Q (l/s)	N	l (mm)	h (mm)	n	A(sides) (mm)	V (m/s)	Re (cylinder)	T/D	P/D	T/l	l/D	A/h	St NewEq	A/h Zima Eq. S=0.2	A/h Zima Eq. S=New Eq.	A/h New Eq T/D<5
		18.33	20	1200	304	1	19	0.05	1114.53	2.5	17.5	0.05	50	0.0625	0.4878	0.025771	0.0044742	0.05618
		18.33	20	1200	234	2	31	0.065	1447.94	2.5	17.5	0.05	50	0.1325	0.4878	0.025771	0.0044742	0.08913
		18.33	20	1200	190	3	31.333	0.08	1783.25	2.5	17.5	0.05	50	0.1649	0.4878	0.025771	0.0044742	0.11677
		18.33	20	1200	155	4	31.667	0.099	2185.92	2.5	17.5	0.05	50	0.2043	0.4878	0.025771	0.0044742	0.14143
60	420	12.22	13	800	230	1	2	0.066	1473.12	2.5	17.5	0.08	33.3	0.0087	0.5623	0.037691	0.0049101	0.05273
		12.22	13	800	175	2	28.333	0.087	1936.1	2.5	17.5	0.08	33.3	0.1619	0.5623	0.037691	0.0049101	0.08366
		12.22	13	800	150	3	15.667	0.102	2258.78	2.5	17.5	0.08	33.3	0.1044	0.5623	0.037691	0.0049101	0.1096
		6.11	7	400	170	1	19	0.09	1993.04	2.5	17.5	0.15	16.7	0.1118	0.6897	0.08118	0.0069996	0.0464
		6.11	7	400	133	2	6.3333	0.115	2547.5	2.5	17.5	0.15	16.7	0.0476	0.6897	0.08118	0.0069996	0.07362
		6.11	7	400	119	3	3	0.128	2847.2	2.5	17.5	0.15	16.7	0.0252	0.6897	0.08118	0.0069996	0.09644

In-line (continued)

T (mm)	P (mm)	Q (l/s)	N	l (mm)	h (mm)	n	A(sides) (mm)	V (m/s)	Re (cylinder)	T/D	P/D	T/l	l/D	A/h	St NewEq	A/h Zima Eq. S=0.2	A/h Zima Eq. S=New Eq.	A/h New Eq T/D≥5
		18.33	10	1200	242	1	26	0.063	1400.07	5	4.38	0.1	50	0.1074	0.3881	0.051543	0.0142047	0.14359
		18.33	10	1200	166	2	37	0.092	2041.07	5	4.38	0.1	50	0.2229	0.3881	0.051543	0.0142047	0.22783
		18.33	10	1200	130	3	40.667	0.118	2606.28	5	4.38	0.1	50	0.3128	0.3881	0.051543	0.0142047	0.29846
120	105	18.33	10	1200	119	4	47.333	0.128	2847.2	5	4.38	0.1	50	0.3978	0.3881	0.051543	0.0142047	0.36149
		12.22	6	800	187	1	21.333	0.082	1811.86	5	4.38	0.15	33.3	0.1141	0.4593	0.069583	0.0136417	0.14076
		12.22	6	800	120	2	42.667	0.127	2823.48	5	4.38	0.15	33.3	0.3556	0.4593	0.069583	0.0136417	0.22334
		12.22	6	800	106	3	41.333	0.144	3196.39	5	4.38	0.15	33.3	0.3899	0.4593	0.069583	0.0136417	0.29258
		6.11	3	400	114	1	31	0.134	2972.08	5	4.38	0.3	16.7	0.2719	0.5774	0.139166	0.0171874	0.15807

In-line

T (mm)	P (mm)	Q (l/s)	N	l (mm)	h (mm)	n	A(sides) (mm)	V (m/s)	Re (cylinder)	T/D	P/D	T/l	l/D	A/h	St NewEq	A/h Zima Eq. S=0.2	A/h Zima Eq. S=New Eq.	A/h New Eq T/D≥5
		18.33	10	1200	240	1	13.667	0.064	1411.74	5	17.5	0.1	50	0.0569	0.3881	0.012886	0.0035512	0.7179
		18.33	10	1200	165	2	23	0.093	2053.44	5	17.5	0.1	50	0.1394	0.3881	0.012886	0.0035512	0.11391
		18.33	10	1200	130	3	25	0.118	2606.28	5	17.5	0.1	50	0.1923	0.3881	0.012886	0.0035512	0.14923
120	420	18.33	10	1200	110	4	25	0.139	3080.15	5	17.5	0.1	50	0.2273	0.3881	0.012886	0.0035512	0.18074
		12.22	7	800	128	2	10	0.119	2647.01	5	17.5	0.15	33.3	0.0781	0.4365	0.020295	0.0044095	0.12697
		12.22	7	800	104	3	9	0.147	3257.86	5	17.5	0.15	33.3	0.0865	0.4365	0.020295	0.0044095	0.16633
		6.11	3	400	128	1	11	0.119	2647.01	5	17.5	0.3	16.7	0.0859	0.5774	0.034791	0.0042969	0.07904

In-line (continued)

T (mm)	P (mm)	Q (l/s)	N	l (mm)	h (mm)	n	A(sides) (mm)	V (m/s)	Re (cylinder)	T/D	P/D	T/l	l/D	A/h	St NewEq	A/h Zima Eq. S=0.2	A/h Zima Eq. S=New Eq.	A/h New Eq T/D≥5
240	105	18.33	5	1200	199	1	15.667	0.077	1702.6	10	4.38	0.2	50	0.0787	0.3087	0.025771	0.0112743	0.10158
		18.33	5	1200	143	2	27.33	0.107	2369.35	10	4.38	0.2	50	0.191	0.3087	0.025771	0.0112743	0.16117
		18.33	5	1200	120	3	22.667	0.127	2823.48	10	4.38	0.2	50	0.1889	0.3087	0.025771	0.0112743	0.21114
		18.33	5	1200	100	4	24	0.153	3388.17	10	4.38	0	50	0.24	0.3087	0.025771	0.0112743	0.25573
		12.22	3	800	110	2	17.333	0.139	3080.15	10	4.38	0.3	33.3	0.1576	0.3654	0.034791	0.0108274	0.158
		6.11	2	400	100	1	13.667	0.153	3388.17	10	4.38	0.6	16.7	0.1367	0.4177	0.092777	0.0220343	0.14209

In-line

T (mm)	P (mm)	Q (l/s)	N	l (mm)	h (mm)	n	A(sides) (mm)	V (m/s)	Re (cylinder)	T/D	P/D	T/l	l/D	A/h	St NewEq	A/h Zima Eq. S=0.2	A/h Zima Eq. S=New Eq.	A/h New Eq T/D≥5
240	420	18.33	5	1200	204	1	1.3333	0.075	1660.87	10	17.5	0.2	50	0.0065	0.3087	0.006443	0.0028186	0.05079
		18.33	5	1200	140	2	12	0.109	2420.12	10	17.5	0.2	50	0.0857	0.3087	0.006443	0.0028186	0.08059
		18.33	5	1200	109	3	8.6667	0.14	3108.41	10	17.5	0.2	50	0.0795	0.3087	0.006443	0.0028186	0.10557
		18.33	5	1200	93	4	9	0.164	3643.19	10	17.5	0.2	50	0.0968	0.3087	0.006443	0.0028186	0.12786

Staggered

T (mm)	P (mm)	Q (l/s)	N	l (mm)	h (mm)	n	A(sides) (mm)	V (m/s)	Re (cylinder)	T/D	P/D	T/l	l/D	A/h	St NewEq	A/h Zima Eq. S=0.2	A/h Zima Eq. S=New Eq.	A/h New Eq T/D≥5
120	105	18.33	10	1200	245	1	21.333	0.062	1382.93	5	4.38	0.1	50	0.0871	0.3881	0.051543	0.0097288	0.13063
		18.33	10	1200	163	2	34	0.094	2078.63	5	4.38	0.1	50	0.2086	0.3881	0.051543	0.0097288	0.20726
		18.33	10	1200	134	3	32	0.114	2528.49	5	4.38	0.1	50	0.2388	0.3881	0.051543	0.0097288	0.27151
		18.33	10	1200	115	4	41.667	0.133	2946.23	5	4.38	0.1	50	0.3623	0.3881	0.051543	0.0097288	0.32885
		12.22	6.5	800	193	1	18.333	0.079	1755.53	5	4.38	0.15	33.3	0.095	0.4473	0.075381	0.0106765	0.13688
		12.22	6.5	800	130	2	30	0.118	2606.28	5	4.38	0.15	33.3	0.2308	0.4473	0.075381	0.0106765	0.21718
		12.22	6.5	800	114	3	31.667	0.134	2972.08	5	4.38	0.15	33.3	0.2778	0.4473	0.075381	0.0106765	0.28451
		6.11	3	400	130	1	18.333	0.118	2606.28	5	4.38	0.3	16.7	0.141	0.5774	0.139166	0.0117716	0.1438
		6.11	3	400	114	2	21.667	0.134	2972.08	5	4.38	0.3	16.7	0.1901	0.5774	0.139166	0.0117716	0.22817

Staggered

T (mm)	P (mm)	Q (l/s)	N	l (mm)	h (mm)	n	A(sides) (mm)	V (m/s)	Re (cylinder)	T/D	P/D	T/l	l/D	A/h	St NewEq	A/h Zima Eq. S=0.2	A/h Zima Eq. S=New Eq.	A/h New Eq T/D≥5
120	315	18.33	10	1200	249	1	11.333	0.061	1360.71	5	13.1	0.1	50	0.0455	0.3881	0.017181	0.0032429	0.07542
		18.33	10	1200	170	2	22	0.09	1993.04	5	13.1	0.1	50	0.1294	0.3881	0.017181	0.0032429	0.11966
		18.33	10	1200	129	3	21.667	0.118	2626.49	5	13.1	0.1	50	0.168	0.3881	0.017181	0.0032429	0.15676
		18.33	10	1200	95	4	18	0.161	3566.49	5	13.1	0.1	50	0.1895	0.3881	0.017181	0.0032429	0.18986
		12.22	6.5	800	210	1	3.6667	0.073	1613.41	5	13.1	0.15	33.3	0.0175	0.4473	0.025127	0.0035588	0.07903
		12.22	6.5	800	133	2	22.333	0.115	2547.5	5	13.1	0.15	33.3	0.1679	0.4473	0.025127	0.0035588	0.12539
		12.22	6.5	800	108	3	11	0.141	3137.19	5	13.1	0.15	33.3	0.1019	0.4473	0.025127	0.0035588	0.16426
		6.11	3	400	133	1	10.667	0.115	2547.5	5	13.1	0.3	16.7	0.0802	0.5774	0.046389	0.0039239	0.08302
		6.11	3	400	90	2	7.6667	0.17	3764.63	5	13.1	0.3	16.7	0.0852	0.5774	0.046389	0.0039239	0.13173

Staggered (continued)

T (mm)	P (mm)	Q (l/s)	N	l (mm)	h (mm)	n	A(sides) (mm)	V (m/s)	Re (cylinder)	T/D	P/D	T/l	l/D	A/h	St NewEq	A/h Zima Eq. S=0.2	A/h Zima Eq. S=New Eq.	A/h New Eq T/D≥5
240	105	18.33	5	1200	277	1	19.333	0.055	1223.17	10	4.38	0.2	50	0.0698	0.3087	0.025771	0.0077218	0.09241
		18.33	5	1200	235	1	19	0.065	1441.77	10	4.38	0.2	50	0.0809	0.3087	0.025771	0.0077218	
		18.33	5	1200	158	2	28.667	0.097	2144.41	10	4.38	0.2	50	0.1814	0.3087	0.025771	0.0077218	0.14662
		18.33	5	1200	120	3	31.667	0.127	2823.48	10	4.38	0.2	50	0.2639	0.3087	0.025771	0.0077218	0.19208
		18.33	5	1200	95	4	28.333	0.161	3566.49	10	4.38	0.2	50	0.2982	0.3087	0.025771	0.0077218	0.23264
		12.22	3	800	185	1	6.6667	0.083	1831.44	10	4.38	0.3	33.3	0.036	0.3654	0.034791	0.0074157	0.09059
		12.22	3	800	117	2	23.333	0.131	2895.87	10	4.38	0.3	33.3	0.1994	0.3654	0.034791	0.0074157	0.14374
		12.22	3	800	93	3	20.333	0.164	3643.19	10	4.38	0.3	33.3	0.2186	0.3654	0.034791	0.0074157	0.1883
		6.11	1.5	400	117	1	18	0.131	2895.87	10	4.38	0.6	16.7	0.1538	0.4593	0.069583	0.0093432	0.10173
		6.11	1.5	400	87	2	9	0.176	3894.45	10	4.38	0.6	16.7	0.1034	0.4593	0.069583	0.0093432	0.16141

Staggered

T (mm)	P (mm)	Q (l/s)	N	l (mm)	h (mm)	n	A(sides) (mm)	V (m/s)	Re (cylinder)	T/D	P/D	T/l	l/D	A/h	St NewEq	A/h Zima Eq. S=0.2	A/h Zima Eq. S=New Eq.	A/h New Eq T/D≥5
240	210	18.33	5	1200	244	1	14	0.063	1388.59	10	8.75	0.2	50	0.0574	0.3087	0.012886	0.0038609	0.06534
		18.33	5	1200	164	2	24.333	0.093	2065.96	10	8.75	0.2	50	0.1484	0.3087	0.012886	0.0038609	0.10368
		18.33	5	1200	125	3	28.333	0.122	2710.54	10	8.75	0.2	50	0.2267	0.3087	0.012886	0.0038609	0.13582
		18.33	5	1200	81	4	10	0.189	4182.93	10	8.75	0.2	50	0.1235	0.3087	0.012886	0.0038609	0.1645

Staggered (continued)

T (mm)	P (mm)	Q (l/s)	N	l (mm)	h (mm)	n	A(sides) (mm)	V (m/s)	Re (cylinder)	T/D	P/D	T/l	l/D	A/h	St NewEq	A/h Zima Eq. S=0.2	A/h Zima Eq. S=New Eq.	A/h New Eq T/D≥5
360	105	18.33	3.5	1200	225	1	15	0.068	1505.85	15	4.38	0.3	50	0.0667	0.2657	0.01804	0.007317	0.0786
		18.33	3.5	1200	150	2	26	0.102	2258.78	15	4.38	0.3	50	0.1733	0.2657	0.01804	0.007317	0.12471
		18.33	3.5	1200	114	3	25.333	0.134	2972.08	15	4.38	0.3	50	0.2222	0.2657	0.01804	0.007317	0.16338
		18.33	3.5	1200	92	4	19.333	0.166	3682.79	15	4.38	0.3	50	0.2101	0.2657	0.01804	0.007317	0.19788
		12.22	2	800	111	1	20.333	0.138	3052.41	15	4.38	0.45	33.3	0.1832	0.3196	0.023194	0.0064782	0.07399
		6.11	1	400	111	2	17	0.138	3052.41	15	4.38	0.9	16.7	0.1532	0.4018	0.046389	0.008162	0.13183
		6.11	1	400	77	3	8	0.198	4400.22	15	4.38	0.9	16.7	0.1039	0.4018	0.046389	0.008162	0.1727

Staggered

T (mm)	P (mm)	Q (l/s)	N	l (mm)	h (mm)	n	A(sides) (mm)	V (m/s)	Re (cylinder)	T/D	P/D	T/l	l/D	A/h	St NewEq	A/h Zima Eq. S=0.2	A/h Zima Eq. S=New Eq.	A/h New Eq T/D≥5
360	315	18.33	3.5	1200	219	1	1.6667	0.07	1547.11	15	13.1	0.3	50	0.0076	0.2657	0.006013	0.002439	0.4538
		18.33	3.5	1200	140	2	5.6667	0.109	2420.12	15	13.1	0.3	50	0.0405	0.2657	0.006013	0.002439	0.072
		18.33	3.5	1200	118	3	8.3333	0.129	2871.33	15	13.1	0.3	50	0.0706	0.2657	0.006013	0.002439	0.09433

In Fig. 7.20 the relative amplitude (A/h), estimated from Equations 7.17 and 7.18, is compared with the measured values. Also, in this figure the line of perfect agreement is shown. It can be seen that the relative amplitude (A/h), calculated using the new equations, agrees much more closely with the measured data.

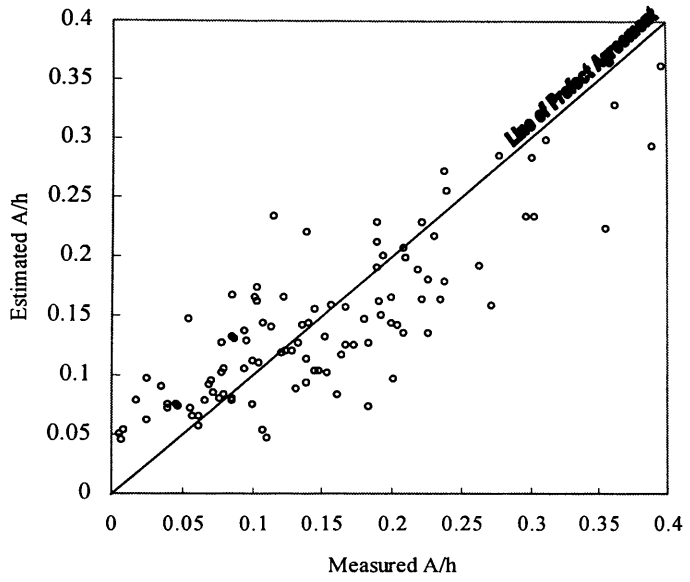

Fig. 7.20 Comparison between relative amplitude (A/h) calculated from the proposed new equation and the measured values.

In Fig. 7.21a, the estimated A/h values obtained using Equations 7.1 and 7.18 and the measured data are compared for a specific batch of the data ($T/D<5$ and $n=1$). This batch of the data is the same as that used in the Zima and Ackermann (2002) study. As can be seen, however, the new equation shows a good agreement with the measured values, but Equation 7.1 also shows reasonable agreement. For the other data, such as that shown in Fig. 7.21b, Equation 7.1 does not show good agreement. Therefore, it can be concluded that Equation 7.1 (Zima and Ackermann 2002) can be used for the specific situation when $T/D<5$ and $n=1$.

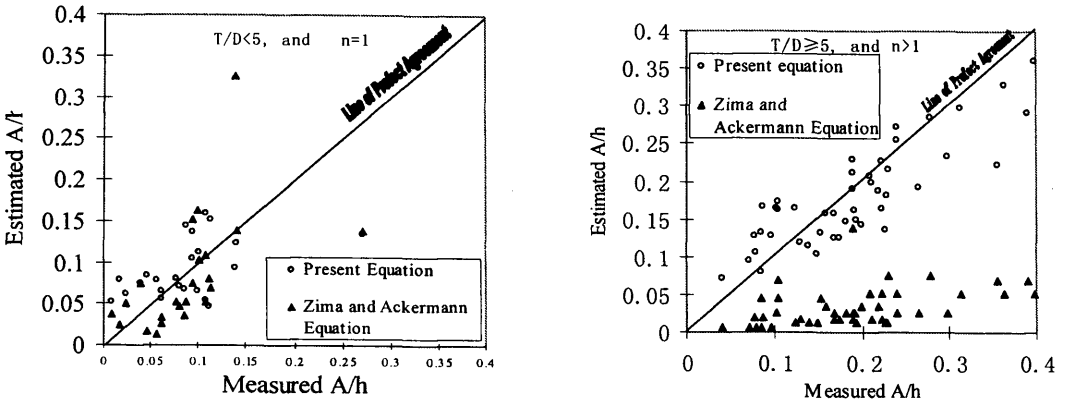

(a) (b)

Fig. 7.21 Comparison between relative amplitude (*A/h*) calculated from the proposed equations 7.1 and 7.18 and the measured values.

In this chapter, attention has focused on the transverse waves generated for open channel flows in a flume of length 10 m and width 1.2 m, and where the flow passes through a cluster of rigid vertical cylinders, with different densities and different arrangements (in-line and staggered), and also with varying channel width. In the first stage, the frequencies of transverse waves were considered and in second stage, the effects of the amplitude of the transverse waves were studied. Results showed that the frequency of the staggered row arrangements was always 22% higher than for the in-line row arrangement. The Strouhal numbers calculated from the measured data were significantly different from those obtained for the widely used Fitz-hugh's map. Hence, dimensional analysis was employed to find a relationship between the Strouhal number and amplitude, as well as other significant parameters. Finally, a new equation was proposed for the Strouhal number and two new equations developed to estimate the wave amplitude.

In summary, these studies have shown that idealised vegetation (in the form of solid rods) can create wave induced oscillations across a flume which, in a practical situation, such as a mangrove forests, could lead to increased flood inundation level. This has been already discussed.

CHAPTER 8
CONCLUSIONS AND FURTHER STUDY

8.1 Summary of research work

A range of experimental studies were first conducted for emergent vegetation conditions on the floodplain and for a compound channel configuration. Further experiments were then carried out for fully and partially emergent and submerged vegetation conditions, for a narrow simple channel and a wide rectangular channel configuration. For the compound and wide rectangular channel experiments, the velocity was measured across the entire channel cross-section, whereas for the narrow simple channel the measurements were taken at several locations within the vegetation array. From these experiments, and a subsequent analysis of the results, a series of conclusions have been drawn. In Chapters 4, 5, and 6 the velocity and turbulence profile characteristics were analysed for flows through rigid vegetation in a compound channel, a narrow simple channel, and a wide rectangular channel. Also in Chapter 7 the frequency and amplitude of transverse waves generated in an open channel were described, where the flow passed through a cluster of rigid vertical vegetation in different densities and arrangements (in-line and staggered).

The main objective of the research, outlined in Chapters 4, 5, and 6, was to investigate the effects of vegetation density on the velocity and turbulence components, for submerged and emergent vegetation, in compound, simple, and wide channel flows. In Chapter 7 the effects of vegetation in creating vortex shedding and transverse waves was investigated.

8.2 Compound channel (Emergent)

When the vegetation density on the floodplain was increased, then the longitudinal velocity in the main channel was found to increase. In other words, whenever the vegetation density increased in the floodplain, then the main flow tended to transfer to the main channel.

In the region of maximum longitudinal velocity in the main channel, a minimum transverse velocity is observed. This means that the longitudinal and transverse velocities are inverse to each other in the region of maximum velocity. In general, the results showed that when one of the components of velocity increased then the other components decreased. Also, for the vertical velocity component, the maximum rate was located in the transition zone and the minimum rate was along the central line of the main channel.

The regions of maximum velocity fluctuation and Reynolds stress components were located at the water surface or transition areas, between the floodplain and main channel. With an increase in the vegetation density, the non-uniformity of the velocity profile and the velocity fluctuation and Reynolds stress components in the main channel increased, with the maximum uniformity being observed for the non-vegetated case.

The velocity fluctuation components were increased significantly by the vegetation, with the non-vegetated state giving the minimum velocity fluctuations in the main channel.

8.3 Simple channel (Submerged)

This study showed that when the vegetation density increased the longitudinal velocity within the vegetated area decreased and within that area it remained

constant and main flow accelerated and diverted towards the upper zones of the flow. Hence, from near the top of rods the velocity increased rapidly to the water surface. When the rod density was increased, the main flow transferred to above the rods. The vegetation density significantly controlled the magnitude of these effects. Hence, for high density vegetation, the velocity difference between that between the rods and that above was high, but for the low density or non-vegetated case, the velocity difference was markedly lower.

As the vegetation density increased, the velocity fluctuation and Reynolds stress components increased with the maximum values occurring near to the top of the rods. The components then decreased towards the water surface. These changes were least noticeable for v', but more pronounced for u' and w'. The velocity fluctuation and Reynolds stress components for the non-vegetated state, showed little variation from the bed to the water surface.

Staggered rods caused the velocity, velocity fluctuation, and Reynolds stress components to scatter to more areas in the flow section. For the medium density state, a high degree of diffusion was observed but for other densities the change was regular.

The experiments indicated that turbulence intensities could vary considerably at different locations. The turbulence intensities were highest directly behind a rod and decreased with increasing distance to downstream. The unobstructed flow region between the rods was less influenced by the wake generated turbulence, causing the turbulence intensity to be lower in this region than the other part of the flow.

As for each emergent profile, the turbulence intensity remained fairly constant throughout the entire flow depth, but for the submerged vegetation changes in the

flow, characteristics were significant. As the velocities decreased within the vegetation zone this created a transition zone between the low velocities within the rods and the higher velocities above the rods, where the turbulence structure was primarily generated. Thus the nature of the flow was identified by a highly turbulent region near the top of the rods.

The interaction of the flow and vegetation and the resulting turbulence characteristics have an important impact on the sediment transport characteristics and channel protection. Vegetation reduces the energy of the flow but also increases the flow depth. The vegetation acts as a baffle, reducing velocities, and resulting in sediment deposition. Also, the vegetation protects the channel bed from erosion because of its high resistance to flow. Since vegetation is aesthetically and environmentally acceptable, it is increasingly recommended for erosion control in open channels.

For the flow structure behind the rods, the longitudinal velocity was observed to be very low; the other velocity components (i.e. transverse and vertical) were high. Also, the velocity fluctuation and Reynolds stress components were high behind the rods. However, when the distance from the rods was increased, the longitudinal velocity increased and other factors decreased.

8.4 Simple channel (Emergent)

For the emergent vegetation state due to the vegetation protruding from the bed to above the water surface for all vegetation densities, the flow parameters remained fairly constant or led to only small variations in the velocity components from the bed to the water surface, at all of the measuring points. Also, the effects of vortex shedding were observed for the submerged conditions to occur near the top of the vegetation, whereas for the emergent conditions the vorticity was only observed

below the water surface. This effect was exacerbated by the staggered nature of the rods and was most noticeable for a medium density and a water depth of 200 mm.

The velocity for all points were almost constant from the bed to the water surface, except for the medium density configuration where the staggering effect caused the velocity to decrease with elevation to about 200 mm above the bed and then increasing again to the surface.

An analysis of the measured time-averaged velocities at the different measuring sites, for the different densities, the velocity profiles behind and in between the rods was found to be significantly different. It was observed that at the points in between the rods the longitudinal velocity ($\overline{U}$) was a maximum and behind the rods the velocity was a minimum. For $\overline{V}$ and $\overline{W}$ the opposite occurred, i.e. points where a high $\overline{U}$ velocity occurred had a low $\overline{V}$ and $\overline{W}$ velocity and vice- versa (see Figs. 5.16-5.18).

The magnitude of the Reynolds stress components (i.e. $\overline{u'v'}$, $\overline{u'w'}$, $\overline{v'w'}$) at the various measuring points were similar in profile with the velocity fluctuation components ($u'rms$, $v'rms$ $w'rms$). This meant that the magnitude of the velocity fluctuation and Reynolds stress components at the points between the rods were minimum and behind the rods these components were maximum.

For all vegetation densities the velocity fluctuation and Reynolds stress components were nearly constant from near the bed to the water surface at all points except for the medium and low density configurations. For the latter two densities, the velocity increased sharply from an elevation of about 150 mm above the bed to reach to its maximum value at an elevation of about 200 mm and then decreased sharply towards the water surface. With an increase in the vegetation

density, the velocity fluctuation and Reynolds stress components increased at all points (see Figs. 5.18-5.24).

8.5 Wide channel fully vegetation

The results showed that, for the submerged vegetation state, as the vegetation density increased then the main flow transferred to the top of the vegetation zone, with the velocity in the vegetated zone being much smaller than that above the vegetation zone. However, as the density was changed to medium and low densities, the velocity effectively increased in the vegetated zone and decreased above this zone.

For the emergent vegetation state, the results showed that the contour lines across the whole profile were nearly vertical between rods, from the bed to the water surface. Hence, the maximum velocity occurred between the rods and minimum behind the rods.

The rod obstruction to the flow created a drag force, opposite to the direction of flow, with vortex shedding occurring behind the rods and secondary currents being observed above the vegetation. Therefore, in the transition zone (i.e. near the vegetation top) a high variation occurred in the velocity fluctuation and Reynolds stress components. The degree of uniformity in the velocity profile also increased as the vegetation density was reduced from high to low and then no vegetation density.

For the submerged state, it is clear that the velocity fluctuation and Reynolds stress components are low and constant, with only small variations occurring in the vegetated zone. As the vegetation decreased to medium and low densities, then the velocity components increased and therefore variations in the velocity fluctuation and Reynolds stress components also increased.

For the emergent state, the results showed that, as the vegetation density increased, the velocity variations and the Reynolds stress components behind and in between the rods also increased. Again, for the high density vegetation, a high variation in the maximum and minimum velocity points occurred, which was higher than that for the medium and low densities.

It was observed that the velocity structures for the high and low densities were similar, with the maximum velocities occurring effectively between the rods, with the velocities being higher for the medium density vegetation. The reason for this difference was due to the staggering of the rods for the medium density, and the in-line configuration for the high and low densities.

In comparing the results of cross-section 4.4 and 1.4, it was clearly concluded that due to proximity of the weir, the variation in the Reynolds stress components at cross-section 1.4 was less than that occurring for cross-section 4.4.

8.6 Wide channel partial one-sided vegetation

For the submerged state, by increasing the vegetation over the vegetated half of the channel, the main flow increasingly flowed through the non-vegetated half of the channel and above the vegetation zone. For the high density configuration, the contour lines at the interface between the vegetation free and the vegetated zones were more vertical, but sloped more with a decrease in the vegetation density.

For the emergent vegetation state, due to the existence of the vegetation over half of the channel, the main flow transferred to the vegetation free half zone. Hence, the velocity difference between the two halves was very pronounced, with the velocities being even higher than for the submerged partial one-sided configuration. With the increase in vegetation, in the vegetated half of the channel the flow almost entirely transferred to the non-vegetated side of the channel.

Hence, in the vegetated half of the channel the velocity was close to zero and the flow was fairly uniform, with the flow shifting almost totally to the vegetation free half of the channel.

With a reduction in the vegetation density, from high to medium and then to low, the average velocity, Reynolds number, and turbulence characteristics decreased in the vegetation free half of the channel. Therefore, the uniformity of the vertical velocity profile decreased and the contour lines changed from near vertical to more circular. The distance between the contour lines also increased, confirming that less variation occurred in the velocity across the flume. Also, with a reduction in the vegetation density on the vegetated half of the channel, the velocity difference between the two halves of the channel decreased.

The area between the vegetated and non-vegetated zones gave the maximum value in the velocity fluctuation and the Reynolds stress components.

8.7 Wide channel partial two-sided vegetation

For the submerged case and with an increase in the vegetation density along the two sides of the channel, the flow was mainly transferred to above the vegetation and to the vegetation free zone in central part of the channel. For the high density case there was a high degree of non-uniformity in the velocity profile. As the vegetation density was decreased to medium and low density, the degree of uniformity in the velocity profile increased.

In the vegetated region along the two sides of the channel, the high and low density cases gave a minimum and maximum longitudinal velocity respectively. This meant that for the high density case the contour lines were closer together than for the low density case. For the high density case, there was a small velocity variation in the vegetated zone on both sides of the channel. Also a peak stress occurred at

the interface between the vegetated and the vegetation free zones and along the two sides of the channel.

For a decrease in the vegetation density to medium and low, the velocity difference between the vegetated and non-vegetated zones decreased. In other words, the uniformity in the velocity profile increased and the distance between the contour lines also increased.

For the emergent state, because the majority of the flow transferred to the vegetation free part of the channel, then the occurrence of higher velocities caused an increase in the Reynolds number and the turbulence characteristics. The uniformity of the vertical velocity profile also increased across the central part of the channel.

For all of the vegetation densities, the velocity along both sides of the channel increased sharply towards the central part of the vegetation free zone and reached a maximum value along the central line of the channel. For all cases, the stresses rose sharply in the vicinity of the boundary between the vegetated and vegetation free zones, reaching a peak and then decreasing to a minimum in the centre of the channel. At the transition between the vegetated and non-vegetated zones, for the high and low density cases, the maximum and minimum peak Reynolds stress components occurred at these locations.

8.8 Wave generation

The first stage of the experiments and a subsequent analysis of the results led to the following conclusions relating to the generation of lateral oscillatory waves:

- Different modes of transverse waves appeared when the velocity of the main flow was increased.

- The vortex shedding frequency occurring for the staggered row arrangement was always 22% higher than the corresponding frequency created for the in-line rod arrangement.
- The Fitz-hugh's map was not a suitable method for calculating the Strouhal number (S_t), when the flowing fluid was water.
- A new formulation for the Strouhal number, as given in Equation (7.14), was obtained from dimensional analysis, which represented a robust estimate of the Strouhal number when the fluid was water.

From an analysis of the results of second stage of experiments, the following conclusions were obtained:

- The maximum wave amplitudes observed in the experiments were 40% of the mean flow depth.
- When the distance between the rods in a row (T) was constant, and the distance between the rod rows (P) was increased, the wave amplitude (A) decreased. Also when the distance between the rod rows (P) was constant, and the distance between rods in the row (T) were increased, the wave amplitude (A) decreased
- The relationship between the relative amplitude (A/h) and the different values of T/D was different. This meant that when the value of T/D was less than 5, the relationship between the relative wave amplitude (A/h) and T/D was in reverse order to that when the value of T/D was more than 5. In other words, when the value of T/D was less than 5 and T/D was increased the ratio A/h increased. However, when the value of T/D was equal to or more than 5 and T/D increased, A/h decreased. (see Fig. 7.19).
- The Zima and Ackermann equation did not present a good estimation for calculating A/h, except for $T/D<5$ and $n=1$ (see Fig. 7.21).

- New formulations, as given in Equations (7.17) and (7.18), were obtained from dimensional analysis, to estimate the amplitude of the transverse wave generated by vortex shedding for the two sets of values of T/D (i.e. $T/D<5$ and $T/D\geq5$).

8.9 Recommendations for further study

1- In the experiments undertaken in this study, the conditions were limited to a fixed rod diameter. This research project could be further extended to include other rod sizes.

2- The minimum distance between the rods for each row was set to 60 mm, and the minimum distance between the rows was 105 cm. In order to analyse the critical points these intervals could be decreased with the hope of providing more accurate profiles of the key velocity and turbulence parameters.

3- The effects of the side walls have been ignored. However, more research needs to be undertaken to investigate the trailing effect. This is a challenging direction of research.

4- Application of Laser Doppler Velocimeter (LDV) instead of Acoustic Doppler Velocimeter (ADV) can lead to better results.

5- The rods used have been considered to be rigid, similar to tree stems, and therefore there has not been any need to investigate the effects of rod flexibility on wave generation. However, in real river basin scenarios the rod may not be rigid. If rod flexibility were taken into account then the complexity of the analysis would increase significantly.

6- The transverse wave characteristics have been analysed for a constant discharge. The influence of a changing discharge, as would occur during a river flood, would provide a valuable extension to the understanding of vortex shedding and wave action in flood inundation modelling.

7- The vortex shedding may be observed and measured more accurately using video cameras as another measurement modality.

8- Changes in the channel and floodplain widths would also provide valuable information for investigating the impact of vegetation on flood inundation.

REFERENCES

Abuodha, P. A. W. and Kairo, J. G. (2001), "Human-induced stresses on mangrove swamps along the Kenya coast." *Hydrobiologia*, 458: 255-265.

Arcement, G. J. and Schneider, V. R. (1989), "Guide for selecting Manning's roughness coefficients for natural channels and flood plain." U.S. Geological Survey Water Resource paper 2339.

Arcement, G. J. and Schneider, V. R. (1987), "Roughness coefficients for densely vegetated flood plains." U.S. Geological Survey Water-Resource Investigations Report 83-4247.

Arcement, G. J. and Schneider, V. R. (1984), "Guide for selecting Manning's roughness coefficients for natural channels and flood plain." U.S.D.T., Federal Highway Administration, Report No. FHWA-TS-84-204.

Bangasser, A. A. (2004), "Modeling the Hydrodynamic processes relating to idealised mangrove vegetation." MSc. thesis, Cardiff University, Cardiff, UK.

Baptist, M. J. (2002), "A flume experiment on sediment transport with flexible, on submergrd." MSc. Thesis, Delft University of Technology, Delft, CN.

Barnes, H. H. (1967), "Roughness characteristics of natural channels." U.S. Geological Survey Water-Resource Paper 1849.

Blevins, R. D. (1977), "*Flow-induced vibrations.*" Van Nostrand Reinhold, New York.

Blevins, R. D. (1985), "The effect of sound on vortex shedding from cylinders." *J. Fluid Mech.*, Vol. 161, 217-237.

Brookes, A. and Shields, F. D. (editors) (1996), "River Channel Restoration: Guiding Principles for Sustainable Projects." John Wiley, Chichester. 440 pages. ISBN 0-471-96139-6.

Carollo, F. G., Ferro V. and Termini D. (2002), "Flow velocity measurements in vegetated channels." Journal of hydraulic Engineering, Vol. 128, No. 7.

Chanson, H. (1999), "*The Hydraulics of Open Channel Flow*" Arnold, London, U.K.

Chaudhry, M. F. (1993), "*Open-channel flow.*" Printice-Hall, Englewood Cliffs, New Jersey, 483 p.

Choi, S.-U. and Kang, H. (2004), "Reynolds stress modelling of vegetated open-channel flows." Journal of Hydraulic Research, IAHR, 42(1), PP. 3-11.

Choi, S.-U. and Yang, W. (2005), "CFD Modelling Vegetated Channel Flows: A State-of-the Art Rewiew." Water Engineering Research, Vol. 6, No. 3, pp. 101-112.

Choi, S.-U. and Kang, H. (2006), "Numerical investigations of mean flow and turbulence structures of partly-vegetated open channel flows using the Reynolds stress model" *Journal of Hydraulic Research* , Vol. 44, No. 2, pp 203-217.

Chow, V. T. (1959), "*Open channel hydraulics.*" McGraw-Hill, NewYork, 680 p.

Christensen, B. A. (1985), "Open channel and sheet flow over flexible roughness." 21st IAHR Congress, Melbourne, Australia, 19-23 August 1985. pp 463-467.

Clay, D., and Tison, G. (1968), "Vortex-induced oscillations at low-head weirs." *J. Hydraulic Div., Am. Soc. Civ. Eng.,* 94(4), 1160.

Cook, H. L. and Campbell, F. B. (1939), "Characteristics of some meadow strip vegetation." Agricultural Engineering 20: 345-348.

Cook, H. L. (1938), "Spartanburg hydraulic laboratory." Civil Engineering 8: 653-655.

Cowen, W. L. (1956), "Estimating hydraulic roughness coefficients." Agri. Engrg., 37(7), P 473-475.

Cox, M. B. (1942), "Tests on vegetated waterways." Oklahoma Agr. Exp. Sta. Tech. Bul. T-15, Stillwater, Okla., 23 p.

Crausse. (1939), "Sur un Phènomene d'Oscillation du Plan d'eau Provoquè Part 1'Ècolement Autour d'Obsticales en forme de Piles du Pont." *Coptes Rendus de Sèances de l'Academie de Sciences*, 209 (in French).

Dean, G. D. and Dalrymple, R. A. (1984), "*Water wave mechanics for engineers and scientific.*" World Scientific, London.

Dunn, C. J. (1996), "Experimental determination of drag coefficients in open channel with simulated vegetation." MSc. Thesis, University of Illinois at Urban-Champaign, Urbana, IL.

Einstein, H.A. and Banks, R. B. (1950), "Fluid resistance of composite roughness." Trans. American Geophysical Union, vol. 31, No. 4, p 603-610.

El-Hakim, O. and Salama, M. M. (1992), "Velocity distribution inside and above branched flexible roughness." Journal of Irrigation and Drainage Engineering, 118, 6, pp 914-927.

Environment Agency (2001a), "Lessons Lerned: Autumn 2000 Floods, Environment Agency, Bristol, UK.

Fairbanks, J. D. (1998), "Velocity and Turbulence Characteristics in Flows Through Rigid Vegetation." MSc Thesis, Blacksburg, Virginia, USA.

Falconer, R. A., Lin, B., Wu, Y., and Harris, E. (2001), "DIVAST Model References and User Manual." Hydroenvironmental Research Centre, School of Engineering, Cardiff University, UK.

Falconer, R. A. (1976), "Mathematical modelling of jet-forced circulation in reservoirs and harbours." PhD Thesis, Imperial College, University of London, London.

Falconer, R. A. (2006), "Editorial in Water Management." ice, Proceeding of The Institution of Civil Engineers, Vol. 159.

Falvey, H. T. (1980), "Bureau of Reclamation Experience with Flow-Induced Vibration." *Practical Experiences with Flow Induced Vibrations*, E. Naudascher and Rockwell, eds., Springer, New York.

Fathi-Moghadam, M. (1996), "Momentom absorption in non-rigid, non-submerged, tallvegetation along rivers." PhD thesis University of Waterloo, Canada.

Fathi-Moghadam, M. and Kouwen, N. (1997), "Nonrigid, nonsubmerged, vegetative roughness on floodplains." J. Hydraulic Engineering, ASCE, Vol. 123(1), pp 51-57.

Fenzel, R. N. and Davis, J. R. (1964), "Hydraulic Resistance Relationships for Surface Flows in Vegetated Channels." Trans. Of ASAE.

Ferro, V. (1999), "Friction factor for gravel-bed channel with high boulder concentration." Journal of Hydraulic Engineering, 125, 7, pp. 771-778.

Fischer-Antze, T., Stoesser, T., Bates, P., and Olsen, N.R.B. (2001), "3-D numerical modeling of open-channel flow with submerged vegetation." *Journal of Hydraulic Engineering*, IAHR, 39(3), pp. 303-310.

Fisher, K. R. (1996), "Handbook for assessment of hydraulic performance of environmental channels." Report SR 490, draft. HR Wallingford, Wallingford, Great Britain. 346 pages.

Fitz-hugh, J. S. (1973), "Flow induced vibration in heat exchangers." *Proc. UKAEA/NPL International Symposium on Vibration Problems in Industry*, Keswick, England, Paper 427, 1-17.

Fleming, G., Frost, L., Huntington, S., Knight, D., Law, F., and Richard, C. (2001), "Learning to live with rivers." Final report of The Institution of Civil Engineers.

French, R. H. (1994), "*Open-channel hydraulics.*" Mc Grow-Hill, Singapore. 739 pages.

Furukawa, K., Wolanski, E., and Mueller, H. (1997), "Currents and sediment transport in mangroveforests." *Estuarine Coastal and Shelf Science*, 44: 301-310.

Ghisalberti, M. and Nepf, H. M. (2002), "Mixing layers and coherent structures in vegetated aquatic flows." Journal of Geophysical Research, Vol. 107, No. C2.

Graf, W. H. and Altinakar, M. S. (1998), "Fluvial hydraulics: Flow and transport processes in channels of simple geometry." Wiley, Chichester, England. 681 pages.

Hagen, L. J. and Skidmore, E. L. (1974), "Reducing turbulent transfer to increase water use efficiency." Agricul. Meteorol. 14, p 153-168.

Hamakawa, H., Fukano, T., Nishida, E., and Aragaki, M. (2001), "Vortex Shedding from a Circular Cylinder with Fin." *Proceeding of 7th AIAA/CEAS Aeroacoustics Conference*, AIAA-2001-2215.

Hanski, M. (2000), "Jokien rakenteellisen tilan arvionti: taustaa EU: n vesipolitiikan puitedirektiivin toimeenpanolle Suomen virtavesissä." Suomen ympäristö, 379. Finnish Environmental Institute (SYKE), Helsinki. 96 Pages.

Ikeda, S. and Kanazawa, M. (1996), "Three dimensional organized vortices above flexible water plants." *Journal of Hydraulic Engineering*, ASCE, 122(11), 634-640.

Järvelä, J. (2002), "Flow resistance of flexible and stiff vegetation: a flume study with natural plants." Journal of Hydrology, 269(1-2): 44-54.

Järvelä, J. (2004), "Flow Resistance in Environmental Channels: Focus on Vegetation." PhD Thesis, Helsinki University of Technology, Espoo, Finland.

Karman, Th. (1912), "Über den Mechanismus des Widerstandes den ein bewegter Körper in einen Flüssigkeit Erfahrt." *Nachr. Königl.* Gesellschaft.

Keulegan, G. H. (1938), "Laws of turbulent flow in open channels." J. Res., Nat. Bureau of Standards, vol. 21, No. 6, p 707-741.

Klaassen, G. J. and Zwaard, J. J. (1974), "Roughness coefficients of vegetated floodplains." J. Hydr. Res. 12(1): 43-63.

Kouwen, N. (1992), "Modern approach to design of grassed channels." J. of Irrigation and Drainage Eng., ASCE, vol. 118, No. 5. P 773-743.

Kouwen, N., Li, R. M., and Simons, D. B. (1981), "Flow resistance in vegetated waterways." Trans. ASAE vol. 24, No. 3, P 684-698.

Kouwen, N. and Li, R. M. (1980), "Biomechanics of vegetated channel linings." J. Hydr. Div., ASCE, vol. 106, No. 6., P 1085-1103.

Kouwen, N., Unny, T. E., and Hill, H. M. (1969), "Flow resistance in vegetated channels." J. Irrig. Drain. Div., Am. Soc. Civ. Eng. (ASCE), 96(2), 329-342.

Krishnappan, B. G. and Lau, Y. L. (1986), "Turbulent modelling of flood plain flows." J. Hydr. Eng., ASCE, vol. 112, No. 4, p 251-266.

Kummu, M. (2002), "Roughness characteristics and velocity profile in vegetated and nonvegetated channel" MSc Thesis in Helsinki University of Technology.

Kutija, V. and Hong, H. M. (1996), "A numerical model for assessing the additional resistance to flow introduced by flexible vegetation." Journal of Hydraulic Research, 34, 1, pp 99-114.

Lemon, E. R. (1967), "Aerodynamic study of CO_2 exchange between the atmosphere and the plant, harvesting the sun: photosynthesis in plant life." Academic Press, New York, p263-290.

Li, R. M. and Shen, H. W. (1973), "Effect of tall vegetation on flow and sediment." J. Hydr. Div. ASCE 99(5): 793-814.

Lienhard, J. H. (1966), "*Synopsis of Lift, Drag and Vortex Frequency Data for Rigid Circular Cylinders.*" Washington State University, College of Engineering, Research Division Bulletin 300.

Lin, B. and Falconer, R. A. (1997), "Three-dimensional Layer-integrated Modelling of Estuarine Flows with Flooding and Drying." Estuarine, Coastal and Shelf Science, 44, pp. 737-751.

López, F. and García, M. H. (2001), "Mean flow and turbulence structure of open-channel flow through non-emergent vegetation." J. Hydr. Engrg. 127(5): 392-402.

Marsh, W. M. (1991), "Landscape Planning: Environmental Applications." John & Willy & Sons. 339 pages.

Masterman, R. and Thorne, C. R. (1992), "Predicting influence of bank vegetation on channel capacity. " J. of Hyd. Eng., ASCE, vol. 118, No. 7, p 1052-1058.

Meijer, D. G. and Van Velzen, E. H. (1998), "Prototype-scale flume experiments on hydraulic roughness of submerged vegetation." HKV Consultants, Lelystad, The Netherlands and Ministry of Transport, Public Works and Water Management, Institute for Inland Water Management and Waste Water Treatment (RIZA), Arnhem, the Netherlands.

Namin, M. M. (2003), "A fully three-dimensional non-hydrostatic free surface flow model for hydro-environmental predictions." PhD Thesis, Cardiff School of Engineering, Cardiff University.

Naot, D., Nezu, I. and Nakagawa, H. (1996a), "Hydrodynamic behavior of partly vegetated open channels." Journal of Hydraulic Engineering, ASCE, Vol. 122, No. 11, pp. 625-633.

Naudascher, E. and Rockwell, D. eds. (1980), "*Practical Experiences with Flow Induced Vibrations.*" Springer, New York.

Nearing, M. A., Ascough, L. D., and Laflen, L. D. (1990), "Sensitivity Analysis of WEPP Hillslope Erosion Model." Transaction, ASCE, 33(3): 839-849.

Nearing, M. A., Lane, L. J., and Laflen, J. M. (1990), "Prediction Technology for soil erosion by water: status and research needs." Soil Sci. Am. J. 54: 1702-1711.

Nepf, H. M. (1999), "Drag, turbulence, and diffusion in flow through emergent vegetation." Water Resources Research 35(2): 479-489.

Nepf, H.M. and Vivoni, E.R. (1999), "Turbulence structure in depth-limited, vegetated flow: Transition between emergent and submerged regimes." *Proceedings of 28th IAHR congress*, Graz, Austria.

Nepf, H. M. and Vivoni, E. R. (2000), "Flow structure in depth-limited, vegetated flow." Journal of Geophysical Research, Vol. 105, No. C12, Pages 28,547-28,557.

Nezu, I. and Rodi, W. (1993), "Experimental study on secondary currents in open-channel flow." 21st IAHR Congress, Melbourne, Australia, 19-23.

Nezu, I. and Nakagawa, H. (1993), "Turbulence in open channel flows." A.A. Balkema: Rotterdam.

Nezu, I. and Onitsuka, K. (2001), "Turbulent structures in partly vegetated open-channel flows with LDA and PIV measurements." *Journal of Hydraulic Research*, IAHR, 39(6), 629-642.

Othman, M. A. (1994), "Value of mangroves in coastal protection." Hydrobiologica 285: 277-282.

Pasche, E. and Rouve, G. (1985), "Overbank flow with vegetatively roughened flood plains." J. Hydr. Eng., ASCE, Vol. 111, No. 9, p 1262-1278.

Petryk, S. (1969), "Drag on cylinders in open channel flow." Ph.D. thesis, Colo.State Univ., Fort Collins.

Petryk, S. and Bosmajian, G., III (1975), "Analysis of flow through vegetation." J. Hydr. Div., ASCE, 101(HY7), p 871-884.

Plate, E. J. and Qurashi, A. A. (1965), "Modelling of velocity distributions inside and above tall crops." J. Applied Meteorol. vol. 4, p 400-408.

Prinos, P. (1990), "Turbulence modelling of main channel-flood plain flows with an algebraic stress model." A paper presented in Inter. Conf. on River Flood Hydr.

Raupach, M. R. and Show, R. H. (1982), "Averaging procedures for flow within vegetation canopies." Bound. L. Meteorol., 22, p 79-90.

Ree, W. O. (1958), "Retardation coefficients for row crops in diversion terraces." Trans. ASAE, vol. 1, p 78-80.

Ree, W. O. and Crow, F. R. (1977), "Friction factor for vegetated waterways of small slope." U.S.D.A., Agri. Research Service, ARS-S-151.

Ree, W. O. and Palmer, V. J. (1949), "Flow of water in channels protected by vegetative linings." U.S.D.A., Soil Cons. Service, Tech. Bulletin No. 967.

Røhde, F. G., Rouve, G., and Pasche, E. (1980), "Self-Excited oscillatory surface waves around cylinders." *Practical Experiences with Flow Induced Vibrations*, E. Naudascher and Rockwell, eds., Springer, New York.

Schnauder, I. (2004), "Interaction processes in a straight compound channel with rigid and flexible emergent floodplain vegetation." PhD Thesis, University of Karlsruhe, Karlsruhe, Germany.

Schuster, J. C. (1967), "Canal Capacity Studies, Wave Formation by Bridge Piers." *Hydraulics Branch Rep., HYD-485*, U.S. Bureau of Reclamation.

Shaw, R. H. and Seginer, I. (1987), "Calculation of velocity skewness in real and artificial plant canopies." Bound. L. Meteorol., 39, p315-332.

Shimizu, Y. and Tsujimoto, T. (1993), "Comparison of Flood-flow Structure Between Compound Channel and Channel with Vegetated Zone." Proc. 25th IAHR Congress, Delft, The Netherlands.

Shimizu, Y. and Tsujimoto, T. (1994), "Numerical analysis of turbulent open-channel flow over a vegetation layer using a k-ε Turbulence Model." Journal of Hydroscience and Hydraulic Engineering. 11(2), pp 57-67.

Stephan, U. (2001), "Zum File βwiderstandsverhalten flexibler Vegetation." Dissertation. Institute of Hydraulics, Hydrology and Water Resources Management; Faculty of Civil Engineering; Vienna University of Technology. 165 pages.

Stephan, U. and Gutknecht, D. (2001), "Hydraulic resistance of submerged flexible vegetation" Journal of Hydrology 269(1-2): 27-43.

Steven, J. G., Jackson, K., and Brusztynsky, T. A. (1986), "Erosion and Sediment Control Handbook." McGraw-Hill Book Company, USA.

Stone, B. M. (1997), "Hydraulics of flow in vegetated channels." MSc thesis, Clarkson Univ., Potsdam, N.Y.

Stone, B. M. and Shen, H. T. (1999), "Hydraulics of flow in vegetated channels." *Proc., Water Resources Engineering*, ASCE, Seattle.

Stone, B. M. and Shen, H. T. (2002), "Hydraulic resistance of flow in channels with cylindrical roughness." Journal of Hydraulic Engineering, Vol. 128, No. 5.

Stormwater Quality Best Management Practices (1991), Prepared by Marshal MacklinMonaghan Limited Concul. Eng. Planners, Thornhill, Ontario. For Envir. Science & Standards/ Water Resources, Ont. Ministry of the Envir., ISBN 0-7729-8478-6.

Strouhal, V. (1878), "Uber eine besondere Art der Tonerregung." *Ann. Physik* (Leipzig).

Temple, D. M. (1983), "Stability of Grass-lined open channels." Transactions, ASAE, 26(4): 1064-1069.

Thom, A. S. (1975), "Momentom, mass and heat exchange of plant communities." In. J. L. Monteith (ed.), Vegetation and the atmosphere, vol.1, Academic Press, London, p57-109.

Thornton, C. I., Abt, S. R., **Morris, C. E., and Fischenich, J. C. (2000),** "Calculating Shear Stress at Channel Overbank Interfaces in Straight Channels with Vegetated Floodplains." Journal of Hydraulic Engineering. Vol. 126, No. 12, pp. 929-936.

Tominaga, A., Ezaki, K., and Nakagawa, H. (1989a), "Three dimensional turbulent structure in straight open-channel flows." *Journal of Hydraulic Research*, IAHR, 27(1), 149-173.

Tsujimoto, T. and Kitamura, T. (1992), "Experimental study on open-channel flow with vegetated zone along sidewall: correlative structures of fluctuations of velocity and free surface." *KHL Progressive Report 1*, Hydr. Lab., Kanazawa University, Japan.

Tsujimoto, T. (1992), "Spectral analysis of velocity and water-surface fluctuations appearing in an open channel with vegetated and non-vegetated regions in a cross-section." *Proc., 6th IAHR Int. Symposium on Stochastic Hydraulics*, Taipei, Taiwan, 361–368.

Tsujimoto, T. and Kitamura, T. (1992), "Transverse mixing associated with surface wave in open-channel flow with longitudinal zone of vegetation." *Proc. Hydraulic Engineering, JSCE,* 36, 273–280.

Tsujimoto, T. and Nagasaki, T. (1992), "Turbulent characteristics of flow over vegetation swaying on a bed." KHL Progressive report 92. Hydr. Lab., Kanazawa Univ., 2-40-20, Kodatsuno, Kanazawa 920, Japan, p 9-19.

Tsujimoto, T.; Shimizu, Y.; Kitamura, T., and Okada, T. (1992), "Turbulent Open-Channel Flow over bed covered by rigid vegetation." Journal of Hydroscience and Hydraulic Engineering. 10, 2, pp. 13-25.

Tsujimoto, T., Kitamura, T., and Okada, T. (1991), "Turbulent structure of flow over rigid vegetation covered bed in open-channels." *KHL Progressive Report 1*, Hydr. Lab., Kanazawa University, Japan.

Tsujimoto, T., Okada, T., and Kitamura, T. (1991), "Turbulent flow over flexible vegetation-covered bed in open channels." KHL Progressive report 91, Hydr. Lab., Kanazawa University, Kanazaw, Japan, p 31-39.

Tsujimoto, T. and Kitamura, T. (1990), "Interaction between flow in vegetated region and flow in non-vegetated region in an open channel." KHL Progressive report 90, Hydr. Lab., Kanazawa Univ., 2-40-20, Kodatsuno, Kanazawa 920, Japan, p 57-68.

Tsujimoto, T., Kitamura, T., Fujii, Y., and Nakagawa, H. (1996), "Hydraulic resistance of flow with flexible vegetation in open channel." Journal of Hydroscience and Hydraulic Engineering 14(1): 47-56.

Tsujimoto, T., Tsuji, A., Izumi, N., and Okada, T. (1995), "Characteristics of Flow in Transitional Reach of a Stream with Vegetation Zone Along a Side Wall." KHL Progressive Report, Kanazawa University, Japan.

USDA (1954), "HGandbook of Channel Design for Soil and Water Conservation." Prepared by Stillwater outdoor hydraulic lab. at Stillwater, Okla., SCS, U.S.D.A., SCS-TP-61.

Walsh, G. E. (1977), "Exploitation of managal." In V. J. Chapman (ed.): Wet Castal Ecosystems. Amesterdam: Elsevier. Pp. 347-362.

Watanabe, T. and Kondo, J. (1990), "The influence of canopy structure and density upon the mixing length within and above vegetation." Journal of Meteorological Society of Japan, 68, 2, pp 227-234.

Weaver, D. S., Fitzpatrick, J. A., and Elkashlan, M. (1986), "Strouhal numbers for heat exchanger tube arrays in cross flow." *Flow Induced Vibration*, 1986, PVP, 104, 193-200.

Westwater, D. (2001), "Modelling hydrodynamic and shallow water processes over vegetated floodplains." PhD thesis, Cardiff University, Cardiff, UK.

World Health Organisation/UNICEF (2000), "Global water supply and sanitation assessment." WH0/UNICEF, Geneva.

Wu, Y., Falconer, R. A., and Lin, B. L. (2001), "The Fate and Impact of Persistent Contaminants in Estuaries and Coastal Waters." Environment Agency, Project Number 7261, Cardiff University, Cardiff.

Xiaohui, S. and Li, C. W. (2002), "Large eddy simulation of free surface turbulent flow in partly vegetated open channels." Dalian University of Technology, Dalian, China.

Ziada, S., Oengoren, A., and Buhlmann, E. T. (1989), "On acoustical resonance in tube arrays -part I: experiments." *J. Fluids Struct.*, 3, 293-314.

Zima, L. and Ackermann, N. L. (2002), "Wave generation in open channels by vortex shedding from channel obstructions." J. of Hydraulic Engineering, 128, No. 6, 596-603.

Žukauskas, A. and Katinas, V. (1979), "Flow-Induced Vibration in Heat Exchanger Tube Banks."

Žukauskas, A., Ulinskas, R., and Katinas, V. (1988), "*Fliud Dynamics and Flow-Indused Vibrations of Tube Banks.*" Hemisphere, New York.